

# ESTABLISHING A FACILITY TO MEASURE THE EFFICIENCY OF STRUCTURED PACKING UNDER TOTAL REFLUX

*by*

Emil Friedrich Paquet

Thesis presented in partial fulfillment  
of the requirements for the Degree



MASTER OF SCIENCE IN ENGINEERING  
(CHEMICAL ENGINEERING)

in the Faculty of Engineering  
at Stellenbosch University

*Supervised by*  
Prof. J.H. Knoetze

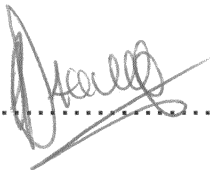
March 2011

---

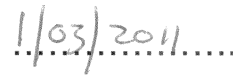
# Declaration

---

By submitting this thesis electronically, I declare that the entirety of the work contained therein is my own, original work, that I am the sole author thereof (save to the extent explicitly otherwise stated), that reproduction and publication thereof by Stellenbosch University will not infringe any third party rights and that I have not previously in its entirety or in part submitted it for obtaining any qualification.

A handwritten signature in black ink, appearing to read 'M. ...', written over a horizontal dotted line.

Signature

A handwritten date '1/03/2011' written in black ink over a horizontal dotted line.

Date

*Copyright © 2011 Stellenbosch University*

*All rights reserved*



---

# Abstract

---

Structured packing is often the preferred choice for column internals because of its low pressure drop and high efficiencies compared to that of trays and random packing. However, the mass transfer phenomena in these gas-liquid contacting devices is still not well understood, even though it is widely used in industry. A contributing factor to this is the lack of understanding and availability of experimental data in the open literature. These shortcomings complicate the design of a distillation column and make practical experience essential. There is thus a need for more experimental data, especially for packings where only limited information is available. The focus of this study was to establish a testing facility that can be used to measure the efficiency of structured packing under total reflux, and not to measure vast quantities of experimental data; the latter will be done in future.

The facilities available at Stellenbosch University limited the internal diameter of the column to 0.2 m, which is sufficient to test higher surface area structured packings ( $\geq 350 \text{ m}^2/\text{m}^3$ ). The column is used with a thermosyphon reboiler that uses steam as the heating source and is equipped with a total condenser. Two sections are used for the packed bed that allow for a total packed height of 3.78 m (2x1.89 m). The column is set up to operate under total reflux and was designed to operate at pressures ranging from 0.3 to 1 bar abs, vapour flow rates of  $0.73 - 3.65 \text{ (m/s) (kg/m}^3)^{0.5}$  and liquid flow rates of  $5 - 25 \text{ m}^3/(\text{m}^2 \cdot \text{h})$ .

It was found that the 2-butanol/iso-butanol and the p-xylene/o-xylene systems are suitable test mixtures for this pilot plant setup. The VLE data from Kutsarov *et al.* (1993) and Zong *et al.* (1983) for p-xylene/o-xylene and 2-butanol/iso-butanol are thermodynamic consistent and was validated by VLE experiments done in this study.

It was found that the experimentally obtained efficiency (HETP) and pressure drop data for Mellapak 350Y compared well with published results of Spiegel and Meier (1987). With regard to the predictive models, it was found that i) the SRP model predicted the HETP of Mellapak 350Y structured packing accurately in the pre-loading region and slightly over predicted the HETP in the loading region, whereas ii) the Delft model over predicted HETP and iii) the Billet and Schultes model under-predicted HETP under the entire tested range (i.e. over-predict efficiency). With regard to the pressure drop data i) the Billet model

accurately predicted the pressure drop over the entire tested range, whereas ii) the SRP model accurately predicted the pressure drop in the pre-loading region and slightly over predicted the pressure drop in the loading region and iii) the Delft model over predicted the pressure drop over the entire range and followed an almost parallel trend to the results from the SRP model.

It was also found that information in the field of mass transfer in a packed column is far from saturated, and there is a need for more experimental data and better understanding of the mass transfer phenomena in packed columns.

---

# Opsomming

---

Gestruktureerde pakking het 'n laer drukval en 'n hoër effektiwiteit in vergelyking met willekeurige pakkings en plate, en is daarom dikwels die voorkeur keuse vir pakkings materiaal in 'n distilleer kolom. Die massa-oordrags verskynsels in hierdie gas-vloeistof kontakters word egter nog nie goed verstaan nie, ten spyte van die grootskaalse aanwending in die nywerheid. 'n Bydraende faktor is die tekort aan eksperimentele data in die ope literatuur. Die tekortkomings bemoeilik die ontwerp van distilleerkolomme en maak praktiese ervaring 'n noodsaaklike vereiste. Daar is dus 'n behoefte aan meer eksperimentele data veral vir pakkings waar daar min of geen data beskikbaar is nie. Die fokus van die studie was om 'n toetsfasiliteit op te rig wat gebruik kan word om die effektiwiteit van gestruktureerde pakking onder totale terugvloei kondisies te bepaal, en dus nie om 'n groot hoeveelheid data te genereer nie; laasgenoemde sal wel deel uitmaak van toekomstige studies.

Die fasiliteite beskikbaar by die Universiteit van Stellenbosch het die binne diameter van die kolom beperk tot 0.2 m. Die diameter is voldoende om gestruktureerde pakkings met 'n hoë oppervlakarea te toets byvoorbeeld pakkings met areas  $350 \text{ m}^2/\text{m}^3$  en hoër. Die kolom gebruik 'n verdamper (met stoom as energie bron) om die vloeistof te verdamp en 'n totale kondensator (verkoel met verkoelingswater) om die damp te laat kondenseer. Twee seksies van 1.89 m elk word gebruik vir die gepakte bed en die kolom het dus 'n totale pakkingshoogte van 3.78 m. Die kolom is opgestel vir totale terugvloei en is ontwerp om bedryf te word by drukke tussen 0.3 en 1 bar abs, damp snelhede van 0.73 tot 3.65 (m/s)  $(\text{kg}/\text{m}^3)^{0.5}$  en vloeistof vloeitempo's tussen 5 en 25  $\text{m}^3/(\text{m}^2.\text{h})$ .

2-butanol/iso-butanol en p-xylene/o-xylene is gevind om geskik te wees as mengsels vir die toetsopstelling. Die damp-vloeistof fase-ewewig data van Kutsarov *et al.* (1993) en Zong *et al.* (1983) vir p-xylene/o-xylene and 2-butanol/iso-butanol is termodinamies konsistent en is gevalideer deur damp-vloeistof fase ewewig toetse in die studie.

Daar is gevind dat die eksperimenteel bepaalde effektiwiteit en drukval data vir Mellapak 350Y pakking goed vergelyk met gepubliseerde data van Spiegel and Meier (1987). Die eksperimenteel bepaalde effektiwiteit data is met waardes van beskikbare modelle model

vergelyk en daar is gevind dat: i) die SRP voorspel die effektiwiteit van Mellapak 350Y pakking akkuraat in die 'pre-loading' gebied maar toon afwykings van die eksperimentele data in die 'loading' gebied, ii) die Delft model voorspel 'n hoër hoogte ekwivalent aan 'n teoreties plaat (HETP) oor die hele gebied terwyl iii) die Billet en Schultes model weer 'n laer HETP voorspel oor die hele gebied. Met betrekking toe die drukval data i) voorspel die Billet model die drukval akkuraat oor die hele gebied, ii) die SRP model voorspel die drukval korrek in die 'pre-loading' gebied maar begin afwyk van die eksperimentele data in die 'loading' gebied en iii) die Delft model voorspel groter waardes vir drukval oor die hele gebied en volg amper 'n parallele tendens met die SRP model.

In die studie is daar gevind dat daarin die gebied van massa-oordrag nog 'n tekort is aan eksperimentele data en daar baie navorsings geleentheid is.

---

# Acknowledgements

---

The author would like to thank the following people how directly and indirectly contributed towards the contents and successful completion of this thesis:

- *To my Lord and Saviour, Jesus Christ, for giving me the ability and strength to successfully complete this project.*
- *My wonderful wife, Tarryn, for her love, patience and constant encouragement during the last two years.*
- *My mother, Susan, and my late father, Arthur, for their constant love, support and encouragement.*
- *My supervisors Prof. J.H. Knoetze and Dr. C.E. Schwarz, for their continuous support, excellent supervision and guidance during the past few years. Without them this thesis would not have been possible.*
- *The personnel in the workshop, especially Anton Cordier and Vincent Carolissen, for their help during the construction and commissioning period of the pilot plant.*
- *Juliana Steyl, for her assistance in ordering equipment. For going out of her way to ensure orders were placed.*
- *Sasol Technology (Pty) Ltd and the South African Department of Trade and Industry through THRIP for their financial contribution.*
- *My mentor at Sasol (Pty) Ltd, Dr. A.E. Erasmus, for his technical assistance and support.*





---

# CONTENTS

---

DECLARATION .....	I
ABSTRACT .....	III
OPSOMMING .....	V
ACKNOWLEDGEMENTS .....	VII
LIST OF FIGURES .....	XIII
LIST OF TABLES .....	XV
NOMENCLATURE.....	XVII
Symbols.....	xvii
Greek .....	xx
Abbreviations .....	xxii
Glossary .....	xxii
<b>1 INTRODUCTION .....</b>	<b>1</b>
1.1 History.....	1
1.2 Column Internals .....	2
1.2.1 Trays .....	2
1.2.2 Packing.....	3
1.3 Motivation Behind this Research.....	4
1.3.1 Hydrodynamics.....	5
1.3.2 Mass Transfer .....	7
1.3.3 Interfacial Area .....	7
1.3.4 Models .....	7
1.3.5 Thermodynamics of Separation.....	8
1.4 Objectives and Scope.....	9
<b>2 LITERATURE REVIEW.....</b>	<b>13</b>
2.1 Introduction to Packed Columns .....	13
2.2 Packing Geometry.....	14
2.3 Effect of Geometric Properties .....	15
2.3.1 Surface Area and Corrugation Angle .....	15
2.3.2 Installation .....	19
2.3.3 High capacity Packings .....	19
2.4 Distributors .....	21
2.4.1 Performance.....	21
2.4.2 Pressure Drop.....	22

2.5	Effect of Column Diameter and Bed Depth on HETP and Pressure Drop .....	23
2.6	Test Mixtures.....	27
2.6.1	Fenske <i>et al.</i> (1938) Rules for a Test System.....	27
2.6.2	Popular Test Mixtures .....	28
2.7	HETP.....	32
2.8	Calculating the HETP from Experimental Data .....	33
2.9	Modelling of Distillation Columns .....	35
2.10	Hydrodynamics .....	36
2.10.1	Billet and Schultes Model.....	38
2.10.2	SRP Model .....	45
2.10.3	Delft Model .....	49
2.11	Effective Interfacial Area .....	51
2.11.1	Billet and Schultes Model.....	51
2.11.2	SRP Model .....	53
2.11.3	Delft Model .....	54
2.12	Mass Transfer.....	55
2.12.1	Billet and Schultes Model.....	55
2.12.2	SRP Model .....	56
2.12.3	Delft Model .....	58
2.13	Evaluation of Models.....	59
<b>3</b>	<b>EXPERIMENTAL SETUP .....</b>	<b>67</b>
3.1	Design Objectives and Limitations .....	67
3.2	Process Concept.....	67
3.3	Design Specifications .....	69
3.3.1	Internal Column Diameter and Height of Packing Section.....	70
3.3.2	Height of Packing Sections.....	70
3.3.3	Test Mixture .....	71
3.3.4	Operating Range .....	71
3.3.5	Distributors .....	71
3.3.6	Sampling.....	72
3.3.7	Materials of Construction.....	72
3.3.8	Sensor Placing.....	72
3.3.9	Insulation .....	73
3.4	Detailed Design Specification .....	73
3.4.1	Reboiler.....	74
3.4.2	Condenser .....	75
3.4.3	Packing Sections .....	76

3.4.4	Distributors .....	77
3.4.5	Sampling.....	79
3.4.6	Packing.....	81
3.4.7	Placement of Sensors.....	81
3.4.8	Steam Tracing.....	85
3.5	Safety.....	86
3.6	Experimental Procedure.....	87
3.7	Selecting a Test Mixtures .....	88
3.8	Vapour-liquid Equilibrium Cell.....	92
3.9	Summary .....	93
<b>4</b>	<b>RESULTS AND DISCUSSION .....</b>	<b>96</b>
4.1	Thermodynamic and Transport Properties. ....	96
4.1.1	VLE Data Verification .....	96
4.1.2	Relative Volatility .....	99
4.2	Commissioning Problems of Pilot Plant .....	102
4.2.1	Problem 1: Incorrect Pressure Drop Trends.....	103
4.2.2	Problem 2: Pressure Drop Oscillations and its Effect on HETP .....	106
4.3	Pilot Plant Data Validation .....	108
4.3.1	Experimental Error.....	109
4.3.2	Time to Reach Equilibrium .....	109
4.3.3	Repeatability .....	111
4.3.4	Influence of Composition on Fenske Equation.....	111
4.4	Results.....	112
4.4.1	Sub-cooling and Heat Losses.....	115
4.4.2	Liquid Distributor.....	117
4.4.3	Property Differences .....	119
4.5	Comparison of Results .....	119
4.5.1	Results Compared to Sulzer™ Brochure and Published Data .....	120
4.5.2	Model Predictions Compared to Experimental Results .....	121
<b>5</b>	<b>CONCLUSIONS .....</b>	<b>128</b>
<b>6</b>	<b>RECOMMENDATIONS.....</b>	<b>134</b>
<b>7</b>	<b>REFERENCES.....</b>	<b>136</b>
<b>8</b>	<b>APPENDIX.....</b>	<b>146</b>
8.1	Boiler Capacity Calculations .....	146
8.1.1	Sample Calculations .....	148
8.2	Constants for Billet and Schultes Model .....	150

<b>8.3</b>	<b>Detailed Drawings.....</b>	<b>152</b>
<b>8.4</b>	<b>Sensor Specifications .....</b>	<b>158</b>
<b>8.5</b>	<b>VLE Operating Procedure .....</b>	<b>159</b>
8.5.1	Preparation .....	159
8.5.2	Start-up .....	159
8.5.3	Running the Experiment.....	159
8.5.4	Sampling.....	160
8.5.5	Shutting Down .....	160
8.5.6	Safety Aspects .....	160
<b>8.6</b>	<b>Total Reflux Distillation Column Operating Procedure and Zoning Report.....</b>	<b>160</b>
8.6.1	Control Loops .....	161
8.6.2	Operating Procedure.....	161
8.6.3	Pressure Regulation .....	164
8.6.4	Sources of Release .....	165
8.6.5	Characteristics of Flammable Solvents Used .....	166
8.6.6	Ventilation.....	167
8.6.7	Conclusions .....	170
8.6.8	Proposed Classification: .....	170
8.6.9	Hazard and Operability Study of Pilot Plant .....	173
<b>8.7</b>	<b>Raoult's Law .....</b>	<b>176</b>
8.7.1	Calculations .....	176
<b>8.8</b>	<b>Thermodynamic Model.....</b>	<b>178</b>
8.8.1	NRTL.....	178
8.8.2	Diffusion Coefficients .....	178
8.8.3	Sample Calculations .....	180
<b>8.9</b>	<b>Experimental Error.....</b>	<b>182</b>
<b>8.10</b>	<b>Results .....</b>	<b>186</b>

---

# LIST OF FIGURES

---

Figure 1 – The link between hydrodynamics, mass transfer and interfacial area .....	6
Figure 2 – Schematic diagram of thesis layout .....	11
Figure 3 – Applications for packed columns a) Distillation, b) Absorption and c) Desorption .....	13
Figure 4 – a) Dimensions of corrugated sheet and b) Corrugation angle .....	14
Figure 5 – Efficiency for Montz™ B1-250 and B1-400 structured packing. Cyclohexane/n-heptane test system at 1.01 bar.....	15
Figure 6 – Pressure drop for Montz™ B1-250 and B1-400 structured packing. Cyclohexane/n-heptane test system at 1.01 bar. ....	16
Figure 7 – Efficiency for Montz™ B1-400 and B1-400.60 structured packing. Cyclohexane/n-heptane test system at 1.01 bar. ....	17
Figure 8 – Pressure drop for Montz™ B1-400 and B1-400.60 structured packing. Cyclohexane/n-heptane test system at 1.01 bar.....	17
Figure 9 – Efficiency for Montz™ B1-250 structured packing. Cyclohexane/n-heptane test system at 4.14 bar, 1.01 bar and 0.33 bar.....	18
Figure 10 – Position of the flat sheet inserted between the corrugated sheets.....	19
Figure 11 – High capacity packings of different vendors.....	20
Figure 12 – The effect of liquid distribution on the efficiency of a packed column .....	22
Figure 13 – influence of wall effects on column diameter .....	25
Figure 14 – VLE curve for mixtures used in distillation pilot plants.....	29
Figure 15 – Pressure drop as a function of gas capacity factor. ....	37
Figure 16 – Liquid hold-up as a function of gas capacity factor .....	38
Figure 17 – Force balance on the liquid film flowing down the surface for the SRP model.....	46
Figure 18 – Graphical evaluation of three semi-empirical liquid hold-up models .....	61
Figure 19 – Graphical evaluation of three semi-empirical liquid hold-up models .....	62
Figure 20 - Graphical evaluation of three semi-empirical effective interfacial area models .....	63
Figure 21 – Graphical evaluation of three semi-empirical liquid mass transfer coefficients .....	64
Figure 22 - Graphical evaluation of three semi-empirical vapour mass transfer coefficients models. 64	
Figure 23 - Graphical evaluation of three semi-empirical overall height of transfer units .....	65
Figure 24 – PFD of distillation column .....	68
Figure 25 – P&ID of the pilot plant setup .....	75
Figure 26 – Reboiler Photos: a) Steam tubes inside the thermosyphon reboiler, b) baffle plate.....	75
Figure 27 – Condenser Photos: a) Cooling water tubes with baffle plates, b) Condenser during operation.....	76
Figure 28 – Structured packing support pins.....	77
Figure 29 – Base design of the distributors .....	78
Figure 30 – Distributors internals a) Drip tubes and b) Chimney tubes .....	78
Figure 31 – Sampling device that was used .....	80
Figure 32 – Steam tracing a) without heating cement b) with heating cement.....	85
Figure 33 – Control loop for steam tracing.....	86
Figure 34 – Process for selecting a test mixture .....	89
Figure 35 – Vapour-liquid equilibrium cell.....	93
Figure 36 – VLE data from Zong et al. (1983) and VLE cell for the 2-butanol/iso-butanol test system 96	
Figure 37 –VLE data from Kutsarov et al. (1993) and VLE cell for p-xylene/o-xylene test system.....	97
Figure 38 – Txy diagram for data obtained from Zong et al. (1983) and the VLE cell, for 2-butanol/iso-butanol test system .....	97
Figure 39 - Txy diagram for data obtained from Kutsarov et al. (1993) and the VLE cell, for p-xylene/o-xylene test system .....	98

Figure 40 – Data for 2-butanol/iso-butanol from Zong et al. (1983) and the VLE data using the NRTL model .....	100
Figure 41 – Data for p-xylene/o-xylene from Kutsarov et al. (1993) and the VLE data using the NRTL model .....	100
Figure 42 – Relative volatility for 2-butanol/iso-butanol versus liquid mole fraction of 2-butanol...	101
Figure 43 – Relative volatility for 2-butanol/iso-butanol versus liquid mole fraction of 2-butanol...	102
Figure 44 – Pressure drop results for 350Y HC packing during commissioning phase. 2-butanol/iso-butanol test system at 1 bar abs, 0.6 bar abs and 0.3 bar abs. ....	103
Figure 45 – Pressure drop results for 350Y HC packing during commissioning phase. p-xylene/o-xylene test system at 1 bar abs, 0.6 bar abs and 0.3 bar abs. ....	103
Figure 46 - Pressure drop results for 350Y HC packing after the nitrogen flushing system was installed. P-xylene/o-xylene test system at 1 bar abs, 0.6 bar abs and 0.3 bar abs. ....	105
Figure 47 - HETP results for 350Y HC packing during commissioning phase. 2-butanol/iso-butanol test system at 1 bar abs, 0.6 bar abs and 0.3 bar abs.....	106
Figure 48 – HETP results for 350Y HC packing during commissioning phase. p-xylene/o-xylene test system at 1 bar abs, 0.6 bar abs and 0.3 bar abs.....	107
Figure 49 – Effect of pressure reducing valve on pressure oscillations.....	108
Figure 50 – Liquid composition from the three distributors versus time.....	110
Figure 51 – HETP versus time.....	110
Figure 52 – Repeatability test for pilot plant setup .....	111
Figure 53 – Repeatability with three different compositions.....	112
Figure 54 – Pressure drop data for Mellapak™ 350Y with 2-butanol/iso-butanol test system at 1 atm .....	113
Figure 55 – HETP data for Mellapak™ 350Y with 2-butanol/iso-butanol test system at 1 atm .....	113
Figure 56 – Number of theoretical stages calculated in Aspen compared to those obtained from the Fenske equation.....	114
Figure 57 – Effect of sub-cooling .....	115
Figure 58 – Temperature profile through the column.....	117
Figure 59 – a) End pieces welded to each drip point. b) Distribution after modifications.....	118
Figure 60 - Efficiencies results before and after modification to liquid distributor .....	118
Figure 61 – Efficiency results compared to published data.....	120
Figure 62 – Pressure drop results compared to published data.....	121
Figure 63 – Comparison between the experimental HETP values and that obtained from predictive models (Rocha et al., 1993; Billet and Schultes, 1999; Olujić et al., 1999; Olujić et al., 2004) .....	122
Figure 64 – Comparison of the HETP experimental values with the Billet model adjusted .....	124
Figure 65 – Comparison of the experimental pressure drop data with predictive values from the SRP (Rocha et al., 1996) and Delft (Olujić et al., 2004) models .....	124
Figure 66 - Comparison of the experimental pressure drop data with Billet et al. (1993) and Billet et al. (1999) .....	125
Figure 67 - Comparison of the experimental pressure drop over distributors with a model proposed by Rix and Olujić (2008) .....	126

---

# LIST OF TABLES

---

Table 1 – Geometric Parameters of J. Montz™ structured packing	15
Table 2 - Properties of test mixtures (for Figure 14)	30
Table 3 – Loading point for the Billet and Schultes model	39
Table 4 – Flooding point for the Billet and Schultes model	40
Table 5 – Liquid hold-up in the pre-loading region for the Billet and Schultes model	41
Table 6 – Dry bed pressure drop for the Billet and Schultes model	43
Table 7 – Wet bed pressure drop (Equations 41 to 44)	44
Table 8 - Liquid hold-up with SRP	47
Table 9 – Pressure drop with SRP	48
Table 10 – Testing conditions for model evaluations	59
Table 11 – SRP model constants	60
Table 12 – Billet model constants proposed by Erasmus (2004)	60
Table 13 – Delft model constants	61
Table 14 – Packing dimensions	81
Table 15 – NRTL constant used in Aspen model	99
Table 16 – Experimental error	109
Table 17 – Composition range of the three different compositions for the bottom packed bed	112
Table 18 – Constants for Billet model available for metal structured packing (Extraction of Table A 5 in Appendix - Section 8.2)	123





---

# Nomenclature

---

## Symbols

Symbol	Description	Units
$a$	Packing surface area	$m^2/m^3$
$A$	Constant for pressure drop	-
$A_c$	Column cross sectional area	$m^2$
$a_e$	Effective interfacial area	$m^2$
$a_h$	Hydraulic area of packing per unit volume of packed bed	$m^2/m^3$
$a_{\text{packing}}$	Total effective packing surface area	$m^2/m^3$
$a_{\text{wall}}$	Wetted wall surface area	$m^2/m^3$
$A_o$	Free column cross sectional area	$m^2$
$b$	Corrugation base length	$m$
$B$	Constant for pressure drop	-
$C_E$	Correction factor for surface renewal	-
$C_{FI}$	Constant for specific packing at flooding point	-
$C_h$	Constant for specific packing for hydraulic area	-
$C_L$	Constant for specific packing for mass transfer in vapour phase	-
$C_{lp}$	Constant for specific packing at loading point	-
$C_p$	Constant for specific packing for pressure drop	-
$C_V$	Constant for specific packing for mass transfer in vapour phase	-
$d_h$	Hydraulic diameter	$m$
$d_{hV}$	Hydraulic diameter for the gas phase	$m$
$D_L$	Liquid phase diffusion coefficient	$m^2/s$
$d_p$	Particle diameter	$m$
$d_s$	Column diameter	$m$
$D_V$	Vapour phase diffusion coefficient	$m^2/s$
$F_c$	Vapour capacity factor	$(m/s)(kg/m^3)^{0.5}$

$F_{c,lp}$	Vapour capacity factor at loading point	$(m/s)(kg/m^3)^{0.5}$
$F_{load}$	Loading effect factor	-
$F_{lp}$	Vapour capacity factor at loading point	-
$Fr_L$	Froude number for liquid flow	-
$F_{SE}$	Surface enhancement factor	-
$F_t$	Correction factor for total hold-up due to effective wetted area	-
$f_w$	Wetting factor	-
$g$	Gravitational constant	$m/s^2$
$g_{eff}$	Effective gravity	$m/s^2$
$h$	Corrugation side length	m
HETP	Height equivalent to theoretical plate	m
$h_L$	Liquid hold-up	$m^3/m^3$
$h_{L,Fl}$	Liquid hold-up at flooding	$m^3/m^3$
$h_{L,pl}$	Liquid hold-up in pre-loading region	$m^3/m^3$
$h_{pb}$	Height of the packed bed	m
$h_{pe}$	Height of the packing element	m
HETP	Height equivalent to a theoretical plate	m
HTU <sub>L</sub>	Height mass transfer unit for the liquid phase	m
HTU <sub>O</sub>	Overall height of a mass transfer unit	m
HTU <sub>V</sub>	Height mass transfer unit for the vapour phase	m
$K$	Wall factor	-
$K_1$	Constant for SRP model	-
$k_L$	Mass transfer coefficient in the liquid phase	m/s
$k_V$	Mass transfer coefficient in the vapour phases	m/s
$k_{V,lam}$	Mass transfer coefficient in a laminar vapour phases	m/s
$k_{V,turb}$	Mass transfer coefficient in a turbulent vapour phases	m/s
$L$	Mass flow of liquid	kg/h
$l_{V,pe}$	Length of gas flow channel in packing element	m
$l_\tau$	Length of flow path	m

$Ma_L$	Marangoni number of liquid	-
$n_{cc}$	Number of chevron collectors	-
$n_{ct}$	Number of chimney-trays	-
$n_{FI}$	Exponent at flooding point	-
$n_{ld}$	Number of liquid distributors	-
$n_{lp}$	Exponent at loading point	-
$N_t$	Number of theoretical plates or stages	-
$Re_L$	Reynolds number for liquid flow	-
$Re_V$	Reynolds number for vapour flow	-
$Re_{Ve}$	Reynolds number effective gas phase	-
$Re_{Vrv}$	Reynolds number relative velocity	-
$s$	Corrugation side length	m
$S_{cV}$	Schmidt number for vapour phase	-
$u_L$	Superficial liquid velocity	m/s
$u_{L,e}$	Effective liquid velocity	m/s
$u_{L,FI}$	Superficial liquid velocity at flooding point	m/s
$u_{L,lp}$	Superficial liquid velocity at loading point	m/s
$u_V$	Superficial vapour velocity	m/s
$u_{V,e}$	Effective vapour velocity	m/s
$u_{V,FI}$	Superficial vapour velocity at flooding point	m/s
$u_{V,lp}$	Superficial vapour velocity at loading point	m/s
$V$	Mass flow of vapour	kg/h
$We_L$	Weber number of liquid of liquid	-
$\Delta d_{DC}$	Pressure drop due to directional changes	Pa
$\Delta p_{GG}$	Pressure drop due to gas-gas interactions	Pa
$\Delta p_{GL}$	Pressure drop due to gas-liquid interactions	Pa
$\Delta p_{int}$	Pressure drop over internals	Pa
$\Delta p_{lp}$	Pressure drop in pre-loading region	Pa
$x_{lk}$	Liquid mole fraction of the light key component in the liquid phase	mole/mole

$\Delta P/\Delta z$	Pressure drop	Pa
$(\Delta P/\Delta z)_d$	Dry bed pressure drop	Pa/m
$(\Delta P/\Delta z)_{Fl}$	Pressure drop at flooding	Pa/m
$(\Delta P/\Delta z)_{pl}$	Pressure drop in pre-loading region	Pa/m
$z$	Unit length	m

## Greek

Symbol	Description	Units
$\alpha$	Relative volatility	
$\alpha_L$	Effective liquid flow angle	°
$\gamma$	Contact angle between solid and liquid film	°
$\delta$	Liquid film thickness	m
$\varepsilon$	Packing porosity	-
$\varepsilon_e$	Effective void fraction	-
$\theta$	Corrugation inclination angle	°
$\lambda$	Stripping factor	-
$\mu_w$	Dynamic viscosity of water at 20°C and 1 atm	kg/m.s
$\mu_L$	Dynamic viscosity of liquid phases	kg/m.s
$\mu_V$	Dynamic viscosity of vapour phases	kg/m.s
$\xi_{bulk}$	Direction change factor for bulk zone	-
$\xi_{wall}$	Direction change factor for wall zone	-
$\xi_{GL}$	Gas-liquid friction factor	-

$\xi_{GG}$	Gas-gas friction factor	-
$\nu_L$	Kinematic viscosity of liquid	$m^2/s$
$\rho_L$	Liquid density	$kg/m^3$
$\rho_V$	Vapour density	$kg/m^3$
$\rho_w$	Density of water at 20°C and 1 atm	$kg/m^3$
$\zeta_{cc}$	Chevron collector loss coefficient	-
$\zeta_{ct}$	Chimney-tray loss coefficient	-
$\zeta_{DC}$	Overall coefficient for direction change losses	-
$\zeta_{GG}$	Overall coefficient for gas-gas friction losses	-
$\zeta_{GL}$	Overall coefficient for gas-liquid friction losses	-
$\sigma_L$	Surface tension in liquid phase	$kg/s$
$\zeta_{ld}$	Liquid distributor loss coefficient	-
$\sigma_w$	Surface tension of water at 20°C and 1 atm	$kg/s$
$\tau_L$	Duration of contact for liquid phase	s
$\tau_V$	Duration of contact for gas phase	s
$\varphi$	Fraction of the triangular flow channel occupied by liquid	-
$\phi$	Relative free area	$m^2/m^2$
$\psi$	Fraction of gas flow channels ending at the column wall	-
$\psi'_L$	Resistance coefficient for wetted bed pressure drop	-
$\psi_{FI}$	Resistance coefficient at flooding point	-

$\psi_L$	Resistance coefficient for wetted bed pressure drop	-
$\psi_{ip}$	Resistance coefficient at loading point	-
$\psi_o$	Resistance coefficient for dry bed pressure drop	-
$\psi_{L,pl}$	Resistance coefficient of liquid in pre-loading region	-
$\Omega$	Fraction of packing surface area occupied by holes	-

## Abbreviations

CFD	Computational fluid dynamics
HAZOP	Hazard and operability study
HETP	Height equivalent to a theoretical plate
MSDS	Material safety data sheet
P&ID	Piping and instrumentation diagram
PFD	Process flow diagram
PID	Proportional–integral–derivative
PLC	Programmable logic computer
PPE	Personnel protective equipment
PTFE	Polytetrafluoroethylene
SANS	South African National Standard
SS	Stainless Steel
TSR	Thermosyphon reboiler
VLE	Vapour-liquid equilibrium

## Glossary

### Liquid hold-up

Amount of liquid present in packed bed.

### Premature flooding

Partial flooding of a packing element. It normally occurs at the transition point between two packing elements, due to abrupt flow changes.

**Vapour flow factor**

The superficial vapour velocity that is corrected for by the density of the vapour phase.

**Distillation**

A method for separation of feed components based on differences in their boiling temperatures at a fixed pressure. Distillation is a physical process and not a chemical reaction.

**HETP value**

Describes the efficiency of packing material based on the mass transfer height that provides one theoretical stage of separation.

**Packed bed**

Confined volume of elements that is designed to improve the contact between the liquid and vapour phases.

**Pressure drop**

Decrease in pressure due to resistance to flow through a device.

**Turndown ratio**

Ratio of maximum hydraulic flow to minimum flow at a constant efficiency.

**Loading point**

The transition point between the pre-loading and loading regions. It is the point where the liquid hold-up as well as the velocity of the liquid film in constant with the vapour phase becomes a function of the vapour flow rate.

**Flooding point**

The transition point between the loading and flooding regions. If the shear stress of the gas counter flow is sufficient to entrain the entire liquid to the top of the column. It is normally associated with a sharp increase in the liquid hold-up and HETP.





---

# 1 Introduction

---

## 1.1 History

Distillation is an age old process that was perfected and changed over the years to serve the need of a given liquid separation process. The Encyclopaedia of Zosimus describes the work of two female alchemists who lived at the beginning of the Christian era, named Cleopatra (a Greek who should not be confused with the temptress of Caesar's time) and Mary the Jewess. Cleopatra wrote a piece entitled, "Chrysopoea", which dealt with gold making, wherein she describes one of the earliest versions of a distillation apparatus. The device consisted of a heating source that heated a cylindrical vessel. Connected to the vessel was a vertical tube leading into an alchemical still, with two condensers. However, the processes that these alchemists employed did not differentiate sharply between sublimation and genuine distillation. Under the reign of Emperor Diocletian most of the Greek records were destroyed, with only a single page of the alchemists' manuscript having survived (Liebmann, 1956).

The word "distillare" or "destillare", means "to drop" or "drip off", and was first used by a member of the Byzantine group that expanded on Aristotle's experimental work on the systematic distillation of seawater. Alexander, a member of the "Peripatetics" who lectured in Athens in approximately 200 A.D. recorded that (free translation): "They boil the sea water and suspend large sponges from the mouth of a brass vessel to absorb what is evaporated, and after drawing the liquid from the sponges they find it to be sweet water" (Liebmann, 1956).

Alcohol was probably the first product of scientific distillation from experiments conducted in the eleventh or twelfth century (Liebmann, 1956). However, the first vertical distillation column was designed in France by Jean Baptiste Cellier-Blumenthal in 1813 (Underwood, 1935). The first packing was used in 1820 by a technologist named Clement, who used 1 inch diameter glass balls in a vertical still to produce alcohol (Kister, 1992). Another reference to a packed column is the early patent of Phillips (European Patent number/year: 110965/1847) that describes a still for alcohol and mentions the use of a column filled with coke or pumice stone instead of using perforated plates (Underwood, 1935).

But it was only at the beginning of the twentieth century that the application of distillation columns spread rapidly from enhancing the alcohol content of beverages to the primary separation technique used to separate crude oil into various products (Kister, 1992). At this time the products of crude oil were mainly used in steam boilers to power ships for the marine industry. However, in 1910, the first oil-fired diesel engines were introduced as an alternative. As society became increasingly industrialised, the use of distillate fuel used in trucks, automobiles and aircrafts increased (Totten *et al.*, 2003). This opened a new area for distillation columns where new internals were developed with improved performance, leading to vast energy and capital savings. Section 1.2 will discuss the development of column internals.

## **1.2 Column Internals**

Column internals provide the contact area for mass transfer and can be divided into two categories, namely trays and packing. Both these categories of column internals are still extensively used in separation columns with each of them having its place in the market. The most popular designs under each category will be discussed briefly.

### **1.2.1 Trays**

For tray distillation columns the contact area is created by a vapour phase that bubbles through a liquid phase. Popular designs for these tray columns can be divided into three main design categories, namely:

- *Bubble cap trays*
- *Sieve trays*
- *Valve tray*

#### ***i. Bubble cap trays***

Bubble cap trays were used as the primary tray type before the 1960s and are seldom used in modern towers (Kister, 1992). The bubble cap tray consists of a perforated tray that is fitted with a gas riser over each hole. A cap is mounted onto each gas riser in such a way that it allows gas to pass through the gas riser and then redirects the gas downwards and discharges through the slot in the cap. Finally, the gas bubbles through the liquid (hence the name 'bubble cap') and flows to the next tray. The main disadvantage of bubble caps is that

they have a higher pressure drop and manufacturing cost compared to that of sieve and valve trays, but they have the advantage of having excellent turndown ratios.

### ***ii. Sieve trays***

Sieve trays are perforated plates that allow gas flow through the holes, thus creating a multi-orifice effect (Kister, 1992). The gas flow rate keeps the liquid from flowing through the holes. At low gas flow rates some of the liquid will flow through the holes (weeping) and therefore bypass some of the trays, and thus reduce the efficiency of the plate. The number, size, and arrangement of the holes are thus important design parameters. The advantage of the sieve tray is its low manufacturing cost, but it has the disadvantage of a low turndown ratio.

### ***iii. Valve trays***

The difference between sieve trays and valve trays is that valve trays are equipped with movable disks. The valves are moved by the gas flow, and rise as the gas flow increases. In the case of no gas flow the valves will close on the holes and thus prevent the weeping of liquid through the holes. The movement of the valve determines its turndown ratio and is limited by the design of the valve. Valve trays have a slightly higher manufacturing cost (approximately 20%) but have a higher turndown ratio than that of sieve trays and are therefore frequently the preferred choice.

Trays still have a large market share in the field of separation technology and new trays are still being developed to increase the efficiency and capacity of a distillation column. However, packing has also started to obtain a considerable market share, although its use is restricted by its comparatively high manufacturing cost (Kister, 1992).

## **1.2.2 Packing**

Packings are often the preferred choice of column internals when a column is designed or revamped. This is due to its low pressure drop and higher capacity compared to that of trays. The capital cost of packed columns is more than that of a tray column and is therefore often restricted to demanding separation (i.e. heat-sensitive distillation and strong vacuum distillation).

In packed columns the liquid wets the surface of the packing and flows down the packing under gravity. Mass transfer occurs where the liquid film is in contact with the counter-current vapour stream. The vapour is thus the continuous phase and the liquid the dispersed phase. Packed column internals can be classified as either random or structured packings.

***i. Random packing***

Random packing is distinct pieces of packing that are dumped or randomly placed inside a column shell (Kister, 1992) and are especially used in high pressure distillation and gas processing applications (Nieuwoudt, 2010). Many different designs, sizes, and construction materials of random packing have led to the improvement and optimisation of distillation columns. Random packing has the advantage that it can operate at a higher liquid load and it is easier to install, remove, and clean than structured packing.

***ii. Structured packing***

Structured packing consists of wire mesh or corrugated sheets that are arranged in an orderly manner to form packing elements and was first used in the 1950s. Its use and applications have since increased tremendously due to the favourable pressure drop and superior efficiency characteristics compared to tray and random packing (Strigle, 1994). Unfortunately, structured packing is also more expensive and labour intensive than trays and random packing, and its use is therefore often restricted to demanding separations that involve a large number of theoretical stages or those requiring high vacuum conditions (Billet, 1995). Consequently, new configurations of structured packing are continuously being developed to improve the efficiency and expand the use of structured packing. A more detailed discussion on structured packing will be given in Chapter 2.

## **1.3 Motivation Behind this Research**

Distillation is by far the most used separation process in the chemical industry. To date, most commercial distillation columns are still being designed based on experimental data from a pilot plant because predictive models fail to accurately predict the hydrodynamic and mass transfer behaviour inside a distillation column (Schultes, 2010). Mean deviation for interpolation of state-of-the-art models range from 10 % for liquid hold-up to 80 % for chemisorptions, and with extrapolation the mean deviation varies between 30% to > 100%

(Schultes, 2010). For this reason, distillation columns are usually over designed and/or are operated conservatively (not at full capacity). The predictive models are, however, useful for the conceptual design of a distillation column and are often even used in the final design stages when there are no experimental data available. A conceptual design is normally generated using simulation programs such as Aspen Plus™, which provide valuable information on the hydrodynamic and number of stages required for separation. Aspen Plus™ gives the user two options when simulating a distillation column, i.e. equilibrium based or rate-based (non-equilibrium) models. With the equilibrium based model it is assumed that the vapour and liquid phases are in thermodynamic equilibrium at each stage, while the rate-based model assumes that the vapour-liquid equilibrium only occurs at the interface. With the rate-based model the column diameter needs to be specified in Aspen Plus™ and the user has an option between two semi-empirical models to predict the column behaviour, namely the Billet and Schultes model (Billet and Schultes, 1993) or the SRP model (Bravo *et al.*, 1992). With the equilibrium model, the diameter of the column is calculated after the flow rates and composition profiles inside the column are determined.

The aim of the semi-empirical models is to accurately predict the capacity and efficiency inside a distillation column. The three different areas that determine the capacity and efficiency of packed columns are the hydrodynamics, mass transfer and interfacial area. These areas overlap as illustrated in Figure 1. Capacity and efficiency are based on the performance of the three key areas, as well as the thermodynamics of the systems (see Figure 1). Each of these key areas will briefly be discussed, with a more detailed discussion in Chapter 2.

### **1.3.1 Hydrodynamics**

Hydrodynamics normally form the base of a predictive model as it predicts the liquid hold-up and pressure drop of the column. The liquid hold-up is the ratio of liquid volume to that of the whole packed volume, and is normally made up of two components: static and dynamic hold-up. The static hold-up is liquid that remains in the packed bed, due to capillary forces, after the liquid flow is stopped. The capillary forces are determined by the structure of the packings and wettability of the packing, as well as by the physical properties of liquid such as surface tension, viscosity and density (Kolev, 2006). The static hold-up usually makes up a small amount of the total liquid hold-up (Kolev, 2006). The dynamic hold-up is the

difference between total hold-up and static hold-up, and is influenced by the liquid and vapour flow rates.

The amount of liquid hold-up inside a distillation column changes the void fraction that is available for gas flow and therefore influences the pressure drop inside a distillation column (Billet and Schultes, 1991). The pressure drop inside a distillation column is of great interest, especially in low vacuum and gas absorption operations, as it also determines the capacity and, therefore, the diameter of the column. The pressure drop and liquid hold-up are a function of the geometric properties of the packing, properties of the fluid, and the gas and liquid velocities. A more detailed discussion of the relationship between gas and liquid velocities on pressure drop and liquid hold-up can be found in section 2.10.

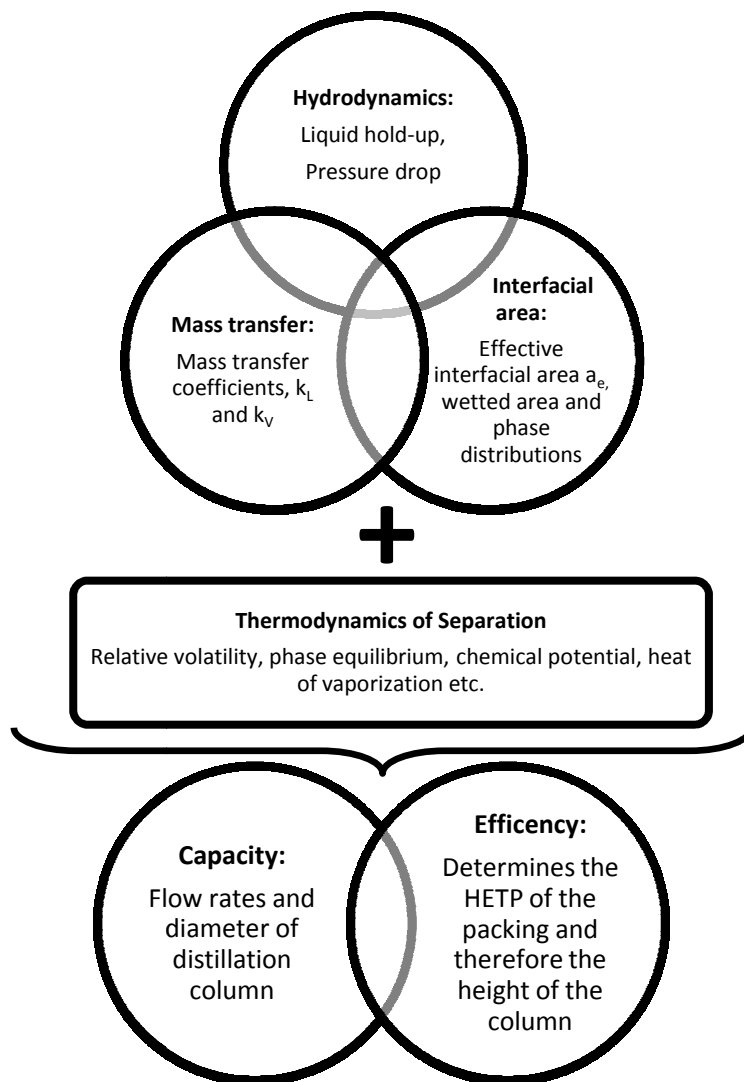


**Figure 1 – The link between hydrodynamics, mass transfer and interfacial area**

### **1.3.2 Mass Transfer**

The concentration difference of a species between the liquid and gas phases relative to its equilibrium concentration serves as the driving force for mass transfer inside a distillation column, and the rate of mass transfer is dependent on both the resistance to mass transfer and the concentration gradient. The overall vapour and liquid mass transfer coefficients,  $k_v$  and  $k_L$ , are diffusion rate constants that relate the mass transfer rate, mass transfer area, and concentration difference, thus giving an indication of the resistance to mass transfer in both liquid and vapour phases (Kolev, 2006). However, the extent of the separation is limited by the thermodynamic equilibrium (Seader and Henley, 2006).

The penetration theory proposed by Higbie and counter-current evaporation in a wetted-wall column is normally used to calculate the vapour and/or liquid mass transfer coefficients (Erasmus, 2004). Efficiency or performance of the mass transfer is usually expressed in terms of height equivalent to a theoretical plate (HETP). The factors that influence the HETP are the type and size of packing, the operating conditions, and the physical properties of the test system (Wang *et al.*, 2005). Thus, the mass transfer performance determines the height of the distillation column.

### **1.3.3 Interfacial Area**

Interfacial area is described in terms of wetted and effective area available for mass transfer. The wetted interfacial area is the actual area of the packing that is wetted by the fluid, and depends on the geometry of the packing and the liquid distributor used. Effective interfacial area is the part of the wetted area that actively contributes to the mass transfer inside a distillation column. Saturated zones inside the packing are created in the packing if there is a lack of constant interfacial surface renewal of the bulk liquid. Effective interfacial area can also include the surfaces of drops, jets and sprays, and can thus have a larger value than the specific surface area of the structured packing (Wang *et al.*, 2006). The effective interfacial area is usually combined with the mass transfer coefficient to form a volumetric mass transfer coefficient that is used to determine the HETP of a distillation column.

### **1.3.4 Models**

Accurate knowledge of the performance characteristics of structured packing is a fundamental requirement for the optimum design of absorption, desorption, and



rectification columns with regard to fluid dynamics and mass transfer. Experimental measurements have led to new concepts and fresh ideas in the field of separation technology and have allowed new mathematical models to be developed that predict the performance characteristics (Billet, 1995). An improved knowledge of the performance of structured packing will lead to improved mass transfer and efficiency models, which will reduce overdesign and energy wastage in distillation processes.

Most models found in literature are semi-empirical, and are therefore based on the experimental data of structured packing. Thus, they normally contain a number of experimentally determined constants that depend on the type of system and packing used. It is risky to use a predictive model outside its range of validation (Engel *et al.*, 2001). Most data found in literature are for Mellapak™ 250Y. Very little work has been reported in the open literature on packings with other specific surface areas. Therefore, predictive models can be expected to deviate from experimentally determined values for larger and smaller specific packing area packings.

The ideal model would be a model that accurately predicts all three key areas as well as the relationship between them. This model would then allow an engineer to design a distillation column without the need to first obtain experimental data in a pilot plant, therefore saving time and money. It would also allow existing distillation columns to be optimised and operated at full capacity.

### **1.3.5 Thermodynamics of Separation**

Thermodynamic equations and properties play a key role in distillation operations as they describe and determine the phase equilibrium and energy balance, therefore influencing the sizing of the equipment. The thermodynamic properties include fugacity, entropy, enthalpy, and density, which are all functions of phase composition, temperature and pressure. It is therefore essential that the thermodynamic models accurately predict the thermodynamic behaviour of the test system, since the thermodynamic properties are used in predictive models. As mentioned, the thermodynamic equilibrium also limits the extent of the separation (Seader and Henley, 2006).

## 1.4 Objectives and Scope

The aim of this study is to establish a facility to investigate the performance of structured packing with high specific surface area under total reflux. The objectives of this study are described as follows:

- i. Conduct a literature survey to gain insight into the behaviour of structured packing, and to evaluate some of the well-known predictive models.*
- ii. Design and construct a pilot plant setup in which data for high specific surface area - for example 350 and 500 m<sup>2</sup>/m<sup>3</sup> - structured packings can be generated.*
- iii. Select a test mixture that is suitable for the pilot plant.*
- iv. Commission the pilot plant setup and obtain the necessary safety documentation.*
- v. Conduct experimental runs with the pilot plant under total reflux.*
- vi. Validate and compare the experimental data with well-known predictive models.*
- vii. Draw conclusions and make recommendations from the experimental results and model predictions.*

Currently only a few data points are available in the open literature for Mellapak™ 350Y structured packing, manufactured by Sulzer™, and no data are published for Flexipack 350YHC, manufactured by Koch-Glitsch™. It would therefore be of great value to generate data for these two packings, as well as to develop a model that can be used to accurately predict the performance of structured packings with a higher surface area. In addition, it would be of value to compare the performance of the two different vendors.

The focus of this study is to construct a pilot plant setup that can be used to generate reliable efficiency data for high surface area structured packing under total reflux. The size of the boiler available in the Department of Process Engineering at the University of Stellenbosch limited the internal diameter of the column to 0.2 m. Thus the study is not focused on the development of a new model, or to generate a vast quantity of data, but rather on the construction and validation of the pilot plant setup. However, the former may be seen as a valuable endeavour for further study.

The study forms part of a larger endeavour that is aimed at the development of a theoretically based model that can predict the efficiency of structured packing. The theoretical model will be based on fundamental understanding and observation gained from work done on the mass transfer coefficients, effective interfacial area, and hydrodynamics of structured packing. The results from the constructed column could thus be used to validate the developed model.

A schematic representation of the layout of the thesis is given in Figure 2. The figure represents the structure of the thesis by giving the main sub-headings under each chapter.

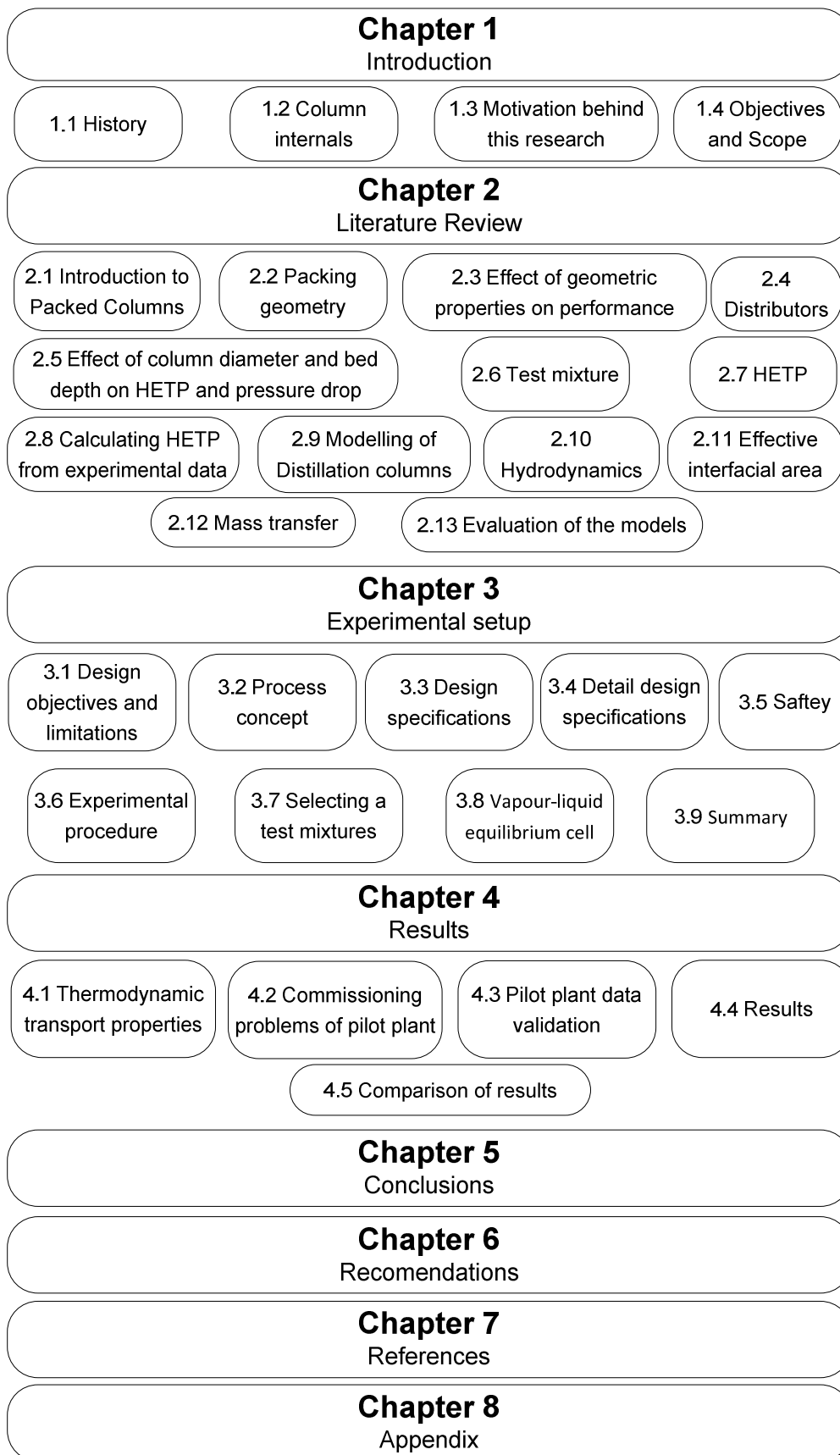


**Figure 2 – Schematic diagram of thesis layout**



---

## 2 Literature Review

---

### 2.1 Introduction to Packed Columns

Packed columns are mainly used in distillation, absorption, and desorption processes to separate vapour-liquid or gas-liquid systems, and can either be filled with random or structured packing (Billet, 1995). Structured packing is often the preferred choice of packing material due to its superior capacity and efficiency compared to random packing. However, structured packing is more expensive than random packing, and its use is often limited to demanding separation processes. Graphical illustrations of distillation, absorption, and desorption are given in Figure 3 and a short description of each process is given thereafter. In this study gas will refer to a component that is still a gas phase at room temperature, whereas a vapour phase is in its natural state a solid or a liquid at room temperature.

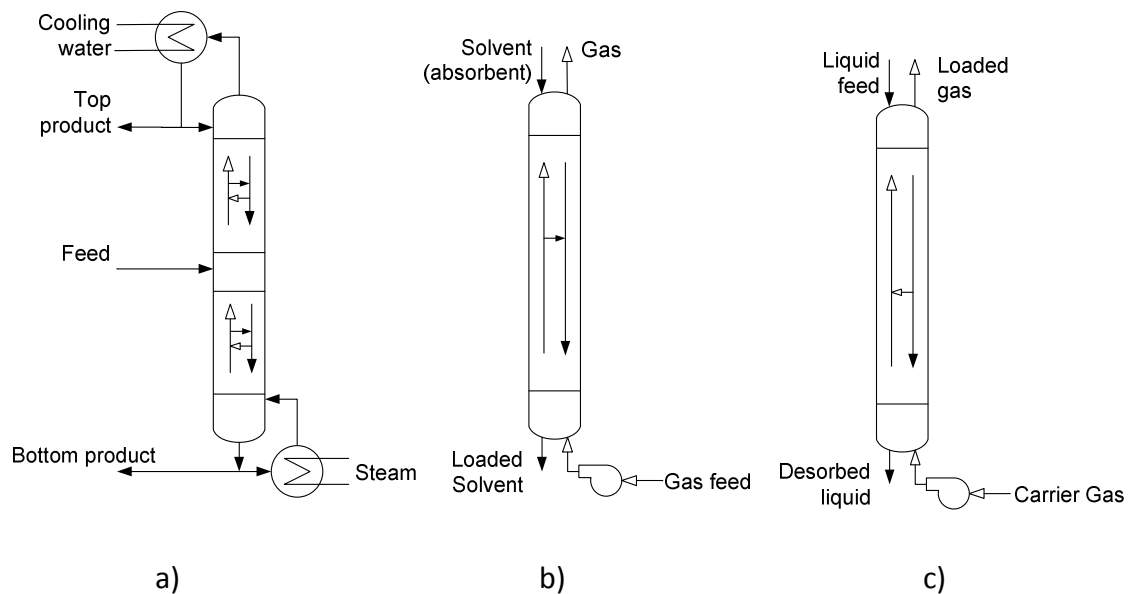


**Figure 3 – Applications for packed columns a) Distillation, b) Absorption and c) Desorption**  
**Source – Redrawn from Billet (1995)**

The physical **absorption** process refers to the transport phenomena of a solute from the gas phase to the liquid phase (Stigle, 1994), whereas **desorption** (or stripping) refers to the mass transfer process that involves the transfer of a solute from the liquid phase to the gas phase (Stigle, 1994). In **absorption** and **desorption** processes a gas stream enters the bottom of the column and comes in contact with a liquid phase that flows down the column. A blower

is normally used to move the gas through the column and it is also used to control the flow rate of the gas.

**Distillation** is a method of separating mixtures based on the difference in relative volatilities. In a distillation process the vapour formed by the reboiler flows up the column and comes in contact with the liquid that is condensed in the condenser. The two phases thus flows counter-currently, and as a result the higher boiling component accumulates in the bottom of the column and flows out of the column as bottom product. The lower boiling point component accumulates in the condenser and leaves the column in the top product (distillate).

Distillation is also more energy intensive than absorption and desorption columns due to the vast amount of energy required to vaporise the liquid mixture in the reboiler. Therefore substantial energy saving can be achieved by increasing the efficiency of distillation column internals (Billet, 1995). Selecting the correct column internals are therefore crucial when designing or refitting the column with new internals. The rest of the literature review will focus on the classification, performance, efficiency, and modelling of structured packing inside a distillation column.

## 2.2 Packing Geometry

Structured packing geometry is normally described in terms of the specific surface area ( $a$ ), the corrugation height ( $h$ ), the corrugation angle ( $\theta$ ), the corrugation side length ( $s$ ), the corrugation base length ( $b$ ) and the height of the packing element ( $h_{pe}$ ). These dimensions are illustrated in Figure 4, where the corrugation angle refers to the inclination angle of the flow paths in the packing. The liquid film thickness ( $\delta$ ) on the packing is also illustrated in Figure 4. The influence of the geometric properties on the performance of structured packing will be discussed in section 2.3.

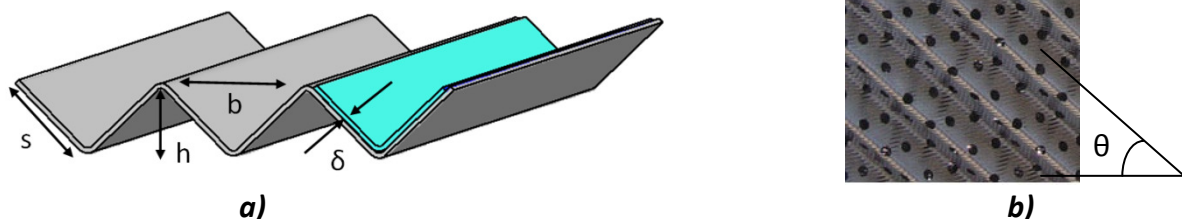


**Figure 4 – a) Dimensions of corrugated sheet and b) Corrugation angle**  
**Source – a) Olujć et al. (1999), b) Koch-Glitsch™ Flexipak-HC™ (Reprinted with permission of Koch-Glitsch™)**

## 2.3 Effect of Geometric Properties

### 2.3.1 Surface Area and Corrugation Angle

There is always a trade-off between capacity and mass transfer efficiency (HETP) in a distillation column. Capacity is defined as the maximum vapour flow rate allowed in a packed column, hence defined by the flooding point. Flooding point is discussed in detail in Section 2.10. Increasing the surface area of structured packing generally decreases the HETP and capacity (Billingham and Lockett, 1999). This is illustrated in Figure 5 and Figure 6. The vapour capacity factor is plotted against HETP in Figure 5 and against the pressure drop in Figure 6. The main corrugation-related dimensions of the packings are presented in Table 1. The vapour capacity factor ( $F_c$ ) is defined as the superficial vapour velocity ( $u_v$ ) times the square root of the vapour density ( $\rho_v$ ).

**Table 1 – Geometric Parameters of J. Montz™ structured packing**

Packing	$a$ (m <sup>2</sup> /m <sup>3</sup> )	$\theta$ (°)	$\epsilon$	$h_{pe}$	$h$ (m)	$b$ (m)	Data obtained from
B1-250	244	45	0.98	0.197	0.012	0.0224	Olujić <i>et al.</i> (2000)
B1-400	394	45	0.96	0.197	0.0074	0.0140	Olujić <i>et al.</i> (2000)
B1-400.60	390	60	0.96	0.215	0.0074	0.0143	Olujić <i>et al.</i> (2000)

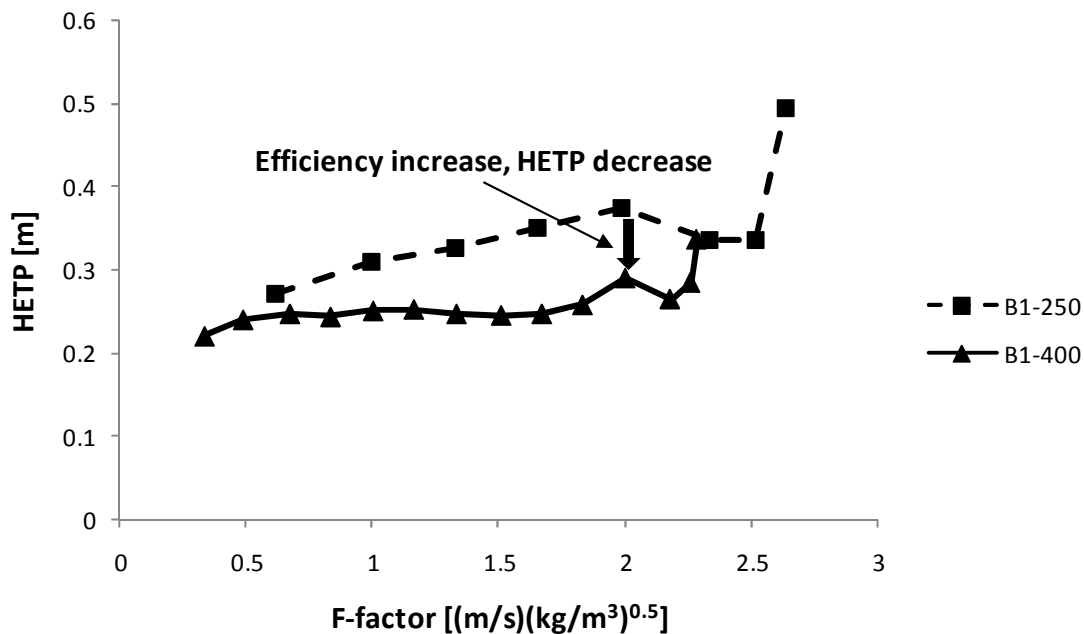


**Figure 5 – Efficiency for Montz™ B1-250 and B1-400 structured packing. Cyclohexane/n-heptane test system at 1.01 bar. Source - Olujić *et al.* (2000)**



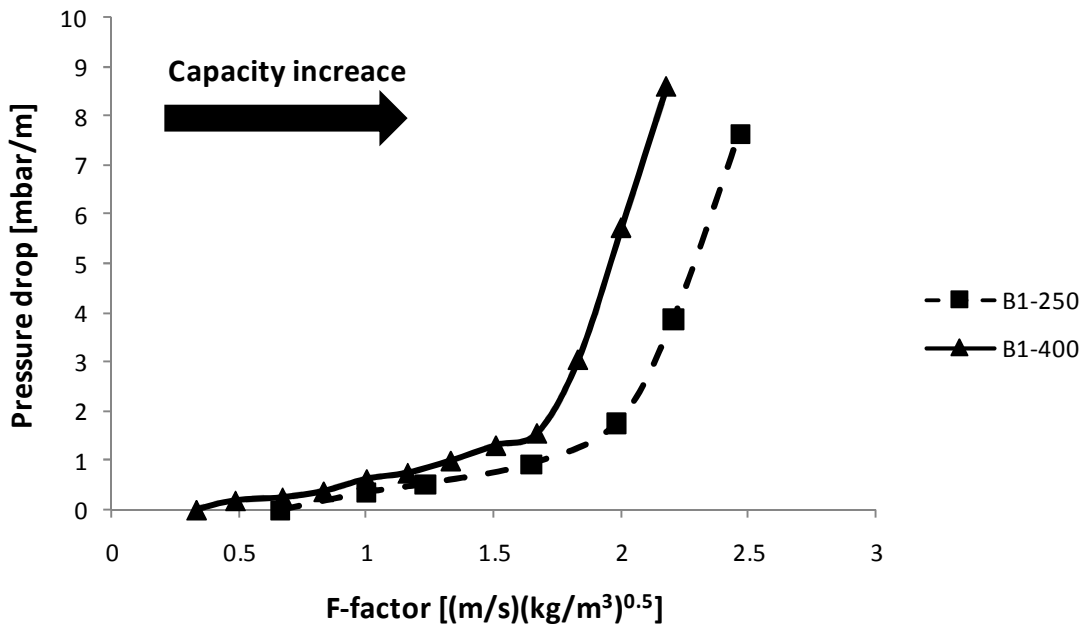


**Figure 6 – Pressure drop for Montz™ B1-250 and B1-400 structured packing. Cyclohexane/n-heptane test system at 1.01 bar. Source - Olujić et al. (2000)**

It is important to note that the HETP of the B1-250Y packing increases up to a point where after it decreases until flooding is reached and then increases rapidly thereafter (see Figure 5). However, the HETP of B1-400Y packings is only slightly influenced by the increased flow rates, but starts to decrease to some extent up until the flooding point is reached after which it increases (Olujić *et al.*, 2000). The efficiency hump present with the B1-400 packing usually occurs at high operating pressures (Fritz *et al.*, 1999). The decrease in capacity with the increase in surface area is mainly due to the reduction in open flow area for the gas phase. From Figure 6 it can be seen that the B1-250 can operate at a higher vapour flow factor than the B1-400 packing and therefore has a higher capacity but lower efficiency.

The influence of the corrugation angle and surface structure of the packing was investigated, where it was found that the capacity of the column increased with an increase in the corrugation angle, but at the expense of efficiency (Olujić *et al.*, 2000). These effects are illustrated in Figure 7 and Figure 8. Olujić *et al.* (2000) also investigated the effect of perforated and non-perforated corrugation sheets, finding that the perforated corrugated sheet yields a higher capacity before flooding occurs.

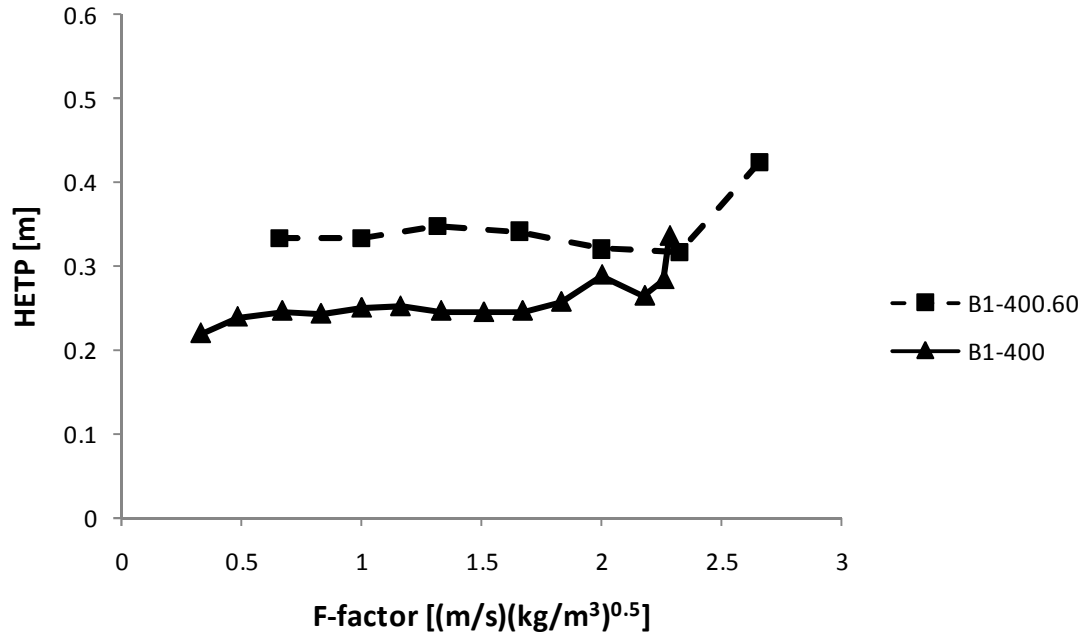


**Figure 7 – Efficiency for Montz™ B1-400 and B1-400.60 structured packing.  
Cyclohexane/n-heptane test system at 1.01 bar.  
Source – Olujić et al. (2000)**

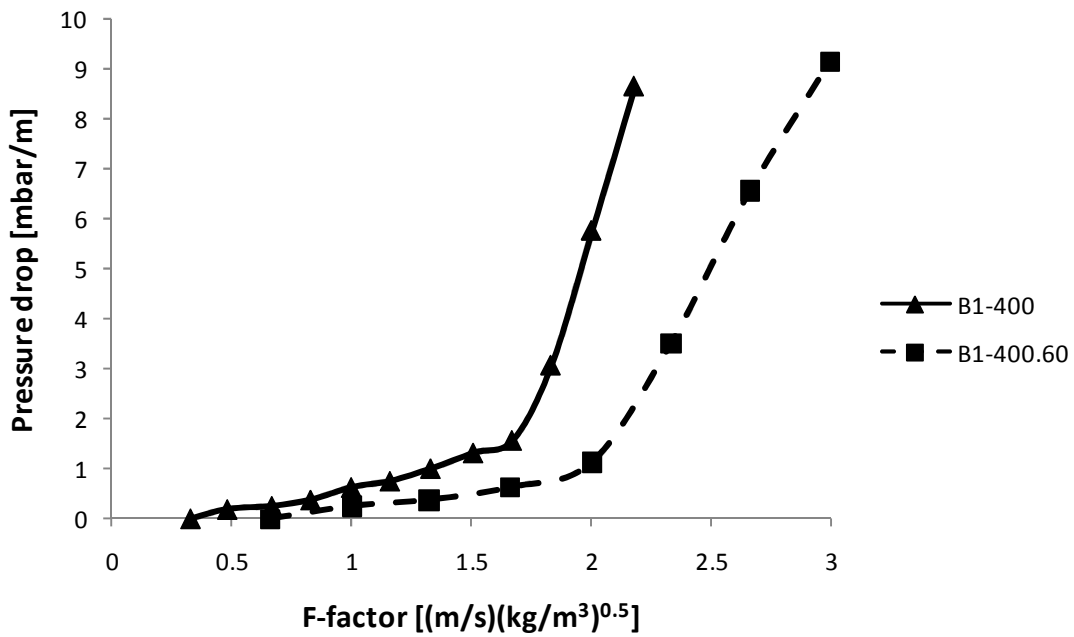


**Figure 8 – Pressure drop for Montz™ B1-400 and B1-400.60 structured packing.  
Cyclohexane/n-heptane test system at 1.01 bar.  
Source - Olujić et al. (2000)**

The efficiency and capacity of structured packing are also influenced by the operating pressure of the column. As illustrated in Figure 9, the efficiency increases with a higher operating pressure, but at the expense of a decrease in capacity. The liquid is entrained in the packed bed by the shear forces between the gas and liquid phase and by the increase of liquid flow by a factor of  $\sqrt{\rho_1/\rho_0}$ . Thus, the decrease in capacity is a result of gas having a higher density and liquid having a higher flow rate at elevated operating pressure which leads to greater shear forces exerted by the gas phase on the liquid phase.

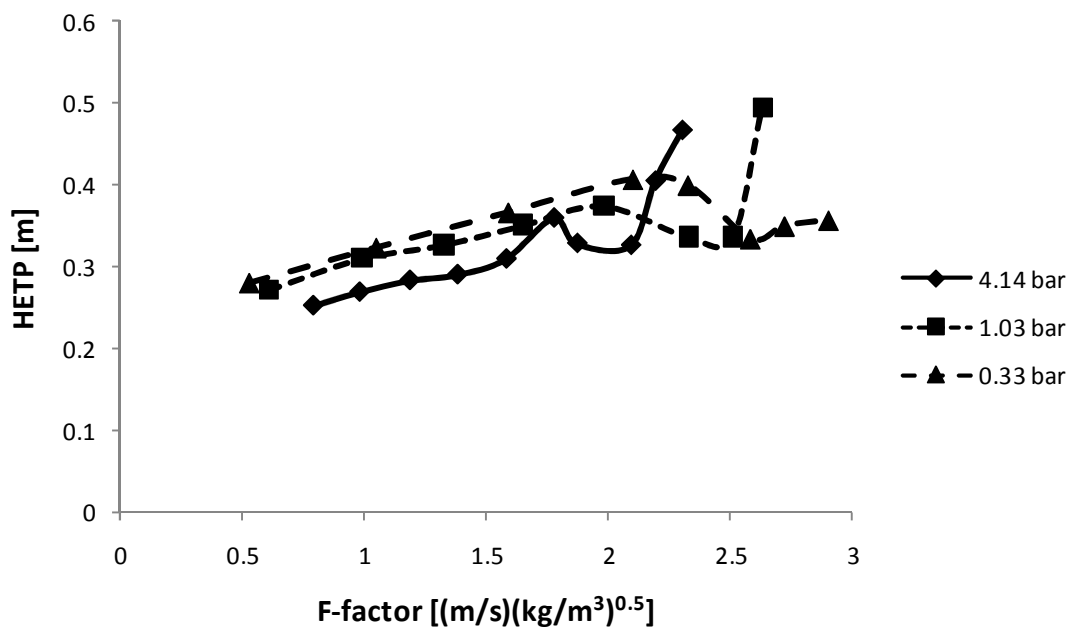


**Figure 9 – Efficiency for Montz™ B1-250 structured packing. Cyclohexane/n-heptane test system at 4.14 bar, 1.01 bar and 0.33 bar**  
**Source - Olujić et al. (1999)**

Olujić *et al.* (2001) also increased the capacity of Montz™ B1-250 structured packing by inserting a flat sheet in between the corrugated sheets. This eliminated the gas-gas interaction, which is the main contributor to pressure drop. However, this led to a large increase in the HETP due to liquid maldistribution. The flat sheet inserted between the corrugated plates is illustrated in Figure 10.

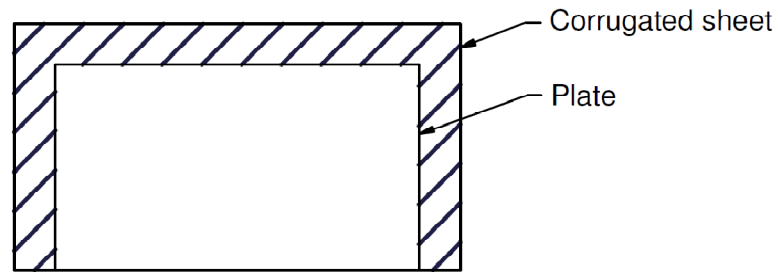


**Figure 10 – Position of the flat sheet inserted between the corrugated sheets**  
**Source – Redrawn from Olujić et al. (2001)**

Luo *et al.* (2008) investigated the effect of the channel opening angle on the hydrodynamic and mass transfer performance of Mellapak™ structured packing. The investigation included both numerical (using computational fluid dynamics (CFD)) and experimental analyses. From their results it was found that decreasing the channel opening angle from 90° to 20° led to a 35% pressure drop decrease and a 13% increase in the mass transfer efficiency.

### 2.3.2 Installation

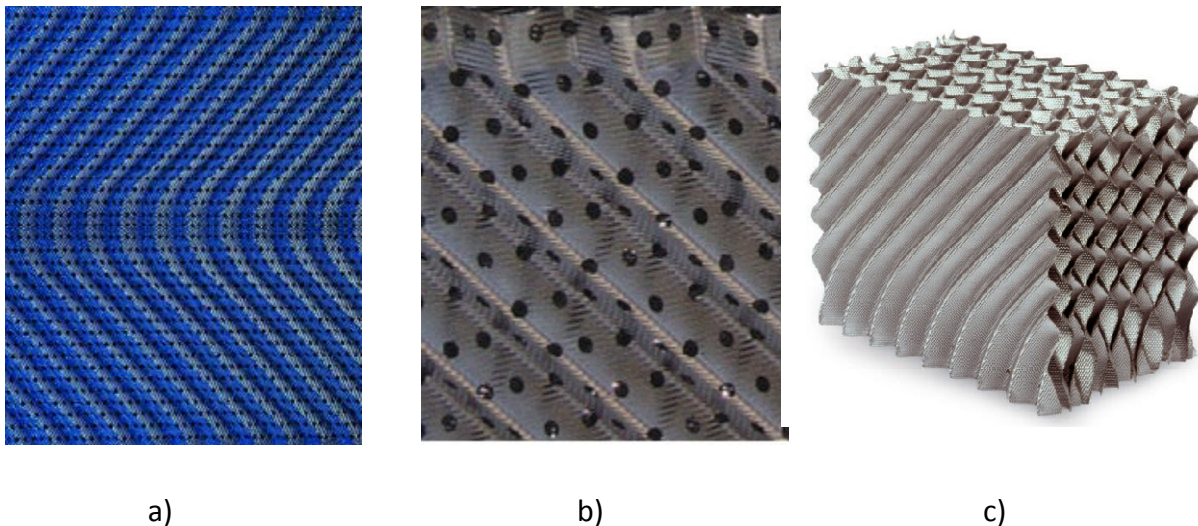
During installation of structured packing, the packing elements are rotated 90° with respect to one another. This promotes a uniform spreading of the vapour and liquid flows in all radial planes throughout the packed bed. In addition, each structured packing segment is equipped with wall wipers, to direct the liquid flow at the column wall back into the packed bed (Strigle, 1994).

It was observed that liquid starts to accumulate at the transition area between two packing segments (partial flooding), which happens as a result of the abrupt obstruction to gas and liquid flows (Suess and Spiegel, 1992). This partial flooding at the bottom of the packing element is defined as premature flooding of the packed column (Parkinson and Ondrey, 1999). The observation of premature flooding led to the development of new high-capacity packings.

### 2.3.3 High capacity Packings

More effective packing has been developed, but at higher manufacturing costs. The trade-off between packing performance and capital cost then started playing a role, with the more effective packing usually only justified in more demanding processes and debottlenecking of columns (Billingham and Lockett, 1999). There is therefore a need for a packing that has a higher capacity, lower manufacturing cost, and does not result in loss of efficiency.

Billingham and Lockett (1999) were the first to design a packing that has the same mass transfer efficiency, but with higher capacity compared to conventional packings, entitled high-capacity packing. Their design was based on the observation by Sues and Spiegel (1992) that flooding started to occur at the bottom of a packing element. To eliminate this premature flooding they equipped the packing with a sharper bend at the bottom of each packing element. The patent for the packing was granted in 1997 to Billingham and Lockett, and Koch-Glitsch™ was awarded with a licence for all applications other than industrial gas. As a result of the high-capacity packing entering the market, the other main competitors (Sulzer™ and J. Montz™) have designed similar high-capacity packings. Typical high capacity packings are shown in Figure 11.



a)

b)

c)

**Figure 11 – High capacity packings of different vendors**

**a) Sulzer™ Mellapak™-Plus, b) Koch-Glitsch™ Flexipak-HC and c) Montz-pak type M/MN  
(Reprinted with permission of Sulzer™, Koch-Glitsch™ and J. Montz™)**

As seen in Figure 11 a, Sulzer™s' high capacity packing (Mellapak™-Plus) has smooth bends at the transition area between the two packing elements. The smooth bends are present at the top and bottom of the packing element, unlike the Montz™ high-capacity packing (Montz™-Pak M/MN) that only has a smooth bend at the bottom of the packing element (see Figure 11c). The Koch-Glitsch™ packing (Figure 11b) is based on the patent from Billingham and Lockett (1997), and has a more abrupt and shorter change, typically 20 mm, (Luo et al. 2008) to the flow angle at the transition area.

Data for the Montz™ high capacity packing have been published by Olujić *et al.* (2001, 2003, 2006). However, it is not the case for that of Koch-Glitsch and Sulzer™ high-capacity structured packings. Parkinson and Ondrey (1999) have reported that Mellapak-Plus™ as well as Flexipack high-capacity packings showed capacity increases between 20-30% while maintaining the same separation efficiency, compared to traditional Mellapak™ and Flexipack™ packings.

## 2.4 Distributors

### 2.4.1 Performance

Good and effective liquid distribution is an important factor in achieving the best performance of structured packing (Perry *et al.*, 1990). Many studies have been dedicated to evaluating the performance of a distributor. Helling and DesJardin (1994) found that liquid distribution has been the primary cause for poor liquid distribution when pilot plant data are scaled-up. Experimental studies relating to liquid distribution over structured packing have been conducted (Stikkelman *et al.*, 1989; Fitz Jr. *et al.*, 1999; Pavlenko *et al.*, 2006; Alekseenko *et al.*, 2008), as well as the optimisation of distribution (Perry *et al.*, 1990), the effect of bed length, maldistribution and redistribution (Schultes, 2000; Cai *et al.*, 2003), the effect of initial distribution on structured packing (Olujić and de Graauw, 1990; Olujić *et al.*, 2004), and the quantification and evaluation of the liquid distribution (Edwards *et al.*, 1999; Spiegel, 2006).

In addition, Kister (1990) graphically describes the effect of good, poor, and very poor liquid distribution on the performance of structured packing as illustrated in Figure 12. This diagram can be used to make a quick evaluation of the distributor's performance if the efficiency data of the packing are available. It must be kept in mind that the hydrodynamic and mass transfer processes are extremely complex and Figure 12 is based on ideal situations, and therefore can deviate from real situations (Kister, 1992).

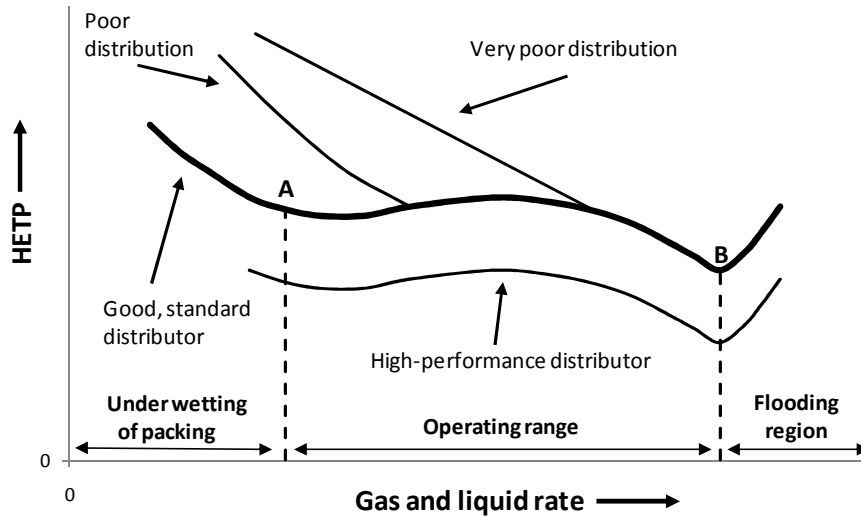


**Figure 12 – The effect of liquid distribution on the efficiency of a packed column**  
**Source – Redrawn from Kister (1992)**

From Figure 12, in region A-B the packing is well wetted with a turbulent liquid film by the distributor, which gives almost constant efficiency of the packing, and thus this region is ideal for distillation column design and operation. Point A represents the distributor's turndown limit and will shift to the right with poor liquid distribution, because more liquid is required to fully wet the packing (Kister, 1992). In the case of very poor liquid distribution, point A might not be observed and the column's efficiency might take the form of a V-shaped curve as seen in Figure 12 (Kister, 1992).

## 2.4.2 Pressure Drop

The pressure drop over distributors and redistributors is normally small compared to the pressure drop of the packed bed and therefore can be neglected in many situations. However, in heat-sensitive distillations, the total allowable pressure drop is normally specified and therefore the pressure drop over the distributors and redistributors cannot be neglected (Rix and Olujić, 2008).

Rix and Olujić (2008) developed a simple pressure drop model from first principles that can be used to predict the pressure drop of liquid distributors and redistributors. The ratio of open area for gas flow ( $A_o$ ) to the column's cross sectional area ( $A_c$ ) is usually a key factor when designing and predicting the pressure drop for liquid distributors and redistributors, and normally ranges between 40% and 70%. Working equations to calculate the pressure drop of a liquid distributor include:

$$\zeta_{cc} = 1.5(2.5 - 2.5\phi) \quad 1$$

$$\zeta_{ct} = 1.2[1 + 2.5(1 - \phi)] \quad 2$$

$$\zeta_{ld} = 1.2[1.5 - \phi(2.5 - \phi)] \quad 3$$

$$\Delta p_{\text{int}} = \left( \frac{n_{cc}\zeta_{cc}}{\phi_{cc}^2} + \frac{n_{ct}\zeta_{ct}}{\phi_{ct}^2} + \frac{n_{ld}\zeta_{ld}}{\phi_{ld}^2} \right) \frac{F_c^2}{2} \quad 4$$

$$\phi = \frac{A_o}{A_c} \quad 5$$

Where the contraction loss coefficient ( $\zeta$ ) with subscripts cc, ct and ld refer to chevron collector, chimney-tray and liquid distributor respectively,  $\phi$  is the relative free area defined as the ratio between the cross sectional area of the column and the open area for flow, n denotes the number of contractions and  $F_v$  the vapour capacity factor.

The model by Rix and Olujić (2008) is the only model found in literature that predicts the pressure drop over a distributor reasonably, and can thus be employed to revise the initial design of distributors. The next section will discuss the effect of column diameter and bed depth on HETP and pressure drop for structured packing inside a distillation column.

## 2.5 Effect of Column Diameter and Bed Depth on HETP and Pressure Drop

Meier *et al.* (1979) conducted efficiency and hydrodynamic tests on Mellapak™ 250Y with pilot plants that had internal diameters of 0.16, 0.25 and 1 m respectively. It was found that the HETP is not influenced by the column diameter, and that the pressure drop results between the 0.25 m and 1 m diameter columns compared well, with the exception at the lowest tested liquid load of 5 m<sup>3</sup>/m<sup>2</sup>h. At this flow rate the 0.25 m internal diameter column gave a higher pressure drop than the 1 m diameter column over the entire tested range. Additionally, they investigated the effect of packing height in a 1 m diameter column, and found that the packing efficiencies can be maintained up to a packing height of 6.6 m without intermediate redistribution.

Wu and Chen (1987) did experimental work to test the efficiency of structured and random packing, using a 0.15 m internal diameter distillation column for efficiency tests and 0.3 m



and 0.9 m internal diameter hydrodynamic columns for the capacity and pressure drop tests. From their study it was found that, in most cases, the type of packing to be used in a commercial design can be tested in a pilot plant column. They also studied the effect of wall effects and internal diameter. The ratio of wetted inner surface area of the column ( $a_{wall}$ ) versus the total effective packing surface area ( $a_{packing}$ ) can be calculated with equation 6 where  $d_s$  is the internal diameter of the column and  $a_e$  the specific surface area of the packing.

$$\frac{a_{wall}}{a_{packing}} = \frac{\pi d_s z}{\left(\frac{\pi d_s^2}{4}\right) a_e} = \frac{4}{d_s a_e} \quad 6$$

From equation 6 it can be seen that the smaller the column, the greater the wall effect would be. Thus the contribution of the wetted inner surface of the column to mass transfer becomes more pronounced for smaller columns and for packing with a smaller internal surface area. Wu and Chen (1987) found that this effect was true for random packing, but, due to the much higher effective surface area within structured packing, this effect was not observed for structured packing. They also used the data from the pilot plants to design a 1.5 m internal diameter column. The column was built and operated successfully.

Helling and DesJardin (1994) used a pilot plant distillation column with internal diameter of 0.22m to generate data for a 1.27 m column. Notably, they could not obtain the same efficiency as what they obtained from the pilot plant and attributed the difference to poor liquid distribution. After a thorough investigation of the distributor, as well as adjustments to the liquid distributor, and bed depth, the column's efficiency was increased. Thereafter, the results compared fairly well with the pilot plant data. Similar results were observed by Kunesh *et al.* (1987).

Gualito *et al.* (1997) did a computer simulation to obtain a better understanding of the change in column height on HETP. Their simulation indicated higher efficiencies at the bottom of the bed than for the top of the bed. It was thus deduced that HETP is affected by i) the temperature difference in the top and bottom part of the packed bed and ii) the stripping factor, which is dependent on the equilibrium curve. The effect was more

pronounced with ceramic packing at atmospheric pressure than with metal structured packing at 4.14 bar.

Deible *et al.* (1997) investigated the influence of wall effects on column diameter. The wall effects that were studied included wall flow, heat loss, and control sensitivity. It was found that these wall effects were almost independent of the column diameter in columns larger than 0.1 m, but below 0.05 m the effects increased sharply (see Figure 13).

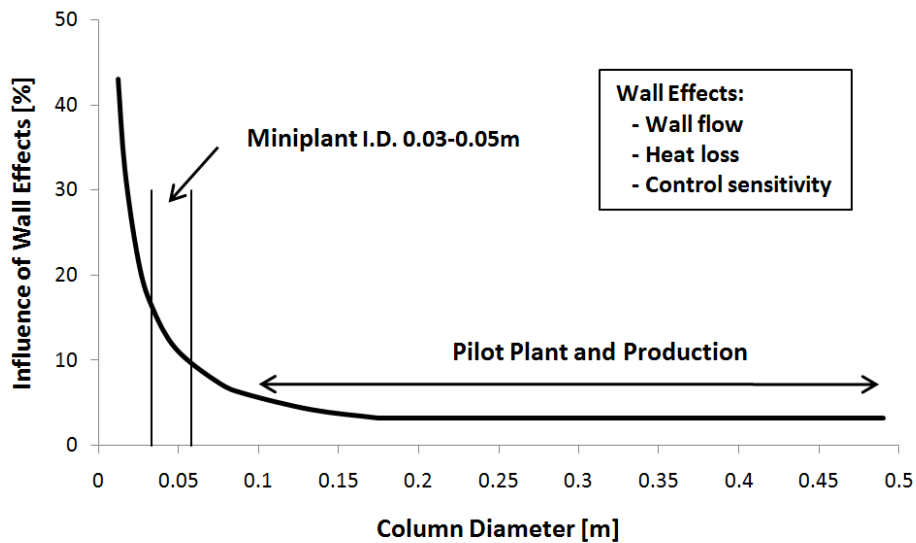


**Figure 13 – influence of wall effects on column diameter**  
**Source - Redrawn from Deibele et al. (1997)**

Olujć (1999) studied the effect of column diameter on the pressure drop over the packing. The study was done on Montz™-pak B1-250 with an air/water system in perspex columns with internal diameters of 0.2 m, 0.45 m, 0.8 m and 1.4 m. It was found that columns smaller than 1 m in diameter resulted in a higher pressure drop than larger diameter columns. Further, the effect was more pronounced in columns where the diameter of the column was more or less equal to the packing height. In smaller diameter columns there are more sharp directional changes than in larger beds, as there are more gas flow channels ending at the column walls. Therefore the effect is strongly related to the number of sharp directional changes.

The directional change of the gas flow makes up a part of the pressure drop inside a distillation column. Consequently, the more directional changes, the higher the pressure drop will be. Olujć (1999) also reported that data published by Meier *et al.* (1979) suggested

considerable diameter effects on pressure drop, where the latter reported that the pressure drop data between columns with internal column diameters of 0.25 m and 1 m compared well, with an exception of the liquid rate  $5 \text{ m}^3/\text{m}^2\cdot\text{h}$ . Olujić's (1999) study was, however, only done on one type of packing and it would be of value to see if packing with a larger surface area would have the same effect. Furthermore, the experiments were only conducted with an air/water system and the effect was not validated through total reflux experiments. Different setups were used for the experiments, for which no detailed description was given. This would have been beneficial for external consideration, especially the way the gas flow rate was measured, as it can influence the vapour capacity factor and therefore the capacity of the packing. Erasmus (2004) observed that an additional corrugation sheet could increase the pressure drop of the structured packing. An indication as to whether the ratio between the packed sheets per column diameter was constant throughout all the test setups would be helpful.

Olujić (2008) proposed a standardised pilot plant that can be used to measure the efficiency of structured packing. It was suggested that the column diameter should be as large as possible to reduce the wall effects, and that the column diameter should at least be double the size of the height of the packing element. Thus for Montz™ and Sulzer™ packings (with an element height between 0.15 m and 0.2 m) a column diameter of 0.45 m is recommended and for Koch-Glitsch™ and former Norton packing (with an element height between 0.25 m and 0.3 m) a diameter of 0.6 m. Olujić (2008) recommended that a column diameter of 0.45 m should be sufficient to test the performance of structured packing.

In conclusion, from the finding of Meier *et al.* (1979), Wu and Chen (1987) and Deible *et al.* (1997) it is clear that the HETP is not influenced by the column diameter and that the wall effects are almost independent of the column diameter in columns larger than 0.1 m. The wall effects are dependent on the ratio of the column's surface area to packing surface area, and can be decreased by either increasing the column diameter or increasing the surface area of the packing (see equation 6). From this, it is recommended to use a larger diameter column to study the effects of structured packing with a smaller surface area, but that a 0.2 m internal diameter distillation column can be used to determine the efficiency of 350Y structured packings.

From a hydrodynamic point of view, tests done by Olujić (1999) showed that column diameter has an effect on the pressure drop of structured packing. It is thus recommended that hydrodynamic tests should be done in as large a column size as possible. The effect of column diameter on pressure drop could be less for larger surface area packings, but this still needs to be proven experimentally.

Increasing the column diameter will increase the time to reach steady state, as well as energy consumption (Ottenbacher *et al.*, 2010). Five times more energy is required to operate a 0.45 m internal diameter distillation column than a 0.2 m column using a water/methanol test mixture (see calculations in Appendix – Section 8.1). It is also necessary to minimise any heat losses to the environment. The hydrodynamic studies do not require any vaporisation or condensation of the test mixture, and therefore the operating costs are considerably lower than those of distillation tests. For this reason it is also desirable to keep the column diameter as small as possible, and to minimise the heat losses to the environment for distillation testing to determine the efficiency, and as large as possible for hydrodynamic testing to determine the capacity of the packing, as was done by Wu and Chen (1987).

## 2.6 Test Mixtures

It is crucial to select the correct test mixture for a specific pilot plant design (Olujić, 2008). To do so, certain factors need to be taken into account. To address these factors, Fenske *et al.* (1938) formulated seven fundamental rules for fractional distillation columns; these rules still apply today and are quoted below. Thereafter the popular test mixtures used in pilot plant test setups are discussed.

### 2.6.1 Fenske *et al.* (1938) Rules for a Test System

- i. A binary mixture whose vapour-liquid equilibrium data are known should be used. If the number of theoretical plates is calculated by an equation using the relative volatility ( $\alpha$ ), the numerical value of ( $\alpha$ ) should be known accurately over the composition range used.*
- ii. The binary mixture should give results at least approximately the same as other binary mixtures. If the binary mixture is new, it should be compared in a distillation column with one of the well known binary mixtures.*

- iii. *The original concentration of the binary mixture should be chosen so that at equilibrium the concentration of the less volatile component in the distillate or the more volatile component in the still is not too small. That is, whenever possible, the middle portion of the vapour-liquid diagram should be used. In n-heptane/methylcyclohexane mixture differences of analyses due to refractive index reading only 0.0002 apart may, when still concentrations of n-heptane or distillate concentrations of methylcyclohexane are obtained, cause differences of eight theoretical plates when these concentrations lie near the ends of the vapour-liquid diagram.*
- iv. *The components of the binary mixture should be pure.*
- v. *A sufficient number of tests should be made to ensure the reliability of the results.*
- vi. *The column should be operated for sufficient periods of time so that steady conditions are realized.*
- vii. *Efficiencies should be determined over the entire throughput range of the column.*

### **2.6.2 Popular Test Mixtures**

The VLE curves for the most popular systems used by the well-established facilities (SRP, FRI and Delft) are plotted in Figure 14 (Rocha *et al.*, 1996; Fitz *et al.*, 1999; Olujić, 1999). The methanol/ethanol system has been omitted because it lies directly on top of the cyclohexane/n-heptane system, and the 2-butanol/iso-butanol was added for comparison. As this is the test system used to determine the performance of structured packing in this study. As seen in Figure 14, the 2-butanol/iso-butanol test system lies almost right in the middle of the popular cyclohexane/n-heptane and chlorobenzene/ethylbenzene systems.

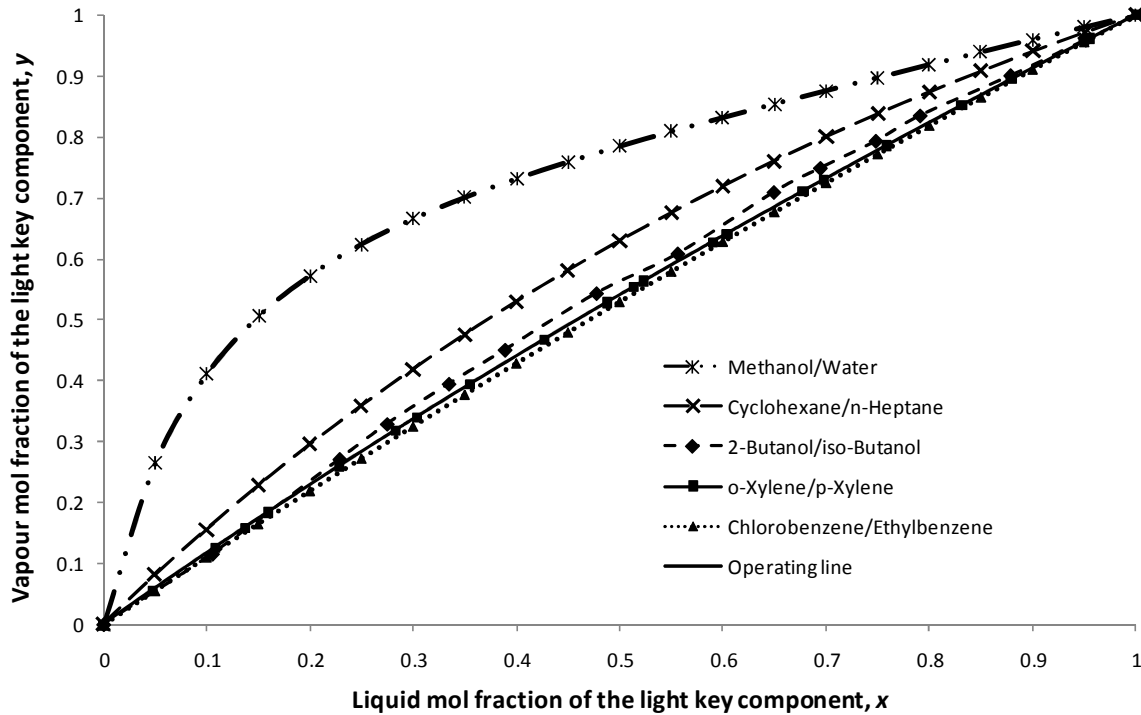


**Figure 14 – VLE curve for mixtures used in distillation pilot plants**  
**Source - Kutsarov et al. (1993), Zong et al. (1983) and (Onken and Arlt, 1990)**

The surface tension of a test mixture also influences the wettability of the system and therefore the wetted area. It can be expected that a system with a smaller surface tension will have better wetting characteristics than a system with a larger surface tension. A test system can be classified as neutral, positive, or negative with regard to surface tension. A decrease in the surface tension along the liquid flow path is termed a negative system and, with an increase of surface tension, the system is termed positive, and when the surface tension stays constant along the flow path, a neutral system is referred to (Billet and Schultes, 1993).

It can be expected that different test systems will produce different HETP results because of physical property differences between the test mixtures (Ottenbacher *et al.*, 2010). Some of the pure component properties that will influence the properties of a test mixture are the heat of vaporisation, molecular weight, boiling point, and surface tension. The pure component properties of the test mixtures given in Figure 14 are presented in Table 2. The HETP will also be influenced by the test mixture properties which include the relative volatility and the mixing properties. Each of the test mixtures in Figure 14 and Table 2 will be discussed briefly.

**Table 2 - Properties of test mixtures (for Figure 14)**

Test mixture	Components	$\alpha$	Boiling point at 1 atm [°C]	$M_r$ [g/mol]	$\sigma$ at bp [N/m]	$h_{vap}$ at bp [kJ/kg]	$\mu$ at bp [mPa.s]
Methanol/water	Methanol	2.61 -	64.7	32.04	0.0189	1095	0.329
	Water	6.83	100.0	18.02	0.0589	2257	0.282
Cyclohexane/n-Heptane	Cyclohexane	1.65 -	80.8	84.16	0.0177	357	0.422
	n-Heptane	1.72	98.4	100.21	0.0126	328	0.201
2-Butanol/iso-butanol	2-Butanol	1.28 -	99.7	74.12	0.0149	549	0.375
	iso-butanol	1.37	107.7	74.12	0.0159	565	0.374
o-Xylene/p-Xylene	o-Xylene	1.19 -	144.0	106.17	0.0170	341	0.263
	p-Xylene	1.16	138.4	106.17	0.0164	336	0.219
Chlorobenzene/Ethylbenzene	Chlorobenzene	1.12 -	131.8	112.56	0.0205	324	0.287
	Ethylbenzene	1.12	136.2	106.17	0.0170	337	0.236

**i. Methanol/Water**

The methanol/water system is one of the test mixtures recommended by Onken and Arlt (1990). The system has a large relative volatility and is therefore normally used in a short bed where four or less theoretical stages are present. Exceeding four theoretical stages leads to operating in the pinch zone, and this may lead to large analytical errors. Water also does not wet a metallic surface well, due to its large surface tension and therefore under wetting of the packing can be expected. It might be noted that a water system wets a metallic surface about 23% as well as an organic liquid wets the same surface (Rocha *et al.*, 1996). Another negative aspect of the methanol/water system is the large difference in molecular weight, which leads to a large density difference between the top and bottom of the packed bed. This effect is not always accounted for when working out the F-factor. Also the large difference between the heat of vaporisation in the two components is undesirable.

**ii. Cyclohexane/n-Heptane**

Cyclohexane/n-heptane also forms part of the recommended test mixture of Oken and Arlt (1990) and is one of the test mixtures used by SRP, FRI and Delft UT. The systems are normally used in columns where the number of plates varies between 3 and 7; going above this will lead to working in the pinch region. Relative deviations in efficiency of as much as 25 % have been observed when working with this test mixture. These deviations or uncertainties are highly undesirable for the manufacturer and end users (Ottenbacher *et al.*, 2010). The tests were done with the same packing and in the same experimental setup.

Another problem with working with this test mixture is the large differences in the molecular weight and heat of vaporisation, which will cause a density gradient throughout the column, which is not easy to take into account.

**iii. *2-Butanol/iso-Butanol***

The butanol system does not form part of the recommended test mixtures of Onken and Arlt (1990). The butanol system can be used for columns containing 10 to 16 theoretical stages. An advantage of the butanol system is that it consists of two isomers, thus eliminating the density gradient within the column. One drawback of the butanol system is its higher heat of vaporisation, which increases the operating costs and energy requirements of the experimental setup. The butanol system also has a relatively high viscosity, and its results could be valuable to the industry, since there is almost no data available for high viscosity mixtures in the open literature.

**iv. *o-Xylene/p-Xylene***

The p-xylene/o-xylene test mixture also does not form part of the recommended test mixtures of Onken and Arlt (1990), but is used by the FRI as a test mixture. The p-xylene/o-xylene test mixture is almost the ideal test system due to its low and almost constant relative volatility, and is recommended for use in columns containing 15 to 35 theoretical plates. Other advantages are its low surface tension, the small difference in heats of vaporisation, and no difference in its molecular weight. Low surface tension will ensure good spreading and wetting on the packed surface, and the constant molecular weight and heats of vaporisation will ensure that there is no density gradient and that the molar flow rate is constant.

**v. *Chlorobenzene/Ethylbenzene***

The chlorobenzene/ethylbenzene test mixture is one of the recommended test mixtures by Onken and Arlt (1990) and is used by Bayer Technology Services and Sulzer™. This system was also used by Billet and Schultes (1993). Recommended use for the chlorobenzene/ethylbenzene test system is in a column with 16 to 40 theoretical plates. The constant relative volatility makes it ideal for analysis, and the small difference between the molecular weights will have a small effect on the density within the column. The change in heat of vaporisation between the two components was identified as a weak point for the test



system (Schultes, 2010). Ethylbenzene is also classified as carcinogenic (Science Lab, 2010) and because of this safety reason this test system is not recommended for pilot plant use.

## 2.7 HETP

Mass transfer performance in packed columns is often expressed in terms of the HETP. According to the double film theory, the relationship between the HETP and overall height of a mass transfer unit (HTU<sub>o</sub>) is given by Equation 7 (Wang *et al.*, 2005).

$$\text{HETP} = \frac{\ln \lambda}{\lambda - 1} (\text{HTU}_o) \quad 7$$

Where  $\lambda$  is the stripping factor and for total reflux can be defined as (Billet, 1995):

$$\lambda = \frac{\alpha}{[1 + x_{tk}(\alpha - 1)^2]} \quad 8$$

The overall mass transfer unit consists of the height of a mass transfer unit for the vapour phase (HTU<sub>v</sub>) and that of the liquid phase (HTU<sub>L</sub>). Their relationship can be expressed as (Billet and Schultes, 1999):

$$\text{HTU}_o = \text{HTU}_v + \lambda \cdot \text{HTU}_L \quad 9$$

The height of mass transfer units for the vapour and liquid phase (Wang *et al.*, 2005) is defined as:

$$\text{HTU}_v = \frac{u_v}{k_v a_e} \quad 10$$

$$\text{HTU}_L = \frac{u_L}{k_L a_e} \quad 11$$

Where  $u_v$  and  $u_L$  are the superficial vapour and liquid velocities of the vapour and liquid phases,  $k_L$  and  $k_v$  the mass transfer coefficients for the liquid and vapour phase, and  $a_e$  the effective surface area.

## 2.8 Calculating the HETP from Experimental Data

The efficiency (HETP) of packed columns can be determined from Equation 12:

$$\text{HETP} = \frac{h_{pb}}{N_t} \quad 12$$

where  $h_{pb}$  is the height of the packed bed and  $N_t$  the number of theoretical stages. The number of theoretical stages can be calculated by the Fenske equation (Equation 13) (Fenske, 1932), with a process simulator such as Aspen Plus™ or with a graphical method such as the McCabe-Thiele method (McCabe and Thiele, 1925).

$$N_t = \frac{\ln \left[ \left( \frac{x_{lk}}{1-x_{lk}} \right)_{Dist} \left( \frac{1-x_{lk}}{x_{lk}} \right)_{Bot} \right]}{\ln \alpha} \quad 13$$

The Fenske equation is used by the Delft UT (Olujić, 2008) and the SRP model (Gualito *et al.*, 1997) to calculate the number of theoretical stages in a distillation column. The accuracy of the Fenske equation is dependent on the accuracy of the relative volatility, and small deviations in the relative volatility will cause large errors in the determination of the number of theoretical stages. Coulson and Herington (1948) state that if the relative volatility is 1.10, an error of 0.01 in the relative volatility will introduce an error of 10 % when calculating the number of theoretical stages using the Fenske equation. If the relative volatility is 1.2 the error will be 5 %. For this reason, it is important to have reliable VLE data from which the relative volatility can be accurately calculated over the entire composition range when calculating the number of equilibrium stages with the Fenske equation. Olujić *et al.* (2007) used an analytical method which is equivalent to the graphical McCabe-Thiele method to calculate the number of equilibrium stages for the non-ideal methanol/water test system. However, to use the McCabe-Thiele method accurately certain assumptions need to be valid (Seader and Henley 2006), namely:

- i. Both components of the binary mixture should have equal and constant molar enthalpies of vaporisation.
- ii. Heat of mixing and sensible-enthalpy changes ( $C_p\Delta T$ ) are negligible compared to latent heat changes.
- iii. The column is well insulated, with negligible heat losses to the environment.
- iv. The pressure is uniform throughout the column.

These assumptions do not hold true for the methanol/water system, because of the large difference in heats of vaporisation (see Table 2). It is therefore recommended to rather use the Ponchon-Savarit method to calculate the number of theoretical stages for the methanol/water test system.

The HETP and pressure drop is normally plotted against the vapour capacity factor (F-factor), which is defined as the superficial vapour velocity of the gas times the square root of the vapour density (Equation 14).

$$F_c = u_v \sqrt{\rho_v} \quad 14$$

The F-factor is therefore dependent on the density of the vapour, and density is a function of the temperature, composition of the test mixture, and operating pressure of the system. Thus, the F-factor varies along the column (Olujić *et al.*, 2007).

The difference in density is not always taken into account when specifying the F-factor. It is therefore desirable to choose a test mixture which has i) two components where the boiling points are close to one another to eliminate the temperature difference between the top and the bottom of the column, ii) components that have similar molecular weights to eliminate the effect of compositional changes on the density, and iii) a reasonably constant heat of vaporisation to ensure constant molar flow rate through the column. The effect of pressure difference between the top and bottom of the column is dependent on the type of packing and distributors used. Delft UT and FRI prefer to use the geometric average between the top and bottom conditions in the column to define the F-factor, whereas the SRP uses the bottom conditions (Olujić *et al.*, 2007).

## 2.9 Modelling of Distillation Columns

Many different approaches have been applied to model the hydrodynamic and mass transfer phenomena in a distillation column. These approaches include:

- *Capacity charts (McNulty and Hsieh, 1982; Robbins, 1991) and empirical correlations fitted to experimental data (Spiegel and Meier, 1987)*
- *Semi-empirical models (Rocha et al., 1993 and 1996; Billet and Schultes, 1999; Maćkowiak, 1990, 1991 and 2009; Olujić et al., 2004)*
- *Process simulations (Pro II™ and Aspen Plus™)*
- *Film models (Shetty and Cerro, 1997)*
- *CFD models (Haghshenas Fard et al., 2007)*
- *Neural networks (Whaley et al., 1999; Pollock and Eldridge, 2000)*
- *Short cut methods (Kister, 1992; Strigle, 1994; Lockett 1998; Carrillo et al., 2000)*

Process simulation packages are powerful tools to simulate and predict the behaviour of distillation columns. They also incorporate some of the semi-empirical models to predict the performance of a distillation column. Aspen Plus™ uses the Billet (Billet and Schultes, 1993) and SRP (Bravo et al., 1985; 1992) models to predict the performance of structured packing. However, newer versions of the Billet and SRP models are available and a summary of the working equations of the Billet model is given in Billet and Schultes (1999) whereas Fair et al. (2000) summarise the latest working equations for the SRP model.

The other well known semi-empirical model is the Delft model, which was developed at the Delft UT with the working equations summarised in Olujić et al. (2004). Brunazzi et al. (1995) developed a model to predict the interfacial area of Mellapak 250Y and later extended the model to predict the liquid film mass transfer coefficient (Bruanzzzi and Paglianti, 1997a) and pressure drop (Bruanzzzi and Paglianti, 1997b) of Mellapak 250Y structured packing.

Maćkowiak (1990, 1991, 2009) developed a model that can be used to predict the hydrodynamic behaviour of random as well as structured packing. The model was first developed to predict the irrigated pressure drop in a packed column (Maćkowiak 1990), and then later extended to predict the liquid hold-up and vapour velocity at flooding conditions. Recently, Maćkowiak (2009) further extended the model to predict the dry bed pressure

drop in packed columns. Maćkowiak's model was validated over an extended range of packings and operating conditions. The model also does not require any experimentally predetermined constants, and therefore making the model favourable to predict the hydrodynamic behaviour of packed columns.

Recently Rejl *et al.* (2010) developed a "profile method" to predict the concentration profile and thus the efficiency of structured packing in a distillation column. Experiments were done with Mellapak 250Y structured packing in a 0.15 m internal diameter column. The Billet, Delft and SRP models were then fitted on the experimental data to obtain a corrected model of the Billet, Delft and SRP models that is used to predict the mass transfer coefficients.

The rest of the discussion will only focus on the Billet, Delft and SRP models, as these models include both hydrodynamic as well mass transfer behaviour of packed columns and have been validated on an extended data bank with a wide variety of packings and test mixtures. The three different models will be discussed in terms of their:

- *Hydrodynamic behaviour*
- *Effective interfacial area and*
- *Mass transfer predictions*

After all the models are presented they will be graphically compared with one another.

## **2.10 Hydrodynamics**

The hydrodynamic behaviour within a distillation column describe the flow rates, pressure drop and transition points. There are two transition points (loading and flooding point) that divide the operating curve of the distillation column into three operating regions, i.e. the pre-loading, loading, and flooding regions. The three operating regions are illustrated in Figure 15 and Figure 16. In Figure 15 the pressure drop and in Figure 16 the liquid hold-up of a packed column are plotted against the vapour capacity factor. The loading points of each curve fall on line A-A and the flooding points on line B-B.

The loading and flooding points were first described as the lower and upper "breaking point", thereby dividing the curve into three different regions. The loading point refers to

the point where the pressure drop curve “breaks away” from its linear relationship in the pre-loading region; see Figure 15 (Zenz, 1947).

In the pre-loading region the liquid trickles down the packed bed and is uninfluenced by the counter-current flow of gas (see Figure 16). As the gas velocity is increased, the shear stress at the liquid film boundary layer also increases to such an extent that it causes the liquid velocity at the boundary layer to drop. The point at which the liquid film velocity at the boundary layer becomes zero represents the loading point (line A-A on Figure 15 and Figure 16). Above this point, the shear stress in the gas will cause some of the liquid flow to be impeded. The flooding point (line B-B) is reached when the shear stress is sufficient to entrain the entire liquid volume in the column (Valluri *et al.*, 2002). The loading region is the area between the loading and flooding points (see Figure 15 and Figure 16). The flooding region is the region at higher gas flow rates. The transition points characterise the capacity of the column.

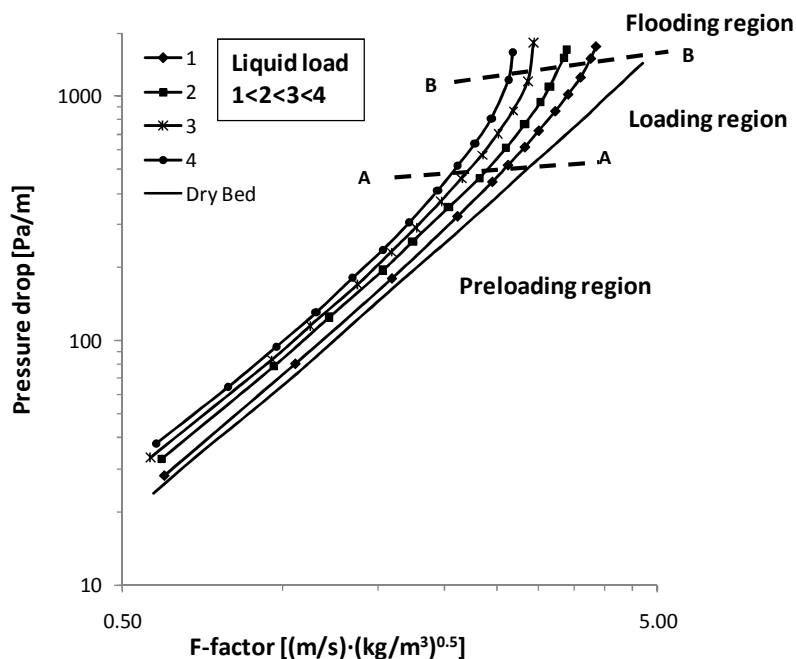


**Figure 15 – Pressure drop as a function of gas capacity factor.  
Source – Data from Lamprecht (2010)**

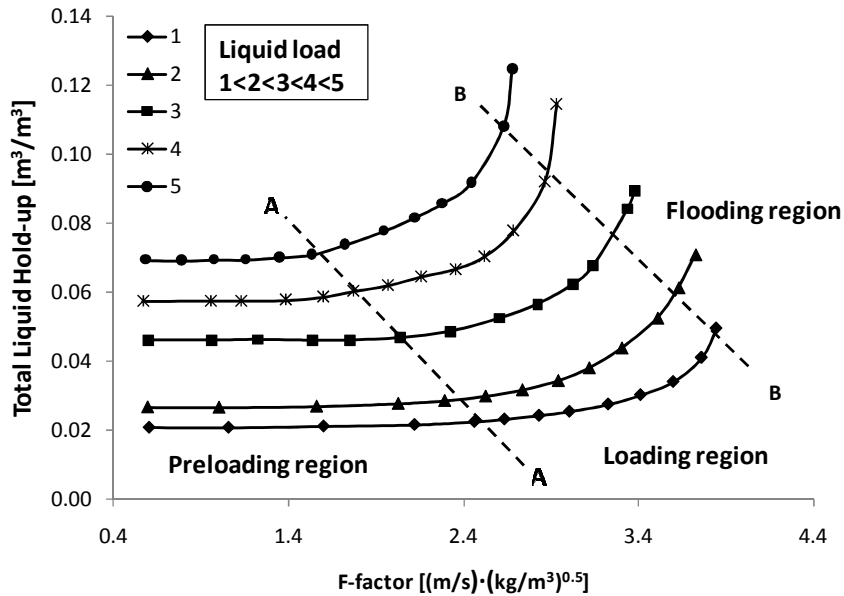


**Figure 16 – Liquid hold-up as a function of gas capacity factor**  
**Source - Data from Lamprecht (2010)**

Columns normally operate between 70 and 80 % of their capacity (Billet and Schultes, 1999), therefore it is important to accurately predict the flooding point of a distillation column. Over-predicting the flooding point will cause the distillation column to operate deep into its loading region, causing high pressure drops over the packing. A higher pressure drop over the column leads to a larger temperature difference between the top and the bottom of the column; which could be problematic for reactive and heat-sensitive distillations (Helling and DesJardin, 1994). Under-predicting the flooding point will lead to an over design of the column, and therefore hinder the distillation column from operating at its optimal conditions and full capacity; this leads to excessive capital costs.

### 2.10.1 Billet and Schultes Model

The Billet model is a theoretically based model first derived for random packing, but later extended to structured packing (Billet and Schultes, 1993). The drawback of this model is that it requires six packing constants for each type of packing. Packing constants for 70 types of packings (60 random and 10 structured) can be found in Billet and Schultes (1999). The structured packings that were tested included packing made from metal, ceramic, and plastic with surface areas of 110, 200, 250 and 300 m<sup>2</sup>/m<sup>3</sup> (Billet and Schultes, 1999). A

summary of the constants available for structured packing are given in Table A 5 in Section 8.2.

The six constants in the Billet model is used in semi-empirical correlations to predict the i) loading point, ii) flooding point, iii) liquid hold-up, iv) pressure drop, v) liquid-side mass transfer coefficient, and vi) vapour-side mass transfer coefficient. Each of these semi-empirical correlations will be discussed.

### ***i. Loading and Flooding Points***

The Billet model consists of several equations that describe the pressure drop and liquid hold-up in the pre-loading and loading regions. It is therefore important for this model to accurately predict the loading and flooding points. The equations that determine the loading and flooding points are semi-empirical models, which are based on theoretical and experimental studies (Billet and Schultes, 1993). The assumption made is that the void fraction in the packed bed can be represented by multiple vertical channels through which the liquid flows down as a film to the counter-current gas stream. The Billet model does not account for the inclination angle caused by the packing geometry. The equations used to determine the loading and flooding velocities is presented in Table 3 and Table 4. In both situations an iterative approach is taken in solving the series of equations. The fourth order equation for the liquid hold-up at flooding velocity (Equation 24) has only one solution of physical significance that lies between  $\epsilon/3$  and  $\epsilon$ . First, the right hand side of Equation 24 must be positive, which implies that the liquid hold-up at the flooding point cannot be less than  $\epsilon/3$ . Secondly, it is physically impossible for the liquid hold-up to exceed the void fraction (Billet and Schultes, 1987).

**Table 3 – Loading point for the Billet and Schultes model  
(Equations 15 to 19)**

<p>Vapour velocity at loading point:</p> $u_{V,lp} = \sqrt{\frac{g}{\psi_{lp}}} \left( \frac{\epsilon}{a^{1/6}} - a^{1/2} \left( 12 \frac{1}{g} \frac{\mu_L}{\rho_L} u_{L,lp} \right)^{1/3} \right) \left( 12 \frac{1}{g} \frac{\mu_L}{\rho_L} u_{L,lp} \right)^{1/6} \sqrt{\frac{\rho_L}{\rho_V}}$	15
---	----



**Table 3 (Continue) - Loading point for the Billet and Schultes model**

Resistance coefficient at the loading point defined by:	
$\psi_{lp} = \frac{g}{C_{lp}^2 \left[ \frac{L}{V} \sqrt{\frac{\rho_V}{\rho_L}} \left( \frac{\mu_L}{\mu_V} \right)^{0.4} \right]^{2n_{lp}}}$	16
Where $C_{lp}$ is the packing specific constant and:	
$\frac{L}{V} \sqrt{\frac{\rho_V}{\rho_L}} \leq 0.4 \rightarrow n_{lp} = -0.326$ <p>with <math>C_{lp} = C_{lp}</math></p>	17
$\frac{L}{V} \sqrt{\frac{\rho_V}{\rho_L}} > 0.4 \rightarrow n_{lp} = -0.723$ <p>with <math>C_{lp} = 0.695 C_{lp} \left( \frac{\mu_L}{\mu_V} \right)^{0.1588}</math></p>	18
$u_{L,lp} = \frac{\rho_V}{\rho_L} \frac{L}{V} u_{V,lp}$	19

**Table 4 – Flooding point for the Billet and Schultes model  
(Equations 20 to 26)**

Vapour velocity at flood point:	
$u_{V,Fl} = \sqrt{\frac{2g}{\psi_{Fl}} \frac{(\varepsilon - h_{L,Fl})^{3/2}}{\varepsilon^{1/2}}} \sqrt{\frac{h_{L,Fl}}{a}} \sqrt{\frac{\rho_L}{\rho_V}}$	20
Resistance coefficient at the flooding point defined by:	
$\psi_{Fl} = \frac{g}{C_{Fl}^2 \left[ \frac{L}{V} \sqrt{\frac{\rho_V}{\rho_L}} \left( \frac{\mu_L}{\mu_V} \right)^{0.2} \right]^{2n_{Fl}}}$	21
Where $C_{Fl}$ is the packing specific constant and:	
$\frac{L}{V} \sqrt{\frac{\rho_V}{\rho_L}} \leq 0.4 : n_{Fl} = -0.194; C_{Fl}$	22
And for	
$\frac{L}{V} \sqrt{\frac{\rho_V}{\rho_L}} \geq 0.4 : n_{Fl} = -0.708; C_{Fl} = 0.6244 C_{Fl} \left( \frac{\mu_L}{\mu_V} \right)^{0.1028}$	23

**Table 4 (Continue) - Flooding point for the Billet and Schultes model**

$h_{L,Fl}^3 (3h_{L,Fl} - \varepsilon) = \frac{6}{g} a^2 \varepsilon \frac{\mu_L}{\rho_L} \frac{L}{V} \frac{\rho_V}{\rho_L} u_{V,Fl}$	24
$\frac{\varepsilon}{3} \leq h_{L,Fl} \leq \varepsilon$	25
Rearrange Equation 24 $u_{V,Fl} = \frac{h_{L,Fl}^3 (3h_{L,Fl} - \varepsilon) g \rho_L^2}{6a^2 \varepsilon \left(\frac{L}{V}\right) \mu_L \rho_V}$	26

Solving these equations in an iterative manner, and adhering to the boundary conditions for liquid hold-up, yields the flooding velocity.

**ii. Liquid Hold-up in the Pre-loading Region**

The liquid hold-up in the pre-loading region is calculated with the equations listed in Table 5. Equations 27 and 28 were theoretically derived from a force balance, and from Equation 28 it can be seen that the liquid hold-up in the pre-loading region is only a function of liquid properties and liquid flow rate. The ratio of wetted area to packing area  $a_h/a$  accounts for the area of the packing that is not completely wetted by the liquid flow, and is determined with empirical correlations 29 and 30. These correlations have been verified on 56 packings of various shapes and sizes as well as on 16 characteristic systems (Billet and Schultes, 1993).  $Re_L$  and  $Fr_L$  are the Reynolds and Froude numbers defined by Equations 31 and 32 and the constant  $C_h$  characterises the packing geometry and reflects the difference between the actual liquid flow and that of the physical model (Billet and Schultes, 1999).

**Table 5 – Liquid hold-up in the pre-loading region for the Billet and Schultes model (Equations 27 to 32)**

$\psi_{L,pl} = \frac{h_L}{a_h} \frac{(\varepsilon - h_L)^2}{u_V^2} \frac{\rho_L g}{\rho_V}$	27
$h_{L,pl} = \left( 12 \frac{\mu_L a^2 u_L}{\rho_L g} \right)^{1/3} \left( \frac{a_h}{a} \right)^{2/3}$	28
$\frac{a_h}{a} = C_h Re_L^{0.15} Fr_L^{0.1} \quad \text{for } Re_L < 5$	29
$\frac{a_h}{a} = 0.85 C_h Re_L^{0.25} Fr_L^{0.1} \quad \text{for } Re_L \geq 5$	30

**Table 5 (Continue) - Liquid hold-up in the pre-loading region for the Billet and Schultes model (Equations 27 to 32)**

$\text{Re}_L = \frac{u_L \rho_L}{a \mu_L}$	31
$\text{Fr}_L = \frac{u_L^2 a}{g}$	32

### **iii. Liquid Hold-up in the Loading Region**

To predict the liquid hold-up in the loading region, Billet and Schultes (1993) developed an empirical correlation (Equation 33) that fits the shape of experimental curves in the loading region. In Equation 33, the liquid hold-up is calculated with Equation 34 and not with the theoretical expression given in Equation 24. Equation 34 is obtained from an air/water system where it was found that the liquid hold-up at flooding point is about 2.2 times the value obtained from Equation 28. It is therefore necessary to account for the influence of viscosity and density if systems other than air/water are used (Billet and Schultes, 1993). From this is it clear that the equations used to predict the liquid hold-up in the loading region are purely based on empirical correlations.

$$h_L = h_{L,pl} + (h_{L,Fl} - h_{L,pl}) \left( \frac{u_V}{u_{V,Fl}} \right)^{13} \quad 33$$

$$h_{L,Fl} = 2.2 h_{L,pl} \left( \frac{\mu_L \rho_w}{\mu_w \rho_L} \right)^{0.05} \quad 34$$

### **iv. Pressure Drop in a Dry Bed**

The dry bed pressure drop ( $dP_d/dz$ ) (Equation 35) for gas flowing through a dry bed of height  $z$  was derived from a force balance by applying the shear force/pressure equilibrium and the Newtonian friction law. The equations to calculate the dry pressure drop in a packed bed are presented in Table 6.

**Table 6 – Dry bed pressure drop for the Billet and Schultes model  
(Equations 35 to 39)**

$\left(\frac{dP}{dz}\right)_d = \psi_o \frac{a}{\varepsilon^3} \frac{F_c^2}{2} \frac{1}{K}$	35
$\frac{1}{K} = 1 + \frac{2}{3} \frac{1}{(1-\varepsilon)} \frac{d_p}{d_s}$	36
$d_p = 6 \frac{1-\varepsilon}{a}$	37
$\psi_o = C_p \left( \frac{64}{\text{Re}_v} + \frac{1.8}{\text{Re}_v^{0.08}} \right)$	38
$\text{Re}_v = \frac{u_v d_p \rho_v}{(1-\varepsilon) \mu_v} K$	39

Where,  $d_p$  and  $d_s$  are the particle and column diameter respectively. The particle diameter ( $d_p$ ) in Equation 36 depends on the ratio of volume available to the total area of packing and is calculated using Equation 37. The real packed bed void fraction differs from the theoretical void fraction because there is more free space at the wall of the column. The difference is accounted for by a wall factor (K) in Equation 36. For the dry bed, the resistance coefficient ( $\psi_o$ ) is determined with an empirical correlation (Equation 38), which is derived from experimental data conducted on 54 types of packing. The constant ( $C_p$ ) describes the surface properties and geometry of the dry packing and is thus specific for a given type of packing (Billet and Schultes, 1991). The constants available for structured packing for the Billet and Schultes model can be found in the Appendix – Section 8.2.

**v. Pressure Drop in a Wetted Bed:**

In a wetted bed the liquid hold-up within the bed reduces the volume available for gas flow. This is corrected with an effective void fraction  $\varepsilon_e$  defined by Equation 40.

$$\varepsilon_e = (\varepsilon - h_L) \tag{40}$$

The wetted bed pressure drop can be calculated by substituting the effective void fraction in Equation 35 and introducing a wetting factor ( $f_w$ ) that reflects the change in the packing surface area as a result of wetting. Table 7 lists the equations that are used to calculate the irrigated pressure drop in a packed bed. Here  $\psi_L$  is the resistance coefficient for two-phase

flow. The resistance coefficient and wetting factor are grouped together, and can be defined by the empirical correlation, Equation 42.

**Table 7 – Wet bed pressure drop (Equations 41 to 44)**

$\frac{dP}{dz} = \psi_L \frac{f_w a}{(\varepsilon - h_L)^3} \frac{F_c^2}{2} \frac{1}{K}$	41
$\psi_L' = \psi_L f_w = C_P f(S) \left( \frac{64}{\text{Re}_V} + \frac{1.8}{\text{Re}_V^{0.08}} \right) \left( \frac{\varepsilon - h_L}{\varepsilon} \right)^{(3-x)}$	42
For pre-loading region: $f(S) = \exp\left(\frac{\text{Re}_L}{200}\right) \text{ for } x = 1.5$	43
For flooding region: $f(S) = \left( \frac{h_L}{h_{L,fp}} \right)^{0.3} \exp\left(\frac{\text{Re}_L}{200}\right)$	44

It was found that the pressure drop in high pressure applications with low liquid viscosities can be better described by Equation 45 in terms of the Froude and Reynolds numbers. Therefore a modification was made to Equation 42 (Billet and Schultes, 1999).

$$\psi_L' = C_P \left( \frac{64}{\text{Re}_V} + \frac{1.8}{\text{Re}_V^{0.08}} \right) \left( \frac{\varepsilon - h_L}{\varepsilon} \right)^{1.5} \left( \frac{h_L}{h_{L,fp}} \right)^{0.3} \exp\left(C_1 \sqrt{\text{Fr}_L}\right)$$

with  $C_1 = \frac{13300}{a^{3/2}}$  45

It must also be kept in mind that the Froude numbers used for the pressure drop and effective area also differ from one another:

Pressure drop:

$$\text{Fr}_L = \left( \frac{u_L^2 a}{g} \right)$$
 46

Effective interfacial area:

$$\text{Fr}_L = \left( \frac{u_L^2}{gd_h} \right) \quad 47$$

And

$$d_h = 4 \frac{\varepsilon}{a} \quad 48$$

Substituting  $d_h$  into Equation 47 gives the following equation for the Froude number for interfacial area:

$$\text{Fr}_L = \left( \frac{u_L^2 a}{4\varepsilon g} \right) \quad 49$$

For most structured packings the void fraction is a value close to 1, typically between 0.90-0.97 (Rocha *et al.*, 1999), thus  $4\varepsilon \approx 4$ . Therefore the Froude number used for pressure drop is about 4 times higher than the one used for effective interfacial area.

### 2.10.2 SRP Model

The SRP model was developed at the University of Texas and was refined over the years, and the latest publication with all the relevant working equations can be found in Fair *et al.* (2000). The main variables in this model used to describe the performance of structured packing are pressure drop, maximum flow capacity, and mass transfer efficiency (Rocha *et al.*, 1993). The SRP model considers the void fraction that is available for gas flow as a series of wetted wall columns, with a geometry that depends on the angle and size of the corrugations. The effective gas and liquid velocities,  $u_{V,e}$  and  $u_{L,e}$ , take this into account and are defined by Equation 50 and Equation 51:

$$u_{V,e} = \frac{u_V}{\varepsilon(1-h_L) \sin \theta} \quad 50$$

$$u_{L,e} = \frac{u_L}{\varepsilon h_L \sin \theta} \quad 51$$

where  $u_v$  and  $u_L$  represent the superficial vapour and liquid velocities, while  $h_L$  is the liquid hold-up and  $\varepsilon$  the void fraction.

The SRP model uses effective gravity that accounts for forces that oppose the flow of the liquid film moving down the structured packing. The forces acting on the liquid film flowing down the surface of the packing are expressed in Equation 52. In this force balance the shear force of the liquid on the solid surface is neglected. A graphical illustration of the force balance is given in Figure 17.

$$\begin{aligned} \text{Net downward head} = & \text{gravity head} - \text{buoyancy head} - \text{head caused by gas} \\ & \text{pressure difference} - \text{surface drag head} \end{aligned} \quad 52$$

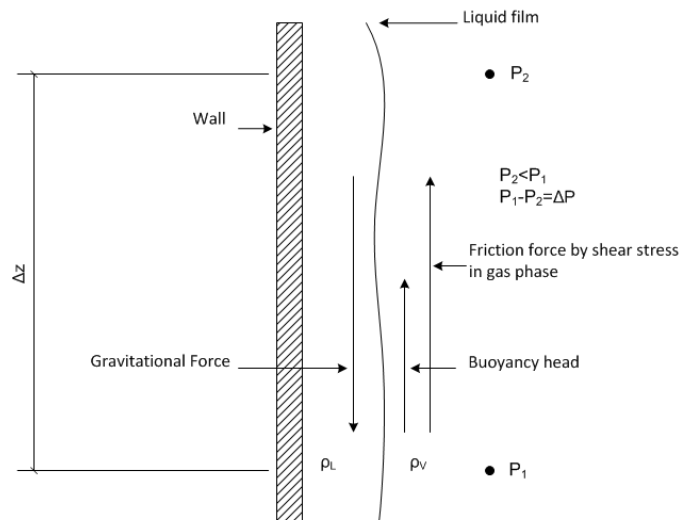


**Figure 17 – Force balance on the liquid film flowing down the surface for the SRP model  
Redrawn from Rocha et al. (1993)**

From the force balance, an effective gravity was derived and is expressed in Equation 53, where  $(\Delta P/\Delta z)_{Fl}$  is the pressure drop at flooding. Flooding occurs when the effective gravity reaches a value of zero.

$$g_{\text{eff}} = g \left[ \left( \frac{\rho_L - \rho_v}{\rho_L} \right) \left( 1 - \frac{\Delta P/\Delta z}{(\Delta P/\Delta z)_{Fl}} \right) \right] \quad 53$$

The liquid hold-up is calculated with an iterative approach using the effective gravity to account for the forces opposing the flow of liquid down the plate. The systematic approach to calculate the liquid hold-up is illustrated in Table 8.

**Table 8 - Liquid hold-up with SRP  
(Equations 54 to 58)**

1.	Obtain $\rho_L, \rho_V, \mu_L, \mu_V, S, \varepsilon, \theta, u_L, u_V$	
2.	Estimate dry pressure drop: $\left(\frac{\Delta P}{\Delta z}\right)_d = \frac{A\rho_V}{s\varepsilon^2(\sin\theta)^2}u_V^2 + \frac{B\mu_V}{s^2\varepsilon\sin\theta}u_V$ <i>A and B are constants for dry bed pressure drop and for sheet metal structured packing A = 0.177 and B = 88.77</i>	54
3.	Calculate the correction factor for total hold-up: $F_t = \frac{29.12(\text{We}_L \text{Fr}_L)^{0.15} S^{0.359}}{\text{Re}_L^{0.2} \varepsilon^{0.6} (1 - 0.93 \cos \gamma)(\sin \theta)^{0.3}}$	55
4.	Set initial conditions for iterations: $\left(\frac{\Delta P}{\Delta z}\right)_{new} = \left(\frac{\Delta P}{\Delta z}\right)_d$	56
5.	Execute iteration process: $h_L = \left[\frac{4F_t}{s}\right]^{2/3} \left[ \frac{3\mu_L u_L}{\rho_L \varepsilon \sin \theta g \left[ \left(\frac{\rho_L - \rho_V}{\rho_L}\right) \left(1 - \frac{(\Delta P/\Delta z)_{new}}{(\Delta P/\Delta z)_{Fl}}\right)\right]} \right]^{1/3}$ $\frac{\Delta P}{\Delta z} = \frac{(\Delta P/\Delta z)_d}{[1 - (0.614 + 71.35S)h_L]^5}$	57
6.	Check for convergence: $\text{if } \frac{\Delta P}{\Delta z} \neq \left(\frac{\Delta P}{\Delta z}\right)_{new} \text{ then } \left(\frac{\Delta P}{\Delta z}\right)_{new} = \left(\frac{\Delta P}{\Delta z}\right); \text{ go to step 5}$ $\text{if } \frac{\Delta P}{\Delta z} \approx \left(\frac{\Delta P}{\Delta z}\right)_{new} \text{ then STOP}$	58

**Source - Gualito et al. (1997)**



The correction factor  $F_t$  is based on the work done by Shi and Mersmann (1985), and accounts for the area of the packing that is not wetted by the liquid film. The model for liquid hold-up was simplified by assuming that the static hold-up in the packed bed can be neglected (Rocha *et al.*, 1993). The model was developed for an air/water system with Flexipack™ and Gempak™ structured packings. Validation of the model was done with a hexane/n-heptane system under total reflux distillation. Gualito *et al.* (1997) extended the model so that it could be used to design applications where the distillation column is filled with ceramic and plastic structured packings. In the SRP model the pressure drop at flooding was taken as 1025 Pa/m. This was done to simplify the model so that only one  $K_1$  value is used for all the packings tested.  $K_1$  is a dimensionless constant that is only dependent on the packing type, and it is expected that  $K_1$  is constant for a particular shape of the packing regardless of size or surface characteristics.

$$K_1 = \frac{(\rho_L - \rho_V) g}{\left(\frac{\Delta P}{\Delta z}\right)_{Fl}} \quad 59$$

#### vi. Calculating Pressure Drop

Pressure drop in the pre-loading region is calculated with the model developed by Rocha *et al.* (1993). For the pressure drop in the loading region, the SRP model incorporated the loading point correlation (Equation 63) developed by Verschoof *et al.* (1999). The equations to calculate the pressure drop with the SRP model are listed in Table 9.

**Table 9 – Pressure drop with SRP  
(Equations 60 to 64)**

$\left(\frac{\Delta P}{\Delta z}\right)_{pl} = \left(\frac{\Delta P}{\Delta z}\right)_d \left(\frac{1}{1 - (0.614 + 71.35s) h_L}\right)$	60
$\left(\frac{\Delta P}{\Delta z}\right)_{loading} = \left(\frac{\Delta P}{\Delta z}\right)_{pl} F_{load}$	61
<p>Pressure drop enhancement factor:</p> $F_{load} = 3.8 \left(\frac{F_c}{F_{c,lp}}\right)^{2/\sin\theta} \left(\frac{u_L^2}{\epsilon^2 g d_{hV}}\right)^{0.13}$	62

**Table 9 (Continue) – Pressure drop with SRP**

<p><i>F</i>-factor at loading point:</p> $F_{c,lp} = \left( 0.053 \varepsilon^2 g d_{hV} (\rho_L - \rho_V) \left( \frac{u_L}{u_V} \sqrt{\frac{\rho_L}{\rho_V}} \right)^{-0.25} (\sin \theta)^{1.15} \right)^{0.5}$	63
<p>Where the triangular gas flow channel diameter is:</p> $d_{hV} = \frac{(bh - 2\delta s)^2}{bh}{\left[ \left( \frac{bh - 2\delta s}{2h} \right)^2 + \left( \frac{bh - 2\delta s}{b} \right)^2 \right]^{0.5} + \frac{bh - 2\delta s}{2h}}$	64

### 2.10.3 Delft Model

The Delft model was developed as an academic spin-off project between Montz™ and Delft UT towards analysis and improvement of the performance of corrugated sheet structured packing (Olujic, 1997; Olujic *et al.*, 1999 and Olujic, 2002). A summary of all the working equations for the Delft model can be found in Olujic *et al.* (2004). The Delft model assumes that the liquid film is evenly spread over the entire area of the packing. Thus, the liquid hold-up is calculated by multiplying the film thickness ( $\delta$ ) with the specific packing area ( $a_p$ ) as shown in Equation 65. The liquid hold-up is therefore only a function of the corrugation angle of the packing and the properties and flow rate of the liquid, and is not dependent on the gas velocity.

*Liquid hold-up:*

$$h_L = \delta a_p \tag{65}$$

$$\delta = \left( \frac{3\mu_L u_L}{\rho_L g a \sin \alpha_L} \right)^{1/3} \tag{66}$$

The Delft model incorporated the effective liquid flow angle ( $\alpha_L$ ) of Spekuljak and Billet (1987), to account for the liquid flowing at a larger angle to that of the corrugation angle. This has led to a minor improvement of the model (Fair *et al.*, 2000). The effective liquid flow angle is defined by Equation 67:

$$\alpha_L = \arctan \left[ \frac{\cos(90 - \theta)}{\sin(90 - \theta) \cos \left[ \arctan \left( \frac{b}{2h} \right) \right]} \right] \quad 67$$

The effective gas and liquid velocities are calculated with Equation 68 and Equation 69:

$$u_{V,e} = \frac{u_V}{(\varepsilon - h_L) \sin \theta} \quad 68$$

$$u_{L,e} = \frac{u_L}{\varepsilon h_L \sin \alpha_L} \quad 69$$

Effective and relative velocity based Reynolds numbers:

$$\text{Re}_{Ve} = \frac{\rho_V u_{V,e} d_{hV}}{\mu_V} \quad 70$$

$$\text{Re}_{Vrv} = \frac{\rho_V (u_{V,e} + u_{L,e}) d_{hV}}{\mu_V} \quad 71$$

The Delft model uses the same hydrodynamic diameter for gas flow ( $d_{hV}$ ), and equations to calculate loading point, pressure drop enhancement factor and pressure drop for the full operating range, as used by the SRP model in Equation 64. Therefore, the pressure drop in the pre-loading region is the only factor that differs from the SRP model.

The Delft model assumes that the gas flows in a zigzag pattern through the packed bed, and uses a combination of three contributors to describe the pressure drop in the pre-loading region (see Equation 72). The three contributors to pressure drop are i) gas/liquid interaction (GL), ii) gas/gas interaction (GG) and, iii) direction change (DC) of the gas.

$$\Delta p_{pl} = \Delta p_{GL} + \Delta p_{GG} + \Delta p_{DC} = (\zeta_{GL} + \zeta_{GG} + \zeta_{DC}) \frac{\rho_V u_{V,e}^2}{2} \quad 72$$

For the gas/liquid interaction:

$$\zeta_{GL} = \varphi \xi_{GL} \frac{h_{pb}}{d_{hV} \sin \theta} \quad 73$$

Where the gas/liquid friction factor,  $\xi_{GL}$  is defined as:

$$\xi_{GL} = \left\{ -2 \log_{10} \left[ \frac{(\delta/d_{hV})}{3.7} - \frac{5.02}{\text{Re}_{Vrv}} \log \left( \frac{(\delta/d_{hV})}{3.7} + \frac{14.5}{\text{Re}_{Vrv}} \right) \right] \right\}^{-2} \quad 74$$

And the gas/gas interaction coefficient,  $\zeta_{GG}$ , is defined as:

$$\zeta_{GG} = (1 - \phi) \xi_{GG} \frac{h_{pb}}{d_{hV} \sin \theta} \quad 75$$

$\xi_{GL}$  is the Gas/Gas friction factor defined as:

$$\xi_{GG} = 0.722 (\cos \theta)^{3.14} \quad 76$$

The direction change losses coefficient,  $\zeta_{DC}$ , can be calculated as:

$$\zeta_{DC} = \frac{h_{pb}}{h_{pe}} (\xi_{bulk} + \psi \xi_{wall}) \quad 77$$

Where  $\psi$  represents the fraction of the channels ending at the column wall

$$\psi = \frac{2h_{pe}}{\pi d_s^2 \tan \theta} \left( d_s^2 - \frac{h_{pe}^2}{\tan^2 \theta} \right)^{0.5} + \frac{2}{\pi} \arcsin \left( \frac{h_{pe}}{d_s \tan \theta} \right) \quad 78$$

$$\xi_{bulk} = 1.76 (\cos \theta)^{1.63} \quad 79$$

$$\xi_{wall} = \frac{4092 u_L^{0.31} + 4715 (\cos \theta)^{0.445}}{\text{Re}_{Ve}} + 34.19 u_L^{0.44} (\cos \theta)^{0.779} \quad 80$$

## 2.11 Effective Interfacial Area

### 2.11.1 Billet and Schultes Model

The Billet model uses a hydraulic surface area ( $a_h$ ) to account for the area that is not completely wetted. This is used to calculate the liquid hold-up, whereas the effective interfacial area ( $a_e$ ) accounts for the wetted area that does not actively take part (dead area) in the mass transfer process, and is used to calculate the volumetric mass transfer coefficients. These two surface areas must not be confused with one another.

Absorption and desorption experiments done on 31 different systems and 67 packings gave rise to Equation 81, which can be used to calculate the effective interfacial area for positive and neutral systems in the pre-loading region (Billet and Schultes, 1993).

Pre-loading region:

$$\begin{aligned} \left(\frac{a_e}{a}\right)_{lp} &= 1.5(ad_h)^{-0.5} \left(\frac{u_L d_h}{v_L}\right)^{-0.2} \left(\frac{u_L^2 \rho_L d_h}{\sigma_L}\right)^{0.75} \left(\frac{u_L^2}{gd_h}\right)^{-0.45} \\ &= 1.5(ad_h)^{-0.5} \text{Re}_L^{-0.2} \text{We}_L^{0.75} \text{Fr}_L^{-0.45} \end{aligned} \quad 81$$

This model was later extended to also predict the effective interfacial area in the loading region up to the flooding point (Equation 82 and Equation 83).

Above the loading point:

$$\left(\frac{a_e}{a}\right)_{u_G > u_{G,lp}} = \left(\frac{a_e}{a}\right)_{lp} + \left[ \left(\frac{a_e}{a}\right)_{Fl} - \left(\frac{a_e}{a}\right)_{lp} \right] \left(\frac{u_{V,lp}}{u_{V,Fl}}\right)^{13} \quad 82$$

$$\left(\frac{a_e}{a}\right)_{Fl} = 7 \left(\frac{\sigma_L}{\sigma_W}\right)^{0.56} \left(\frac{a_e}{a}\right)_{lp} \quad 83$$

The Billet model can also be used to calculate the effective interfacial area for negative systems; this is done by including the Marangoni number ( $Ma_L$ ) which describes the differential change in surface tension along the column (see Equation 84) (Billet and Schultes, 1993).

For negative systems:

$$\left(\frac{a_e}{a}\right)_{neg} = \left(\frac{a_e}{a}\right) \left(1 - 2.4 \times 10^{-4} |Ma_L|^{0.5}\right) \quad 84$$

Systems are classified as neutral, positive or negative based on the criteria given in Section 2.6.

### 2.11.2 SRP Model

The SRP model uses a surface enhancement factor ( $F_{SE}$ ) and liquid hold-up correction factor ( $F_t$ ), which are based on the work done by Shi and Mersmann (1985), to calculate the effective interfacial area (Rocha *et al.*, 1996).

$$\frac{a_e}{a} = F_t F_{SE} \quad 85$$

$$F_{SE} = 0.35 \quad \text{for Flexipac and Mellapak structured packing}$$

The hold-up correction factor can be calculated with:

$$F_t = \frac{29.12 (We_L Fr_L)^{0.15} s^{0.359}}{Re_L^{0.2} \varepsilon^{0.6} (1 - 0.93 \cos \gamma) (\sin \theta)^{0.3}} \quad 86$$

Where  $\gamma$  is the contact angle of the liquid and defined as:

$$\cos \gamma = 0.9 \quad \text{for } \sigma_L < 0.055 \text{ N/m}$$

$$\text{And } \cos \gamma = 5.211 \times 10^{-16.835 \sigma_L} \quad \text{for } \sigma_L > 0.055 \text{ N/m} \quad 87$$

With the dimensionless numbers defined as:

$$Re_L = \frac{u_L s \rho_L}{\mu_L} \quad 88$$

$$Fr_L = \frac{u_L^2}{sg} \quad 89$$

$$We_L = \frac{u_L^2 \rho_L s}{\sigma_L g} \quad 90$$

This model was later improved by Gualito *et al.* (1997) – (Equation 91) and then again by Wang *et al.* (2006) (Equation 92) to correlate the interfacial area at elevated pressures.

Correlation improved by Gualito *et al.* (1997):

$$\frac{a_e}{a} = \left( \frac{a_e}{a} \right)_{SRP} \left[ \frac{1.2}{1 + 0.2 \exp \left( 15 \frac{u_L}{u_V} \right)} \right] \quad 91$$

Correlation refined by Wang *et al.* (2006):

$$\frac{a_e}{a} = \left( \frac{a_e}{a} \right)_{SRP} \times 0.17 \left( \frac{\rho_L}{\rho_V} \right)^{0.6} \exp \left( -\frac{0.15}{u_V} \right) \quad 92$$

### 2.11.3 Delft Model

The Delft model for the interfacial area was, at first, a purely empirical correlation fitted on absorption data of CO<sub>2</sub> in a dilute aqueous solution of NaOH. It was also assumed that all types of structured packing experience the same degree of wetting and liquid spreading. This led to Equation 93, where A and B are the packing type and size specific constants (for Montz™ pak B1-250, A=2.143x10<sup>-6</sup> and B=1.5), and Ω is the fraction of the packing occupied by holes (0.1 for Montz™-pak, BSH, and other packing with holes e.g. Mellapak™ and Flexipac structured packing) (Olujic *et al.*, 1999).

$$a_e = a_p \frac{(1 - \Omega)}{\left( 1 + \frac{A}{u_L^B} \right)} \quad 93$$

Olujic *et al.* (1999) also realized that this was the weakest point in the model for predicting the efficiency of structured packing. Fair *et al.* (2000) suggested that the Delft and SRP models should refine their models by incorporating the effective liquid flow angle that was developed by Spekuljak and Billet (1987), but this only leads to minor improvement in both the SRP and Delft models. Later, Olujic *et al.* (2004) made changes to the effective area correlation by including the effective interfacial area, developed by Onda *et al.* (1968), for random packing, leading to the development of Equation 94 and Equation 95.

$$a_e = (1 - \Omega) a_{e,Onda} \quad 94$$

$$a_{e,Onda} = a \left\{ 1 - \exp \left[ -1.45 \left( \frac{0.075}{\sigma_L} \right)^{0.75} \text{Re}_L^{0.1} \text{Fr}_L^{-0.05} \text{We}_L^{0.2} \right] \right\} \quad 95$$

With the dimensionless numbers defined as:

$$\text{Re}_L = \frac{u_L \rho_L}{a \mu_L} \quad 96$$

$$\text{Fr}_L = \frac{u_L^2 a}{g} \quad 97$$

$$\text{We}_L = \frac{u_L^2 \rho_L}{\sigma_L a} \quad 98$$

## 2.12 Mass Transfer

### 2.12.1 Billet and Schultes Model

#### *i. Mass Transfer in the Liquid Phase*

Billet and Schultes (1993) developed a mass transfer model where they assumed that the liquid is constantly remixed at the surface of the packing and therefore the mass transfer in the liquid phase occurs by non-steady state diffusion, as described by Equation 99.

$$k_L = \frac{2}{\sqrt{\pi}} \sqrt{D_L \frac{1}{\tau_L}} \quad 99$$

In equation 99,  $D_L$  is the diffusion coefficient of the transferring component and  $\tau_L$  is the time necessary for the renewal of the interfacial area. The renewal time is calculated with Equation 100 and takes the liquid hold-up, length of the flow path, and liquid superficial velocity into account. Efficiency of the packing is influenced by the length of the flow path ( $l_t$ ), which determines the contact as well as the residence time of the liquid in the packing. Through a dimensional analysis of the influencing parameters, Billet and Schultes (1993) found that the length of the flow path could be best described by the hydrodynamic diameter ( $d_h$ ) defined by Equation 101:

$$\tau_L = h_L l_t \frac{1}{u_L} \quad 100$$

$$l_t = d_h = 4 \frac{\mathcal{E}}{a} \quad 101$$



A volumetric mass transfer coefficient for the liquid phase (Equation 102) was derived by combining equation 100 and 99 and substituting it into Equation 28.

$$k_L a_e = C_L \left( \frac{g \rho_L}{\mu_L} \right)^{1/6} \left( \frac{D_L}{d_h} \right)^{1/2} a^{2/3} u_L^{1/3} \left( \frac{a_e}{a} \right) \quad 102$$

where  $C_L$  is a constant that characterises the shape of the structured packing.

## ii. Mass Transfer in the Vapour Phase

The volumetric mass transfer coefficient for the vapour phase (equation 104) is determined in a similar manner, with the time interval required for the renewal of the contact area ( $\tau_v$ ) defined in terms of the void fraction, liquid hold-up, flow path, and the superficial gas velocity (Equation 103).

$$\tau_v = (\varepsilon - h_L) l_\tau \frac{1}{u_v} \quad 103$$

$$k_v a_e = C_v \frac{1}{(\varepsilon - h_L)^{1/2}} \frac{a^{3/2}}{l_\tau^{1/2}} D_v \left( \frac{u_v \rho_v}{a \mu_v} \right)^{1/6} \left( \frac{\mu_v}{\rho_v D_v} \right)^{1/3} \left( \frac{a_e}{a} \right) \quad 104$$

Where  $C_v$  is similar to  $C_L$  and also describes the structure and surface area of the packing.

## 2.12.2 SRP Model

### i. Mass Transfer in the Liquid Phase

The SRP model uses the penetration theory to calculate the liquid side mass transfer coefficient (Rocha *et al.*, 1996):

$$k_L = 2 \sqrt{\frac{D_L C_E u_{L,e}}{\pi S}} \quad 105$$

where the factor  $C_E$  accounts for surfaces that do not experience rapid surface renewal.  $C_E$  for structured packing is normally assumed to be 0.9.

In the SRP model, the liquid mass transfer coefficient is noted with  $C_E$  in the nominator in Rocha *et al.* (1996) (see equation 105) and with  $C_E$  in the denominator in Rocha *et al.* (1992) (see equation 106). The  $C_E$  term for both equations 105 and 106 has the same definition and value (0.9 for structured packing), thus a 20% difference between the two predictions for structured packing can be expected. This discrepancy may have originated from a typing error, but it leads to great confusion when applying the model to distillation designs. For example, Rejl *et al.* (2010) use Equation 105, whereas Wang *et al.* (2005) use Equation 106.

$$k_L = 2 \sqrt{\frac{D_L u_{L,e}}{\pi C_E S}} \quad 106$$

The Delft model uses an equation that is similar to equation 106 to predict the liquid phase mass transfer coefficient and from this it seems that equation 99 is the correct form for the SRP equation. However, for the rest of the study the liquid side mass transfer coefficient published in Roch *et al.* (1996) will be used, because it is the latest published version by the authors.

## ii. **Mass Transfer in the Vapour Phase**

The vapour phase mass transfer coefficient used in the SRP model is based on the wetted-wall relationship, which was first derived by Johnstone and Pigford (1942). This coefficient was later used by Bravo *et al.* (1985) for gauze structured packing, where it was assumed that the packing surface area was wetted completely (Equation 107).

$$\frac{k_V S}{D_V} = 0.0338 \left( \frac{u_V S \rho_V}{\mu_V} \right)^{0.8} \left( \frac{\mu_V}{D_V \rho_V} \right)^{0.33} = 0.0338 \text{Re}_g^{0.8} \text{Sc}_g^{0.333} \quad 107$$

Thereafter, this model was extended to sheet metal structured packings where it is known that the surface is not always wetted completely at all liquid loads. The Reynolds number was adjusted by replacing the superficial gas velocity with the relative gas to liquid velocity. The constant 0.0338 was also adjusted to 0.054 by fitting it on experimental data. From this the vapour phase mass transfer coefficient is defined by Equation 108.

$$\frac{k_V s}{D_V} = 0.054 \left( \frac{(u_{V,e} + u_{L,e}) \rho_V s}{\mu_V} \right)^{0.8} \left( \frac{\mu_V}{D_V \rho_V} \right)^{0.33} \quad 108$$

Where the effective vapour  $u_{V,e}$  and liquid  $u_{L,e}$  velocities are defined as:

$$u_{V,e} = \frac{u_V}{\varepsilon(1-h_L) \sin \theta} \quad 109$$

$$u_{L,e} = \frac{u_L}{\varepsilon h_L \sin \theta} \quad 110$$

### 2.12.3 Delft Model

#### iii. Mass Transfer in the Liquid Phase

For the liquid mass transfer coefficient the Delft model uses the penetration theory defined by Fair *et al.* (2000), but prefers the hydrodynamic diameter ( $d_{hG}$ ) to the corrugation side dimension ( $s$ ). From this the liquid mass transfer coefficient is defined by Equation 111.

$$k_L = 2 \sqrt{\frac{D_L u_{L,e}}{\pi d_{hV} 0.9}} \quad 111$$

#### iv. Mass Transfer in the Vapour Phase

The Delft model uses a vapour phase mass transfer coefficient that is the geometric mean between the turbulent and laminar vapour transfer coefficients. Vapour phase mass transfer coefficients in both regimes are described by the Schmidt number and relative gas to liquid Reynolds numbers, the length of the packing element, hydrodynamic diameter, and the gas-liquid friction coefficient. Equations 112 to 114 are used to calculate the vapour mass transfer coefficients.

$$k_V = \sqrt{k_{V,lam}^2 + k_{V,turb}^2} \quad 112$$

$$\frac{k_{V,lam} d_{hV}}{D_V} = 0.664 Sc_V^{1/3} \sqrt{Re_{Vrv} \frac{d_{hV}}{l_{V,pe}}} \quad 113$$

$$\frac{k_{V,turb} d_{hV}}{D_V} = \frac{Re_{V,r} Sc_V \frac{\xi_{GL}\phi}{8}}{1 + 12.7 \sqrt{\frac{\xi_{GL}\phi}{8}} (Sc_V^{2/3} - 1)} \left[ 1 + \left( \frac{d_{hV}}{l_{V,pe}} \right)^{2/3} \right] \quad 114$$

In the above equations the relative Reynolds and Schmidt numbers are defined as:

$$Re_{V,r} = \frac{\rho_V (u_{V,e} + u_{L,e}) d_{hV}}{\mu_V} \quad 115$$

$$Sc_V = \frac{\mu_V}{\rho_V D_V} \quad 116$$

## 2.13 Evaluation of Models

In this section the three semi-empirical models (Billet, SRP and Delft) will be evaluated and compared according to their predictions regarding: i) liquid hold-up, ii) effective interfacial area, iii) liquid and vapour side mass transfer coefficient, and iv) the height equivalent to a theoretical plate. The conditions for the evaluation are given in Table 10, and the constants used for the models are discussed thereafter. The physical properties used for the evaluation are given in Table A 6 in the Appendix.

**Table 10 – Testing conditions for model evaluations**

Pressure	Test mixture	Packing	Manufacture	Surface area	Column diameter
1 bar	2-butanol/iso-butanol	Structured packing	Sulzer	350Y	0.2 m

### **Constants Used**

The SRP model requires four constants to predict the efficiency and pressure drop of corrugated sheet structured packing. The constants used in this study are presented in Table 11. One of the problems when using the generalized SRP model is the pressure drop at flooding (Gualito *et al.*, 1997). In the generalized SRP model it is assumed that most of the structured packing will flood at a pressure drop between 900 and 1200, and a value of 1025 Pa/m was chosen as the flooding pressure drop to simplify the model even further (Rocha *et al.*, 1993). However, this value does not hold true for all packings, and therefore needs to be adjusted to predict the efficiencies over the entire operating range. The same

problem with the flooding pressure drop was observed by Gualito *et al.* (1997) and Uresti-Melendez and Rocha (1993). Therefore, the flooding pressure drop was adjusted from 1025 Pa/m to 1650 Pa/m to solve the equations for hold-up at higher vapour load factors.

**Table 11 – SRP model constants**

Constant	Description	Value
A	Dry $\Delta P/\Delta Z$ friction constant	0.177
B	Dry $\Delta P/\Delta Z$ friction constant	88.77
FSE	Surface enhancement factor	0.35
$(\Delta P/\Delta Z)_{\text{flood}}$	Flooding pressure drop (Pa/m)	1650

The Billet model requires six experimentally determined constants to predict the efficiency and pressure drop of structured packing. However, there are no packing constants available for Mellapak™ 350Y and it was therefore decided to use the same packing constants as used by Erasmus (2004) for Flexipac 350Y (see Table 12), since the specific surface areas of the two packings are the same. The constants used for Flexipac 350Y by Erasmus (2004) are:

- *Dry pressure drop ( $C_p$ ) was fitted on dry pressure drop data for Flexipac 350Y.*
- *Published constants for loading ( $C_s$ ) and flooding ( $C_{FI}$ ) point for Mellapak™ 250Y were found to accurately predict the pressure drop of air/water and air/kerosol systems of Flexipac 350Y.*
- *For the mass transfer coefficients the constants of Montz™pak B1-300 were used as it has a geometric surface area closest to that of Flexipac 350Y.*

**Table 12 – Billet model constants proposed by Erasmus (2004)**

Constant	Description	Value
$C_s$	Constant for loading point resistance factor	3.157
$C_{FI}$	Constant for flooding point resistance factor	2.464
$C_L$	Constant for liquid side mass transfer	1.165
$C_V$	Constant for vapour phase mass transfer	0.422
$C_h$	Ratio of wetted to geometric area	0.482
$C_p$	Constant for dry bed resistance factor	0.172

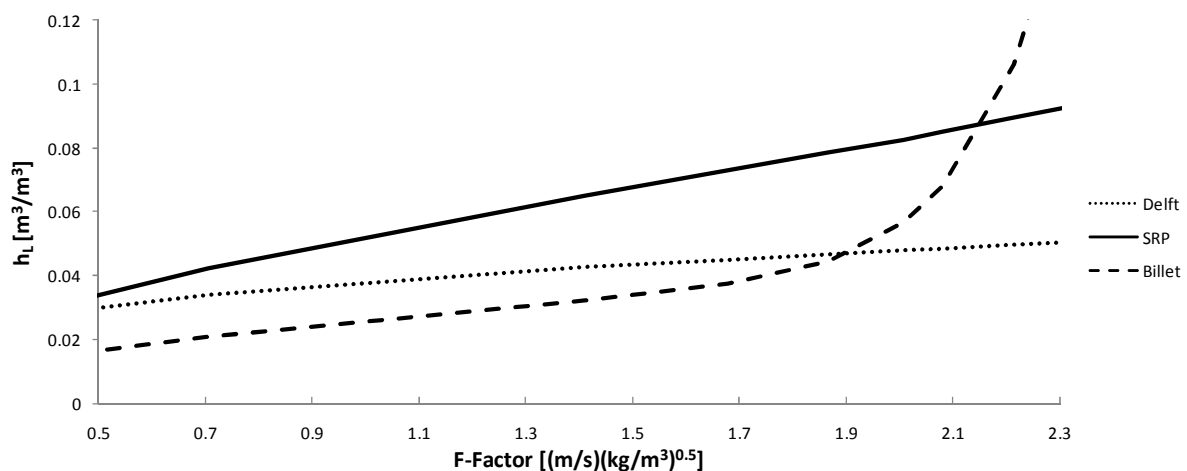
The Delft model needs three geometric related constants and therefore is the only semi-empirical model used in this study that does not require any experimental pre-determined constants. However the newest version of the Delft model uses the effective interfacial area developed by Onda *et al.* (1968) and only requires the constant that represents the fraction of packing surface occupied by holes ( $\Omega$ ) to predict the efficiencies of structured packing. The constants used for the Delft model are presented in Table 13. The Delft model was developed for a column where the packing element height was smaller than the column diameter, which was not the case for this study. It was therefore decided to set the fraction of the channels ending at the wall column equal to one; this was done to avoid any mathematical errors.

**Table 13 – Delft model constants**

Constant	Description	Value
A	For effective interfacial area	2.14E-06
B	For effective interfacial area	1.5
$\Omega$	Fraction of packing surface occupied by holes	0.1

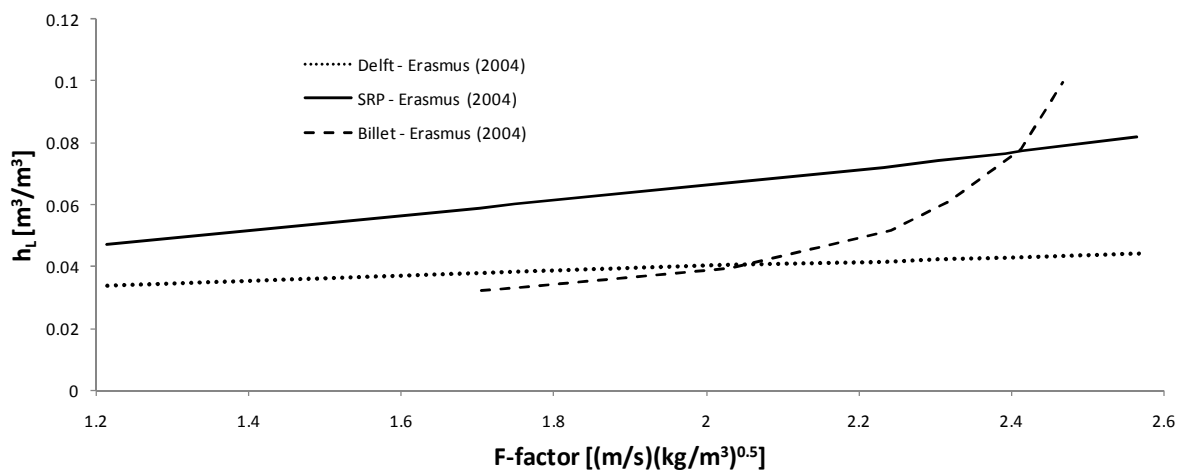
**i. Liquid Hold-up**

The liquid hold-up in a distillation column is of great importance, since it influences the pressure drop as well as the mass transfer efficiency of the column. The three semi-empirical model predictions for liquid hold-up are illustrated in Figure 18 and discussed thereafter.



**Figure 18 – Graphical evaluation of three semi-empirical liquid hold-up models**

The Delft and SRP model predict the liquid hold-up as an almost linear function of superficial gas velocity (see Figure 18). As stated in Section 2.10.1, the liquid hold-up predicted by the Billet model is based on a 13<sup>th</sup> order empirical polynomial correlation derived from experimental observations, therefore taking the shape of the liquid hold-up curve that rapidly increases after the loading point. For this reason it can be expected that the Billet model will show a sharper increase in the HETP as well as the pressure drop for Mellapak™ 350Y packing than the predictions of the SRP and Delft model. Of the three semi-empirical models, the Billet model predicts the shape of the liquid hold-up curve most realistically (see Figure 18). However, the drawback of the model is that it requires six packing constants, and inaccurate prediction of the loading and flooding points will lead to large errors in the model predictions. In Figure 19 liquid hold-up trends for the three predictive models by Erasmus (2004) for Flexipac™ 350Y structured packing at 1 bar abs with chlorobenzene/ethylbenzene are plotted against the vapour capacity factor.



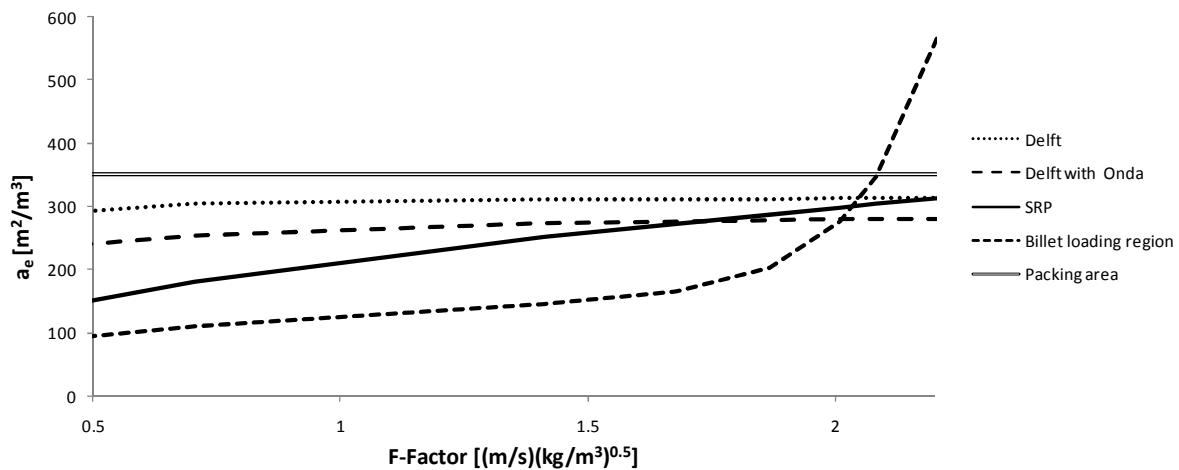
**Figure 19 – Graphical evaluation of three semi-empirical liquid hold-up models  
Redrawn from Erasmus (2004)**

Figure 19 shows that the liquid hold-up from Erasmus has similar trends to that observed in Figure 18, thus indicating that the equations are setup in the correct manner.

## **ii. Effective Interfacial Surface Area**

In Figure 20 the effective surface areas predicted by the three models are graphically compared. It can be seen that the Delft model predicts the effective surface area to be close to the specific area of the packing for the entire operating range, whereas the SRP and Billet

models predict a gradual increase. From Figure 20 it can be seen that the Delft model predicts an effective surface area that is approximately 90 % of the packings' surface area. The Delft model that is corrected with Onda's correlation is also plotted in Figure 21, and only leads to a minor decrease in the prediction of the effective surface area for the model (Fair *et al.*, 2000). Effective interfacial area predicted by the SRP is based on work done by Shi and Mersmann (1985), and the model shows an almost linear increase with increases in the vapour capacity factor. The Billet model predicts an exponential increase in effective interfacial area because it uses a 13<sup>th</sup> polynomial to predict the effective surface area in the loading region. The success of the Billet model will again be dependent on accurate predictions of the loading points.



**Figure 20 - Graphical evaluation of three semi-empirical effective interfacial area models**

### **iii. Liquid and Vapour Mass Transfer Coefficients**

The three semi-empirical liquid and vapour mass transfer models that are studied are graphically compared in Figure 21 and Figure 22.



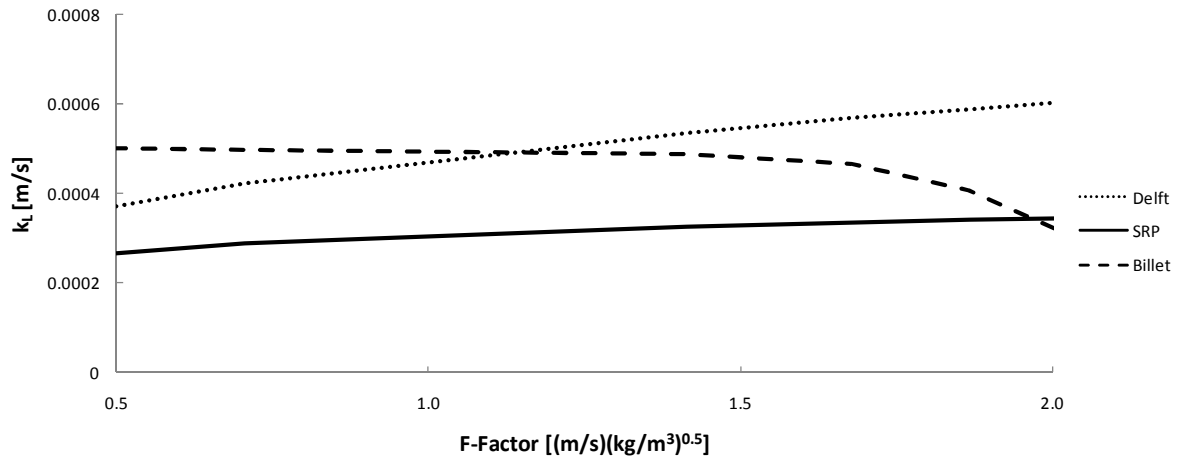


**Figure 21 – Graphical evaluation of three semi-empirical liquid mass transfer coefficients**

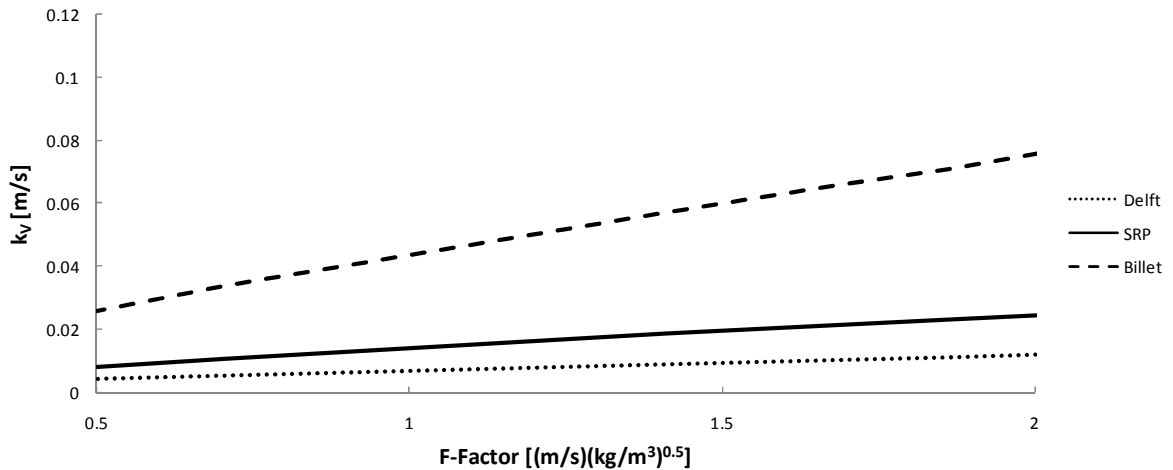


**Figure 22 - Graphical evaluation of three semi-empirical vapour mass transfer coefficients models**

The SRP and Delft models use similar liquid side mass transfer coefficients. The main difference between the two models is that the 0.9 factor is in the numerator of the SRP model (using equation 105) and in the denominator of the Delft model. This difference causes the two models to predict the liquid side mass transfer coefficient with approximately a 20 % difference. The Billet model uses volumetric liquid and vapour mass transfer coefficients when calculating the efficiency of structured packing, which is the product of a mass transfer coefficient and the effective surface area. Thus, the volumetric mass transfer coefficient is divided by the effective surface area (that is predicted by the

Billet model) to obtain a mass transfer coefficient comparable to the SRP and Delft predictive models. The Billet model shows a slight decrease in the liquid mass transfer coefficient in the pre-loading region with a sharp decrease in the loading region. The sharp decrease is due to the empirical 13<sup>th</sup> order polynomial used to predict the effective interfacial area.

In Figure 23 it can be seen that all three models predict an increase in the vapour phase mass transfer coefficient with an increase in the vapour capacity factor. The sharp increase in the Billet model is due to the 13<sup>th</sup> order polynomial for the liquid hold-up. Liquid hold-up decreases the void fraction for vapour flow, and therefore increases the vapour side mass transfer coefficient (see Equation 104). Both SRP and Delft models predict almost linear increases for the vapour as well as the liquid side mass transfer coefficients with an increase in the vapour capacity factor (see Figure 21 and Figure 22).

It is important to notice that the liquid side mass transfer coefficient is approximately 100 times smaller than the vapour side mass transfer coefficient predicted by all three models. Spiegel and Meier (1987) found the opposite that the liquid side mass transfer coefficient is always larger than the vapour side mass transfer coefficient.

#### iv. Height Equivalent to a Theoretical Plate

The HETP predicted by the Billet, Delft and SRP models are given in Figure 22.

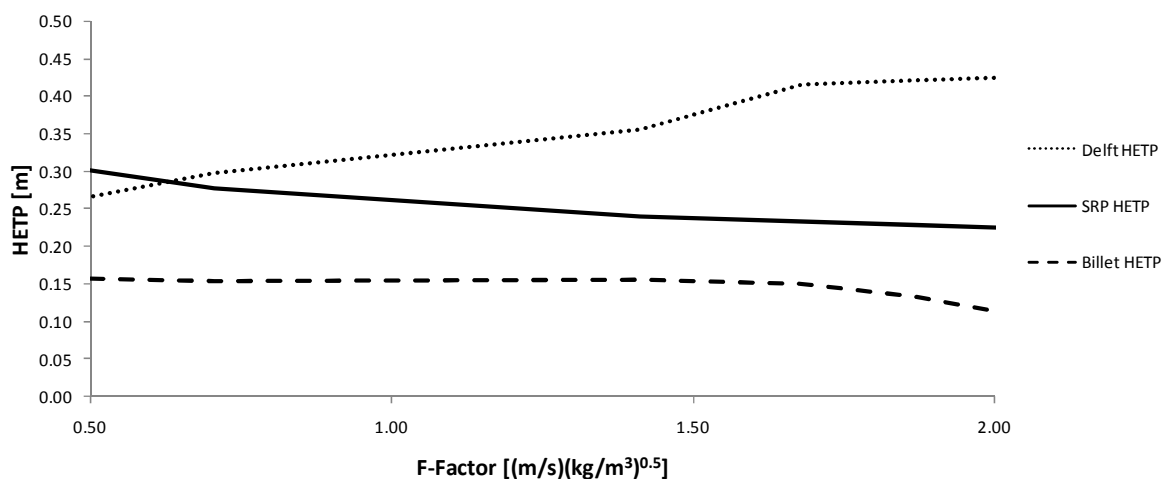


**Figure 23 - Graphical evaluation of three semi-empirical height equivalent to a theoretical plate**

Figure 22 shows that there is a big difference in the predictions of the height equivalent to a theoretical plate predicted by the Billet, Delft and SRP models. The Delft model predicts the largest values for HETP, with the Billet model predicting the smallest values. The decrease in HETP by the Billet model is due to the exponential increase in the liquid hold-up and effective interfacial area. The SRP predicts an HETP that lies almost in the middle of those predicted by the Billet and Delft models. Erasmus (2004) also found that the Delft model predicts the largest values for HETP, followed by the SRP and then the Billet model, thus corresponding to the findings from this study.

From this it is not surprising that the design of packed columns is still mostly based on experimental data obtained from a pilot plant, because predictive models differ in the way they predict the performance of structured packing with a higher surface area.

It is thus essential to generate accurate performance data for structured packing. More data will lead to an improved understanding of the packings' performance and this will lead to the development of new predictive models that can accurately predict the performance of structured packing.

From the findings in the literature review it was decided to construct a test facility that can be used to study the performance of structured packing over the entire operating range. The next chapter will deal with the design and design specifications of the distillation column.

---

## 3 Experimental Setup

---

In the literature review it was found that the Billet and Schultes, Delft and SRP models differ in the way they predict the performance of higher surface area ( $\geq 350 \text{ m}^2/\text{m}^3$ ) structured packing, and therefore it can be expected that it will do the same for the new types of structured packing on the market (Flexipac™ HC™, Mellapak™-Plus™ etc.). There is therefore a need for more experimental data for existing higher area structured packing and new types of packing. The new experimental data will lead to a better understanding of the packings and their performance, and can lead to new and more effective models being developed.

### 3.1 Design Objectives and Limitations

The scope of this study was to design and construct a packed column that can be used to test the efficiency of structured packing. A process concept was developed that allows structured packing to be tested under total reflux. However, provision in the design has been made so that the distillation column can later be converted to a continuous feed column to study the effect of L/V ratio on packing performance. Converting and testing under continuous feed conditions falls beyond the scope of this project. The process concept is discussed in Section 3.2 and the detailed design will be given thereafter.

The main limitation of this project was the size of the available boiler. The steam requirements of the reboiler limited the internal diameter of the column to 0.2m (see calculations in Appendix – Section 8.1). The next section will deal with the design specifications set for the column, and thereafter a detailed design of the column will be given.

### 3.2 Process Concept

The process concept is illustrated in Figure 24. As mentioned in Section 3.1 the pilot plant was designed to operate under total reflux, but can later be converted to a continuous feed column.

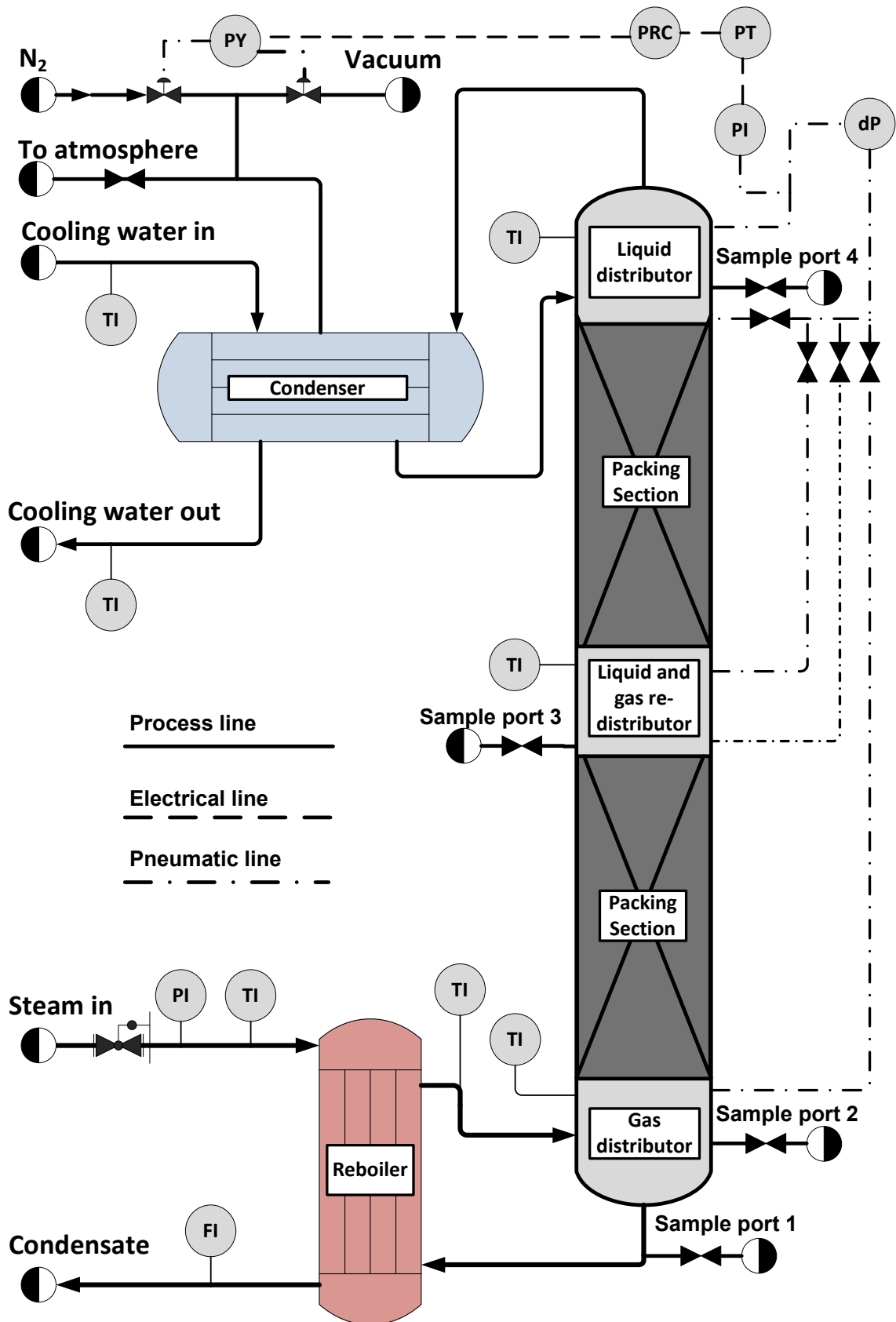


Figure 24 – PFD of distillation column

Total reflux is the condition where no feed streams enter and no product streams are withdrawn from the column. Therefore, all the vapour that leaves the packed bed is condensed in the condenser and the condensate is then returned to the top of the packed bed as reflux. The condensate then flows down under gravity through the packing into the reboiler, where it is vaporised and returned to the packed bed. The vapour and the liquid thus flow counter-currently with respect to one another. The term “total reflux” comes from the fact that all the condensate is returned back to the column and resembles the case where the liquid to vapour flow rate (L/V) ratio is one. The L/V ratio will only be constant throughout the column if there are no heat losses to the environment. Heat losses to the environment may cause some of the rising vapour to condense against the column wall, thereby changing the L/V ratio in the column.

The pilot plant setup had to be built so that it could later be converted to a continuous feed column. For this reason provision had to be made to place an additional feed point on the liquid and gas redistributor. In the case of continuous feed this feed point can be used to convert the column into a continuous feed column, thereby splitting the packed column into absorption and stripping sections.

### **3.3 Design Specifications**

After the literature review and conceptual process design it was found necessary to make certain design specifications and considerations before a detailed design of the packed column could be done. These specifications and considerations are listed below and discussed subsequently. A description of the detailed design is given in Section 3.4.

- *Internal column diameter*
- *Height of packing sections*
- *Test mixture*
- *Operating range*
- *Distribution of vapour and liquid phases*
- *Sampling*
- *Materials of construction*
- *Sensors*
- *Isolation*

### **3.3.1 Internal Column Diameter and Height of Packing Section**

Delft UT is in the process of compiling a document that is aimed at the standardisation of efficiency measurements (Olujić, 2008). In the document a recommendation is made regarding the internal column diameter, namely that when testing the efficiency of structured packing, an internal diameter of at least twice the height of the packing element should be used. Koch-Glitsch™ manufactures packing with element heights ranging from 0.25 m to 0.3 m, thus the recommended column diameter would be 0.6 m. On the other hand Sulzer™ and Montz™ packing element heights range between 0.15 m and 0.21 m and therefore an internal column diameter of 0.4 m would be sufficient. Therefore, Delft UT recommends that a 0.4 m internal diameter column would be a good compromise to test the efficiency of Sulzer™, Montz™ and Koch-Glitsch™ packings.

However, the literature indicates that the efficiency of structured packing is not dependent on the diameter of the packed column, although it does seem to have an effect on the hydrodynamic performance.

The size of the available boiler limited the internal diameter of the column to 0.2 m. This project is also running parallel with another project where the hydrodynamic behaviour of packed columns is characterised. In the hydrodynamic experimental setup the packed column has a column diameter of 0.4 m, and it also allows for systems to be tested other than air/water systems (Lamprecht, 2010).

The efficiency results from the 0.2 m internal diameter column can thus be used in conjunction with the hydrodynamic test to characterise the performance and capacity of structured packing. A similar technique was used by Wu and Chen (1987) with great success.

### **3.3.2 Height of Packing Sections**

The height of the packed section determines the number of theoretical stages of the packed column. It is therefore an important variable that also influences the type of test system used.

Meier *et al.* (1979) found that increasing the packed heights from 1.4 m to 6.6 m showed no effect on efficiency for structured packing. Nevertheless, it is important that a test setup has sufficient height to test the performance of structured packing. It was therefore decided to

equip the column with two packing sections with a liquid and vapour redistributor placed between the two packing sections. Provision for a feed point was made on the liquid and vapour redistributor to later convert the column to a continuous feed column.

More information on the liquid distributors is given in Section 3.4.4 and the detailed design specifications are given in Section 3.4.

### **3.3.3 Test Mixture**

According to the literature (Section 2.6) it is crucial to select the correct test mixture for a specific plant setup. Choosing an incorrect test mixture can lead to high purities in the top and bottom composition that increases the experimental error. Therefore a methodology for the selection process to select a test mixture for a specific distillation application was developed as part of this study. More detail on the methodology is given in Section 3.7.

### **3.3.4 Operating Range**

Modifications to packing have led to capacity increases of packings. New and more effective packings that can operate at F-factors of up to  $4 \text{ (m/s)(kg/m}^3\text{)}^{0.5}$  are entering the market. It can be expected that this value will increase in years to come, and thus provision must be made to accommodate these new types of packing in the pilot plant's testing range. The pilot plant setup must therefore have the capacity to operate at vapour capacity factors of  $0.3 - 4 \text{ (m/s)(kg/m}^3\text{)}^{0.5}$ .

The pressure operating range for most distillation applications lies between 0.1 bar (abs) and 1 bar (abs). It is therefore important that the pilot plant setup is able to operate under vacuum conditions.

### **3.3.5 Distributors**

Good liquid distribution is one of the key requirements to operate a distillation column successfully (Section 2.4). Therefore, it was decided to install a distributor above each bed with a chimney-tray at the bottom of the column to evenly distribute the vapour to the bottom packed section. More information on the design of the distributors is given in Section 3.4.4.

It is also important that the distributor have a high turndown ratio to cover a wide range of liquid loads (Olujić, 2008). The liquid distributor is also normally placed between two to five



centimetres above the packing (Olujić, 2008) and a space of one column diameter is normally left between the chimney-tray and the bottom of the packing (Kister, 1992). The recommended drip points per square meter are between 100 and 150 for testing packing with surface areas from 250 to 500 m<sup>2</sup>/m<sup>3</sup> (Olujić, 2008).

### **3.3.6 Sampling**

High-quality samples are very important when studying the performance of a distillation column, because the HETP of the packing is calculated from the liquid compositions over the packing. It is essential to take a sample that is fresh and representative of the mixture composition at that point. This makes the three distributors ideal for sampling, because they collect and mix all the liquid flowing from each packing section. Additionally, the continuous flow through the distributor ensures that a fresh sample is drawn. It is also important to draw a small sample to ensure that it does not disturb the equilibrium of the system. The sampling technique and sampling device are discussed in detail in Section 3.4.5.

### **3.3.7 Materials of Construction**

Distillation columns normally operate at high temperatures with corrosive solvents. It is therefore important to select the correct materials for construction to prevent leaking of the vapours and spilling of solvents that are harmful to the operator and environment. Leakage of flammable liquids can also lead to an explosion. For these reasons it is necessary to select the correct construction materials and seals. Stainless steel, grade 316SS, is usually the preferred choice for construction materials (Olujić, 2008), and seals made from ceramic fibre or polytetrafluoroethylene (PTFE) can be used with most organic solvents.

### **3.3.8 Sensor Placing**

Temperature and pressure sensors are used to monitor and study the behaviour of packed columns. Thus, the correct choice of sensors and placement of sensors are important to accurately monitor the behaviour of the distillation column. It is also important that the sensors have the right specification and ranges to measure the entire operating range. The placement of the sensors is discussed in Section 3.4.7, and the specifications of each sensor are given in the Appendix – Section 8.4.

### **3.3.9 Insulation**

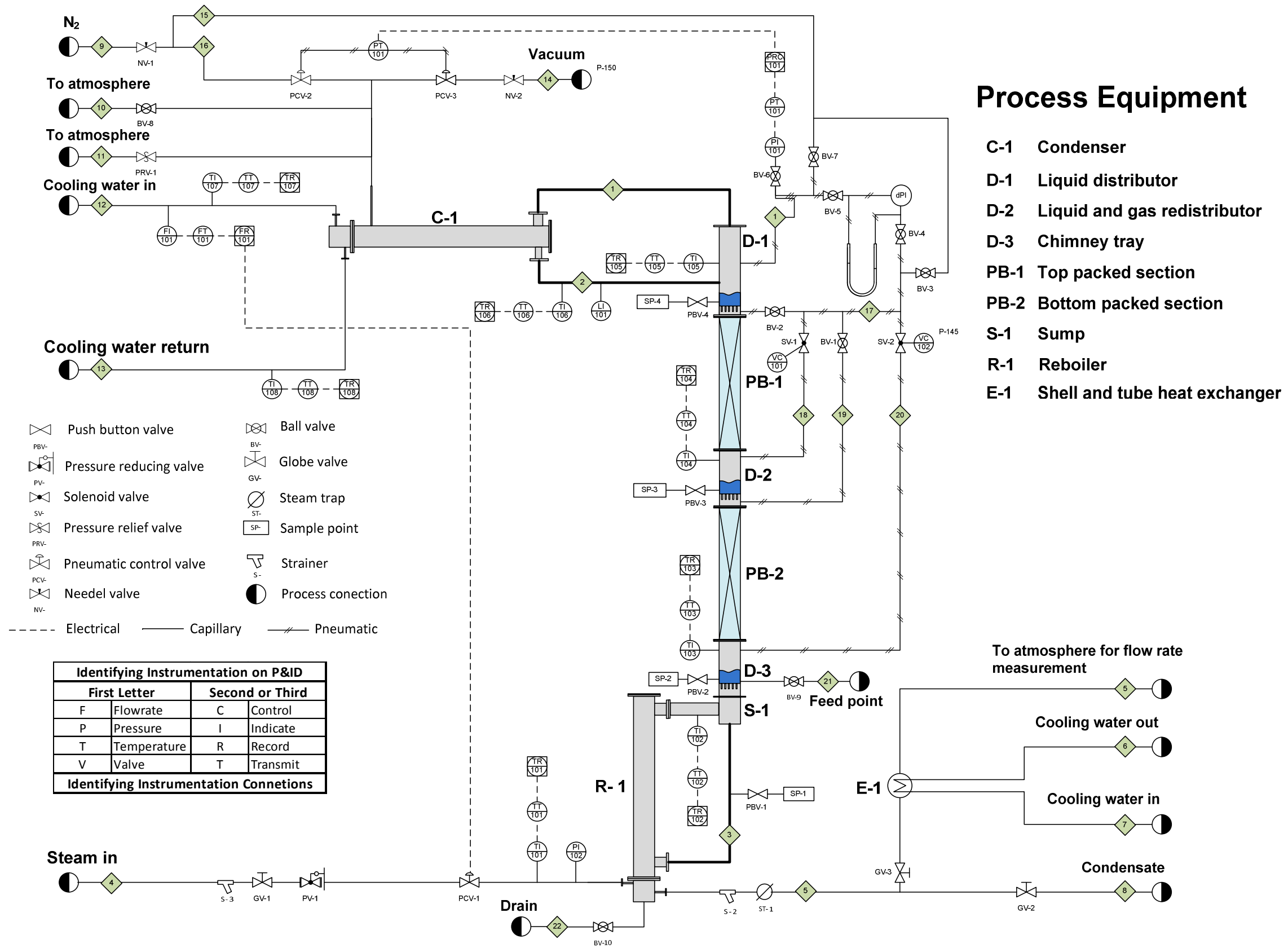
Heat losses to the environment are unwanted because i) they cause some of the rising vapour to condense at the column wall, thus promoting unwanted wall flow and lead to a change in the liquid-to-vapour ratio, and ii) they increase the operating cost of the pilot plant. The pilot plant must therefore be well insulated to minimise the effect of heat losses. Insulation material can be bought in various shapes and sizes to fit around the piping and sections of the column. To minimise heat losses even further, it was decided to equip the pilot plant with a steam tracing system. Section 3.4.8 provides more detail on the steam tracing system.

## **3.4 Detailed Design Specification**

The detailed design was based on the design objective, process concept, and design specifications given in Sections 3.1 to 3.3. The specifications and outcome of the final design specification is given in this section and the detailed drawings of the main components are given in Appendix – Section 8.3.

The pilot plant setup was built on the premises of the University of Stellenbosch and the design and construction of the pilot plant took approximately two years to complete and an additional six months to commission. A process and instrumentation diagram (P&ID) of the column is shown in Figure 25 and each of the main components in the experimental setup is discussed thereafter.







### 3.4.1 Reboiler

The capacity of the boiler determines the amount of heat available to vaporise the liquid mixture, and therefore determines the maximum column diameter that can be used.

A thermosyphon reboiler (TSR) was used in the experimental setup (recall Section 3.2) to vaporise the liquid. The reboiler uses steam (supplied by a diesel boiler) as a heating source. The diesel boiler can supply steam at a pressure of 10 bar and has a maximum capacity of 400 kg/h.

The steam lines that run from the diesel boiler to the TSR is well insulated to minimise any heat losses. Before the steam enters the TSR, it passes through a Y-strainer, isolating valve; pressure reducing valve and a control valve (see Figure 25). A globe valve is used as an isolating valve to seal the line off when the plant is not in operation, where a PN17 valve is used to reduce the pressure from 10 bar to the desired operating value. The PN17 valve works with a pneumatic system that controls the pressure within a 1 % accuracy band. A pneumatic control valve connected to a programmable logic computer (PLC) interface is used to control the steam volumetric flow rate to the reboiler. A constant volumetric flow rate and steam pressure ensures a constant steam supply to the column, and leads to a constant vapour flow rate in the packing sections. The temperature and pressure of the steam are measured with a thermocouple and a pressure gauge before it enters the TSR. Steam is trapped in the reboiler with a ball float steam trap. The condensate is then cooled by a shell-and-tube heat exchanger to ensure all the steam is condensed before the flow rate is measured with a 25 litre water bucket and a stop watch over a period of 10 minutes. Cooling water is used as the cooling medium in the shell-and-tube heat exchanger. The condensate was measured on a scale with an accuracy of up to  $\pm 0.01$  kg, giving an accuracy of 0.13% for the measurements (typical condensate flow rate ranged between 8 – 16 kg). The bucket weight is subtracted and the net weight of the condensate is recorded. The condensate flow rate together with the heat of vaporisation of the steam is then used to calculate the flow rate of the vapour inside the distillation column.

The TSR is positioned vertically and was manufactured from 316 stainless steel (SS). The TSR was finally well insulated with 40mm glass wool and equipped with steam tracing to ensure minimal heat losses. A detailed drawing of the reboiler is presented in Appendix –

Section 8.3 and photos of the steam tubes inside the reboiler are shown in Figure 26. The steam flows through the tubes. The TSR and the sump have a capacity of approximately 50 L.



a)



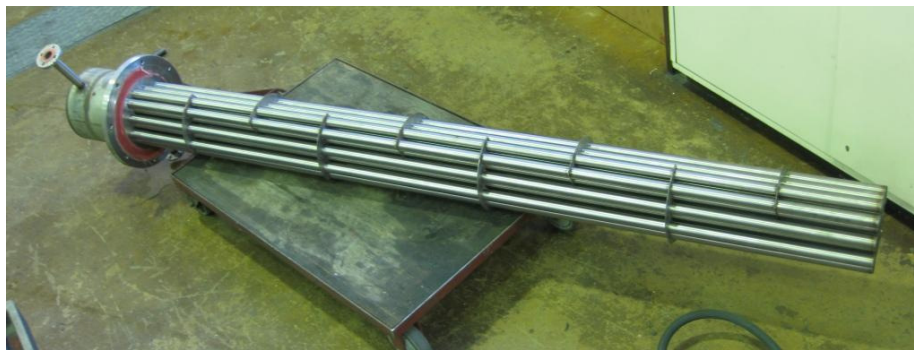
b)

**Figure 26 – Reboiler Photos: a) Steam tubes inside the thermosyphon reboiler, b) baffle plate**

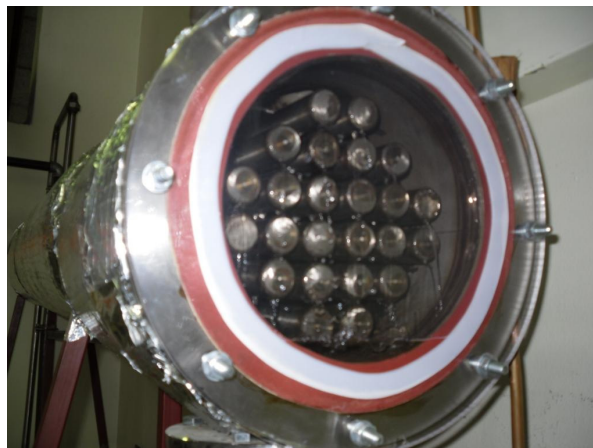
### 3.4.2 Condenser

The condenser is a total condenser and has a similar design to that of the thermosyphon reboiler. However, it is placed horizontally, is equipped with baffle plates and uses cooling water that is supplied via a closed water cooling system to condense the vapour. The condensate is returned to the column by gravity. Stainless steel 316SS is used as construction material and the condenser is well insulated with glass wool to minimise the heat losses. The cooling water flow rate, inlet and outlet temperatures are recorded by the PLC. The cooling water is supplied at a temperature of approximately 17 °C and flow rate of 2.3 kg/s. A pressure control line has been installed for the condenser. The condenser is also placed at a slight angle to ensure all the condensate drains out.

A detailed drawing of the condenser is given in Appendix – Section 8.3. Photos of the cooling water tubes with baffle plates and of the condenser during operation are presented in Figure 27. The photo of the condenser during operation was taken during the commissioning phase, when the plant was operated with water. The photo was taken to observe the flow patterns inside the condenser and to make sure that the flow of liquid back to the column is constant during operation, thus giving a constant liquid flow inside the packed sections. The clear flange is made from polycarbonate. After the test run it was replaced with a 20 mm thick 316SS flange.



a)



b)

**Figure 27 – Condenser Photos: a) Cooling water tubes with baffle plates, b) Condenser during operation.**

### 3.4.3 Packing Sections

The structured packing is found in the two packed sections (recall Figure 24), which can be seen as the heart of the experimental setup, i.e. the targeted area for testing. Both packing sections have a height of 2 m and can hold seven packing elements of Koch-Glitsch™ (350Y HC™ height = 0.27 m) or nine packing elements of Sulzer™ (Mellapak™ 350Y height



0.21 m), thus giving a total packed height per packing section of 1.89 m for both types of structured packing. The total packed height is 3.78 m (2 x 1.89 m).

The outer shells of both the packing sections are manufactured from 316SS, and are well isolated with glass wool. They are also equipped with steam tracing to minimise the heat losses as well as to avoid some of the rising vapour condensing against the wall. The packing elements are supported in the packing section by support pins that are welded to the inside of the packing section wall. Figure 28 shows the support pins.

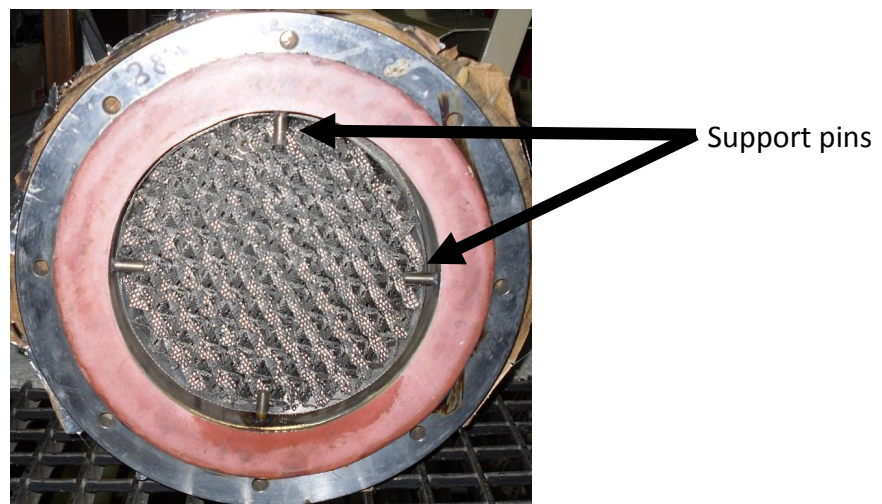


**Figure 28 – Structured packing support pins**

### **3.4.4 Distributors**

As seen in Figure 24, three distributors are used in the experimental setup, namely:

- *Liquid distributor*
- *Gas and liquid redistributor*
- *Gas distributor*

The design of the distributors was provided by Dr A Erasmus from Sasol. Each of these distributors has a similar design but differs in their functionality. The design and functional differences of each distributor will be briefly discussed. The base design of all three distributors is illustrated in Figure 29 and the drip tubes and chimney pipes with hats are illustrated in Figure 30. Liquid samples are drawn from the distributors. Note that sampling techniques are discussed in detail in Section 3.4.5.

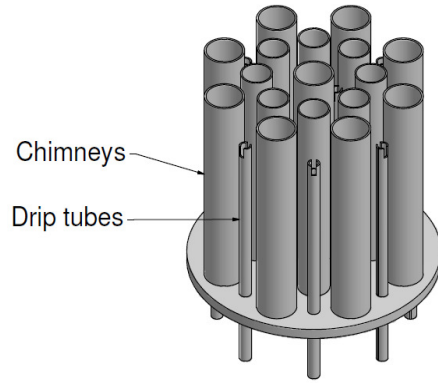


**Figure 29 – Base design of the distributors**

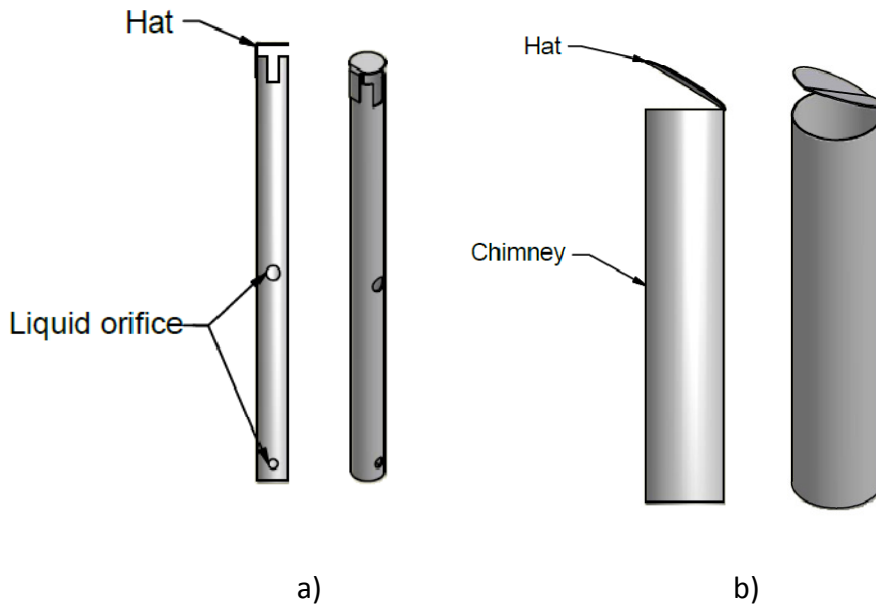


**Figure 30 – Distributors internals a) Drip tubes and b) Chimney tubes**

The basic design of all distributors includes 11 drip tubes and 17 chimney tubes, thus giving a drip point density of 350 drip points/m<sup>2</sup>. Gas flows through the chimney tubes and liquid through the drip tubes (Figure 30). The distributors are manufactured from 316SS and the liquid orifices are sized to handle liquid flow rates between 5 and 25 m<sup>3</sup>/(m<sup>2</sup>.h). The distributor will start to run dry below a flow rate of 5 m<sup>3</sup>/(m<sup>2</sup>.h). Above 25 m<sup>3</sup>/(m<sup>2</sup>.h), the drip tubes will overflow, and flow through the chimney tubes might occur. Both of these conditions are undesirable and must be prevented. All the distributors are placed approximately 5cm above the packed bed, and all the distributor's sections are insulated

with glass wool and equipped with steam tracing. A detailed drawing of the distributing section can be found in Appendix – Section 8.3.

The liquid distributor is used to distribute the condensate evenly over the packing (Figure 29). The condensate enters the distributing section through a feed point which is situated 5cm above the surface of the distributor. No hats are installed on the drip tubes or the gas risers as there is no additional liquid that flows to the distributor from above it, rendering these unnecessary.

The liquid and gas redistributor collects all the liquid from the packing section above and then mixes and redistributes it evenly over the bottom packing section (Figure 29). The gas is also redistributed to the top packing section. Thus, it is necessary that this distributor be equipped with hats on both the drip and chimney tubes to prevent the liquid from interfering with the rising gas flow, as well as to prevent the liquid from bypassing the distributor. If liquid bypasses the distributor, it will lead to a non-representative sample (taken from the distributor). It can be expected that the hats on the chimney tubes will cause an additional pressure drop over the distributors compared to the liquid distributor without the hats.

The gas distributor is used to distribute the vapour from the reboiler evenly over the packing above and to collect all the liquid flowing from the packing to ensure a representative liquid sample. The gas distributor is thus also equipped with hats on both the drip tubes and chimney tubes.

### **3.4.5 Sampling**

#### ***i. Sampling Procedure***

Samples are drawn from each of the three liquid distributors and one from the reboiler (see Figure 24), giving four samples per data point. The samples drawn from the distributors are used to determine the HETP of the top and bottom packed section. The sample taken from the reboiler is used to monitor the column composition between and during runs as well as to estimate the heating properties of the mixture. Figure 31 illustrates one of the sampling devices used.

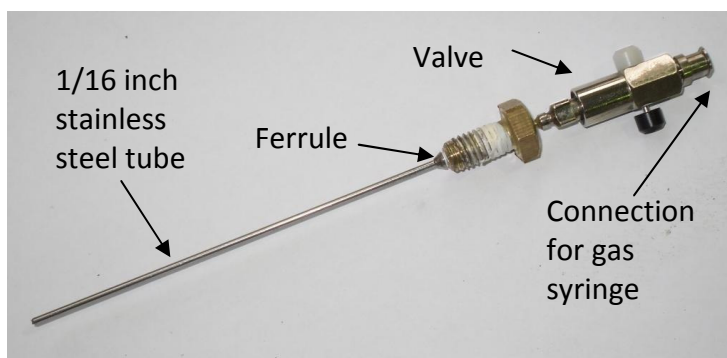


**Figure 31 – Sampling device that was used**

The sampling devices screw into the column and seal tightly on the stainless steel ferrule. A gas tight syringe is then screwed into the sampling device and is used to draw a 1 ml sample through the 1/16" tube. The valve seals off the sampling port when it is not in use. The sample is injected into a 2 ml gas tight sampling bottle, by using the gas tight syringe and a needle (which screws onto the syringe). The reason for using gas tight instrumentation is to ensure that none of the volatile components evaporate during the sampling process, which would lead to an incorrect representation of the actual composition. Sampling lines are flushed before each sample is taken to eliminate the effect of dead volume in the device. Each of the sampling ports has its own syringe. The syringes are washed with acetone and dried in between samplings. All the samples are taken within a period of approximately 5 minutes starting at the reboiler (Sample port 1). Intermediate samples in between the packing elements are not taken in this study. This was not done because it is very difficult to take a good representative sample of the liquid mixture flowing down the packing and, the fact that the height of packing elements from each vendor is different makes it difficult to position the sampling point along the packed sections. Samples are cooled in a freezer before they are prepared for analysis to minimise the possibility of volatile components evaporating during the sample preparation process.

## **ii. Analyses of Samples**

Analytical grade acetone was used to dilute the samples before they were analysed with a Varian CP3380 GC (gas chromatograph) with FID detector and auto sampler using a Zebron ZB-5 (60 m x 0.32 mm x 0.25 µm) column. The GC was calibrated with standard solutions that represented the composition at the top, middle, and bottom of the column. These

three standard solutions were also injected before starting the auto sampling sequence to ensure that the GC remained correctly calibrated. Each sample was injected three times and the average composition of the samples was used. Retention time difference between components for the 2-butanol/iso-butanol system was approximately two minutes, and one minute for the p-xylene/o-xylene system.

### 3.4.6 Packing

#### *i. Specifications*

Flexipac 350Y HC and the Mellapak™ 350Y packings were both used for testing. Both of these packings are made from sheet metal that has a perforated and shallow embossed surface. Dimensions of the two packings are given in Table 14.

**Table 14 – Packing dimensions**

Description	Symbol	Units	Mellapak™ 350Y	Flexipac 350Y HC
Surface area	a	m <sup>2</sup> /m <sup>3</sup>	350	350
Corrugation angel	α	°	45	45
Void fraction	ε	-	0.95	0.984
Height of packing element	h <sub>pe</sub>	m	0.21	0.27
Corrugation side	S	mm	12.1	11
Crimp height	h	mm	8.5	7.5
Channel base	b	mm	17.4	16.5
Reference			(Erasmus, 1999)	(Erasmus, 2004)

#### *ii. Installation of Packing*

The packing elements were carefully installed and each packing element was rotated 90° with respect to the previous one. Wall wipers (made from sheet metal gauze to minimise the pressure drop) were bended outwards to ensure that the wall wipers touched the column wall. After the packing was installed and the column was closed, pressure-checks were done on the column to eliminate any possible leaks. Thereafter, the column was filled with an initial charge.

### 3.4.7 Placement of Sensors

As discussed in the design specification (Section 3.3.8) it is very important that the sensors are placed in strategic places to monitor and record the behaviour of the packed column.

The sensors must also be able to accurately measure the conditions in the packed column over the entire operating range. In this section the sensors used are listed first and a discussion on their placement and function in the column are given thereafter.

The following types of sensors were used to monitor the hydrodynamic and thermal behaviour of the distillation column:

- *Pressure sensors*
- *Differential pressure transmitter*
- *Manometer*
- *Absolute pressure transmitter*
- *Temperature sensors*
- *PT 100's*
- *Temperature gauges*
- *Type K thermocouples*
- *Flow meter*
- *Magnetic flow meter*

All the electronic sensors were calibrated and installed by an external company. The specifications of all the sensors are given in Appendix – Section 8.4. The control was done with the help of a PLC interface, which was also used to log all the temperatures, pressures and flow rates of the cooling water.

#### ***i. Differential Pressure Transmitter and Manometer***

A differential pressure transmitter is used to monitor the hydrodynamic behaviour of the column. The pressure transmitter is connected in such a way that the pressure drop over various sections of the column can be measured by opening and closing the correct valves (see Figure 24). The sections of the column that can be monitored with the differential pressure transmitter are listed below:

- *Liquid distributor*
- *Top packing section*
- *Gas and liquid redistributor*
- *Bottom packing section*

A manometer was also installed on the differential pressure lines to enable spot checks on the calibration of the differential pressure transmitter. The placement of the pressure taps are shown in Figure 24 and a detailed sketch of the placement of the pressure connection over the distributors are given in Appendix – Section 8.3. The detailed drawing in the Appendix shows that the pressure taps are made using a large diameter pipe that reduces to a smaller diameter pipe. This was done so that the vapour in the pressure tap can cool down and condense against the larger pipe diameter without blocking the smaller lines that are connected to the pressure transmitters. The condensate flows back to the column under gravity. A nitrogen flushing system was also installed on the pressure lines to flush the lines during experimental runs. This ensures that there is no condensate in the smaller pressure line. Condensate in the pressure lines can lead to incorrect readings on both the differential pressure transmitter and manometer and therefore makes it difficult to detect.

During normal operation, the differential pressure drop reading over the top packing section bed and bottom packing bed was alternated with two solenoid valves that open and close every 10 minutes.

## ***ii. Absolute Pressure Transmitter***

An absolute pressure transmitter is used to measure the operating pressure at the top of the column. As seen in Figure 24, the absolute pressure transmitter shares a pressure tap with the differential pressure transmitter. The measurement of the absolute pressure transmitter is used by a PID controller to control the operating pressure inside the column. The pressure control loop is shown in Figure 24 and the control philosophy behind the control loop will now be discussed.

The control loop works on a push-pull system, with pressurised nitrogen on the one side and a vacuum pump on the other side. If the operating pressure drops below the set point, the pneumatic valve on the nitrogen line will open and the pneumatic valve on the vacuum line will close simultaneously. If the operating pressure goes above the set point, the pneumatic valve on the vacuum line will open and the pneumatic valve in the nitrogen line will close. Both the pneumatic valves on the nitrogen and vacuum lines are closed when operating at the desired set point. The pneumatic valve in the nitrogen line is fail close and the vacuum line is fail open. This is done to prevent a pressure build up in the column in case of a power

failure. A detailed description of the control philosophy and safety interlocks can be found in Appendix – Section 8.6. Needle valves are also installed on both the pressurised nitrogen and vacuum lines to damp the pressure inside the lines, making the control system less aggressive. The needle valves are also used to close both lines when the experimental setup is not in use. A safety relief valve is also installed on the pressure control system to make provision for unforeseen pressure surges. When operating at atmospheric conditions the two needle valves are closed and the valve connected to the atmosphere is opened.

### **iii. Temperature**

Temperature sensors have been placed at strategic places on the inside and outside of the column to monitor the thermal behaviour of the column. The following temperatures were measured and a brief explanation of each one will be given thereafter:

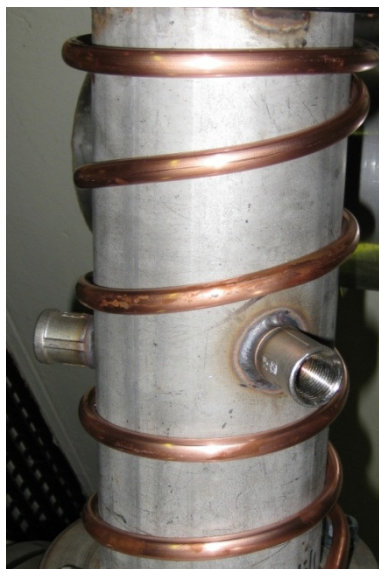
- *Temperature of the vapour space above and below each packing section (PT100)*
- *Temperature in the reboiler (PT100)*
- *Reflux return temperature (PT100)*
- *Steam inlet temperature (thermocouple)*
- *Outside wall temperature of the column (thermocouple)*
- *Cooling water inlet (thermocouple)*
- *Cooling water outlet (PT100)*

The temperatures of the vapour space above and below each packing section were used to calculate the diffusion coefficients as well as the vapour densities. Vapour densities are necessary to calculate the gas capacity factor. The temperature in the reboiler was used to calculate the specific heat capacities of the test mixture. The reflux return temperature was used to calculate the amount of sub-cooling. Steam inlet temperature, together with the inlet pressure, was used to determine the heat of vaporisation of the steam. The outside wall temperature of the column was used to assist with the control of the steam tracing system and the cooling water inlet and outlet temperatures together with the cooling water flow rate were used to enable an energy balance around the condenser. The cooling water flow rates were measured and recorded using a magnetic flow meter that is connected to the PLC interface. Manual temperature gauges were installed with the PT100s to obtain a direct indication of the temperature.



### 3.4.8 Steam Tracing

The experimental setup is fitted with steam tracing to minimise the heat losses and to prevent condensation of the vapour against the column wall. Steam tracing is kept at approximately 3 °C lower than the operating temperature of the column. This is done to prevent the steam tracing from adding external heat to the column and causing some of the liquid flowing down the column to be evaporated. The main purpose of steam tracing is to keep the column at equilibrium conditions and prevent heat loss to the surroundings, i.e. to ensure adiabatic operating conditions. Steam tracing is installed on the whole column except on the condenser and 3/8" copper tubes are used for the steam tracing. Heat transfer cement is used to increase the surface area for heat transfer as well as to eliminate the void fraction between the copper tube and the wall of the column. Illustration of the steam tracing with and without heating cement can be seen in Figure 32.



a)



b)

**Figure 32 – Steam tracing a) without heating cement b) with heating cement**

The steam tracing control loop is shown in Figure 33, and the control philosophy behind the control loop for the steam tracing will now be discussed.

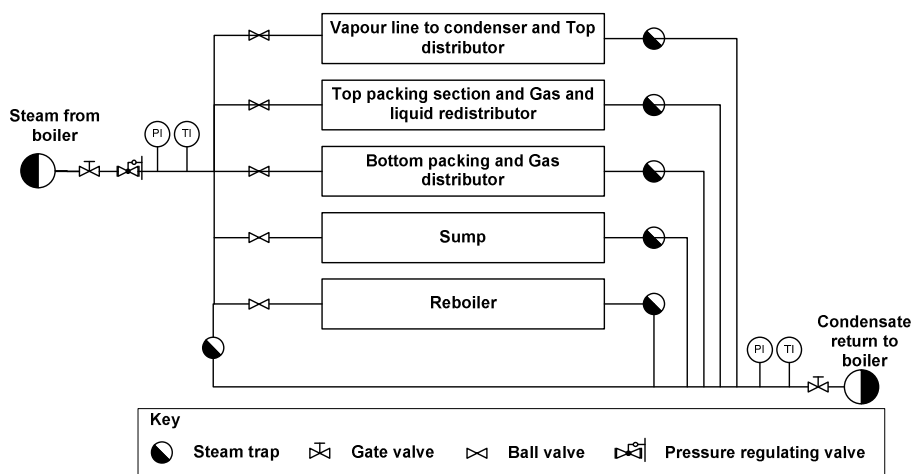


**Figure 33 – Control loop for steam tracing**

The inlet pressure of the steam was controlled manually with a pressure regulating valve. Thus the control of the steam tracing was done manually. A manifold equipped with isolating valves for the various sections was used to distribute the steam to the various sections in the column. Steam tracing should always follow the rule “one tracer – one steam trap” (SpiraxSarco, 1995). According to this rule, each section was equipped with its own steam trap. A steam trap was also used as a draining valve at the lowest point in the manifold, as seen in Figure 33.

### 3.5 Safety

The column is constructed inside a laboratory shared with other students and, the test systems used to evaluate the performance of a distillation column are usually flammable and hazardous. It is therefore essential to use the correct equipment, ensure the safe operation of the column, and to wear the correct personal protective equipment at all times. The correct classification of hazardous and non-hazardous areas are also important, as the sensor selection is based on the classification of the area, i.e. zone 0, zone 1 or zone 2.

The following are the zones defined according to SANS (Standards South Africa, 2005):

**Zone 0:** “Location in which an explosive gas atmosphere is present continuously or for long periods of time.”

**Zone 1:** “Location in which an explosive gas atmosphere is likely to occur in normal operation.”

**Zone 2:** “Location in which an explosive gas atmosphere is not likely to occur in normal operation and, if it does occur, it is likely to do so only infrequently and to exist for a short period only.”

All the zones and sensors must be classified and selected according to SANS 10108:2005 (Standards South Africa, 2005). Calculations for the volume occupied by each zone are based on regulations found in SABS IEC 79-10:1995 (Standards South Africa, 1997). After the zoning process was completed it was found necessary to use intrinsically safe and explosion-proof equipment. The zoning of the column was done in parallel with a hazard and operability study (HAZOP) to incorporate safety interlocks. The installation of all the instruments was done according to SANS 10086-1:2003 (Standards South Africa, 2004) and, thereafter, a certificate of competency (COC) was issued by an approved master electrician. The zoning report and HAZOP can be found in Appendix – Section 8.6.9.

### **3.6 Experimental Procedure**

A short description of the experimental procedure will be given here and a more detailed procedure can be found in Appendix - Section 8.6.

1. Feed the column with the chosen test system.
2. Load the column with nitrogen.
3. Start the flow of the cooling water to the condenser.
4. Start the boiler.
5. Adjust the pressure to the desired operating pressure.
6. Start the flow of the steam to the reboiler and steam tracing.
7. Operate the column at flooding conditions for 5 minutes, to ensure that the packing is well wetted.
8. Reduce the steam flow to the reboiler until desired operating conditions are reached.
9. Reach hydrodynamic steady state (usually 15 minutes).
10. Wait four hours to ensure that mass transfer steady state is reached.

11. Take samples at sampling ports 1 to 5.
12. Increase the steam flow rate to the reboiler and repeat step 8 to 10.
13. At the end of each experimental day, close the steam valve to the reboiler and steam tracing.
14. Compressed N<sub>2</sub> is then used to control the pressure in the column.
15. Leave the cooling water running for an hour after the steam valve has been closed, thereafter the flow of cooling water to the condenser can be stopped.
16. The compressed N<sub>2</sub> is then used to bring the column to atmospheric pressure.
17. After the column has been shut down, prepare the samples for analysis and analyse with the GC (with auto sampler) during the night.

### **3.7 Selecting a Test Mixtures**

It is crucial that an appropriate test mixture is selected for a pilot plant setup. The most popular test mixtures are discussed in detail in Section 2.6. From that it was found that there is a need for a procedure to select a test mixture for a specific pilot plant application. For this reason a method for selecting a test mixture was developed in this study.

The methodology of the selection process to select a test mixture is explained with the aid of a flow diagram (Figure 34).

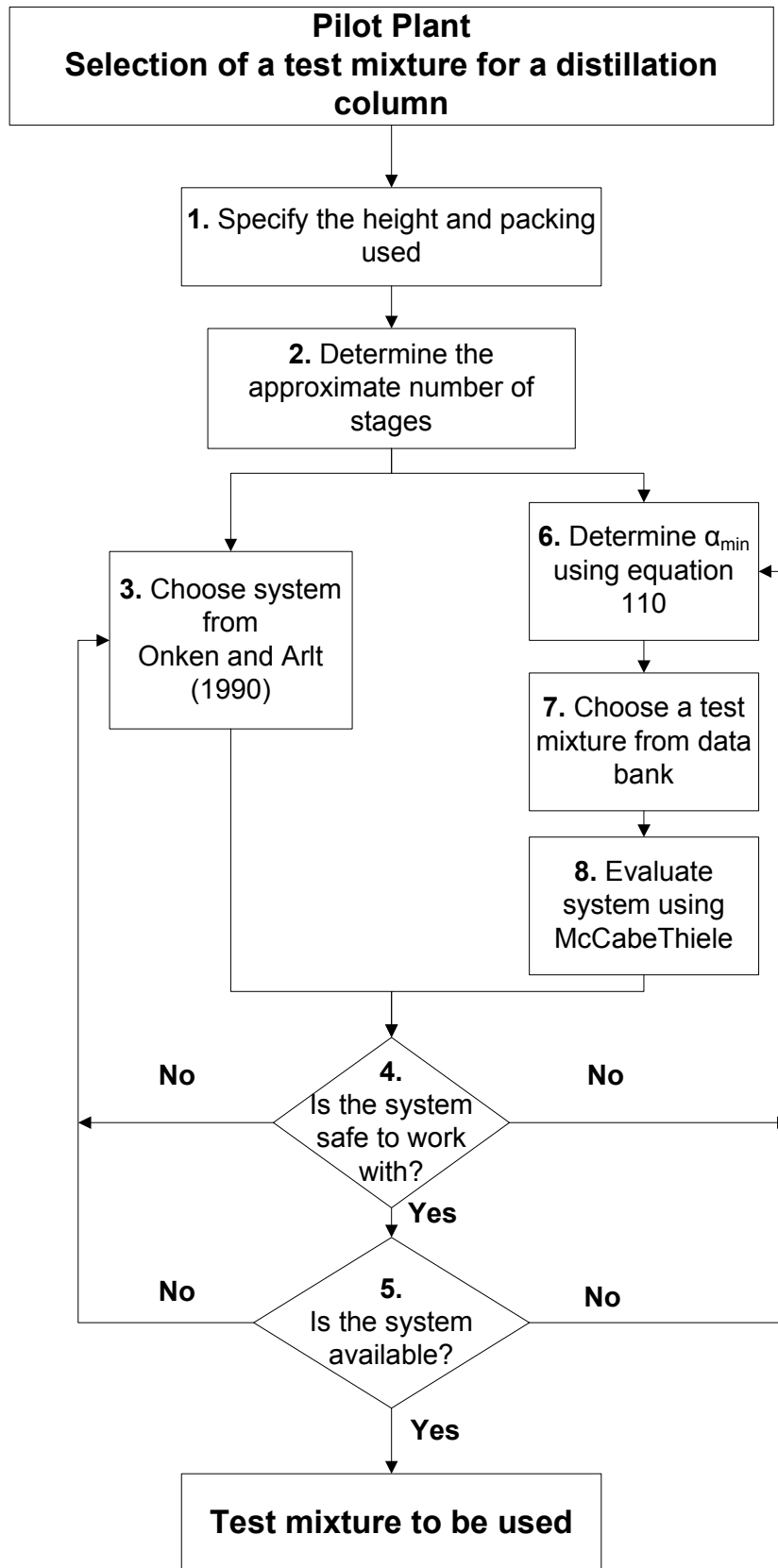


**Figure 34 – Process for selecting a test mixture**

### **Step 1**

Specify the packed height of the pilot plant that will be used, for testing the performance of the packing.

### **Step 2**

When selecting a test mixture for a pilot plant it is important to have an idea of how many theoretical stages will be encountered, because these stages determine the degree of separation and therefore the purities of the top and bottom composition. The number of stages is dependent on the type of packing used and the height of the distillation column. Different packings have different HETPs (as discussed in section 2.2) and a good approximation of HETP for different packings can usually be found in the brochures of suppliers. From this the number of stages expected can be estimated by dividing the height of the packing section by the HETP obtained from the brochures.

### **Step 3**

Mixtures commonly used to evaluate the performance of a distillation column can be found in Onken and Arlt (1990) where full sets of VLE data are given. Recommendations on the number of stages in the distillation column are also made. The VLE data are corrected with the aid of suitable thermodynamic models, e.g. NRTL or Wilson Margules, and a correlation for the relative volatility of each isobaric data set is provided. In the second edition of Onken and Arlt (1990), the systems that contain pure benzene were omitted due to health reasons.

### **Step 4**

A pilot plant is normally operated where other personnel/students are at work. It is therefore very important to choose a safe and chemically stable system when making a choice (Deibele *et al.*, 1997). However, it is not always possible to work with a safe test mixture and therefore it is always important to wear the correct personal protective equipment. If this system is found to be too dangerous to work with an alternative system from Onken and Arlt (1990) should be chosen (Step 3), else continue to step 6.

### **Step 5**

It is also very important that the components for the system can be purchased from a reliable chemical supplier. At this stage it is a good idea to compare different systems in terms of cost and availability. If the systems are too expensive and cannot be supplied in large quantities by the chemical supplier repeat step 3, and if no test mixture can be found to evaluate the test system move on to step 6.

### **Step 6**

To determine the relative volatility for the test mixture the method developed by Peacock (1967) can be used. Equation 117 calculates the relative volatility ( $\alpha_{\min}$ ) that would give the minimum sensitivity to analytical errors for a pilot plant if the number of theoretical stages ( $N_t$ ) is specified.

$$N_t \log_{10} \alpha_{\min} = 1.34 \qquad 117$$

Where 1.34 is a constant determined through statistical analysis and a band within +/- 20% of  $\alpha_{\min}$  would be highly suitable for the selected test mixture (Peacock, 1967).

### **Step 7**

By having a relative volatility, a test mixture can be selected from a data bank. The most popular data banks available are NIST (National Institute of Standards and Technology), Dortmund Data Bank and DECHEMA. These data banks contain experimentally measured VLE data.

### **Step 8**

The test system can be evaluated by using the McCabe-Thiele method. This is done by plotting the VLE curve and operating line (45° line through the origin for total reflux) and by stepping off the number of stages specified, starting at 90% liquid mole fraction of the more volatile component. If the last of the equilibrium stages falls between the 10% and 90% region of the more volatile component, then proceed to step 4, if not, return to step 7 and select a different mixture. The assumptions made by the McCabe-Thiele method are discussed in Section 2.7 and must also be kept in mind when selecting a test mixture.

By going through the selection process it was found that the popular chlorobenzene/ethylbenzene mixture given by Onken and Arlt (1990) can be used. However, due to safety and health reasons, this system was not considered as a test system. Ethylbenzene is classified as carcinogenic (class 2B – possible for humans). Through the selection process discussed in Chapter 2, it was found that iso-butanol/2-butanol and p-xylene/o-xylene would be suitable for the experimental setup. The p-xylene/o-xylene is used by the FRI when doing experiments under high vacuum conditions. However, only tests at atmosphere pressures were conducted to validate the working of the column in this study, but tests at vacuum conditions were done during commissioning.

The initial composition of the test mixture was chosen to avoid working in the pinch zones of the VLE for the systems investigated. Pinch zones are under 10% of the light component at the bottom and above 90 % of the light key component at the top of the column.

### **3.8 Vapour-liquid Equilibrium Cell**

As discussed in Chapter 2, it is extremely important to use accurate VLE data together with a proper thermodynamic model when calculating the HETP of the packing. Data for p-xylene/o-xylene and 2-butanol/iso-butanol systems can be found in the DECHEMA data series (Zong *et al.*, 1983 and Kutsarov *et al.*, 1993). To ensure absolute accuracy in the calculation of the HETP, it was decided to verify the data of Kutsarov *et al.* (1993) and Zong *et al.* (1983) by using the vapour-liquid equilibrium cell available at the University of Stellenbosch. A PFD of the VLE cell is represented in Figure 35 and the operating procedure is given in Appendix – Section 8.5. The VLE cell can operate at atmospheric pressure and at a slight vacuum. For the purpose of this study, all the VLE experiments were conducted at atmospheric pressure and the results are discussed in Chapter 4. The flow paths of vapour and liquid phase are illustrated in Figure 35.

The initial liquid mixture is loaded into the collective chamber. A heating element is then used to vaporise the mixture in the collective chamber; this forces the flow of the mixture up through the coil and into the equilibrium cell. The equilibrium cell is then used to flash the mixture into saturated liquid and vapour phases. Liquid leaves at the bottom of the equilibrium cell and flows to the liquid chamber, while the vapour leaves at the top of the equilibrium cell to the vapour chamber. The liquid and vapour phases then flow from the



liquid and vapour chambers to the collective chamber, where they are mixed and returned to the heating element. The pressure connections are connected to the atmosphere and the condensers are used to ensure that none of the volatile components escape to the atmosphere.

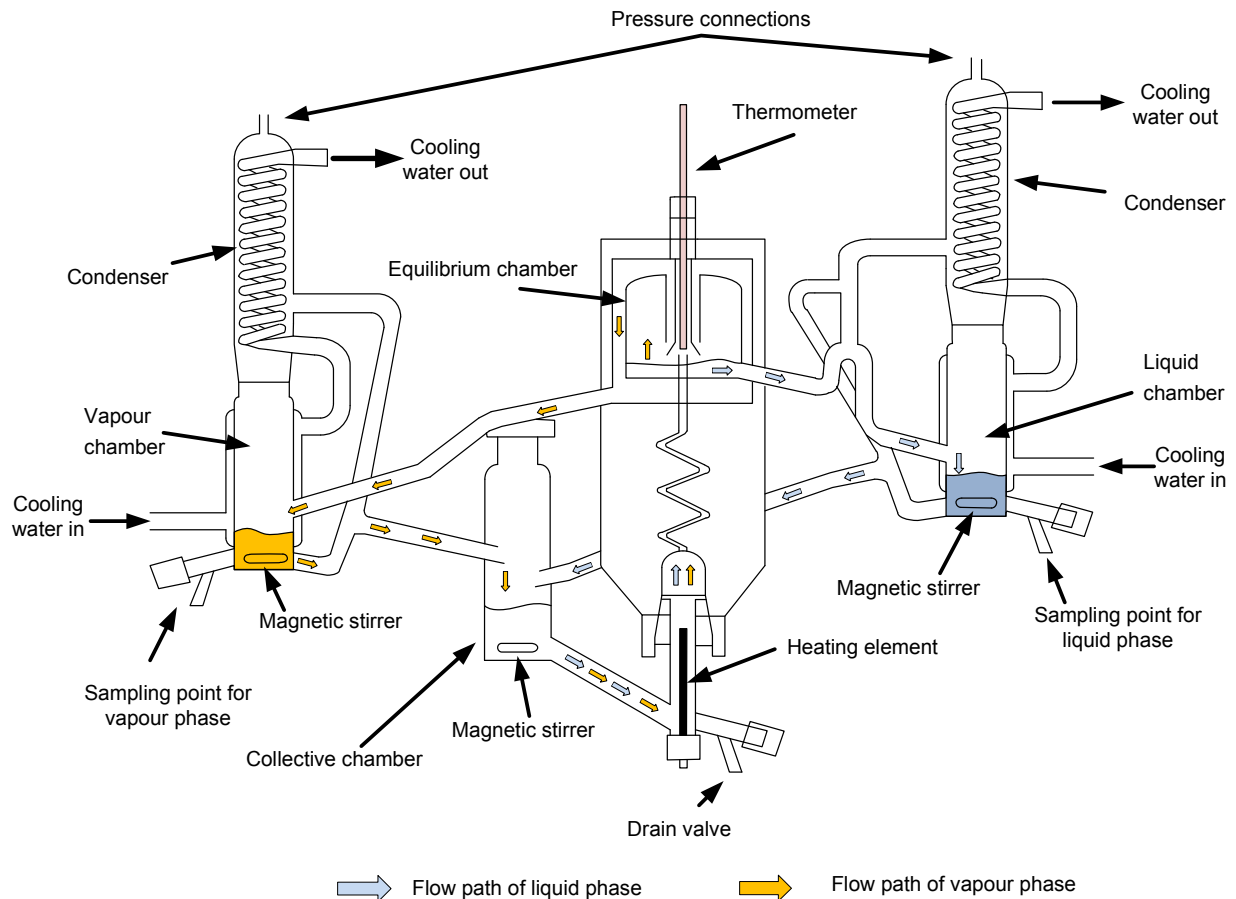


**Figure 35 – Vapour-liquid equilibrium cell**

### 3.9 Summary

The experimental setup constructed in this study consists of a distillation column, designed to test the performance of structured packing under total reflux. Provision was made to modify the column to a continuous feed column with overheads and bottoms product streams to study the effect of the liquid to vapour ratio. Efficiency, in terms of the HETP of the packing, and pressure drop were chosen as performance parameters.

The column consists of two packing sections, each with an inner diameter and height of 0.2 m and 2 m respectively. Liquid distributors are fitted at the top and middle of the

distillation column to ensure even liquid distribution onto the packing and a chimney-tray was installed at the bottom of the column, to evenly distribute the vapour flowing to the packing and to collect the liquid flowing down from the packing.

Steam tracing and insulation were fitted to the outside of the distillation column to minimise heat losses to the environment. The temperature of the steam inside the steam tracing was set at approximately 3 °C lower than the operating temperature of the column, to ensure that the liquid in contact with the inside of the column wall is not vaporised by the steam tracing. Heat transfer cement was applied to the steam tracing to ensure effective heat transfer to the column. A PFD for the experimental setup is shown in Figure 24 with a detailed P&ID given in Figure 25. Sensors were strategically placed to monitor and control the behaviour of the pilot plant setup.



---

# 4 Results and Discussion

---

## 4.1 Thermodynamic and Transport Properties.

As stated in Chapter 2.6 it is important to use accurate VLE data when calculating the efficiency of structured packing. It was therefore decided to confirm the reliability of the VLE data obtained from Kutsarov *et al.* (1993) and Zong *et al.* (1983) and VLE experiments were thus carried out in the vapour equilibrium cell (as described in Chapter 3.8). In the following section, the results from the experiments are compared with the data obtained from Kutsarov *et al.* (1993) and Zong *et al.* (1983).

### 4.1.1 VLE Data Verification

The VLE curves for data obtained from Kutsarov *et al.* (1993) and Zong *et al.* (1983) and the experiments conducted as part of this study are presented in Figure 36 and Figure 37. This data was then plotted on a Txy diagram in Figure 38 and Figure 39 to observe the effect of equilibrium temperature on the composition of the data. Both the 2-butanol/iso-butanol and the p-xylene/o-xylene VLE data sets tested thermodynamic consistent with the point test of Byer *et al.* (1973).

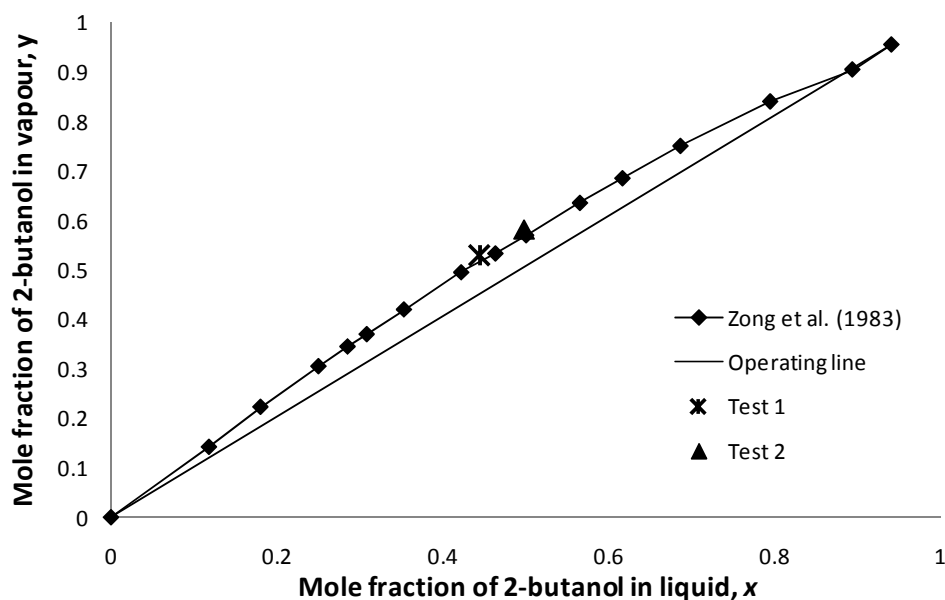


**Figure 36 – VLE data from Zong *et al.* (1983) and VLE cell for the 2-butanol/iso-butanol test system**

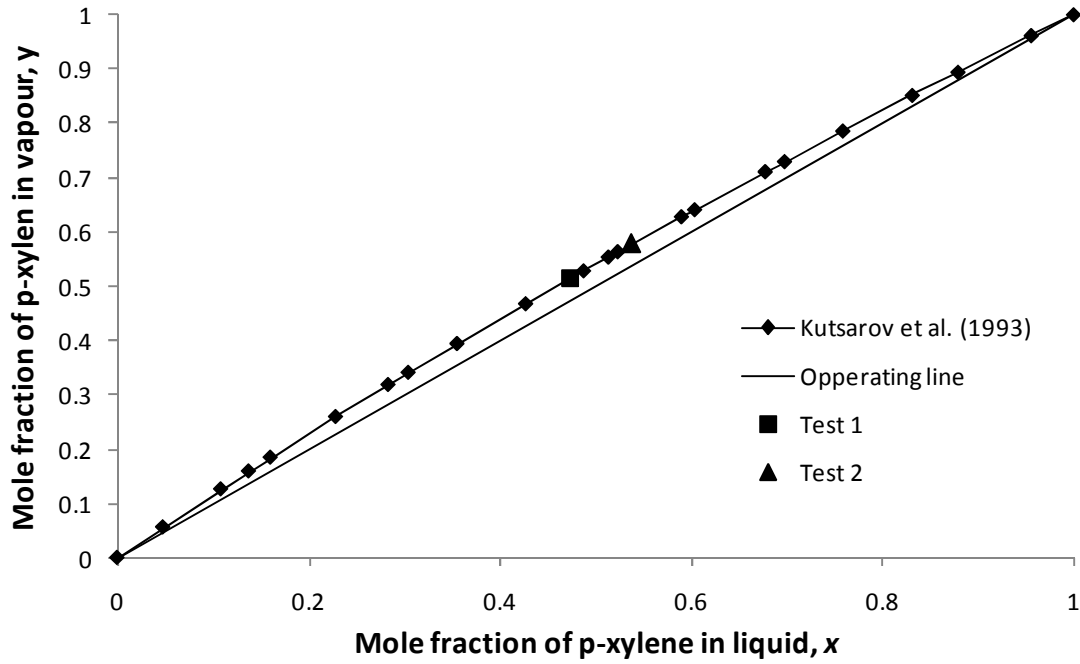


**Figure 37 –VLE data from Kutsarov et al. (1993) and VLE cell for p-xylene/o-xylene test system**

As shown in both Figure 36 and Figure 37, the data obtained from the DECHEMA data series and from the conducted experiments corresponded well.

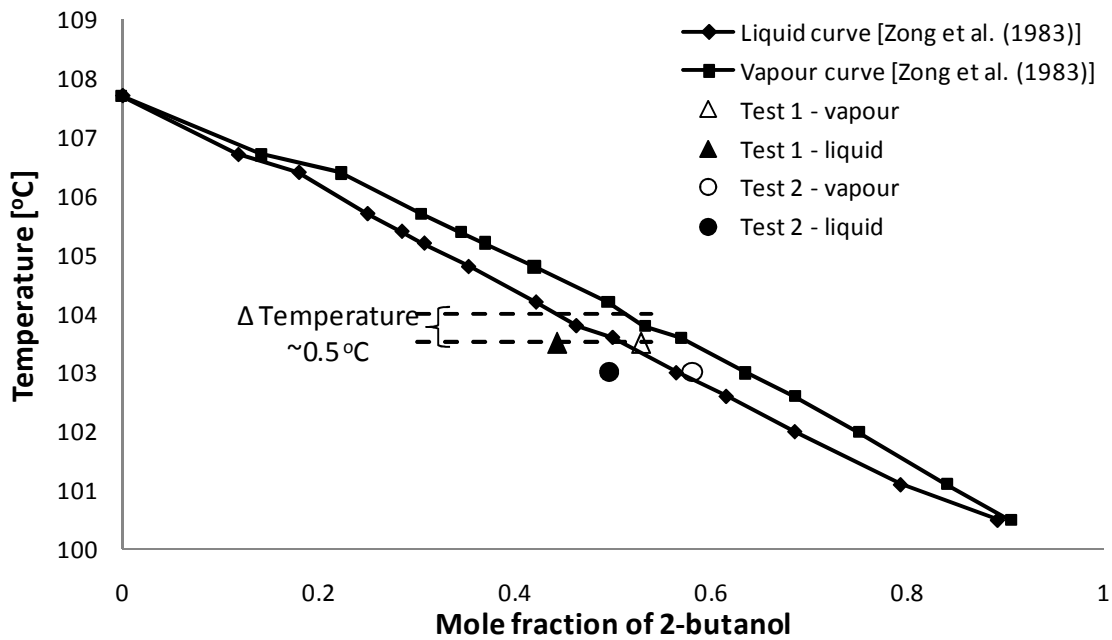


**Figure 38 – Txy diagram for data obtained from Zong et al. (1983) and the VLE cell, for 2-butanol/iso-butanol test system**

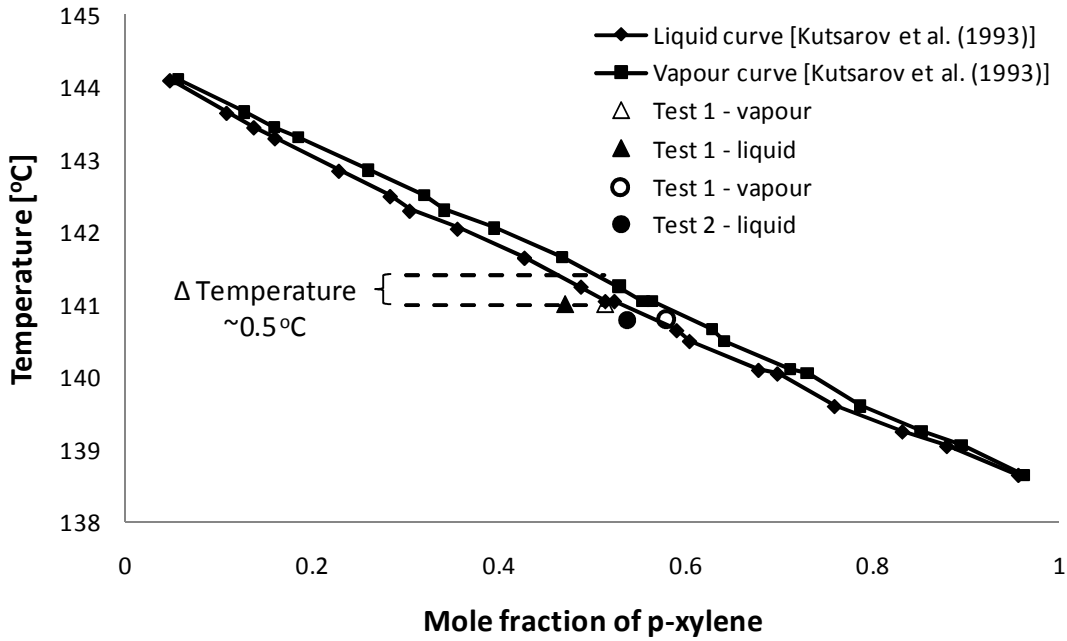


**Figure 39 - Txy diagram for data obtained from Kutsarov et al. (1993) and the VLE cell, for p-xylene/o-xylene test system**

In Figure 38 and Figure 39 a temperature difference of approximately 0.5 °C was observed between the data of Kutsarov *et al.* (1993) and Zong *et al.* (1983) and the data from the experiments conducted. The data Kutsarov *et al.* (1993) and Zong *et al.* (1983) was obtained at pressures of 1.013 bar, whereas the atmospheric pressure in Stellenbosch was measured to be 0.998 bar, therefore it is expected that the data from Kutsarov *et al.* (1993) and Zong *et al.* (1983) will be at a slightly higher temperature than the data obtained from this study. In addition, it should be remembered that the mercury thermometer used in the experiments had a scale division of 1 °C and accuracy of approximately 1 °C and thus temperature differences observed can be due to the difference in operating pressure and/or inaccuracy of the thermometers used.

However, despite of the accuracy of the thermometer, the approximately 0.5 °C difference observed in temperature can be explained according to Raoult's law (see calculations in Appendix – Section 8.7). From the investigation (see Figures 36 to Figure 39) and according to Raoult's law the DECEMA data was deemed accurate and therefore can be utilised in calculations using the Fenske equation. The next section will focus on the way the relative volatility of the mixtures was determined in this study.

### 4.1.2 Relative Volatility

Onken and Arlt (1990) corrected the VLE data with a suitable thermodynamic model and obtained an expression to calculate the relative volatility. The thermodynamic models that were used included the Margules, van Laar, Wilson, NRTL and UNIQUAC and for the systems that showed a deviation from Raoult's law, the Wilson equation was used. Neither the 2-butanol/iso-butanol, nor the p-xylene/o-xylene systems used in this study were obtained from the recommended test mixtures given by Onken (1990) and data from Kutsarov *et al.* (1993) and Zong *et al.* (1983) were found to be accurate and was therefore used in the rest of the study.

The DECHEMA data series provides VLE data together with interaction constants for the different thermodynamic models that can be used to predict the VLE behaviour of the system. Aspen Plus™ was then used with the NRTL thermodynamic model and its recommended constants to generate VLE data for the two systems. The constants from the DECHEMA data series used in the NRTL model can be found in Table 15 and more detailed explanation of how they are used in the model can be found in Appendix - Section 8.8.1. To verify the accuracy of the NRTL model the VLE data obtained from Kutsarov *et al.* (1993) and Zong *et al.* (1983) are plotted with the predicted values of the thermodynamic model in Figure 40 and Figure 41 respectively.

**Table 15 – NRTL constant used in Aspen model**

NRTL constants	$g_{12} - g_{22}$	$g_{21} - g_{11}$	$\alpha_{12}$
2-butanol	-138.8580	127.9478	0.3048
iso-butanol			
p-xylene	-150.7750	173.4618	0.3128
o-xylene			

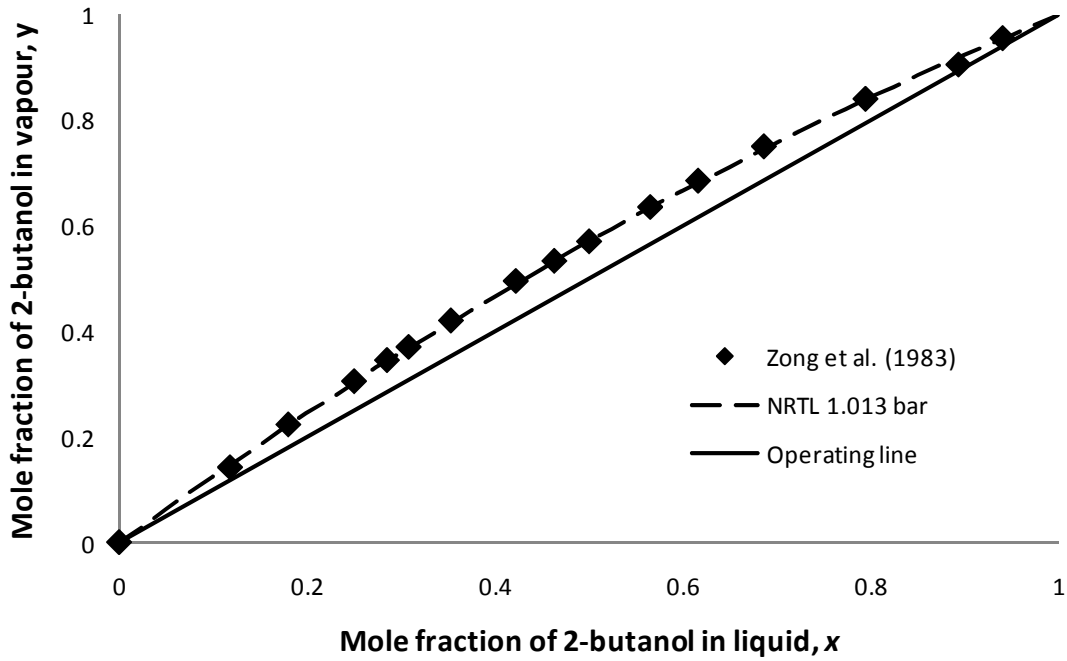


**Figure 40 – Data for 2-butanol/iso-butanol from Zong et al. (1983) and the VLE data using the NRTL model**

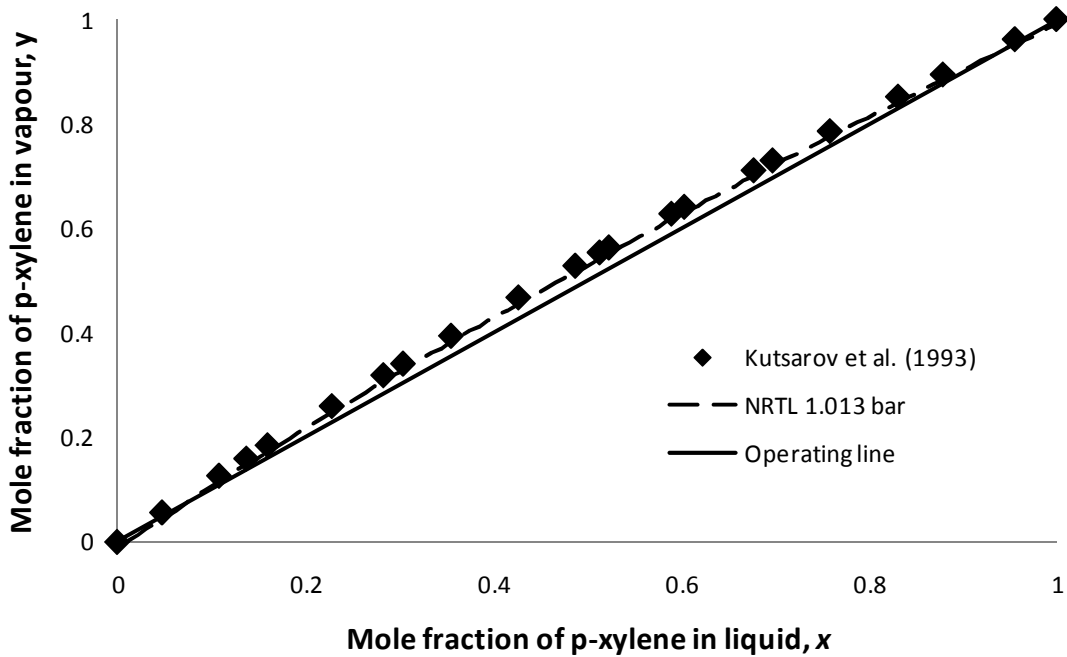


**Figure 41 – Data for p-xylene/o-xylene from Kutsarov et al. (1993) and the VLE data using the NRTL model**

In Figure 40 and Figure 41 it can be seen that the predicted values from the NRTL model correspond excellently with the data obtained from Kutsarov *et al.* (1993) and Zong *et al.*



(1983). Therefore the NRTL thermodynamic model can be used to generate accurate VLE data for the 2-butanol/iso-butanol as well as the p-xylene/o-xylene systems over the entire composition range.

The NRTL thermodynamic model was then used to generate 100 VLE data points for the 2-butanol/iso-butanol system over the entire composition range. The relative volatility was calculated from this data and plotted against the liquid mole fraction of 2-butanol as shown in Figure 42. Here, it can be seen that the relative volatility for 2-butanol/iso-butanol can be expressed as a linear function in terms of liquid mole fraction of 2-butanol. A linear trend line was then fitted to the data to obtain an expression that can be used to accurately calculate the relative volatility over the entire composition range. The same was done for the p-xylene/o-xylene system and the plot for the relative volatility against the liquid mole fraction of p-xylene is shown in Figure 43. Unlike the butanol test system the xylene system showed a decrease in relative volatility with an increase in the liquid mole fraction of the lighter key component, and instead of a linear trend it showed a polynomial trend. Thus for the p-xylene/o-xylene test mixture, a second order polynomial was fitted on relative volatility data.

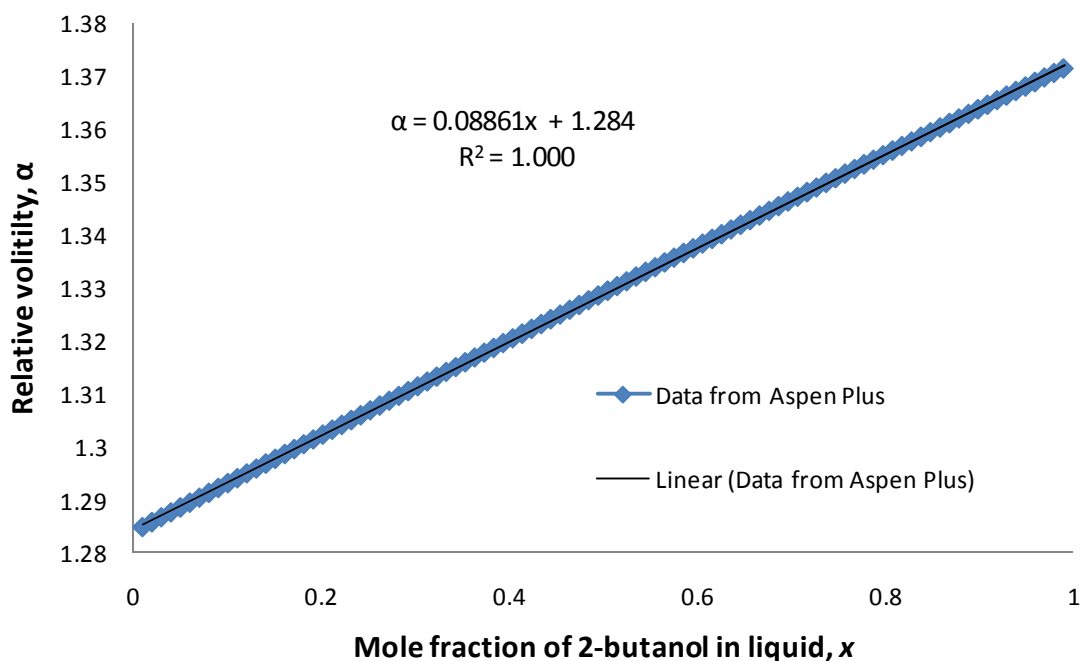


**Figure 42 – Relative volatility for 2-butanol/iso-butanol versus liquid mole fraction of 2-butanol**

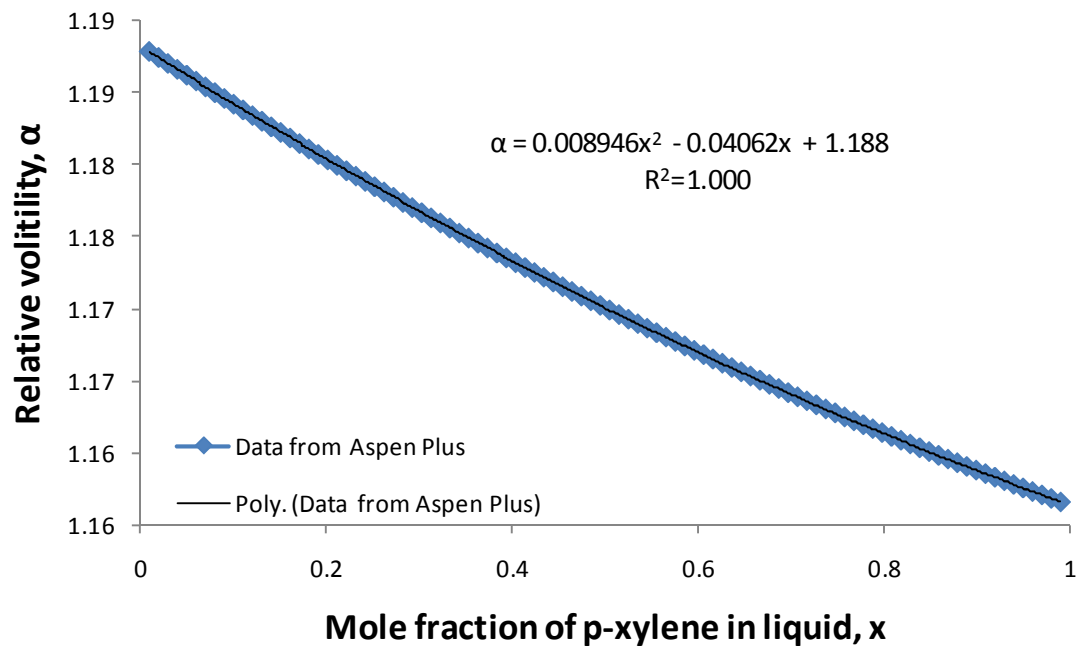


**Figure 43 – Relative volatility for 2-butanol/iso-butanol versus liquid mole fraction of 2-butanol**

The expressions derived for relative volatility were used in the rest of the study to predict the relative volatility of the 2-butanol/iso-butanol and p-xylene/o-xylene test systems when calculating the HETP of the packing by using the Fenske equation. The next section deals with some of the commissioning problems that were encountered after the pilot plant was build.

## 4.2 Commissioning Problems of Pilot Plant

The plant was first commissioned using a water test mixture, to test the working of the reboiler and condenser. Thereafter tests were done with Flexipac 350Y HC structured using 2-butanol/iso-butanol and p-xylene/o-xylene test mixtures at pressures of 0.3 bar (abs), 0.6 bar (abs) and 1 bar (abs) respectively. Analysing the results clearly indicated that some part of the pilot plant was malfunctioning, and therefore it was necessary to closely analyse the working of the pilot plant. In this section these problems and how they were resolved are discussed.

### 4.2.1 Problem 1: Incorrect Pressure Drop Trends

Pressure drop result for 350Y HC packing using 2-butanol/iso-butanol and p-xylene/o-xylene as test mixtures at 0.3 bar, 0.6 bar and 1 bar are shown in Figure 44 and Figure 45.

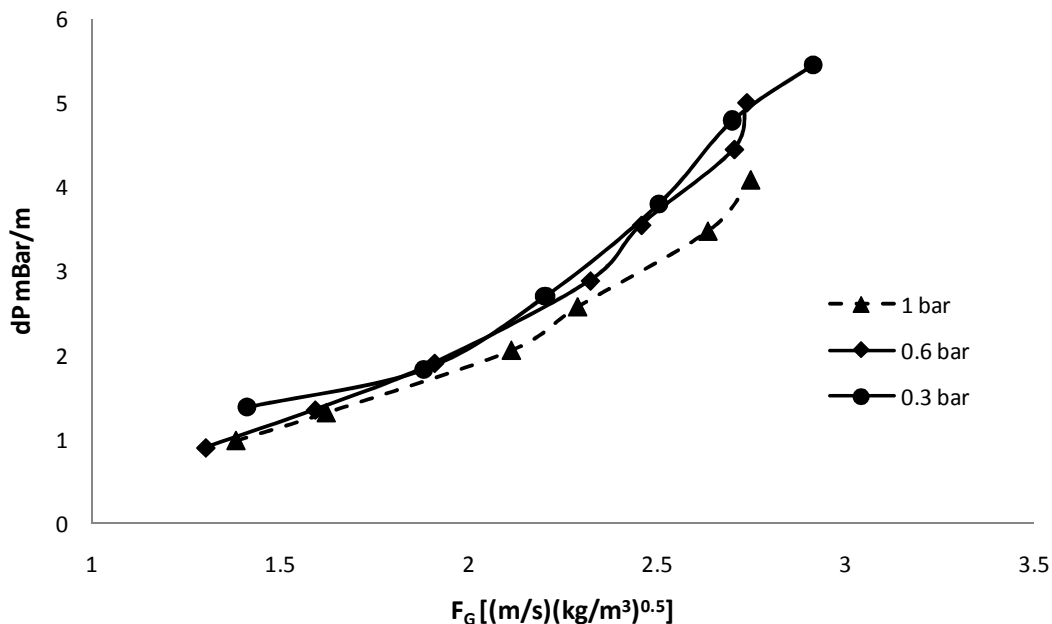


**Figure 44 – Pressure drop results for 350Y HC packing during commissioning phase. 2-butanol/iso-butanol test system at 1 bar abs, 0.6 bar abs and 0.3 bar abs.**

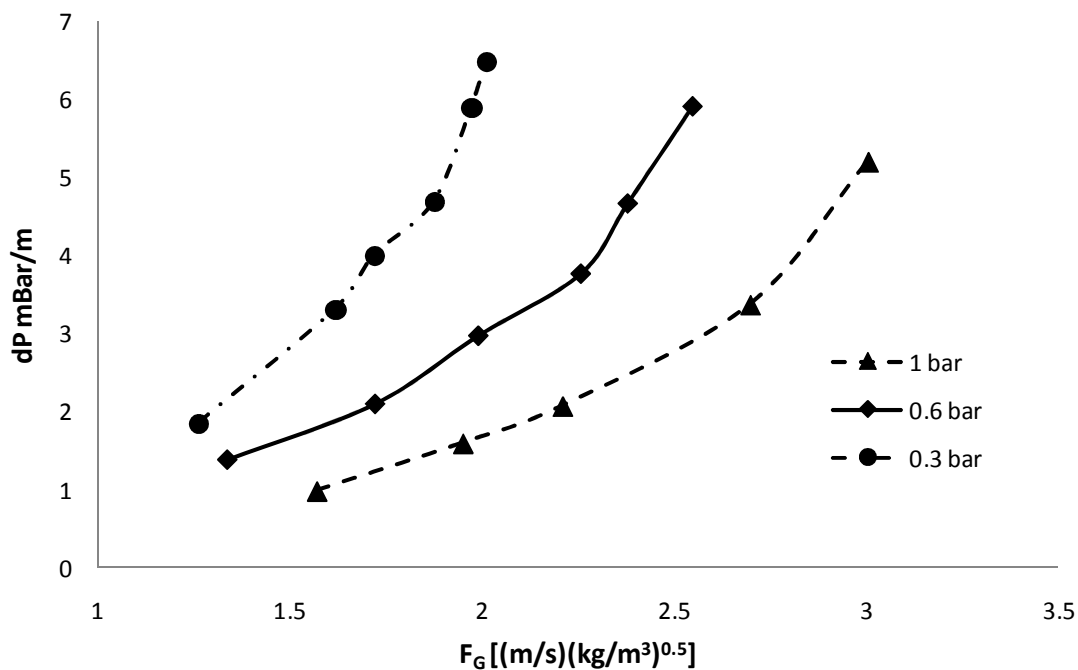


**Figure 45 – Pressure drop results for 350Y HC packing during commissioning phase. p-xylene/o-xylene test system at 1 bar abs, 0.6 bar abs and 0.3 bar abs.**

Figure 44 shows that there is very little difference between the pressure drop curves for 350Y HC with 2-butanol/iso-butanol test system operating at pressures of 0.3 bar abs, 0.6 bar abs and 1 bar abs. This effect is not as worrying as the fact that the pressure drop curve at 0.3 bar is above the pressure drop at 1 bar. This effect is more evident with the results of the p-xylene/o-xylene mixture (see Figure 45).

As discussed in the literature review (Section 2.3), the gas will entrain more of the liquid in the packed column under higher operating pressure. According to the ideal gas law the density of the vapour phase will generally increase as the operating pressure increase. An increase in the vapour density will increase the shear force between the gas and liquid phase and thus allow the vapour phase to entrain more liquid at a lower vapour flow rate. It is therefore expected that these trends should be the inverse of those observed in Figure 44 and Figure 45.

These pressure drop results clearly indicated that there is a problem with the pilot plant setup. This problem can either originate from the differential pressure cell or from the pilot plant setup. The possible problems with each of these are investigated and their implications will be discussed.

#### ***i. Differential Pressure Cell***

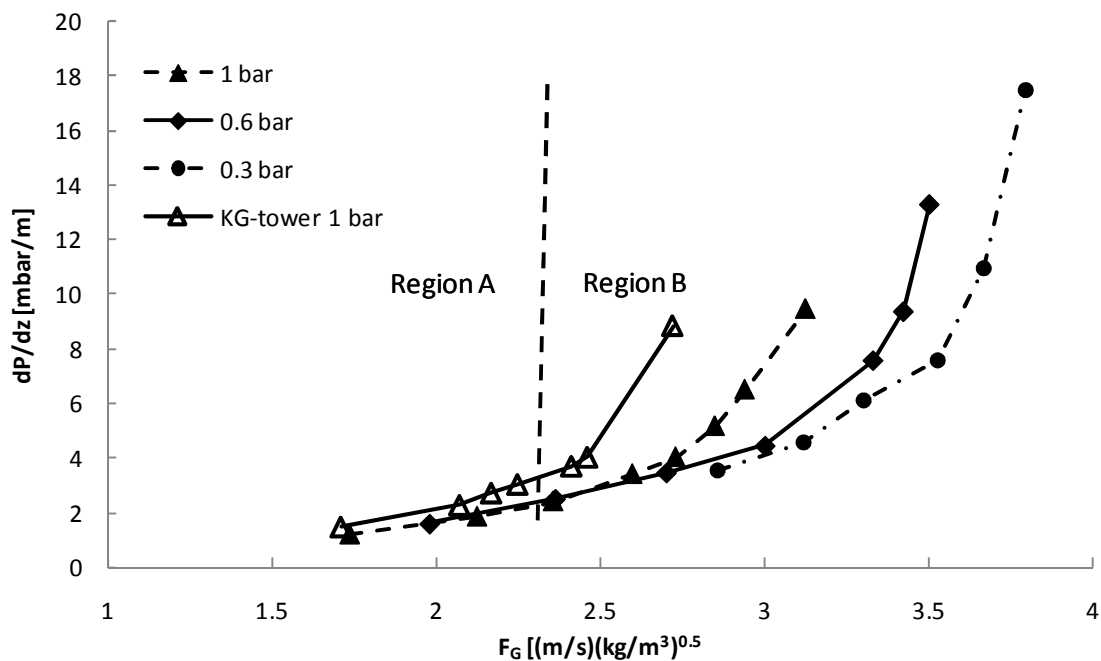
As discussed in Section 3.4.7 a differential pressure cell is used to measure the pressure drop over the packed bed, and any malfunctioning of the differential pressure cell will result in incorrect pressure drop readings. Two possible problems with the differential pressure cell could be that i) the diaphragm used by the differential pressure cell to measure the pressure drop is broken, or ii) the pressure drop cell is wrongly calibrated. To eliminate these possible causes the differential pressure cell was sent back to the supplier for fault detection and recalibration. However, no problems with the differential pressure cell could be found and therefore the problem with the pressure drop trends had to lie with the pilot plant setup. After this it was also decided to equip the pilot plant setup with a manometer so that regular spot checks can be done.

## ii. Pilot Plant Setup

Other factors that might influence incorrect pressure drop readings in the pilot plant setup were identified as i) leakage in the process connection between the differential pressure cell and pilot plant or ii) condensate build up in pressure lines.

**Leakage in the process connections** will give rise to incorrect pressure drop readings by the differential pressure drop cell as well as the manometer in the pilot plant setup up, and thus is hard to detect. However, a pressure test done on the column indicated no leakage in the connection lines and therefore it was eliminated as a possible source of error.

**Build up of condensate** in the pressure lines will also influence the pressure drop readings of both the differential pressure cell and manometer. The fact that 6 mm tubes were used for process connections made this problem the most likely cause of the incorrect pressure drop readings. To eliminate this problem, a nitrogen flushing system was installed to the pressure connections; that can be used to flush the pressure connections before and during operation. After the flushing system was installed tests were done with the xylene test mixture and the new pressure drop results are presented in Figure 46.



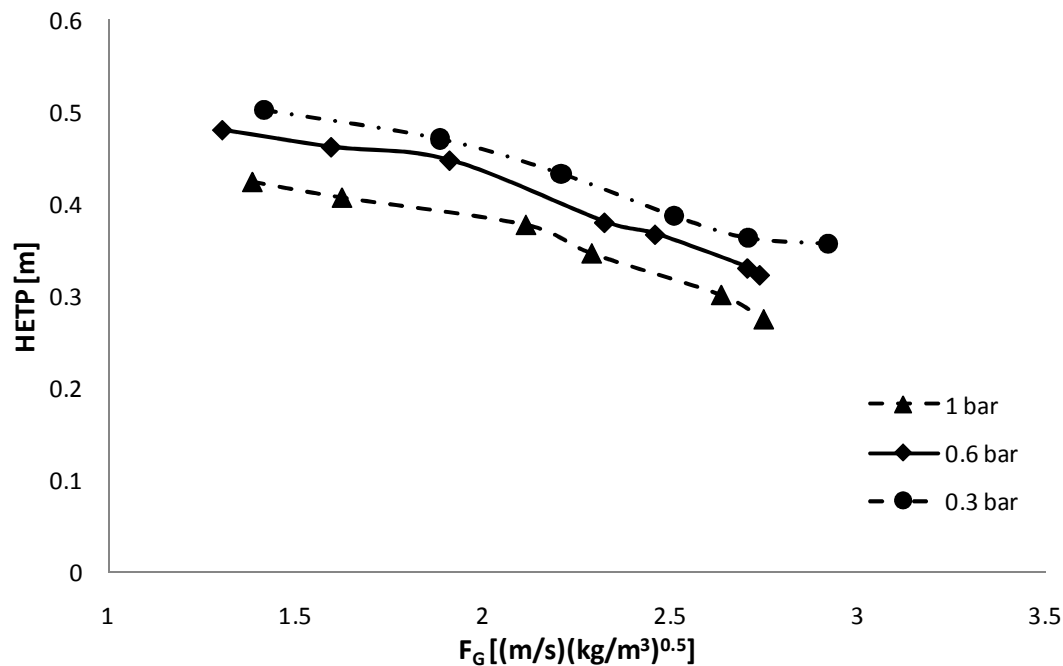
**Figure 46 - Pressure drop results for 350Y HC packing after the nitrogen flushing system was installed. p-xylene/o-xylene test system at 1 bar abs, 0.6 bar abs and 0.3 bar abs.**

Figure 46 shows that the nitrogen flushing line eliminated the problem of incorrect pressure readings. The results were also compared with KG-tower. KG-tower is simulation software develop by Koch-Glitsch™ to predict the pressure drop of packings developed by Koch-Glitsch™. Region A falls within the loading limits of the software package and region B falls outside these limits. The KG-tower software over-predicts the results obtained in this study over the entire operating region.

However, pressure drop readings oscillated during the experimental runs and therefore these results cannot be deemed as accurate. The pressure drop oscillation can also be the reason why the results obtained from this study differ from the results generated by KG-tower. The next section focuses on the pressure oscillations observed and how this problem was resolved. The pressure drop oscillations had an amplitude of 13% of the absolute value with a frequency of 0.01 Hz.

#### 4.2.2 Problem 2: Pressure Drop Oscillations and its Effect on HETP

The HETP results from the commissioning for 2-butanol/iso-butanol and p-xylene/o-xylene test mixture are discussed in this section. The results are presented in Figure 47 and Figure 48.



**Figure 47 - HETP results for 350Y HC packing during commissioning phase. 2-butnao/iso-butanol test system at 1 bar abs, 0.6 bar abs and 0.3 bar abs.**

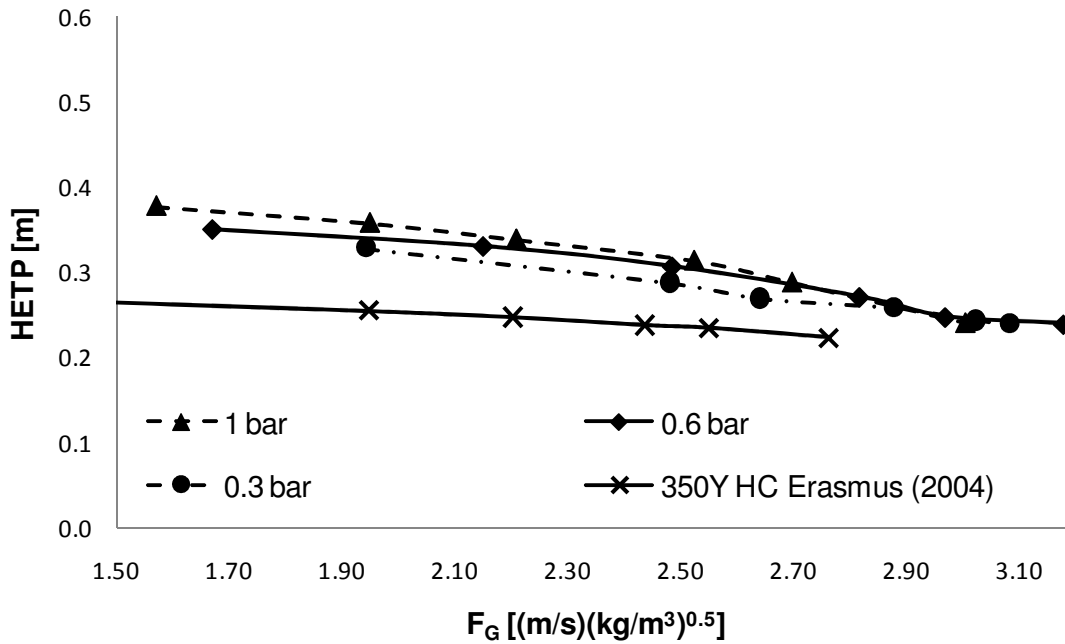


**Figure 48 – HETP results for 350Y HC packing during commissioning phase. p-xylene/o-xylene test system at 1 bar abs, 0.6 bar abs and 0.3 bar abs.**

Section 2.3 discusses the performance of structured packing, and from this it is expected that the HETP of higher surface area structured packing will have a slight decrease with an increase in the vapour capacity factor. However, the decrease observed for 350Y HC with both 2-butanol/iso-butanol and p-xylene/o-xylene system showed a sharper decrease than expected. The decrease observed in Figure 47 and Figure 48 represents more the behaviour of random packing and therefore the results obtained were questionable. In Figure 48 the xylene results were also compared against the performance data for Flexipac 350Y packing generated by Erasmus (2004) and a 30% difference was observed. The possible causes for this behaviour were investigated and the results of the investigation are discussed next.

The vapour and liquid flow rates influence the HETP of packed columns and it is thus important that these phases are in equilibrium with one another. For equilibrium to be established between these two phases it is important that the liquid flow and vapour phase flow rates are constant. Both these flow rates influence the pressure drop in a packed column and therefore the pressure oscillations observed (as discussed in Section 4.2.1) can be the reason for poor HETP behaviour of the packing.

The source of the pressure drop oscillations was identified as the BRV2S pressure valve that was installed in the main steam line. The BRV2S regulating valve worked with a spring action to regulate the pressure. The spring used in this valve gave 10 % oscillation in the set steam pressure. This problem was overcome by installing a DN17 pressure regulating valve that works on a pneumatic control system; this minimised the pressure oscillations in the steam line to 1 % of the set value. Figure 49 shows the effect of the pressure reducing valves on the pressure drop oscillations.

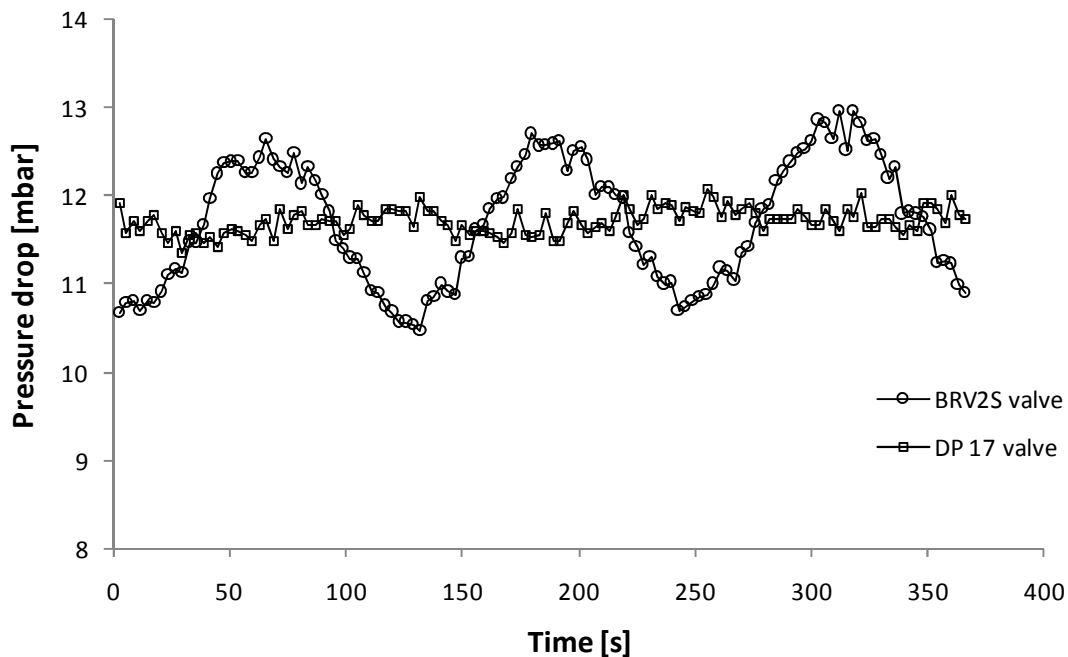


**Figure 49 – Effect of pressure reducing valve on pressure oscillations**

Unfortunately, no further experiments could be conducted with the Flexipac 350Y HC packing because the packing was severely damaged when it was removed from the packed sections. For this reason only the results for Mellapak™ 350Y were used to validate the working of the column, and these results are discussed in the next section. The rest of the results from the commissioning phase can be found in Appendix – Section 8.10.

### 4.3 Pilot Plant Data Validation

Experiments with the 2-butanol/iso-butanol test system using Mellapak™ 350Y structured packing at atmospheric pressure were used to validate the results obtained from the



distillation pilot plant constructed. For the pilot plant validation it is important to know the following:

- *Experimental error*
- *Time to reach equilibrium*
- *Repeatability*

These factors were investigated and will be discussed in this section. The influence of composition on the results of the Fenske equation is also investigated in this section, and thereafter the results are discussed and compared with Aspen Plus™ simulations, published data, and predictive models.

### **4.3.1 Measurement Error**

An error analysis was performed on the pilot plant to calculate the experimental error associated with each data point and is given in Table 16. The percentage error associated with each instrument was used to calculate the maximum percentage error. It must be noted that these error are independent error. The detailed calculation of these errors is given in Appendix – Section 8.9.

***Table 16 – Experimental error***

F-factor	0.32%
Pressure drop	0.58%
HETP	1.7%

### **4.3.2 Time to Reach Equilibrium**

To ensure that the system was in equilibrium, the experimental setup was operated for six hours, with liquid samples drawn from the top, middle, and bottom distributors every hour during that period. The liquid samples were then analysed, and their composition plotted against time (see Figure 50). The compositions were then used to calculate the HETP over the top packing section, bottom packing section, and over both the packing sections together, and then plotted against time (see Figure 51). The pure component heat transfer properties used to calculate the vapour capacity factors were obtained from the NIST data bank.

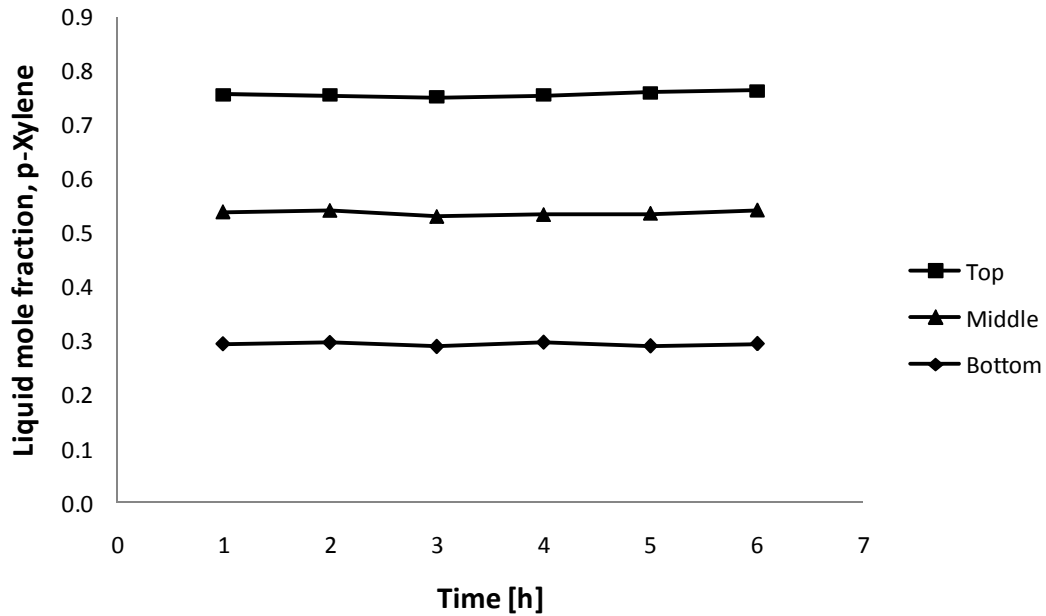


**Figure 50 – Liquid composition from the three distributors versus time**

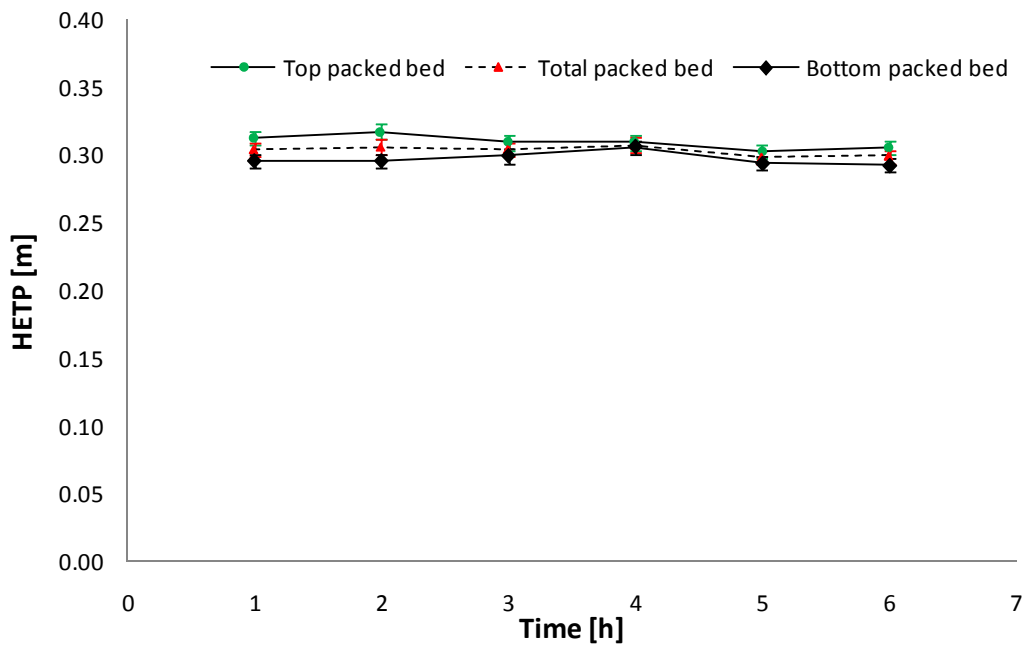


**Figure 51 – HETP versus time**

As seen in Figure 50, the compositions do not vary much with time; but in consideration of Figure 51, it can be seen that the HETP seems to stabilise after three hours. For this reason it was decided to wait at least three hours before taking a sample after any changes were made to the test system.

### 4.3.3 Repeatability

It is also necessary that the pilot plant setup have repeatable experimental data. Therefore an experimental data set was repeated under the same conditions and the results for the repeatability test are illustrated in Figure 52.

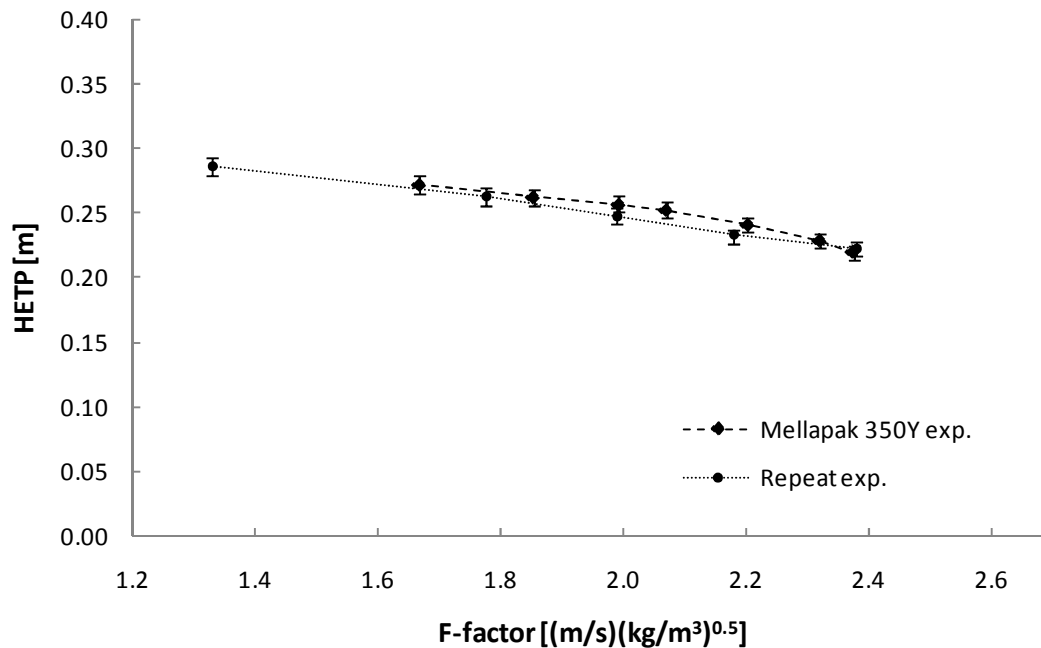


**Figure 52 – Repeatability test for pilot plant setup**

Figure 52 shows that all the data points for the repeatability test fall within the errors bars of the data set, and from this it can be concluded that the pilot plant setup gives repeatable data.

### 4.3.4 Influence of Composition on Fenske Equation

Three compositions of the 2-butanol/iso-butanol test mixtures were used to test the influence of composition on the Fenske equation. The relative volatility of the different compositions are calculated with the relative volatility equations (see Section 4.1), and the geometric average of the relative volatility calculated above and below each bed was used to calculate the HETP of the packing. The composition ranges over the bottom packed bed for the three compositions are given in Table 17, and the HETP obtained over the bottom packed bed is plotted in Figure 53.

**Table 17 – Composition range of the three different compositions for the bottom packed bed**

Location	Composition 1	Composition 2	Composition 3
Bottom distributor	0.54	0.37	0.15
Middle distributor	0.90	0.80	0.53

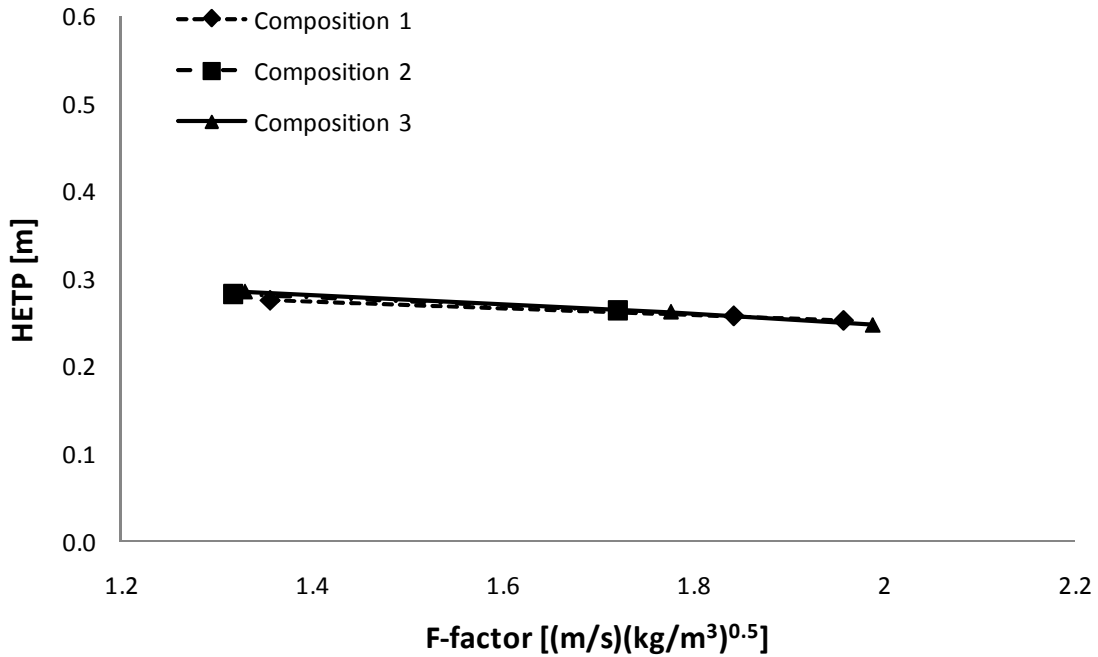


**Figure 53 – Repeatability with three different compositions**

Figure 53 indicates that the Fenske equation is not influenced by composition changes, and that the equations derived for relative volatility in Section 4.1 can be used with the Fenske equation to calculate the HETP of the packing.

The results obtained from tests with Mellapak™ 350Y will be presented and discussed in the next section.

## 4.4 Results

In this section the results obtained during the experimental phase of this study are discussed, and in Section 4.5 the results are compared against the data found in literature, and the predictions from predictive models. Results from the experiments conducted with

Mellapak™ 350Y using the 2-butanol/iso-butanol test system at atmospheric pressure are shown in Figure 54 and Figure 55.

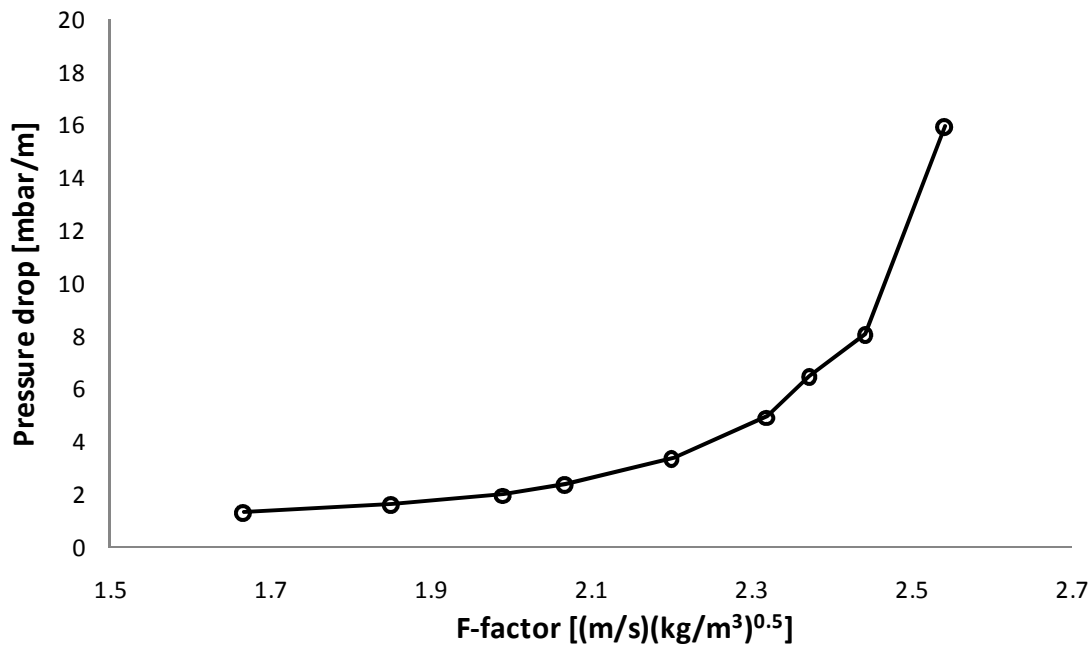


**Figure 54 – Pressure drop data for Mellapak™ 350Y with 2-butanol/iso-butanol test system at 1 atm**

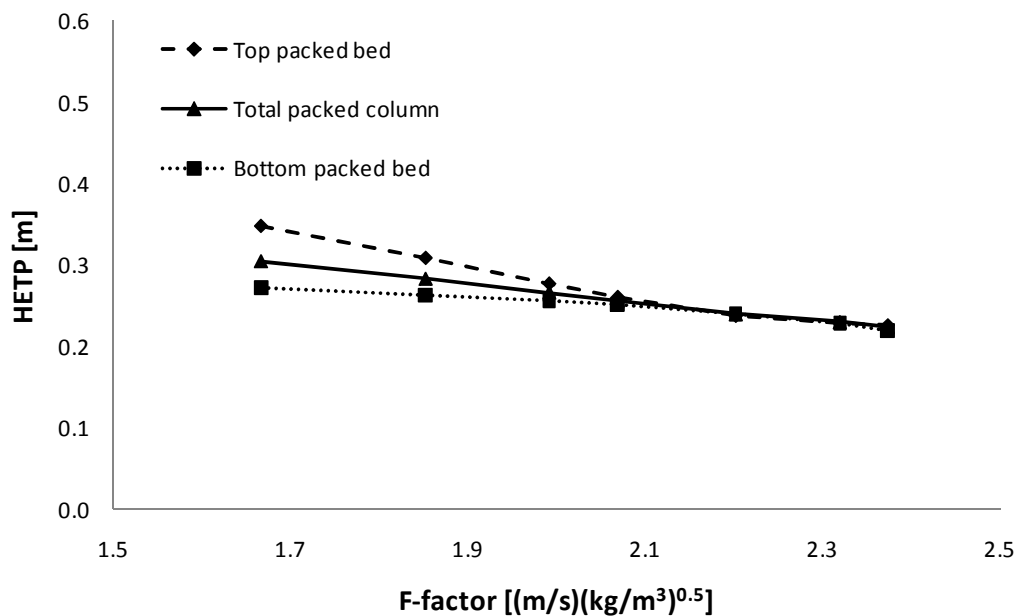


**Figure 55 – HETP data for Mellapak™ 350Y with 2-butanol/iso-butanol test system at 1 atm**

Figure 55 indicates that there is a difference in the efficiencies obtained from the top and bottom section of the packed bed, and that the efficiency over both packing sections is almost at an average value between the two packed sections. The difference between the top and bottom packed section is more significant at low flow rates and then starts to decrease until a “pinch point” is reached. Thereafter the efficiencies coincide, and remain the same for the rest of the operating range.

The number of theoretical stages was also validated through Aspen Plus™ simulations. The Aspen Plus™ simulations were configured to evaluate the number of theoretical stages calculated from the Fenske equation. To do this the bottom composition in the simulation was set to a value close to the liquid composition obtained from the bottom composition. Then, the number of stages was varied to obtain the composition at the middle and top distributors respectively. Once this was done, the number of stages was calculated by interpolating between the stages. The results obtained from the Aspen Plus™ simulations were plotted with the experimental values in Figure 56.

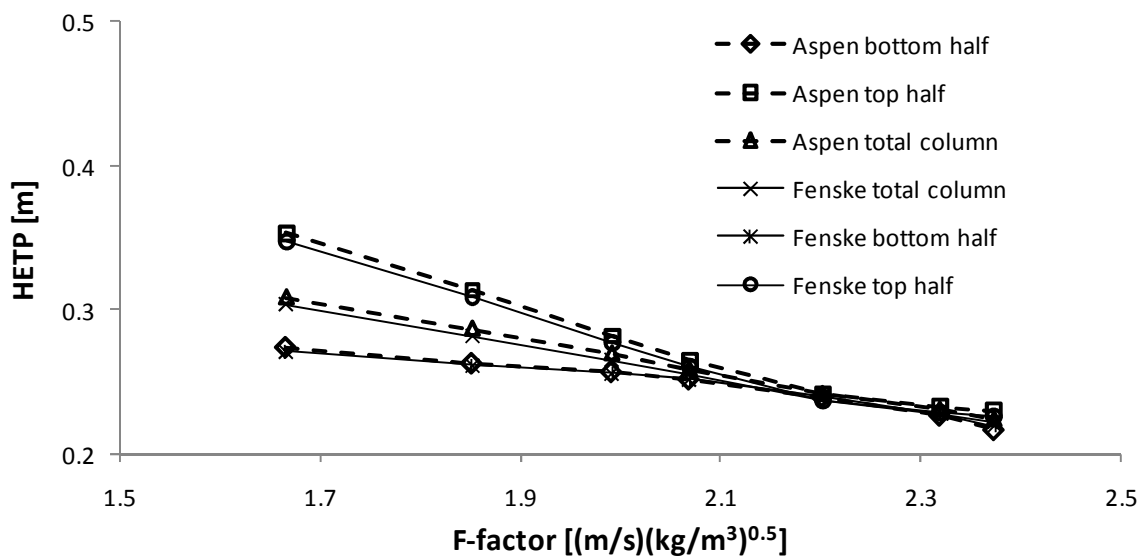


**Figure 56 – Number of theoretical stages calculated in Aspen compared to those obtained from the Fenske equation**

From Figure 56 it can be concluded that the HETP results obtained from the Fenske equation and Aspen simulations compare well in terms of HETP predictions. Therefore the number of theoretical stages calculated from the Fenske equation can be used to calculate the HETP

for the experimental test runs conducted with the 2-butanol/iso-butanol test system. However, the difference observed between the top and bottom packing sections could be attributed to:

- *Sub-cooling in the condenser and heat losses from the column to the environment*
- *Malfunctioning of the liquid distributor; or*
- *Property differences in the bottom and top packed beds as observed by Gualito et al. (1997).*

Each of the above was investigated and will be discussed in the following section.

#### 4.4.1 Sub-cooling and Heat Losses

After analysing the duties of the reboiler and condenser it was found that on average there was a 5 kW difference between the reboiler and condenser duties. The energy usage of the reboiler ranged between 46 and 69 kW. The difference observed could be due to a combined effect of sub-cooling of the condensate and heat losses to the environment. The steam tracing was not used during this experimental run due to the low operating temperature when the butanol test mixture is used. Steam tracing may then lead to additional heat being added to the column, rather than to prevent heat losses to the atmosphere. Temperatures measured at the vapour spaces below and above each packing section varied from 106°C (below the bottom packed bed) to 99°C (above the top packed section) with a condensate temperature of 93°C (returning to the top of the column). A possible effect of the sub-cooling is illustrated with the aid of Figure 57.

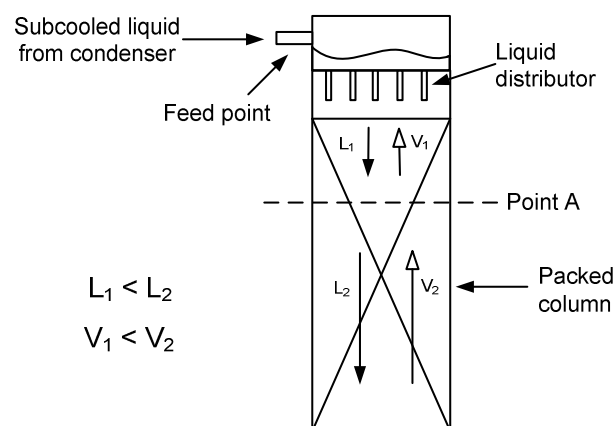


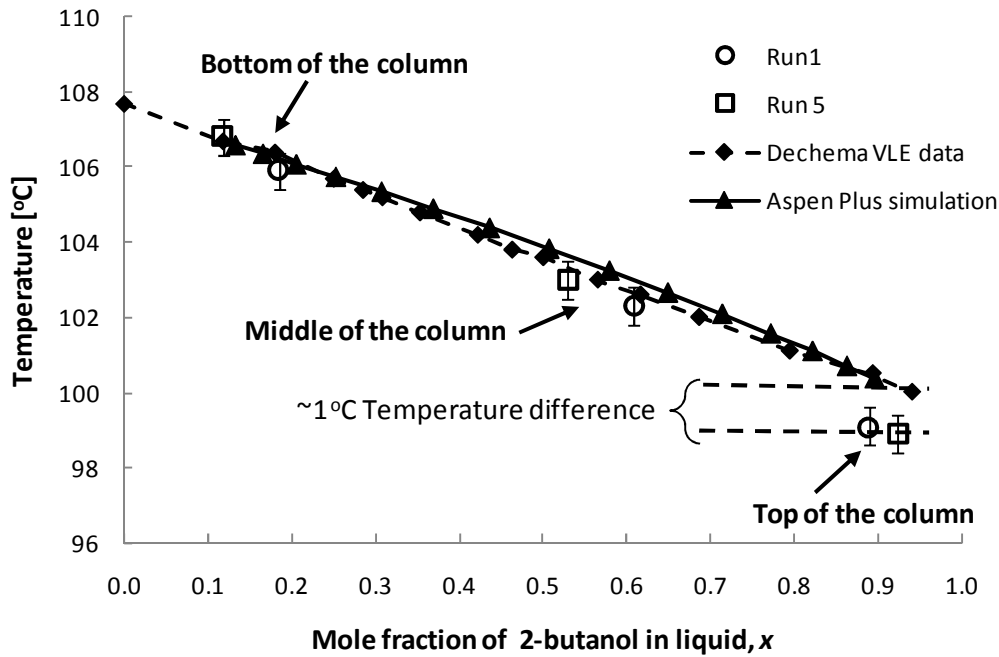
**Figure 57 – Effect of sub-cooling**

Sub-cooling in the condenser will cause the liquid reflux to be at a temperature below the equilibrium temperature of the column. The sub-cooled liquid is distributed evenly over the top packed section, and flows down under gravity. As the sub-cooled liquid flows down the packed section it gets heated by the rising vapour, and thus causes some of the vapour to condense. This will happen until point A (see Figure 57), where the sub-cooled liquid is brought to its equilibrium temperature. Thus, above point A the liquid and vapour phase will have a lower volumetric flow rate than below point A, leading to irregular flow in the top packed section. The vapour that is condensed by the sub-cooled liquid will skip the liquid distributor and this may cause maldistribution in the top packed bed. The effect of sub-cooling is related to the amount of sub-cooled liquid that enters the column, and will increase proportionally as the liquid and vapour flow rates increase in the column. The effect will thus lead to an efficiency difference throughout the operating range.

Heat losses to the environment will have a constant value throughout the operating range, as the operating temperature throughout the column stays almost constant. The slight changes in temperature are due to compositional changes in the column. Heat losses will cause additional vapour to condense against the walls of the distillation column. It is therefore expected that the heat losses to the environment will have a greater effect at low flow rates than at higher flow rates, therefore affecting the efficiency more at lower flow rates than at higher flow rates. This could thus be seen as a possible explanation for the efficiency difference between the top and bottom packed section.

In Figure 58 the temperature profile measured in the column is plotted with the temperature profile of the VLE data as well as the temperature profile from an adiabatic Aspen Plus™ simulation.





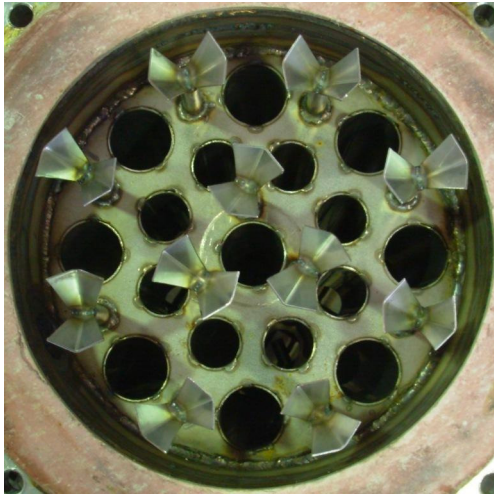
**Figure 58 – Temperature profile through the column**

Figure 58 shows that the vapour at the bottom and middle sections of the column are in equilibrium with the liquid phase. The temperature differences observed at the top of the column indicate that the liquid and vapour phase are not in equilibrium, and can thus be the reason why the top packed bed has a higher HETP than the bottom packed bed.

#### 4.4.2 Liquid Distributor

The top and bottom bed use a similar liquid distributor design, but when comparing the efficiency trends in Figure 55 with those in Figure 10, it could be argued that the efficiency difference might be due to poor liquid distribution. To eliminate the possibility of poor liquid distribution, the top liquid distributor was modified to give four times the number of drip points, thus increasing the drip point density from 350 to 1400 drip points/m<sup>2</sup>. This number of drip points per square metre is almost ten times more than the recommended number of drip points of 150 drip points/m<sup>2</sup>; it can thus be assumed that the packing will be well wetted by the distributor.

The increased number of drip points was achieved by welding an end piece to the tip of each drip point which effectively split each drip point into four drip points. The end pieces that are welded to the drip points are presented in Figure 59 (a), while Figure 59 (b) shows the distribution after modification.



a)



b)

**Figure 59 – a) End pieces welded to each drip point. b) Distribution after modifications**

The efficiency results of the top section from before and after the modification was made is presented in Figure 60.

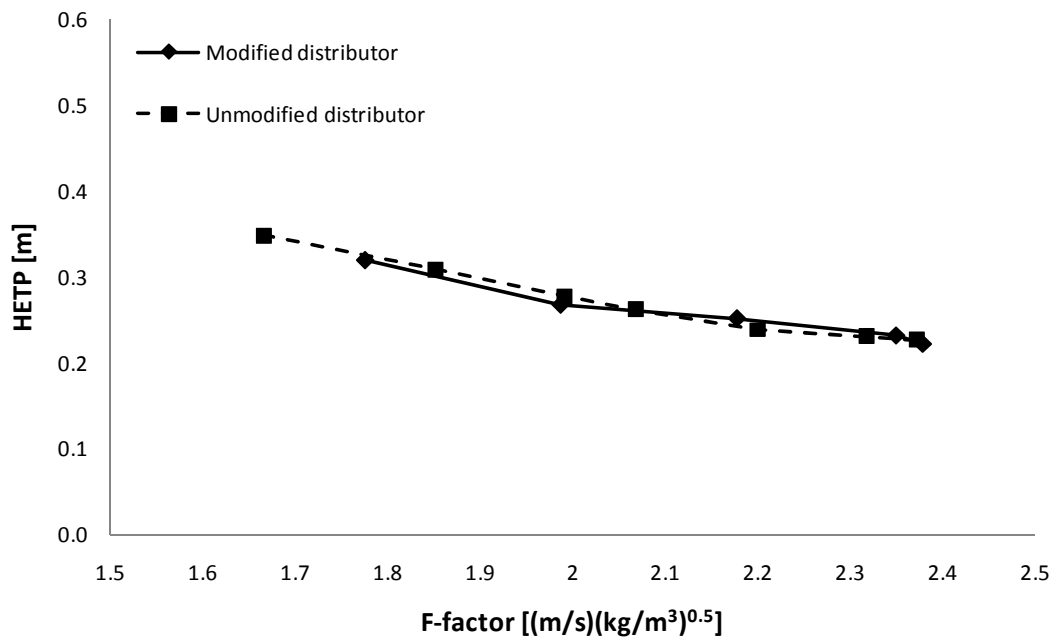


**Figure 60 - Efficiencies results before and after modification to liquid distributor**

Increasing the number of drip points from 11 to 44 did not make any difference in the efficiency of the top section (see Figure 60). Therefore, the performance difference between

the top and bottom bed could not be attributed to poor liquid distribution from the distributor. However, this test also verified the data presented here.

### **4.4.3 Property Differences**

Increased HETP values at the bottom of the column can be ascribed to the butanol mixture having a lower viscosity at the bottom (0.383 cP) compared to the top (0.456 cP) of the column. These viscosity values were generated using the same Aspen Plus™ simulation as discussed in section 4.2 and can thus only be used as estimated values for the bottom and top conditions in the packing bed. The lower viscosity promotes better spreading of the liquid in the bottom section than in the top section, thus giving a larger wettable and effective interfacial area. The values for surface tension generated by Aspen Plus™ indicated an increase in surface tension for the liquid mixture from 15 mN/m at the top of the column to 15.6 mN/m at the bottom of the column. The increase in surface tension will decrease the wetting characteristic of the liquid mixture and therefore reduce the wetted area.

The above sections have shown that the efficiency difference between the top and bottom section could be due to a number of reasons. Thus, efficiencies from only the more stable bottom packed section were used to compare it to published data and predictive models. However, more experimental testing should be done to clarify this efficiency difference between the top and bottom sections.

The next section focuses on comparing the results from the bottom section with published results and predictive models. The bottom section is chosen because it is not affected by the sub-cooling of the condenser and thus much more stable flow rates of the vapour and liquid phases can be expected. The bottom section also resembles more the HETP curve of high surface area structured packing, found in literature, better.

## **4.5 Comparison of Results**

In this section the results from this study are compared with the results published in the literature, and thereafter the results are compared with the predictions of predictive models.

### 4.5.1 Results Compared to Sulzer™ Brochure and Published Data

The only data found in the literature for Mellapak™ 350Y is that published by Spiegel and Meier (1987), which consists of four data points with a trend line. These trend lines are also used in the Sulzer’s brochure (Sulzer™ Chemtech, n.d.). The Spiegel and Meier (1987) experiments were conducted in a 1 m internal diameter column with the chlorobenzene/ethylbenzene test mixture at 0.96 bar abs. These data points and trend lines for the efficiency and pressure drop are compared with results obtained from this study in Figure 61 and Figure 62.

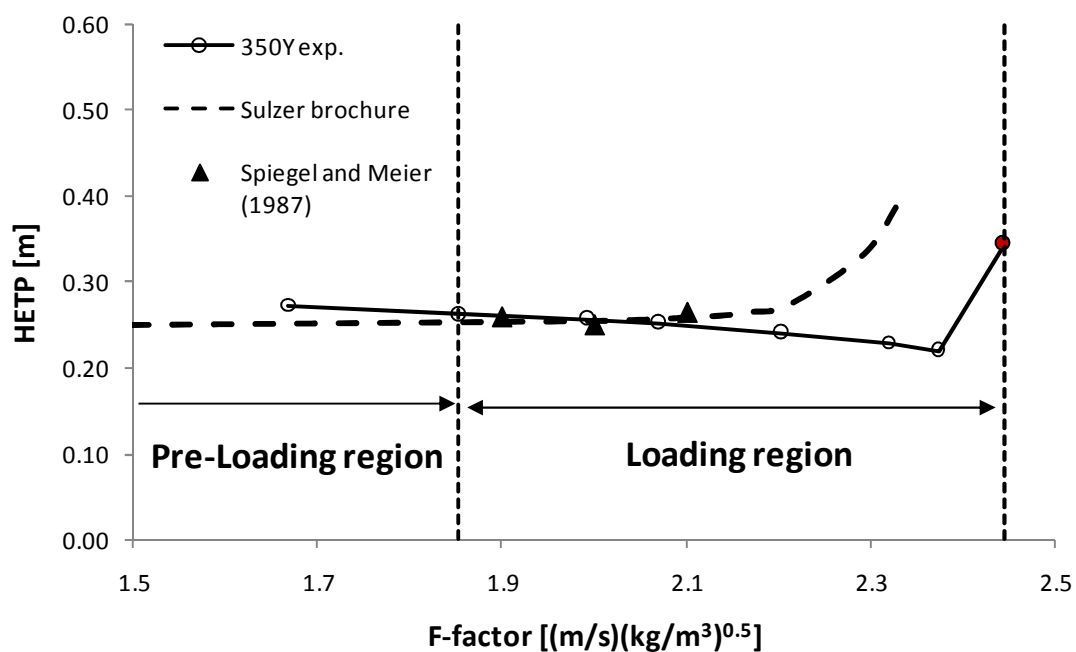


**Figure 61 – Efficiency results compared to published data**

Data obtained from a 0.2m internal diameter column in this study compares well with data from a 1m diameter column (see Figure 61). The trend line from the Sulzer™ brochure indicates that 350Y has a lower capacity than observed in this study. After flooding point, liquid started to accumulate in the condensate return line, and therefore the system cannot be viewed as a total reflux system, since not all the liquid can be returned to the packed section. For this reason the results after flooding were not included in Figure 61 but can be found in Appendix - Section 8.10. Liquid accumulating in the condensate return line starts to occur when the shear stress of the vapour phase is sufficient to hold the liquid flowing down the column.

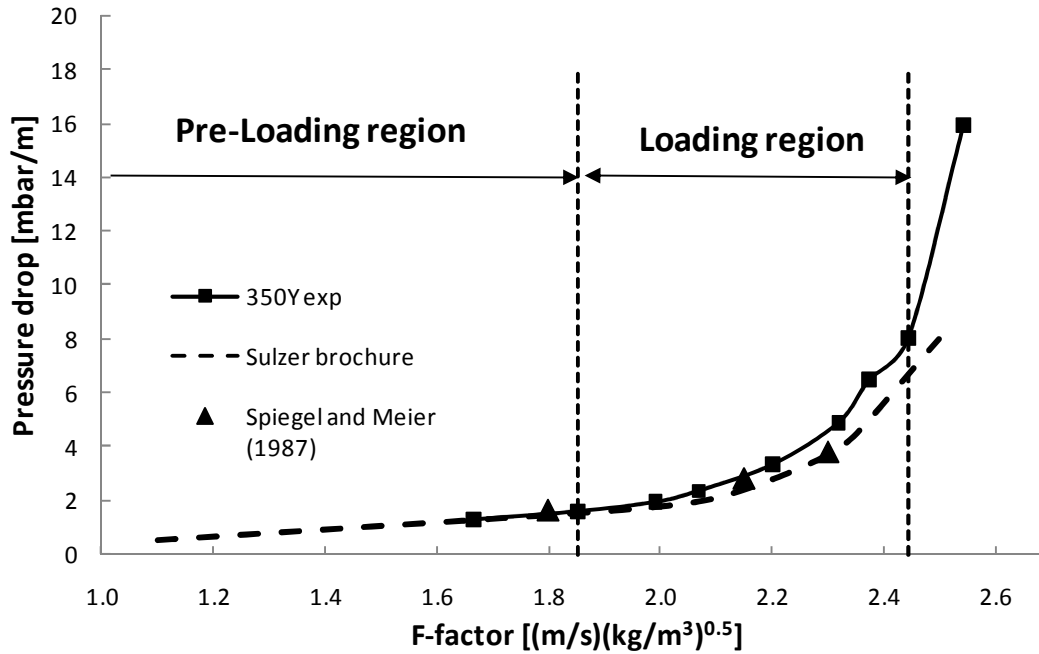


**Figure 62 – Pressure drop results compared to published data**

In Figure 62 the data from Spiegel and Meier (1987), together with trend line from the brochure, are plotted with the pressure drop data measured during the experimental phase. The data published by Spiegel and Meier (1987) compares well with the data from this study (see Figure 62). However, the trend line from the brochure starts to deviate from the experimental values at higher gas flow rates; which could be as a result of the diameter difference. A larger diameter column will have less flow channels ending at the column wall than the smaller diameter column. Directional changes by the gas contribute to the pressure drop over the packed bed, and therefore could be a reason for the higher pressure drop observed in the 0.2 m column than in the 1 m column. Moreover, the effect of column diameter on the pressure drop is not as pronounced as that which Olujić (1999) observed for B1-250Y structured packing. This could be due to the fact that the Sulzer™ 350 m<sup>2</sup>/m<sup>3</sup> has a higher surface area than B1-250Y packing. The larger surface area will reduce the wall effect exerted by the column wall. It can be expected that the effect of column diameter will further decrease as the packing surface area increase.

#### 4.5.2 Model Predictions Compared to Experimental Results

In this subsection the results obtained for the Mellapak™ 350Y will be compared with results obtained from the predictive models discussed in Chapter 2.

In Figure 63 to Figure 66, the experimental results are compared against the three predictive models. The predicted and experimental efficiencies are plotted against the vapour capacity factor in Figure 63 and Figure 64, whereas the predicted pressure drop and experimental pressure drop are plotted in Figure 65 and Figure 66.

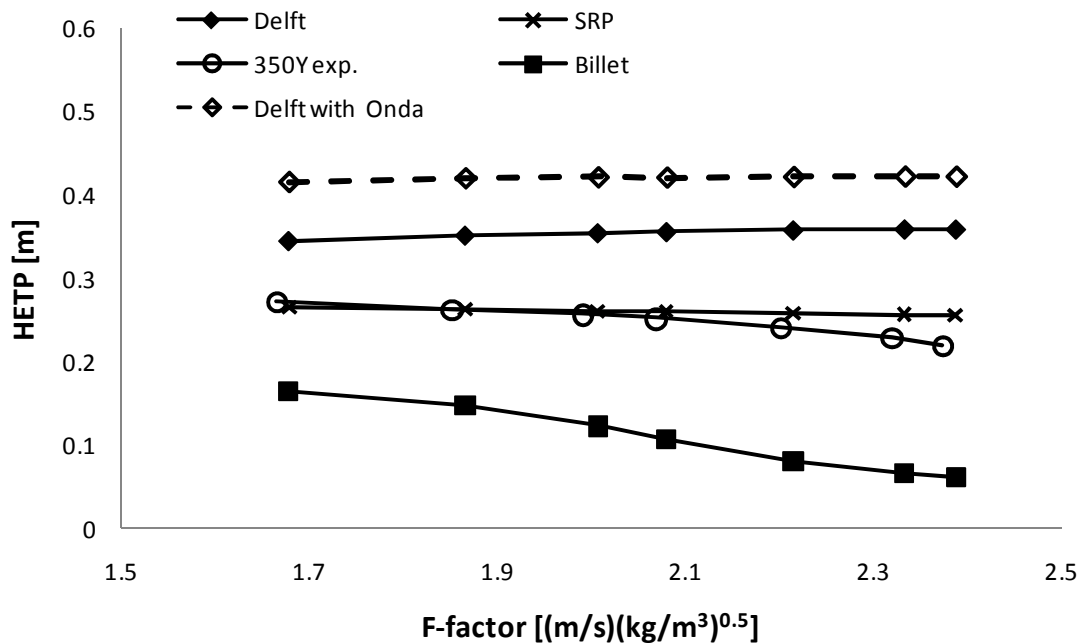


**Figure 63 – Comparison between the experimental HETP values and that obtained from predictive models (Rocha *et al.*, 1993; Billet and Schultes, 1999; Olujić *et al.*, 1999; Olujić *et al.*, 2004)**

Figure 63 shows that both the Delft model (Olujić *et al.*, 1999), and the Delft model with Onda (Olujić *et al.*, 2004), over-predict the HETP. Both models reflect a slight linear increase in HETP as the vapour capacity factor increases. The increase can be attributed to the mass transfer coefficients for the vapour and liquid phases that increase linearly with an increase in vapour capacity factor (see Figure 20 and Figure 21). The effective interfacial surface area stays almost constant with an increase in vapour capacity factor, and is thus almost independent of the liquid load (see Figure 19). The Delft model with Onda also has a lower effective interfacial surface area than the original Delft model (see Figure 19), which leads to the latter giving a lower prediction of HETP.

The SRP model prediction of the efficiency is excellent in the pre-loading region but starts to deviate in the loading region. Liquid hold-up starts to increase exponentially in the loading region, which increases the effective interfacial area for mass transfer. In the loading region

the SRP model only predicts a linear increase in the liquid hold-up (see Figure 18) which explains the slight over prediction of the HETP in the loading region. Despite this, the prediction by the SRP is excellent and the predictions given for the loading region are on the safe side.

As mentioned in Chapter 2, it is important for the Billet model to accurately predict the flooding point. The Billet model under-predicts the HETP with a sharp decrease in the HETP. The main reason for the poor prediction and sharp decrease in HETP is because the Billet model under-predicts the flooding point. The flooding velocity predicted by the Billet model is  $u_{FI} = 1.4 \text{ m/s}$  ( $2.15 \text{ (m/s)(kg/m}^3)^{0.5}$ ) and the experimentally observed flooding velocity was  $u_{FI} = 1.6 \text{ m/s}$  ( $2.49 \text{ (m/s)(kg/m}^3)^{0.5}$ ). After adjusting the predicted flooding point to the observed flooding velocity, the Billet model follows the correct trend for the HETP, but still under-predicts the efficiency (see Figure 64). This under-prediction of the flooding point and HETP may be a result of the packing constants used in the model. The constants available for metal structured packing used for flooding velocity, vapour mass transfer coefficient and liquid mass transfer coefficient for the Billet model are given in Table 18 and a summary of all the constants available for structured packing is given in Appendix – Section 8.2.

**Table 18 – Constants for Billet model available for metal structured packing (Extraction of Table A 5 in Appendix - Section 8.2)**

Manufacture	Material	Description	a [m <sup>2</sup> /m <sup>3</sup> ]	ε [m <sup>3</sup> /m <sup>3</sup> ]	C <sub>FI</sub>	C <sub>L</sub>	C <sub>V</sub>
Ralu pak	Metal	YC -250	250	0.945	2.558	1.334	0.385
Mellapak™	Metal	250Y	250	0.97	2.464		
Gempack	Metal	A2T-304	202	0.977	2.099		
Impulse packing	Metal	250	250	0.975	1.996	0.983	0.27
Montz™ packing	Metal	B1-200	200	0.979	2.339	0.971	0.39
		B2-300	300	0.93	2.464	1.165	0.422

From Table 18, it can be seen that the constant for flooding velocity for structured packings with the same surface area can vary as much as 0.562 from one another. Since no packing constants are available for Mellapak™ 350Y, the constant for Mellapak™ 250Y packing was used in the model predictions. However, the Billet model predicts the observed HETP within its confidence level (see Figure 64), when the flooding velocity constant is adjusted from 2.464 to 2.775 and when the mass transfer constants (C<sub>L</sub> and C<sub>V</sub>) for Impulse 250 packing

are used instead of that of Montz™ B2-300 packing. The main reason for the Billet model's success in predicting the correct trend for the HETP (in the loading region) can be attributed to its accurate prediction of the shape of the liquid hold-up curve in the loading region.

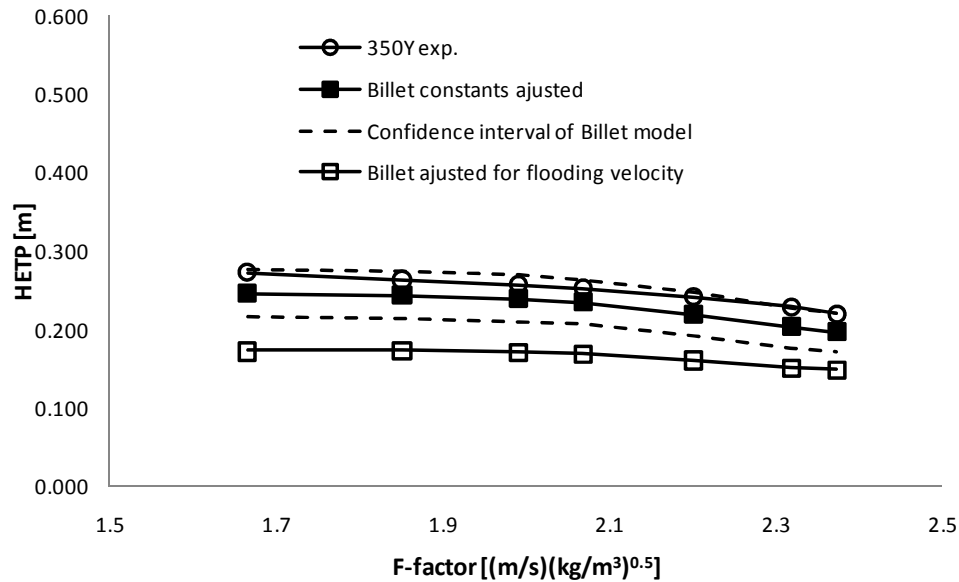


**Figure 64 – Comparison of the HETP experimental values with the Billet model adjusted**

In Figure 65, experimental pressure drop data is compared with the SRP and Delft predictive models and in Figure 66 the two Billet models are plotted together with the experimental values.

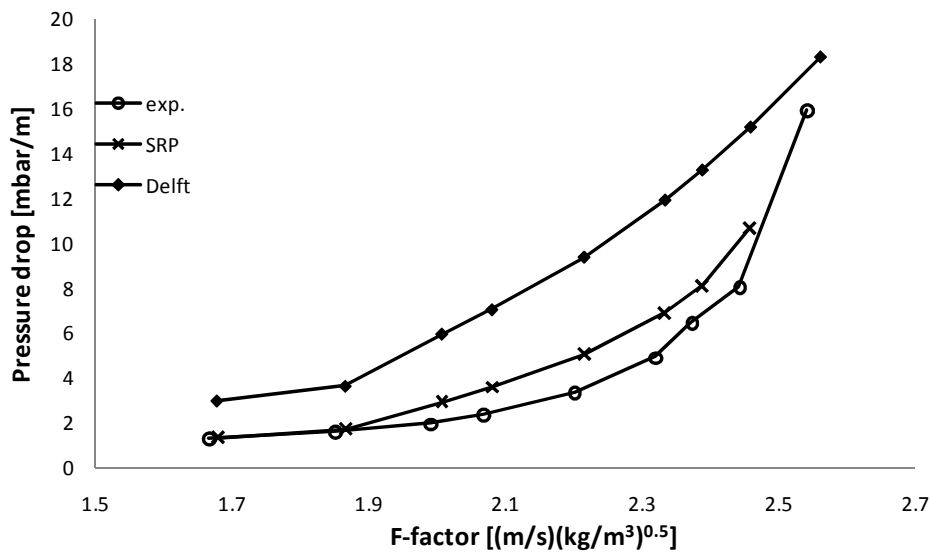


**Figure 65 – Comparison of the experimental pressure drop data with predictive values from the SRP (Rocha et al., 1996) and Delft (Olujić et al., 2004) models**



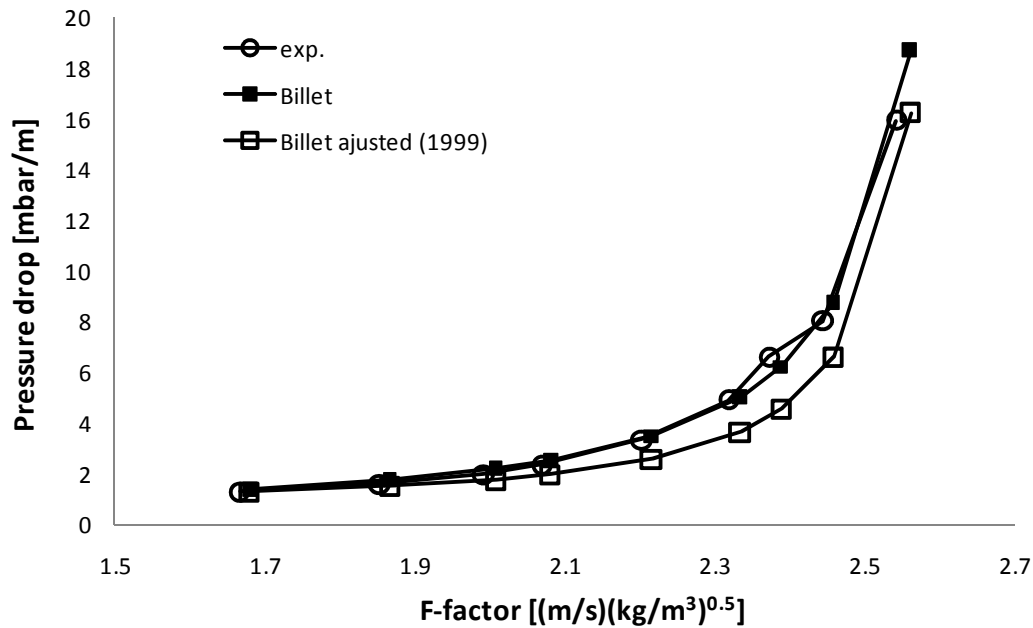


**Figure 66 - Comparison of the experimental pressure drop data with Billet et al. (1993) and Billet et al. (1999)**

Figure 65 indicates that both the Delft and SRP models over-predict the pressure drop, with the latter giving values closer to that observed in this study. Both models give almost parallel predictive trends, which are expected because both models used the same correlation developed by Verschoof *et al.* (1999) to predict the loading point and the pressure drop in the loading region. The only difference in the two models is the way they predict the pre-loading pressure drop.

Figure 66 shows that the Billet model predicts the pressure drop accurately over the entire operating range. In addition, the Billet model (adjusted), with the liquid resistance coefficient expressed in terms of the Froude number instead of the Reynolds, under-predicts the pressure drop in the loading region, but accurately predicts the pressure drop in the pre-loading region (Figure 66). The reason for the accurate prediction of the Billet model could be due to the fact that the constant for the dry pressure drop used was fitted by Erasmus (2004) on experimental data of Flexipac 350Y, which is similar to the Mellapak™ 350Y.

In Figure 67, the pressure drop data for the distributors obtained from the experimental runs are compared with the predictions from the model of Rix and Olujić (2008).

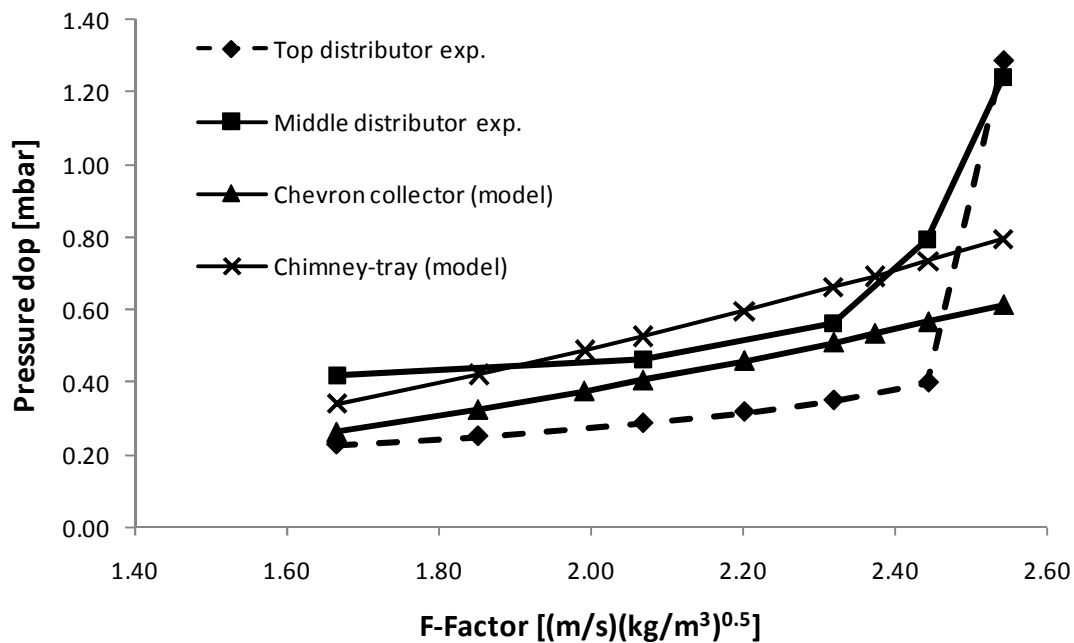


**Figure 67 - Comparison of the experimental pressure drop over distributors with a model proposed by Rix and Olujić (2008)**

As expected, the pressure drop over the middle distributor is higher than that of the top distributor. This is because the middle distributor is equipped with hats on the chimney tubes, whereas the top distributor is not fitted with hats (see Chapter 3). The pressure drop model for the chimney-tray collector represents the pressure drop for the middle distributor well, while the chevron collector falls more in the middle of the two distributors. The models predict the pressure drops well considering the fact that they are based on a simple contraction model for gas flow, and do not take any liquid flow into account. For this reason this model can be used to give an estimation of what the pressure drop over the distributor will be during operation.



---

## 5 Conclusions

---

The main aim of this study was to establish a facility that can be used to generate performance data for high surface area structured packing. To achieve this goal, it was necessary to conduct a thorough literature review and to evaluate the experimental results generated in this study.

From the literature review it was found that:

1. Distributors play an important role in the performance of structured packing, and poor liquid distribution may have a detrimental effect on the performance of packing. It is therefore essential that the correct liquid distributor be used.
2. Pressure drop over distributors is small compared to the pressure drop over the packing and is thus neglected in most cases. However, pressure drop over the distributors becomes crucial in heat-sensitive distillation. The only reliable model available to predict the pressure drop over distributors is the one developed by Rix and Olujić (2008).
3. The internal column diameter does not have an effect on the HETP of structured packing for columns larger than 0.15 m (Meier et al., 1979; Wu and Chen, 1987 and Deible et al., 1997). The wall effects are a function of column diameter and packing surface area, and can be minimised by either increasing the column diameter, or increasing the surface area of the packing.
4. A study by Olujić (1999) reportedly showed that the internal column diameter does have an effect on the pressure drop, and therefore capacity, of structured packing. The study was done on Montz™ B1-250 structured packing in internal diameter columns sizes ranging from 0.2 to 1.4 m. It was also found that this effect is limited to column diameters below 1 m, and becomes more prominent as the column diameter approaches the height of the packing element. Therefore it is recommended that a column diameter of at least twice the height of the packing element is used. Olujić (2008) proposed that a standardised pilot plant should be used to determine the efficiency of structured packing. In his report a

0.4 m internal diameter column is recommended as the standard, because it serves as a good compromise to study the performance of Sulzer™, Montz™ and Koch-Glitsch™ packings.

5. It is not always possible to use Onken's (1990) recommended test mixtures for a specific pilot plant application and there is therefore a need for a method that can be used to select a test mixture for a pilot plant setup.
6. There are quite a few models and modelling techniques available to predict the efficiency of structured packing. These modelling techniques include the use of empirical and semi-empirical correlations, neural network, film models, CFD and even short cut methods. The SRP, Billet and Delft models often form the base from which new correlations are developed and for this reason were selected as models to predict the performance and efficiency of structured packing.
7. The different performance and capacities of various packings make it difficult to model structured packing using semi-empirical models. This is because one or more constants of the semi-empirical models are based on the experimental data of a specific packing type and, in some cases, require predetermined constants. It can thus be expected that the models will fail to accurately predict the efficiency and capacity of the structured packing when i) there are no experimental constants available (for a specific structured packing) and ii) the models are applied outside their validation conditions. The drawback of the Billet model is that it requires six packing constants that are not always available for a specific type of packing. It can therefore be expected that predictions with the Billet model will deviate from experimental conditions if the wrong constants are used. The SRP model requires four constants and the Delft model requires no experimentally determined constants.
8. The Billet and Schultes, SRP and Delft models differ in their methods of predicting the liquid and vapour mass transfer coefficients. This leads to different performance predictions when using these models to predict the performance of a continuous distillation column with L/V ratios that differs from unity (for total reflux,  $L/V=1$ ).
9. The models differ in the way that they predict the pressure drop, loading and flooding points, hold-up and effective surface area. However, the SRP and Delft

models do share similarities in some aspects, e.g. both models use correlations developed by Verschoof *et al.* (1999) to predict the loading point and pressure drop over the packing in the flooding region.

10. There is a large difference in the predictions of the HETP for Mellapak 350Y structured packing by the Billet, Delft and SRP models.

Thus, due to the lack of understanding of the behaviour of packed columns and their differences in predicting the height equivalent to a theoretical plate for Mellapak 350Y structured packing, a packed column with an internal diameter of 0.2 m equipped with two packed sections of 2 m was designed, constructed, and commissioned. The column can be used to generate HETP and pressure drop data from structured packing under total reflux and is designed to operate at pressures ranging from 0.3 to 1 bar abs, vapour flow rates of  $0.73 - 3.65 \text{ m/s (kg/m}^3)^{0.5}$  and liquid flow rates of  $5 - 25 \text{ m}^3/\text{m}^2\cdot\text{h}$ . Provision was made in the design to later convert the setup to a continuous column so that the effect of L/V ratio on the efficiency can be studied. The main aim of this study was thus to establish a facility that can be used to investigate the performance of structured packing with high specific surface area under total reflux.

The hazardous areas around the column were also classified according to SANS. After this the necessary explosion-proof and intrinsically safe sensors were chosen and installed. Once the installation of all the sensors was completed, a COC was issued by a master electrician to certify the proper and safe installation of electrical sensors and equipment.

A methodology to help in the selection of a test mixture for a specific pilot plant was also developed in this study (see Section 3.7). From this it was found that 2-butanol/iso-butanol and p-xylene/o-xylene were suitable test mixtures for the pilot plant setup. However, these mixtures do not form part of the recommended test mixtures of Onken and Arlt (1990) and therefore it was necessary to validate the VLE data found in literature.

#### **Vapour-liquid equilibrium results:**

1. The VLE data for 2-butanol/iso-butanol and o-xylene/p-xylene systems, obtained from Kutsarov *et al.* (1993) and Zong *et al.* (1983), compares well with the experimental VLE data obtained from this study. Therefore, the data from

Kutsarov *et al.* (1993) and Zong *et al.* (1983) can be deemed as accurate and can be used to calculate the HETP of structured packing.

2. The NRTL model with the interaction coefficients recommended by Kutsarov *et al.* (1993) and Zong *et al.* (1983) fits the experimental data well and can thus be used to predict the phase equilibrium of the mixtures.
3. The NRTL model was then also further used to derive an equation to accurately calculate the relative volatility at a given liquid composition.

The 2-butanol/iso-butanol system was then used to validate the working of the pilot plant, and the results for the total reflux experiments are summarised below. Results are also compared against the predictions of the Delft, SRP and Billet models.

#### **Total reflux results:**

1. It was found that a four hour period is sufficient for the system to reach phase equilibrium.
2. A difference in the efficiency of the top and bottom section of the packed bed was observed. This can be attributed to changes in the physical properties (i.e. viscosity and surface tension) from top to bottom, heat losses to the environment and sub-cooling of the condensate return.
3. Increasing the amount of drip points from 11 to 44 did not influence the efficiency of the structured packing.
4. Efficiency and pressure drop results for Mellapak™ 350Y structured packing compared well with the data published by Spiegel and Meier (1987) that was obtained in a 1 m internal diameter column with the chlorobenzene/ethylbenzene system.
5. The efficiency and pressure drop results compared well with the trend lines published in the Sulzer™ brochure in the pre-loading region, but start to deviate in the loading region. The deviation of the pressure drop data could be ascribed to the differences in column diameter (see Section 2.5).
6. A comparison of the efficiency results of the Mellapak™ 350Y packing with predictive models showed that:

- a. The SRP model accurately predicts the efficiency of this particular structured packing in the pre-loading region, but starts to over-predict the HETP of the packing in the loading region.
  - b. The Billet model under-predicts the HETP of the packing over the entire range. The Billet model also under-predicts the flooding point. By adjusting the flooding constant from 2.464 (for Mellapak™ 250Y) to 2.775 the observed flooding point is predicted by the Billet model. The deviation in the Billet model may thus be due to the constants used in the predictive model. No packing constants for the Billet model were available for this packing and therefore the constants proposed by Erasmus (2004) were used (Section 4.5.2). However, the Billet model accurately predicts the experimental HETP values within its confidence level, if the constants for liquid and vapour mass transfer coefficients of Impulse 250 are used instead of the constants proposed by Erasmus (2004). Erasmus (2004) used the constants for Montz™ B2-300 because it has the closest surface area when compared to Flexipac 350Y.
  - c. The Delft model over-predicts the HETP over the entire range. No packing constants are needed for this model. The original Delft model (Olujić *et al.*, 1999) gave better predictions than the Delft model that is corrected with Onda's correlation (Olujić *et al.*, 2004).
7. A comparison of the pressure drop results of the Mellapak™ 350Y packing with predictive models showed that:
- a. The SRP model accurately predicts the pressure drop in the pre-loading region and slightly over-predicts the pressure drop in the loading region.
  - b. The Delft model over-predicts the pressure drop over the entire region.
  - c. The SRP and Delft models predict almost identical pressure drop trends. This is due to the pressure drop models only differing in the way they predict the dry bed pressure drop. The loading point predicted by the two models is the same, since both models use the relations developed by Verschoof *et al.* (1999).
  - d. The Billet model, developed in 1991, described in terms of Reynolds number, accurately predicts the pressure drop over the entire liquid



range. On the other hand, the Billet model, adjusted in 1999 to include the Froude number, accurately predicts the pressure drop in the pre-loading region but under-predicts the pressure drop in the loading region.

8. Pressure drop over distributors:

- a. The pressure drop over the middle distributor is higher than that of the top liquid distributor, most probably because the middle distributor is equipped with chimney hats and the top distributor is without hats.
- b. The model developed by Rix and Olujić (2008) for chimney-tray collectors predicts the pressure drop for the middle distributor well, whereas the model for the chevron-type collectors falls almost in the middle of the top and middle distributors' pressure drop.
- c. The predicted pressure drops are of the correct order of magnitude and this model can therefore be used when an estimated value for the pressure drop is required.

From the results it was concluded that the distillation column constructed in this study can be used to generate efficiency data for high surface area structured packing.

---

## 6 Recommendations

---

The main aim of this study was to construct an experimental setup so that the performance of high surface area structured packing can be evaluated. However, future research will be aimed towards the generation of efficiency data, specifically for high surface area structured packing. Future experimental work may include:

1. Tests under different pressures, vacuum and pressures above atmospheric pressure. Packed columns are normally operated under various pressures and tests done under different operating pressures will give insight into the mass transfer and hydrodynamic behaviour of packings.
2. Tests must also be done in cases where no sub-cooling is present. These results will be valuable and can lead to an explanation of the differences observed between the top and bottom section.
3. Tests with different test mixtures. These can include test mixtures from Onken (1990) or test mixtures selected from the method developed in this study. Testing different test systems, which differ in their physical as well as thermodynamic transport properties, will help understand the influence of these factors on the mass transfer efficiency.
4. Tests using different types of high surface area structure packing, which may include studies with 350Y, 500Y and even 700Y structured packings. Limited data are available for higher order structured packings and this data could give insight into the mass transfer phenomena.
5. Wetted wall experimental work, a study on the effect of column diameter on pressure drop for high surface area structured packing, and hydraulic testing of the capacity of structured packing with air/water and other systems would prove beneficial to help fundamentally understand the mass transfer as well as hydrodynamic performance of structured packing.

6. Tests conducted under feed conditions to study the effect of reflux ratio and L/V ratio on the efficiency of structured packing. This will be done to study column loads typically encountered in industry.
7. Tests can also be conducted with high product purities at the top and bottom of the column and with extreme fluid properties such as high viscosity and surface tension mixtures to study the effect of physical properties on the interfacial mass transfer area and therefore the mass transfer of structured packing.

The results from the above suggested experimental work may lead to the development of a new model, or the modification of existing models, in order to accurately predict the performance of higher surface structured packing over the entire operating range.

Possible improvements of existing models include:

1. Both the SRP and Delft models do not accurately predict the trend of the liquid hold-up in the loading region, and the models can be improved if the correlation for liquid hold-up is adjusted.
2. As seen in this study the success of the Billet model is dependent on the experimentally determined constants. It would therefore be beneficial if more constants for different types of packings are experimentally determined.
3. All three (Billet, Delft and SRP) models give different predictions for vapour and mass transfer coefficients. This may prove problematic when working at continuous feed conditions where the liquid and vapour velocities differ from that of total reflux conditions. Predictive models are normally only validated with total reflux conditions and therefore it can be expected that their performance might deteriorate under continuous feed conditions. Therefore, a fundamental study of the liquid and vapour mass transfer coefficients and doing tests at conditions, where L/V differs from unity, will help to improve the understanding of the mass transfer phenomena.
4. Studying the vapour and liquid mass transfer coefficients, since all three models give different predictions for these coefficients.

From this study it is clear that the study of packed columns is most certainly not old hat and that there is still much room for exploration and improvements to the current predictive models.

---

## 7 References

---

- Alekseenko, S. V., Markovich, D. M., Evseev, A. R., Bobylev, A. V., Tarasov, B. B. and Karsten, V. M., 2008. "Experimental investigation of liquid distribution over structured packing." *American Institute of Chemical Engineers Journal* 54:1424-1430.
- Billet, R. and Schultes, M., 1993. "A physical model for the prediction of liquid hold-up in two-phase counter-current columns." *Chemical Engineering & Technology* 16:370-375.
- Billet, R. and Schultes, M., 1987. "Capacity studies of gas-Liquid two-phase counter-current-flow columns." *Institution of Chemical Engineers Symposium Series 104*, Brighton Centre, Brighton 2:B255-B261
- Billet, R. and Schultes, M., 1991. "Modelling of pressure drop in packed columns." *Chemical Engineering & Technology* 14:89-95.
- Billet, R. and Schultes, M., 1993. "Predicting mass transfer in packed columns." *Chemical Engineering & Technology* 16:1-9.
- Billet, R. and Schultes, M., 1999. "Prediction of mass transfer columns with dumped and arranged packings: Updated summary of the calculation method of Billet and Schultes." *Chemical Engineering Research and Design* 77:498-504.
- Billet, R. 1995. *Packed towers in processing and environmental technology*. Weinheim; New York: VCH.
- Billingham, J. F. and Lockett, M. J., 1999. "Development of a new generation of structured packings for distillation." *Chemical Engineering Research and Design* 77:583-587.
- Billingham, J. F. and Lockett, M. J., 1997. "Packing with improved capacity for rectification systems." US Patent 5632934.
- Bravo, J. L., Rocha, J. A. and Fair, J. R., 1992. "A comprehensive model for the performance of columns containing structured packings." *Institution of Chemical Engineers Symposium Series 128*, Birmingham 1:A489-A507
- Bravo, J. L., Rocha, J. A. and Fair, J. R., 1985. "Mass transfer in gauze packings." *Hydrocarbon Processing* 64:91-95.
- Brunazzi, E., Nardini, G., Paglianti, A. and Petarca, L., 1995. "Interfacial area of Mellapak packing: Absorption of 1,1,1-Trichloroethane by Genosorb 300." *Chemical Engineering & Technology* 18:248-255.

- Brunazzi, E., and Paglianti, A., 1997a. "Liquid film mass transfer coefficient in a column equipped with structured packings." *Industrial & Engineering Chemistry Research* 36:3792-3799.
- Brunazzi, E., and Paglianti, A., 1997b. "Mechanistic pressure drop model for columns containing structured packings." *American Institute of Chemical Engineers Journal* 43:317-327.
- Byer, S. M., Gibbs, R. E. and Van Ness, H. C., 1973. "Vapour-liquid equilibrium: Part II. Correlations from P-x data for 15 systems." *American Institute of Chemical Engineers Journal* 19:245-251.
- Cai, T. J., Chen, G. X., Fitz, C. W. and Kunesh, J. G., 2003. "Effect of bed length and vapour maldistribution on structured packing performance." *Chemical Engineering Research and Design* 81:85-93.
- Carrillo, F., Martin, A. and Rosello, A., 2000. "A shortcut method for the estimation of structured packings HEPT in distillation." *Chemical Engineering & Technology* 23:425-428.
- Coulson, E. A. and Herington, E. F. G., 1948. "Fractional distillation. I. The selection of test mixtures for estimating the efficiency of fractionating columns." *Transactions of the Faraday Society* 44:629-636.
- Deible, L., Goedecke, R. and Schoenmaker, H., 1997. "Investigations into the scale-up of laboratory distillation columns." *Institution of Chemical Engineers Symposium Series* 142 Maastricht, Netherlands 2:1021-1030
- Edwards, D. P., Krishnamurthy, K. R. and Potthoff, R. W., 1999. "Development of an improved method to quantify maldistribution and its effect on structured packing column performance." *Institution of Chemical Engineers* 77:656-662.
- Engel, V., Stichlmair, J. and Geipel, W., 2001. "Fluid dynamics of packings for gas-liquid contactors." *Chemical Engineering & Technology* 24:459.
- Erasmus, A. B., 2004. "Mass transfer in structured packing." PhD, Stellenbosch: University of Stellenbosch.
- Erasmus, A. B., 1999. "Mass transfer in structured packing." MSc, Stellenbosch: University of Stellenbosch.
- Fair, J. R., Seibert, A. F., Behrens, M., Saraber, P. P. and Olujić, Ž., 2000. "Structured packing performance experimental evaluation of two predictive models." *Industrial & Engineering Chemistry Research* 39:1788-1796.

- Fenske, M. R., 1932. "Fractionation of straight-run Pennsylvania gasoline." *Industrial & Engineering Chemistry* 24:482-485.
- Fenske, M. R., Lawroski, S. and Tongberg, C. O., 1938. "Packing materials." *Industrial & Engineering Chemistry* 30:297-300.
- Fitz, Jr., C. W., King, D. W. and Kunesh, J. G., 1999. "Controlled liquid maldistribution studies on structured packing." *Chemical Engineering Research and Design* 77:482-486.
- Fritz, C. W., Kunesh, J. G. and Shariat, A., 1999. "Performance of structured packing in a commercial-scale column at pressures of 0.02-27.6 bar." *Industrial & Engineering Chemistry Research* 38:512-518.
- Fuller, E.N., Ensley, K. & Giddings, J.C., 1969. Diffusion of halogenated hydrocarbons in helium. The effect of structure on collision cross sections. *The Journal of Physical Chemistry*, 73(11), pp.3679-3685.
- Fuller, E.N., Schettler, P.D. & Giddings, J.C., 1966. New method for prediction of binary gas-phase diffusion coefficients. *Industrial & Engineering Chemistry*, 58(5), pp.18-27.
- Gualito, J. J., Cerino, F. J., Cardenas, J. C. and Rocha, J. A., 1997. "Design method for distillation columns filled with metallic, ceramic, or plastic structured packings." *Industrial & Engineering Chemistry Research* 36:1747-1757.
- Haghshenas Fard, M., Zivdar, M., Rahimi, R., Nasr Esfahany, M., Afacan, A., Nandakumar, K. and Chuang, K. T., 2007. "CFD simulation of mass transfer efficiency and pressure drop in a structured packed distillation column." *Chemical Engineering & Technology* 30:854-861.
- Gude, M. & Teja, A.S., 1995. Vapor-Liquid Critical Properties of Elements and Compounds. 4. Aliphatic Alkanols. *Journal of Chemical & Engineering Data*, 40(5), pp.1025-1036.
- Helling, R. K. and DesJardin, M. A., 1994. "Get the best performance from structured packing." *Chemical Engineering Progress* 62-66.
- Johnstone, H. F. and Pigford, R. L., 1942. "Distillation in a wetted-wall column." *Transactions of American Institute of Chemical Engineers* 38:25-51.
- Kister, H., 1992. *Distillation design*. New York: McGraw-Hill.
- Kister, H., 1990. *Distillation operations*. New York: McGraw-Hill.
- Kolev, N., 2006. *Packed bed columns: for absorption, desorption, rectification and direct heat transfer*. 1st ed. Amsterdam ;Boston: Elsevier.

- Kunesh, J. G., Lahm, L. and Yanagi, T., 1987. "Commercial scale experiments that provide insight on packed tower distributors." *Industrial & Engineering Chemistry Research* 26:1845-1850.
- Kutsarov, R., Ralev, N. and Sharlopov, V., 1993. "Liquid-vapour phase equilibrium of binary systems from C6-8 aromatic hydrocarbons." *Zhurnal Prikladnoi Khimii* 66:567 - 573.
- Lamprecht, S. M., 2010. "Establishing a facility to measure packed column hydrodynamics." MSc, Stellenbosch: University of Stellenbosch.
- Liebmann, A. J., 1956. "History of distillation." *Journal of Chemical Education* 33:166.
- Lockett, M. J., 1998. "Easily predict structured packing HETP." *Chemical Engineering Progress* 94:60-65.
- Luo, S. J., Fei, W. Y., Song, X. Y. and Li, H. Z., 2008. "Effect of channel opening angle on the performance of structured packings." *Chemical Engineering Journal* 144:227-234.
- Mackowiak, J., 2009. Extended channel model for prediction of the pressure drop in single-phase flow in packed columns. *Chemical Engineering Research and Design*, 87(2), pp.123-134.
- Maćkowiak, J., 1990. Determination of flooding gas velocity and liquid hold-up at flooding in packed columns for gas/liquid systems. *Chemical Engineering & Technology*, 13(1), pp.184-196.
- Maćkowiak, J., 1991. Pressure drop in irrigated packed columns. *Chemical Engineering and Processing: Process Intensification*, 29(2), pp.93-105.
- Majer, V.; Svoboda, V., 1985. *Enthalpies of Vaporization of Organic Compounds: A Critical Review and Data Compilation*, Blackwell Scientific Publications, Oxford
- McCabe, W. L., and E. W. Thiele. 1925. "Graphical design of fractionating columns." *Industrial & Engineering Chemistry* 17:605-611.
- McNulty, K. J., and Hsieh, C. L., 1982. "Hydraulic performance and efficiency of Koch Flexipac structured packings." *Annual meeting of the American Institute of Chemical Engineers* Los Angeles, California.
- Meier, W., Hunkeler, R. and Stöcker, D., 1979. "Performance of the new regular tower packing "Mellapak" *Institution of Chemical Engineers Symposium Series* 56, 1:3.3/1
- Nieuwoudt, I., 2010a. "Intalox® Ultra™ random packing – Pushing the envelope." *Distillation Absorption*, Eindhoven, The Netherlands. 677-680
- Olujić, Ž., 1999. "Effect of column diameter on pressure drop of a corrugated sheet

structured packing." *Chemical Engineering Research and Design* 77:505-510.

- Olujic, Ž., 2008. *Standardisation of structured packing efficiency measurements*. Delft University of Technology:  
<http://www.tkk.fi/Units/ChemEng/efce/2008/presentations/Olujic-document.pdf>
- Olujic, Ž., Behrens, M., Colli, L. and Paglianti, A., 2004. "Predicting the efficiency of corrugated sheet structured packings with large specific surface area." *Chemical and Biochemical Engineering Quarterly* 18:89-96
- Olujic, Ž., Behrens, M. and Spiegel, L., 2007. "Experimental characterisation and modelling of the performance of a large-specific-area high-capacity structured packing." *Industrial & Engineering Chemistry Research* 46:883-893.
- Olujic, Ž., and de Graauw, J., 1990. "Experimental studies on the interaction between the initial liquid distribution and the performance of structured packings." *Separation Science and Technology* 25:1723-1735.
- Olujic, Ž., Jansen, H., Kaibel, B., Rietfort, T., and Zich, E., 2001. "Stretching the capacity of structured packings." *Industrial & Engineering Chemistry Research* 40:6172-6180.
- Olujic, Ž., Kaibel, B., Jansen, H., Rietfort, T., Zich, E. and Frey, G., 2003. "Distillation column internals/configurations for process intensification." *Chemical and biochemical engineering quarterly* 17:301-309.
- Olujic, Ž., Kamerbeek, A. B. and de Graauw, J., 1999. "A corrugation geometry based model for efficiency of structured distillation packing." *Chemical Engineering and Processing* 38:683-695.
- Olujic, Ž., Mohamed Ali, A. and Jansens, P. J., 2004. "Effect of the initial gas maldistribution on the pressure drop of structured packings." *Chemical Engineering and Processing* 43:465-476.
- Olujic, Ž., Seibert, A. F., Kaibel, B., Jansen, H., Rietfort, T. and Zich, E., 2003. "Performance characteristics of a new high-capacity structured packing." *Chemical Engineering and Processing* 42:55-60.
- Olujic, Ž., Seibert, A. F., and Fair, J. R., 2000. "Influence of corrugation geometry on the performance of structured packings: an experimental study." *Chemical Engineering and Processing* 39:335-342.
- Olujic, Ž., Van Baak, R., Haaring, J., Kaibel, B. and Jansen, H., 2006. "Liquid distribution properties of conventional and high-capacity structured packings." *Chemical Engineering Research and Design* 84:867-874.



- Onda, K., Takeuchi, H. and Okumoto, Y., 1968. "Mass transfer coefficients between gas and liquid phases in packed columns." *Journal of Chemical Engineering of Japan* 1:56-62.
- Onken, U. and Arlt, W., 1990. *Recommended test mixtures for distillation columns*. Second edition. Rugby: The Institution of Chemical Engineers.
- Ottenbacher, M., Olujić, Ž., Jödecke, M. and Großmann, C., 2010. "Structured packing efficiency - vital information for the chemical industry." *Distillation Absorption*, Eindhoven, The Netherlands 575 - 580
- Parkinson, G. and Ondrey, G., 1999. "Packing towers." *Chemical Engineering*, December.
- Pavlenko, A. N., Pecherken, N. I., Chekhovich, V. Yu., Zhukov, V. E., Sunder, S., Houghton, P., Serov, A. F., and Nazarov, A. D., 2006. "Separation of mixtures and distribution of a liquid on a structured packing in a large-scale model of a distillation column." *Theoretical Foundations of Chemical Engineering* 40:329-338.
- Peacock, D.G. 1967. "The selection of test mixtures for distillation columns." *Chemical Engineering Science* 22:957-961.
- Perry, D., Nutter, D. E., and Hale, A., 1990. "Liquid distribution for optimum packing performance." *Chemical Engineering Progress* 86:30-35.
- Pollock, G. S., and Eldridge, R. B., 2000. "Neural network modelling of structured packing height equivalent to a theoretical plate." *Industrial & Engineering Chemistry Research* 39:1520-1525.
- Rejl, F. J., Valenz, L. and Linek, V., 2010. "'Profile Method" for the measurement of  $k_{La}$  and  $k_{Va}$  in distillation columns. Validation of rate-based distillation models using concentration profiles measured along the column." *Industrial & Engineering Chemistry Research* 49:4383-4398.
- Rix, A, and Olujić, Ž., 2008. "Pressure drop of internals for packed columns." *Chemical Engineering and Processing: Process Intensification* 47:1520-1529.
- Robbins, L. A. 1991. "Improve pressure-drop prediction with a new correlation." *Chemical Engineering Progress* 87:87-91.
- Rocha, J. A., Bravo, J. L. and Fair, J. R., 1993. "Distillation columns containing structured packings: A comprehensive model for their performance. 1. Hydraulic models." *Industrial & Engineering Chemistry Research* 32:641-651.
- Rocha, J. A., Bravo, J. L. and Fair, J. R., 1996. "Distillation columns containing structured packings: A comprehensive model for their performance. 2. Mass-transfer Model." *Industrial & Engineering Chemistry Research* 35:1660-1667.
- Rocha, J. A., Bravo, J. L. and Fair, J. R., 1999. "Rebuttal to the comments of Dr. Jun-Hong Qiu

- on "Distillation columns containing structured packings: A comprehensive model for their performance. 1. Hydraulic models".” *Industrial & Engineering Chemistry Research* 38:3188-3189.
- Science Lab. 2010. "Material safety data sheet Ethylbenzene" [online] Available at: <<http://www.sciencelab.com/msds.php?msdsId=9923958>> [Accessed 28 February 2011]
- Schultes, M. 2000. "Influence of liquid redistributors on the mass-transfer efficiency of packed columns." *Industrial & Engineering Chemistry Research* 39:1381-1389.
- Schultes, M. 2010. "Research on mass transfer columns "Old hat or still relevant?"" *Distillation Absorption*, Eindhoven, The Netherlands. 37-42
- Seader, J. D., and Henley, E. J., 2006. *Separation process principles*. 2nd ed. Hoboken N.J.: Wiley.
- Shetty, S. and Cerro, R. L., 1997. "Fundamental liquid flow correlations for the computation of design parameters for ordered packings." *Industrial & Engineering Chemistry Research* 36:771-783.
- Shi, M. G. and Mersmann, A., 1985. "Effective interfacial area in packed columns." *German Chemical Engineering* 8:87-96.
- Spekuljak, Z., and Billet, R., 1987. "Mass transfer in regular packing." *Rev. Latinoam. Transferencia Calor. Mater.* 11:63-72.
- Spiegel, L. 2006. "A new method to assess liquid distributor quality." *Chemical Engineering and Processing* 45:1011-1017.
- Spiegel, L., and Meier, W., 1987. "Correlations of the performance characteristics of the various Mellapak types (Capacity, Pressure drop and Efficiency)." *Institution of Chemical Engineers Symposium Series 104*, Brighton Centre, Brighton 1: A203-A215
- SpiraxSarco. 1995. *Steam in the oil and chemical industries*. England: Spirax-Sarco Limited.
- Standards South Africa. 1997. *Electrical apparatus for explosive gas atmospheres*.
- Standards South Africa. 2005. *The classification of hazardous locations and the selection of apparatus for use in such locations*. 5th ed. Pretoria
- Standards South Africa. 2004. *The installation, inspection and maintenance of equipment used in explosive atmospheres*. 3rd ed. Pretoria
- Stikkelman, R., de Graauw, J., Olujić, Ž, Teeuw, H. and Wesselingh, H., 1989. "A study of gas and liquid distributions in structured packings." *Chemical Engineering & Technology* 12:445-449.

- Strigle Jr., R. F., 1994. *Packed tower design and applications: random and structured packings*. 2nd ed. Houston: Gulf Pub. Co.
- Suess, P, and Spiegel, L., 1992. "Hold-up of Mellapak structured packings." *Chemical Engineering and Processing* 31:119-124.
- Sulzer Chemtech. n.d. "Structured packings for distillation, absorption and reactive distillation."
- Totten, G., Westbrook, S. R. and Shah, R. J., 2003. *Fuels and lubricants handbook: technology, properties, performance, and testing*. West Conshohocken PA: ASTM International.
- Tyn, M.T. and Calus, W.F., 1975a. Diffusion coefficients in dilute binary liquid mixtures. *Journal of Chemical & Engineering Data*, 20(1), pp.106-109.
- Tyn, M.T. and Calus, W.F., 1975b. Estimating liquid molar volume. *Processing*, 21(4), pp.16-17.
- Underwood, A. J. V. 1935. "The Historical development of distilling plant." *Chemical Engineering Research and Design* 13a:34 - 62.
- Uresti-Melendez, J. and Rocha, J. A., 1993. "Pressure drop in ceramic structured packings." *Industrial & Engineering Chemistry Research* 32:2247-2253.
- Valluri, P., Matar, O. K., Mendes, M. A. and Hewitt, G. F., 2002. "Modelling hydrodynamics and mass transfer in structured packings - a review." *Multiphase Science and Technology* 14:303-348.
- Verschoof, H.-J., Olujić, Ž. and Fair, J. R., 1999. "A general correlation for predicting the loading point of corrugated sheet structured packings." *Industrial & Engineering Chemistry Research* 38:3663-3669.
- Wang, G. Q., Yuan, X. G. and Yu, K. T., 2005. "Review of mass-transfer correlations for packed columns." *Industrial & Engineering Chemistry Research* 44:8715-8729.
- Wang, G. Q., Yuan, X. G. and Yu, K. T., 2006. "A method for calculating effective interfacial area of structured packed distillation columns under elevated pressures." *Chemical Engineering and Processing* 45:691-697.
- Whaley, A. K., Bode, C. A., Ghosh, J. and Eldridge, R. B., 1999. "HETP and pressure drop prediction for structured packing distillation columns using a neural network model." *Industrial & Engineering Chemistry Research* 38:1736-1739.

- Wu, K. Y., and Chen, G. K., 1987. "Large-scale pilot column and packed column scale-up." *Institution of Chemical Engineers Symposium Series 104*, Brighton Centre, Brighton, 2:B225-B245
- Zenz, F. A. 1947. "Mechanism of counter-current gas liquid flow through packed towers." *Chemical Engineering Progress* 43:415-428.
- Zong, Z.-L., Yang, X.-H. and Zheng, X.-Y., 1983. "Determination and correlation of vapour-liquid equilibriums of alcohol solutions." *Journal of Chemical Engineering of Japan* 16:1-6.



---

# 8 Appendix

---

## 8.1 Boiler Capacity Calculations

In this section the total amount of heat available for the boiler will be discussed. Thereafter its effect on column diameter is studied. The boiler specifications and maximum heat output is given in Table A 1.

**Table A 1 – Heat available**

Max steam flow rate of boiler	400	kg/h
Pressure of steam	10	bar
Heat of vaporisation of saturated steam	1999.67	kJ/kg
Heat available	222	kW

From Table A 1 it can be seen that only 222 kW is available to vaporise the liquid mixture in the reboiler. Water/methanol mixture was chosen to evaluate the effect on column diameter because both water and methanol have very high heat of vaporisations and thus will give a good representation of the max capacity of the boiler system. The pure component properties as well as the mixture properties for a 50/50 water/methanol mixture are given in Table A 2.

**Table A 2 - Properties of water/methanol mixture from Onken and Arlt (1990)**

Component	Composition	Heat of vaporisation kJ/kg	Boiling point [°C]	Molar weight [g/mol]
Water	0.5	1095	100	18.015
Methanol	0.5	2257	64.65	32.042
Mixture	1	1676	82.3	25.0285

The conditions in the column for the calculations are given in Table A 3 as well as the vapour density in the reboiler (calculated with the ideal gas law).

**Table A 3 – Column conditions**

Pressure	1	bar abs
Temperature in reboiler	82.3	°C
Vapour density of mixture	0.846	kg/m <sup>3</sup>

Under these conditions and from the heat available from the boiler the maximum volumetric flow rate was calculated and is given in Table A 4.

**Table A 4 – Maximum flow rate**

Mass flow rate	0.132	kg/s
Volumetric flow rate	0.156	m <sup>3</sup> /s

Using these conditions the maximum vapour capacity factor can be calculated for different size internal diameter column. This is done and is illustrated in Figure A 1. From Figure A 1 it can be seen that a flow factor of 4 m/s (kg/m<sup>3</sup>)<sup>0.5</sup> can still be obtained at column diameter of 0.2 m. Thereafter the flow factor becomes insufficient over the entire operating range for most structured packings.

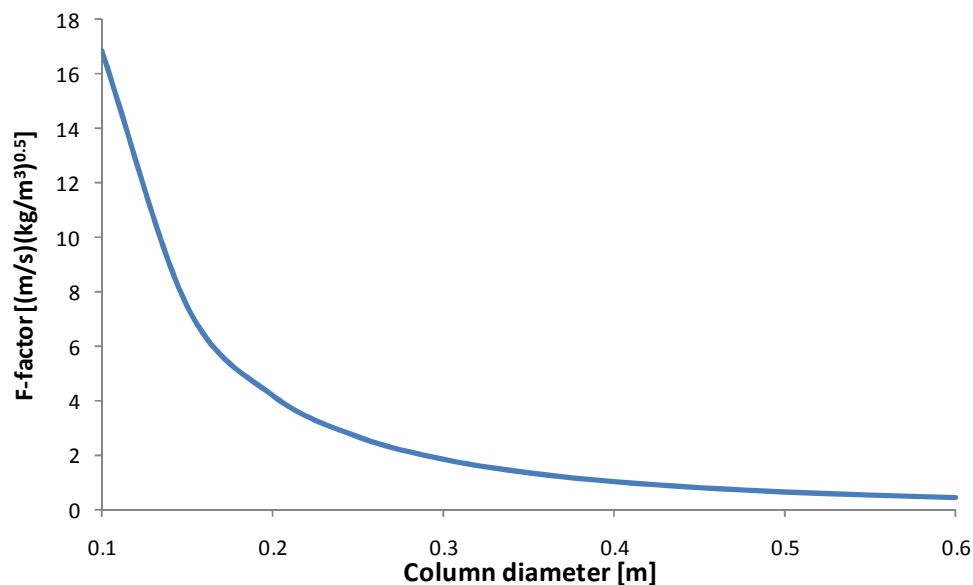


**Figure A 1 – Relationship between flow rate and column diameter for heat available**

Five times more energy is required to operate a 0.45 m column at a flow factor of 4 than is required to operate a 0.2 m column at the same conditions. This is illustrated in the sample calculations.

### 8.1.1 Sample Calculations

The energy required in having an F-factor of 4 m/s (kg/m<sup>3</sup>)<sup>0.5</sup> in a 0.45 m internal diameter column with a methanol/water system is illustrated with the working example given below. The same testing conditions are used that were used with the 0.2 m column.

To calculate the superficial vapour velocity of vapour in the column for an F-factor of 4:

$$\begin{aligned} u_v &= \frac{F_c}{\sqrt{\rho}} \\ &= \frac{4}{\sqrt{0.846}} \\ &= 4.72 \text{ m/s} \end{aligned}$$

Where  $F_c$  is the F-factor [m/s (kg/m<sup>3</sup>)<sup>0.5</sup>] and  $\rho$  is the density (kg/m<sup>3</sup>) of the vapour phase (given in Table A 3).

The superficial vapour velocity is then used to calculate the volumetric flow rate:

$$\begin{aligned} \dot{V} &= A_c \cdot u_v \\ &= \pi \left( \frac{0.45}{2} \right)^2 4.72 \\ &= 0.7512 \text{ m}^3/\text{s} \end{aligned}$$

From this the mass flow rate of the gas can be determined by multiplying the volumetric flow rate with the vapour density.

$$\begin{aligned} \dot{M}_v &= \dot{V} \rho \\ &= 0.7512(0.846) \\ &= 0.6355 \text{ kg/s} \end{aligned}$$

The heat required can now be calculated by multiplying the heat of vaporisation for the mixture (given Table A 2) with the mass flow rate.



$$\begin{aligned}\text{Heat required} &= \dot{M}_v \cdot h_{vp} \\ &= 0.6355(1676) \\ &= 1065 \text{ kW}\end{aligned}$$

Therefore a 0.45 m column requires 1065 kW energy to operate, which means about 5 times more to operate a 0.2 m column (heat required 222 kW) at the same flow factor of  $4 \text{ (m/s)(kg/m}^3\text{)}^{0.5}$ .

## 8.2 Constants for Billet and Schultes Model

All the constants available for structured packing for the Billet model are presented in Table A 5 (Billet and Schultes, 1999).

*Table A 5 – Constants for Billet Schultes model*

Manufacture	Material	Description	$a$ [ $m^2 m^{-3}$ ]	$\epsilon$ [ $m^3 m^{-3}$ ]	$C_{ip}$	$C_{FI}$	$C_h$	$C_{P,0}$	$C_L$	$C_V$
Ralu pak	Metal	YC -250	250	0.945	3.178	2.558		0.191	1.334	0.385
Mellapak	Metal	250Y	250	0.97	3.157	2.464	0.554	0.292		
Gempack	Metal	A2T-304	202	0.977	2.986	2.099	0.678	0.344		
Impulse packing	Metal	250	250	0.975	2.610	1.996	0.431	0.262	0.983	0.270
	Ceramic	100	91.4	0.838	2.664	1.655	1.900	0.417	1.317	0.327
Montz packing	Metal	B1-200	200	0.979	3.116	2.339	0.547	0.355	0.971	0.390
		B2-300	300	0.930	3.098	2.464	0.482	0.295	1.165	0.422
	Plastic	C1-200	200	0.954				0.453	1.006	0.412
		C2-200	200	0.900	2.653	1.973		0.481	0.739	
Euroform	Plastic	PN-110	110	0.936	3.075	1.975	0.511	0.250	0.973	0.167

**Table A 6 – Properties of 2-butanol/iso-butanol test mixture used to evaluate the models**

Description	Symbols	Liquid	Gas	Water	Units
Molecular weight	M	74.12	74.12	18.016	kg/kmol
Density	$\rho$	719.9763	2.359018	1000	kg/m <sup>3</sup>
Dynamic viscosity	$\mu$	0.000417	9.33E-06	0.000158	kg.m/s
Surface tension	$\sigma$	0.015384		0.072	kg/s <sup>2</sup>

### 8.3 Detailed Drawings

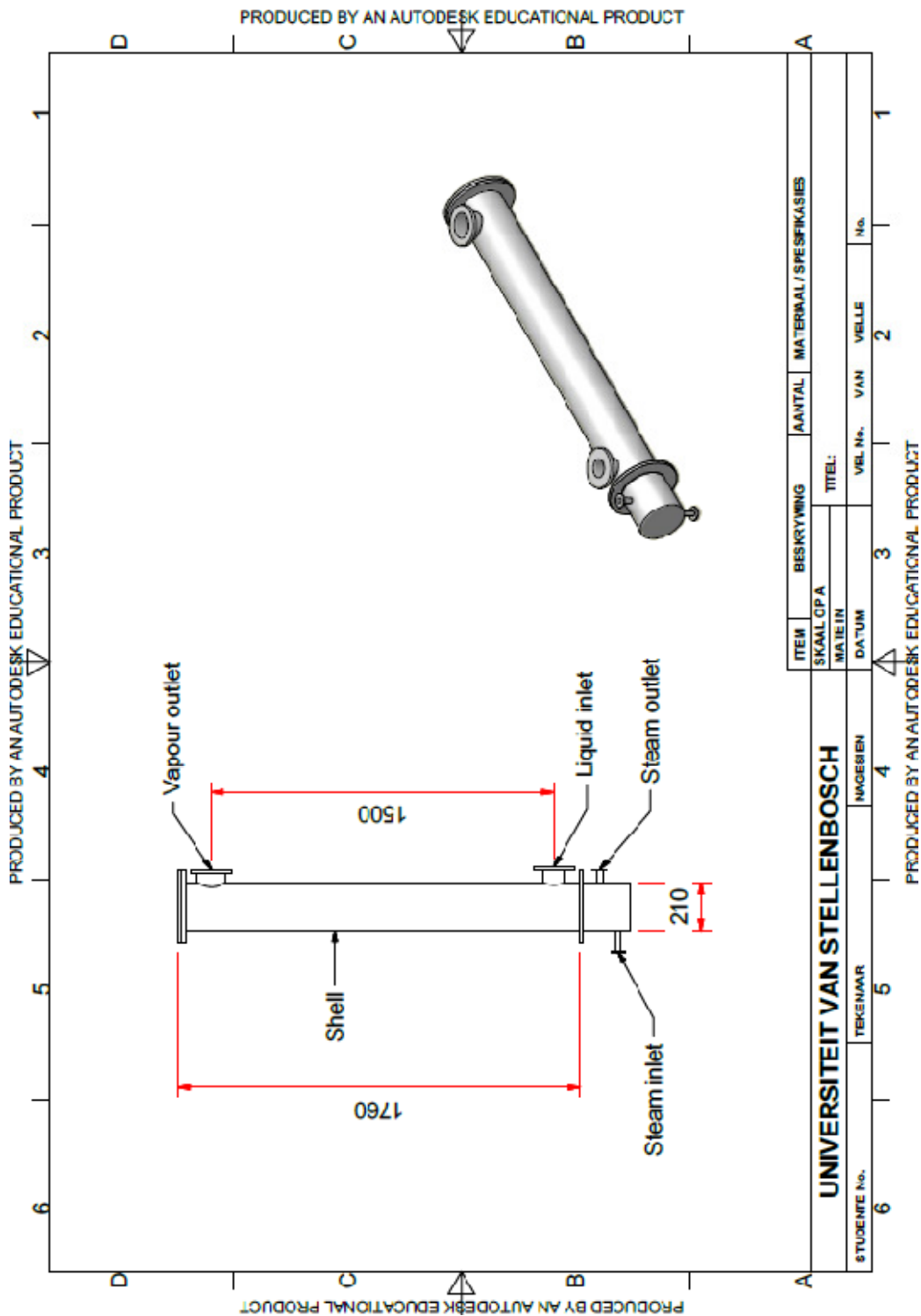
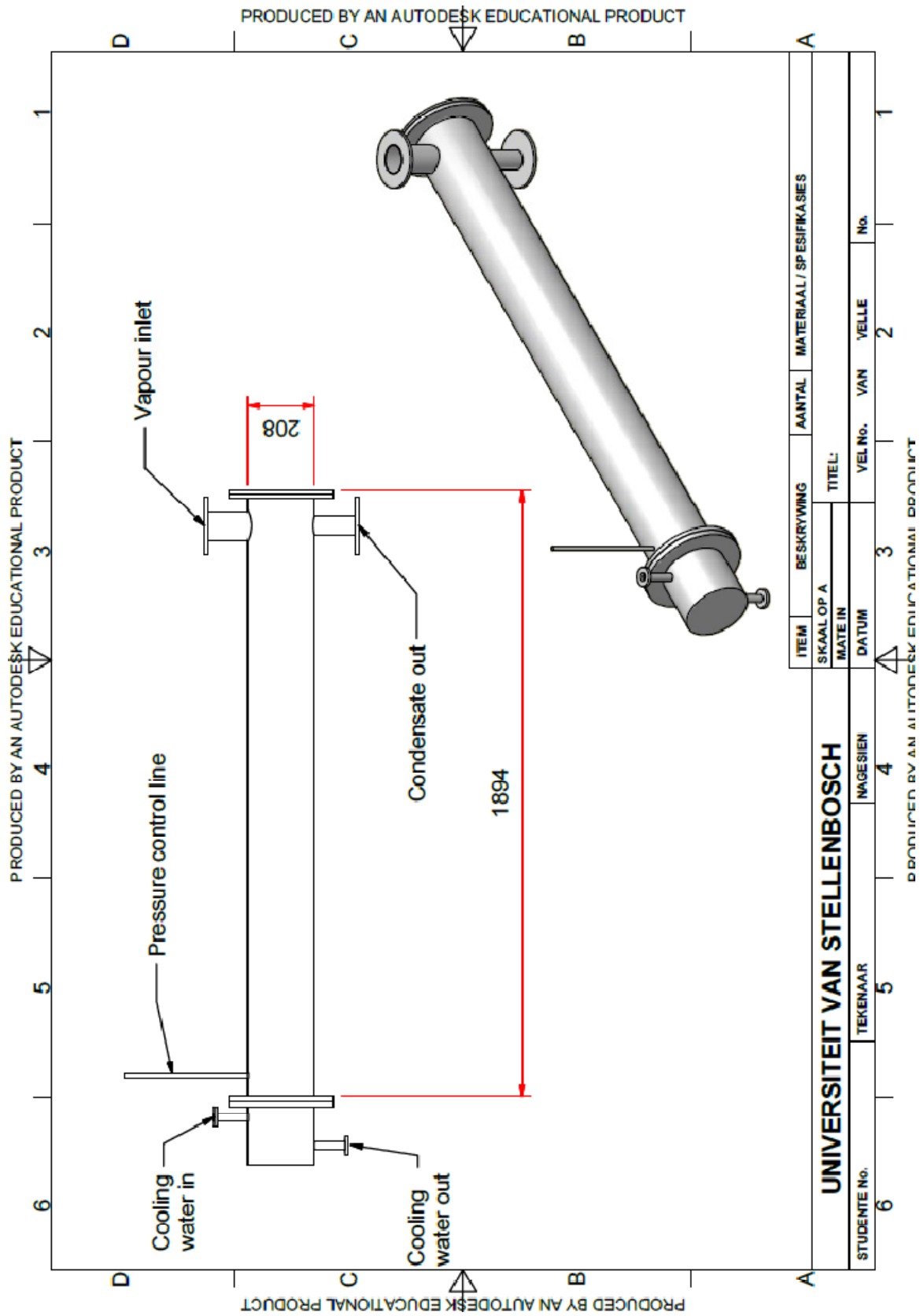


Figure A 2– Detailed drawing of reboiler



**Figure A 3 – Detailed drawing of condenser**

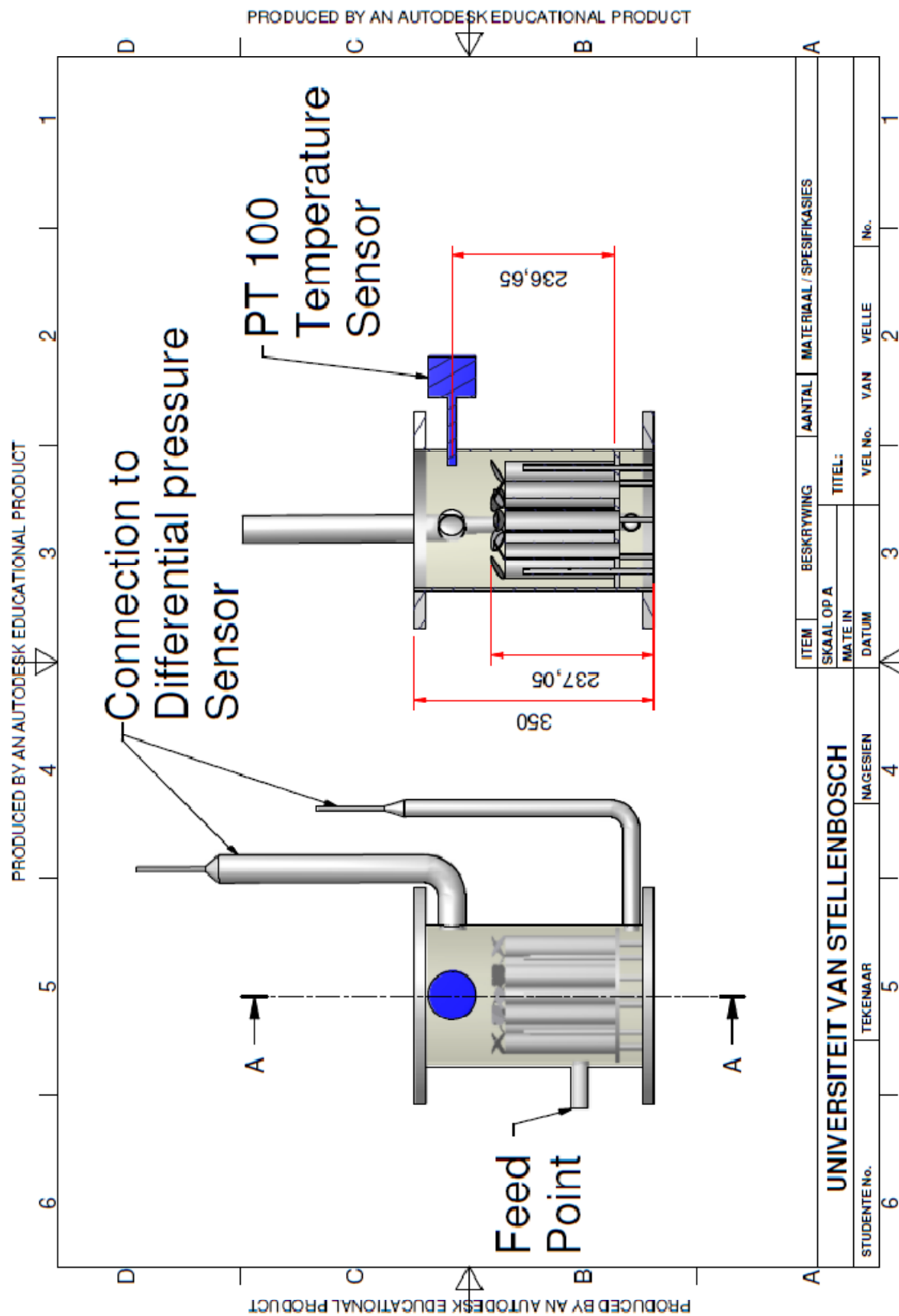


Figure A 4 – Placement of distributors

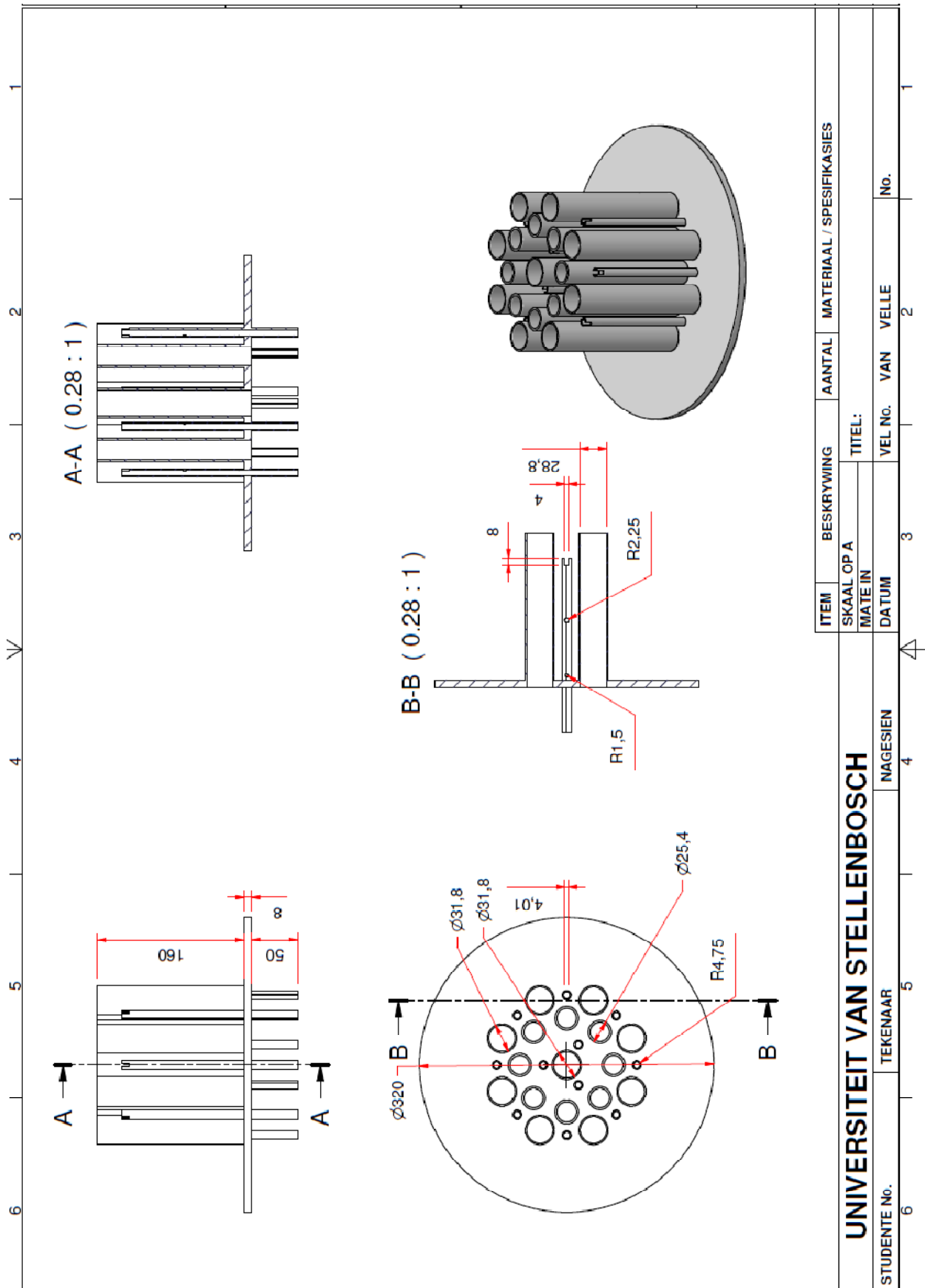


Figure A 5 – Liquid distributor and gas and liquid redistributor

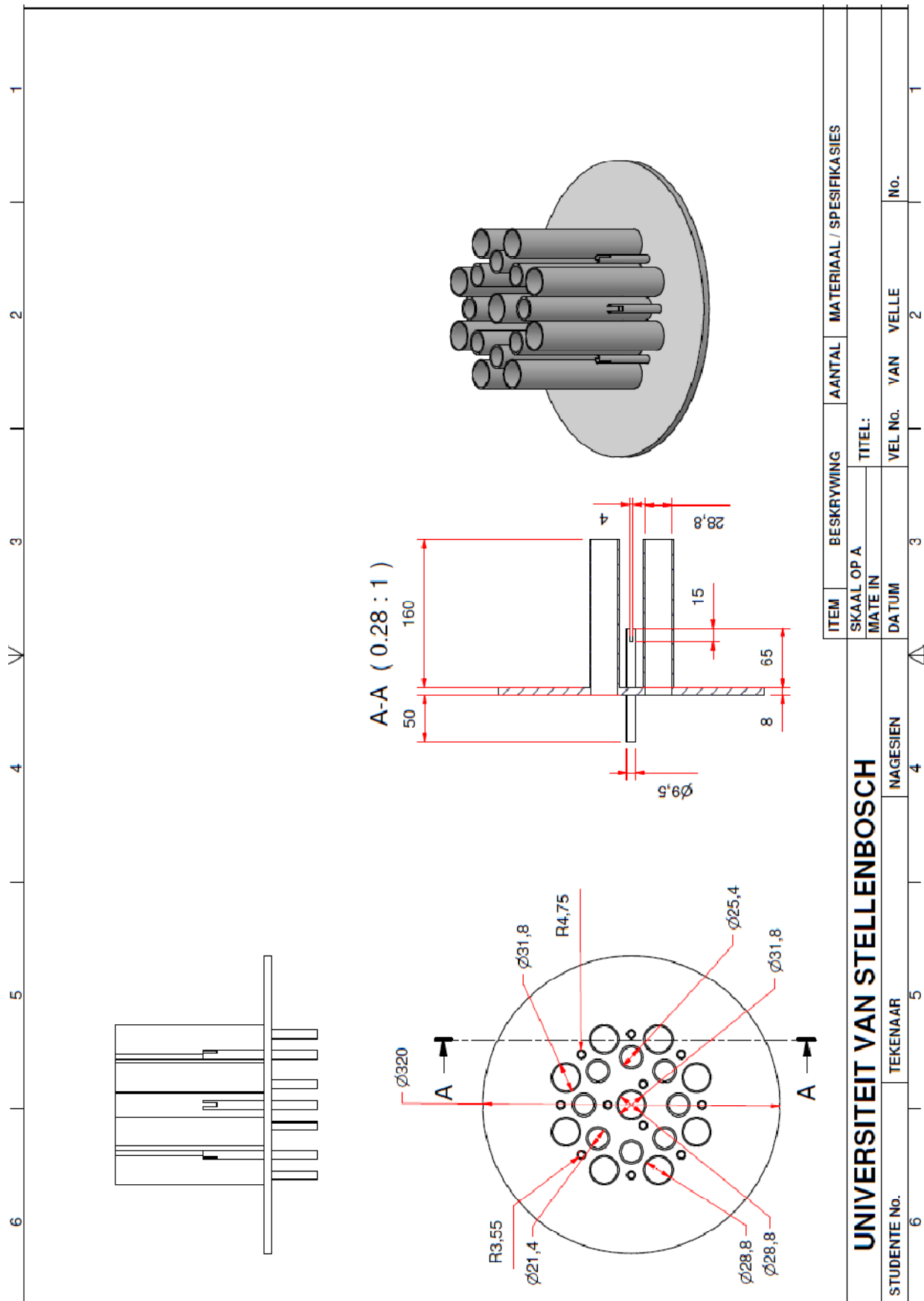
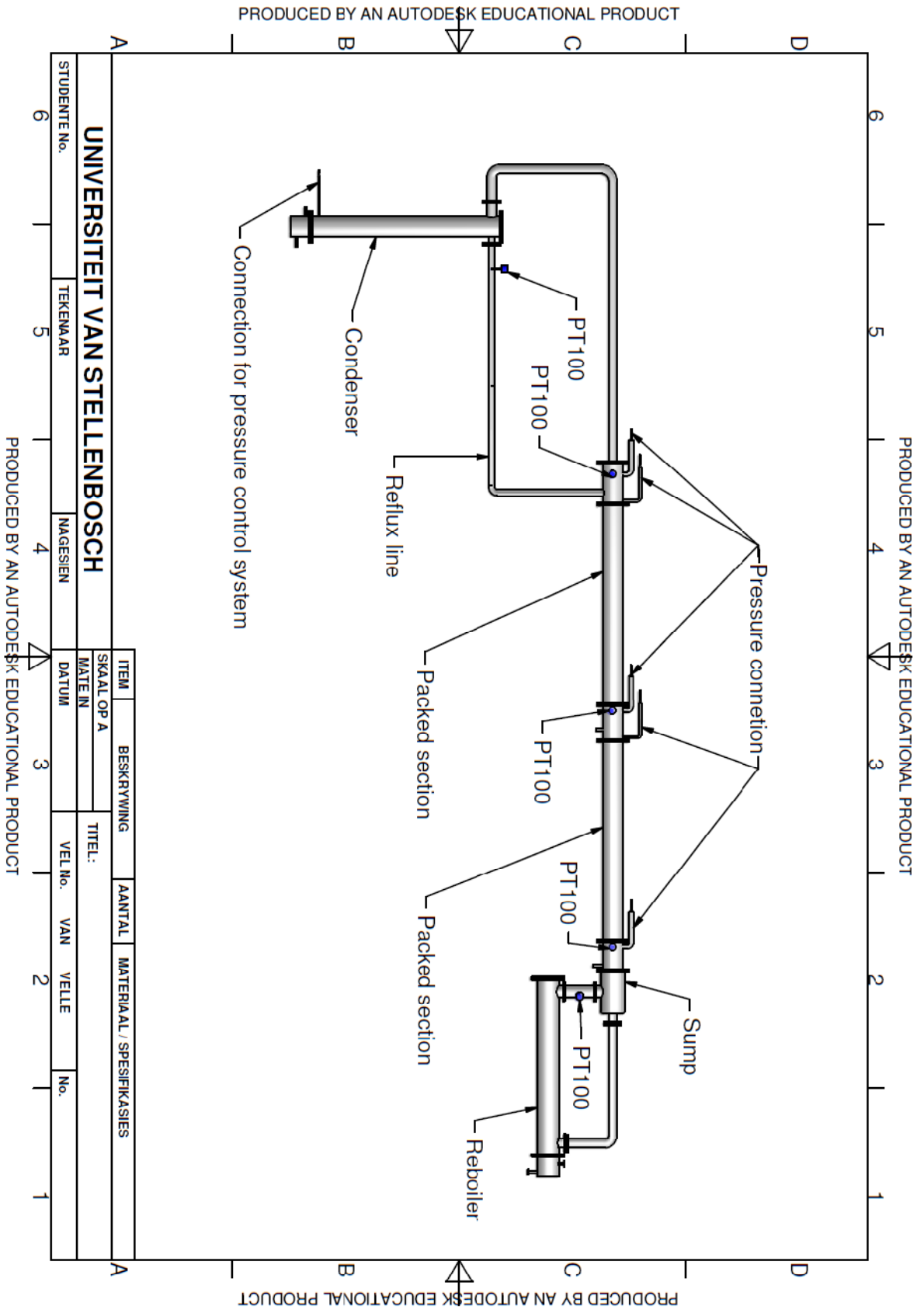


Figure A 6 –Chimney-tray





**Figure A 7 – Detailed drawing of total column**

## 8.4 Sensor Specifications

**Table A 7 - Absolute pressure transmitter specifications**

Make	Siemens
Measuring range	0 - 200 kPa absolute
Measuring accuracy	± 0.05 %
Special Classification	ATEX II 2G EEx d IIC T6
Membrane Material	316 L
Fill fluid	Silicone oil
Output	0 - 20 mA

**Table A 8 - Differential pressure transmitter specifications**

Make	Siemens
Measuring range	2.5 – 250mbar
Measuring accuracy	± 0.58 %
Special Classification	ATEX II 2G EEx d IIC T6
Membrane Material	316 L
Seal	Viton
Output	0 - 20 mA

**Table A 9 - Manometer specifications**

Fluid	Water
Length	1 m
Tube side	1/2"
Material	Glass

**Table A 10 - P100 specifications**

Make	Wika
Type	3 wire
Accuracy	0.10%

**Table A 11 - Thermocouple specifications**

Type	K
Accuracy	1%

## 8.5 VLE Operating Procedure

The flow diagram for the VLE cell is illustrated in Figure 35 (Section 3.8), where flow paths of both the vapour and liquid phases are illustrated. In this section the necessary preparation, start-up, sampling, shut down, and safety aspects will be discussed. The control procedure is obtained from the operating manual.

### 8.5.1 Preparation

1. Mix the correct amount of both testing component as accurately as possible [Total volume = 200 ml].
2. Ensure that the VLE is cell is drained and clean. If not drain the setup and blow out all remaining liquid with pressurised air.
3. To ensure that the system runs at atmospheric pressure, fully open the gate valve that connects the system to the atmosphere.
4. Load the VLE cell by pouring the mixture prepared in step 1 into the collective chamber.

### 8.5.2 Start-up

1. Start the flow of the cooling water to the system.
2. Set the power of the heating rod to an initial setting of 80 watts to heat the system.
3. Allow enough time for the entire still heat.

### 8.5.3 Running the Experiment

1. Try to set the element wattage to a level that forces the boiling liquid up through the glass coil, so much so that the flow rate of condensate and liquid to the catchment container is approximately equal. These flow rates can be compared by observing the relative rate at which the droplets return to the catchment container. To increase the liquid flow rate, increase the power to the element. The increased power pushes the liquid upward through the coil more forcefully. Similarly, the power must be decreased to lower the liquid flow rate (or to increase the vapour flow relative to the liquid flow).
2. Mechanical equilibrium is achieved once the recycle flow rates of the vapour and liquid appear to be equal. Thereafter leave the system to reach chemical

equilibrium. In this study the column was operated for seven hour before any samples were drawn.

#### **8.5.4 Sampling**

1. Capture small amounts of sample solution from the sampling points and close the sample containers to prevent vaporisation of the volatile component.
2. Clearly mark the samples, according to date and sample description.

#### **8.5.5 Shutting Down**

1. Turn off the power to the heating rod.
2. Wait for the system to cool down and thereafter stop the flow of the cooling water.
3. Thereafter drain the solution from the system back into the container from which it was stored.

#### **8.5.6 Safety Aspects**

1. Never power the heating rod while the boiling column is empty.
2. Remember to start the flow of cooling water through the condensers before the heating system is switched on.
3. In the next the operating procedure for the total reflux column will be discussed and the hazardous areas will also be classified.

### **8.6 Total Reflux Distillation Column Operating Procedure and Zoning Report**

It was necessary to classify the hazardous area around the column. This was done together with a HAZOP to ensure safe operation of the system. The following factors are taken into consideration in the zoning report (classification of hazardous areas) and the HAZOP of the system is found Section 8.6.9.

1. Control loops
2. Operating procedures
3. Pressure regulation
4. Source of release

5. Characteristics of flammable solvents used
6. Ventilation
7. Proposed classification
8. Conditions concerning proposed classification

### **8.6.1 Control Loops**

The control of the experimental setup is partly manual and partly automated. Manual control loops include the temperature of the steam tracing which is controlled with a regulating valve. Thermocouples are installed to the outside surface of the column to monitor the wall temperature of the pilot plant. The steam tracing is normally set at 3°C below the operating temperature of the column.

The control of the pressure inside the column is automated with a PID (proportional–integral–derivative) controller, absolute pressure transmitter and with two pneumatic valves. The two pneumatic valves are connected to a vacuum and nitrogen line respectively. Temperatures inside the column and pressure drop over the beds and distributors are measured with PT100s and a dP cell respectively.

### **8.6.2 Operating Procedure**

#### ***i. Before Start-up***

##### **Feed the column with the chosen system:**

The column is set up with one feed point that is situated just above the sump (see P&ID) and will be used to feed the distillation column. The procedure to load the column is as follow:

1. Make sure that the draining valves (BV-10) are closed,
2. Fill the column through the feed point until the sump is full.
3. Make sure that the feed valve (BV-9) is closed after filling.

#### ***ii. Pre-start-up Checks***

1. Drain valve (BV-10) and feed valve (BV-9) are close
2. Luberlock valves at sampling ports are closed

3. Sufficient amount of nitrogen in bottle
4. Diesel level of the boiler
5. Switchboard C2E and C1G must be switch off before the experiment start and must remain switch off during the duration of the experiment

### **iii. Safety Interlocks**

The necessary safety interlocks there put in place after the HAZOP of the column were complete. The HAZOP for the system can be found in Section 8.6.9.

1. Pneumatic valve on the main steam line will close automatically went no cooling water is flowing through the condenser.
2. An alarm will go of if the ventilation system trips.
3. A pressure relieve valve will mechanically open if the pressure exceeds 3 bar abs.
4. The main steam pneumatic valve will close automatically in the case of power failure.

### **iv. Start-up**

1. Switch on the Mechanical ventilation system
2. Switch on the ventilation fans.
3. Check that all the ventilation fans are on.
4. If the ventilation fans do not work, do not continue with the start-up.
5. Start the flow of the cooling water
6. Switch on the cooling water feed pump.
7. Make sure that cooling water is flowing through the system, by checking the flow rate on the cooling water flow meter (FI 101).
8. If no cooling water is flowing through the system, do not continue with the start-up procedure.
9. Open the valve (BV-11 and BV-12) that supplies cooling water to the reboiler's steam outlet line (line 5).
10. Open the nitrogen gas bottle
11. Open the bottle of nitrogen.
12. Regulate the pressure of the nitrogen to 1 bar above desired operating pressure.
13. Slightly open the needle valve (NV-1).

14. Switch on the Vacuum pump
15. Slightly open the needle valve (NV-2) on the vacuum line (line 14).
16. Switch on the boiler
17. Consult boiler's operating procedure.

**v. *Steam Tracing***

1. Make sure that valve on the condensate line is open.
2. Close the regulating valve.
3. Open the main steam valve that supplies steam to the steam tracing.
4. Regulate the pressure of the steam, with the regulating valve until the desired operating pressure and temperature is obtain.
5. Start opening the valves on the stream tracing's manifold.
6. Wait until the wall temperature is near the desired operating pressure.
7. After the system is preheated open the steam valve to the reboiler.

**vi. *Reboiler***

1. Make sure that the valve (GV-2) on the reboiler's condensate line (line 8) is open.
2. Open the main steam isolating valve (GV-1) on line 4.
3. Regulate the steam pressure with the regulating valve (PC-1) to the desired inlet pressure.
4. Open the pneumatic valve (PCV-1) on the control board until the desired pressure drop is reached.

**vii. *Running the Setup:***

1. Wait for the system to reach mechanical equilibrium after the start-up procedure is completed.
2. Thereafter allow sufficient time for chemical equilibrium before taking liquid samples.

**viii. *Shutdown Procedure***

1. Close the:
  - a. Pneumatic control valve (PCV-1).
  - b. Isolating valve (GV-1) that supplies steam to the reboiler.
  - c. Isolating valve to the steam tracing.

- d. Valves on the steam tracing manifold.
2. Shut down the reboiler.
3. Wait for system to cool down.
4. Switch of the cooling water feed pump.
5. Switch of the vacuum pump.
6. Close the nitrogen bottle.

**ix. *Emergency Shutdown Procedure***

1. Close the pneumatic valve that supplies steam to the reboiler.
2. Can be done on the control panel.
3. Close the steam tracings isolating valve.
4. Follow onwards form step two of the shutdown procedure.

**x. *Unloading Procedure***

The column must be unloaded and chemicals must be stored inside the chemical store room if the pilot plant setup is not used for a period of time. The column can be unloaded by opening the draining valve (BV-10), and letting the chemicals flow into the storage containers.

### **8.6.3 Pressure Regulation**

The distillation column can be operated at pressures ranging from vacuum to 3 bar (g). Thus this system is classified as a pressurised system according to the Occupational Health and Safety Act, 1993, and therefore is subjected to its regulations.

Regulations include:

- i. Automatic controls and indicators, installed in the right order and manner and approved by an approved inspection authority*
- ii. Access to exits should be unobstructed*
- iii. Inspection and test*

**i. *Automatic Controls and Indicators***

All the control and instrumentation for this distillation column was installed in the correct manner according to SANS standards by Indecon.



## **ii. Access to Exits**

All the exits is open and without obstructing.

## **iii. Inspection and Testing**

The column was testing with water, before testing it with the o-xylene/p-xylene and 2-butanol/iso-butanol systems, to ensure that there are:

1. No leaks
2. Control system is working
3. Operating procedures are correctly formulated

The distillation column is fitted with a safety relieve valve to prevent unwanted pressure build up inside the column. Safety release valve (PRV-1) is set at a pressure of 3 bar (g), by SparixSarco. Outlet of the pressure relief valve blows off into a container in the bund wall area.

### **8.6.4 Sources of Release**

#### **i. Sources**

All the sources of release of flammable material can be classified as secondary grade of release, because they are not expected to release any flammable material under normal operating conditions. The sources of release are listed below with a brief description:

- **Flanges:** *All flanges are equipped with gaskets and new gaskets must to be installed every time the column is stripped to change the structure packing inside the column.*
- **Relief valve:** *Relief valve was described in detail in section 3.4.*
- **Sample points:** *Liquid and gas sampling will be drawn through a Luberlock valve that can be open or close with a push-pull button. The Luberlock valve has a 0.8mm opening from which the sample will be drawn. An air tide syringe is screwed on directly onto the Luberlock valve to ensure that there is no leakage of vapour or liquid out of the system. All sampling must be in the closed position before start-up can commence. Sample size varies from 0.5 ml to 1 ml.*

- **Leakage:** Leakage can occur in the unlikely event where one of the seals breaks, therefore allowing vapour or liquid to be released into the surrounding area. The area around the column is fitted with a bund wall to contain all the liquid in a safe area. Operations will be stop immediately once such an event occurs.
- **Spillage:** Spillage can occur when the column is being loaded, therefore it is important that the operator where the corrected PPE and that there is no source of possible ignition. All spillage must be cleaned up before operations can start.

## **ii. Grade of Release**

The grade of release is influenced by the differential pressure between inside and outside of the distillation column. The column will be operated at pressure ranges from vacuum to just above atmospheric pressures of the column. These two operating conditions will briefly discussed.

### **Operating Under Vacuum:**

In this case if any leakage occurs, air will be sucked into the column, where the concentration of the flammable vapour is above the upper explosion limit.

### **Operating Near Atmospheric Conditions:**

The rate of release of flammable materials will be low if the column is operating at a pressure which is close to atmospheric pressure. Therefore the classification of the area is dependent on the ventilation system available.

## **8.6.5 Characteristics of Flammable Solvents Used**

### **i. Characteristics of the Solvents Used**

The following testing system is going to be distilled inside this test setup, namely p-xylene/o-xylene and 2-butanol/iso-butanol.

**Table A 12 – Explosion limits of pure components**

Product	Self igniting temp (°C)	Flash Point (°C)	Lower Explosion Limit (%)	Upper Explosion Limit (%)	Density air=1
o-Xylene	463	17	0.9	6.7	3.7
p-Xylene	527	28.9	1.1	7	3.7
2-Butanol	406.1	23.9	1.7	9.8	2.55
Iso-Butanol	415.56	23	1.2	10.9	2.55

**ii. Xylene Mixture**

Xylene is a chemical with a very distinctive smell, and can be smelled at levels as low as 40 ppm, at 200 ppm xylene cause irritation to human skin, and at level of 700 ppm it will make a human nauseous. Thus it will be detected by human senses before it reaches the lower explosion limit of 9000 ppm.

**iii. Volatility of Flammable Liquid**

Flash points of all components are close to room temperature and therefore it is likely that it will lead to a hazardous area around the column when a valve is left open to the atmosphere. The column is also operating at a temperature that is close the boiling point temperatures of the mixture, it is thus necessary for the column not to have any continuous leakages.

**iv. Relative Density of the Gas or Vapour when it is Released**

All components are heavier than air so the vapour will accumulate in the bund wall area or be ventilated away if any leakage would occur.

### **8.6.6 Ventilation**

A proper ventilation system is essential when working with flammable gasses and therefore needs to be evaluated. The SABS give a few guidelines of how a ventilation system can be evaluated in IEC 79-10:1995.

**i. Number of Fresh Air Changes, C**

The lab where the distillation column is based has a volume of 9560m<sup>3</sup> and is equipped with an artificial ventilation system which consisted out of two fans at the bottom and three fans at the top of the building. Based on experimental data, each of the bottom fans has a capacity of 12 m<sup>3</sup>/s, thus giving a total fresh air flow rate of 24 m<sup>3</sup>/s for both fans. From this

the number of fresh air changes per unit time (C) can be calculated with the following equation:

$$C = \frac{dV_{tot}/dt}{V_o} = \frac{24m^3 / s}{9560m^3} = 2.58 \times 10^{-3} s^{-1} \quad \mathbf{A \ 1}$$

Where

$dV_{tot}/dt$  is the total flow rate of fresh air, and

$V_o$  is the total volume being ventilated.

## ii. Calculations

The experiment is performed with a mixture of gasses and not with pure components, for this reason it was decided to take the characteristics of flammable components with the lowest LEL (lower explosion limit) for calculations.

### Characteristics of release

Flammable material	Xylene vapour
Source of release	Failure of flange
LEL	0.04 kg/m <sup>3</sup> (0.9 % vol.)
Grade of release	Secondary
Safety factor, k	0.5
Release rate, (dG/dt) <sub>max</sub>	6x10 <sup>-4</sup> kg/s

Ventilation characteristics

Indoor situation

Number of air changes, C	9.2/h (2.58x10 <sup>-3</sup> s <sup>-1</sup> )
--------------------------	--

Quality factor, f	2
Ambient temperature, T	20°C
Temperature coefficient, (T/293 K)	1

Minimum volumetric flow rate of fresh air:

$$\left(\frac{dV}{dt}\right)_{\min} = \frac{\left(\frac{dG}{dt}\right) T}{k \times LEL \times 293} = \frac{6 \times 10^{-4} \times 293}{0.5(0.04) \times 293} = 0.03 \text{ m}^3/\text{s} \quad \mathbf{A \ 2}$$

Evaluation of hypothetical volume  $V_z$ :

$$V_z = \frac{f \times \left(\frac{dV}{dt}\right)_{\min}}{C} = \frac{2 \times 0.03}{2.58 \times 10^{-3}} = 23.26 \text{ m}^3 \quad \mathbf{A \ 3}$$

Time of persistence:

$$t = \frac{-f}{C} \ln \frac{LEL \times k}{X_0} = \frac{-2}{9.2} \ln \frac{0.9 \times 0.5}{100} = 1.17 \text{ h (70min)} \quad \mathbf{A \ 4}$$

The hypothetical volume takes the shape of a sphere because of the low rate of release of the flammable vapour. Therefore the distance in all directions (radius of sphere) from the source of release that is classified as a zone 2 area, can be calculated by manipulating the formula that is used to calculate the volume of a sphere. This give rise to the following equitation:

$$r = \sqrt[3]{\frac{3 \times V_z}{4 \times \pi}} = 1.7 \text{ m} \quad \mathbf{A \ 5}$$

### 8.6.7 Conclusions

Zone 2 area is 1.7m in all directions from the source of release. From these calculations it can be seen that the value for the hypothetical volume  $V_z$  is significant but can be controlled. The degree of ventilation is considered as medium with regard to the source of release and based on the persistence time; the concept of a zone 2 area would be met.

### 8.6.8 Proposed Classification:

#### Ventilation

Type .....Artificial

Degree.....Medium

Availability.....Good

#### Source of Release

#### Grade of release

Valves, pump seals and flanges.....Secondary

#### Product

Vapour.....Xylene mixture / Butanol mixture

Vapour density.....Greater than air (Xylene = 3.7; Butanol = 2.5)

The zoning sketches can be seen in Figure A 8 and Figure A 9, please note that the sketches is not according to scale. 1.7m in all direction is calcified as a zone 2 area and the bund wall area is classified as a zone 1 area because the vapour of all the flammable material is heavier than air.

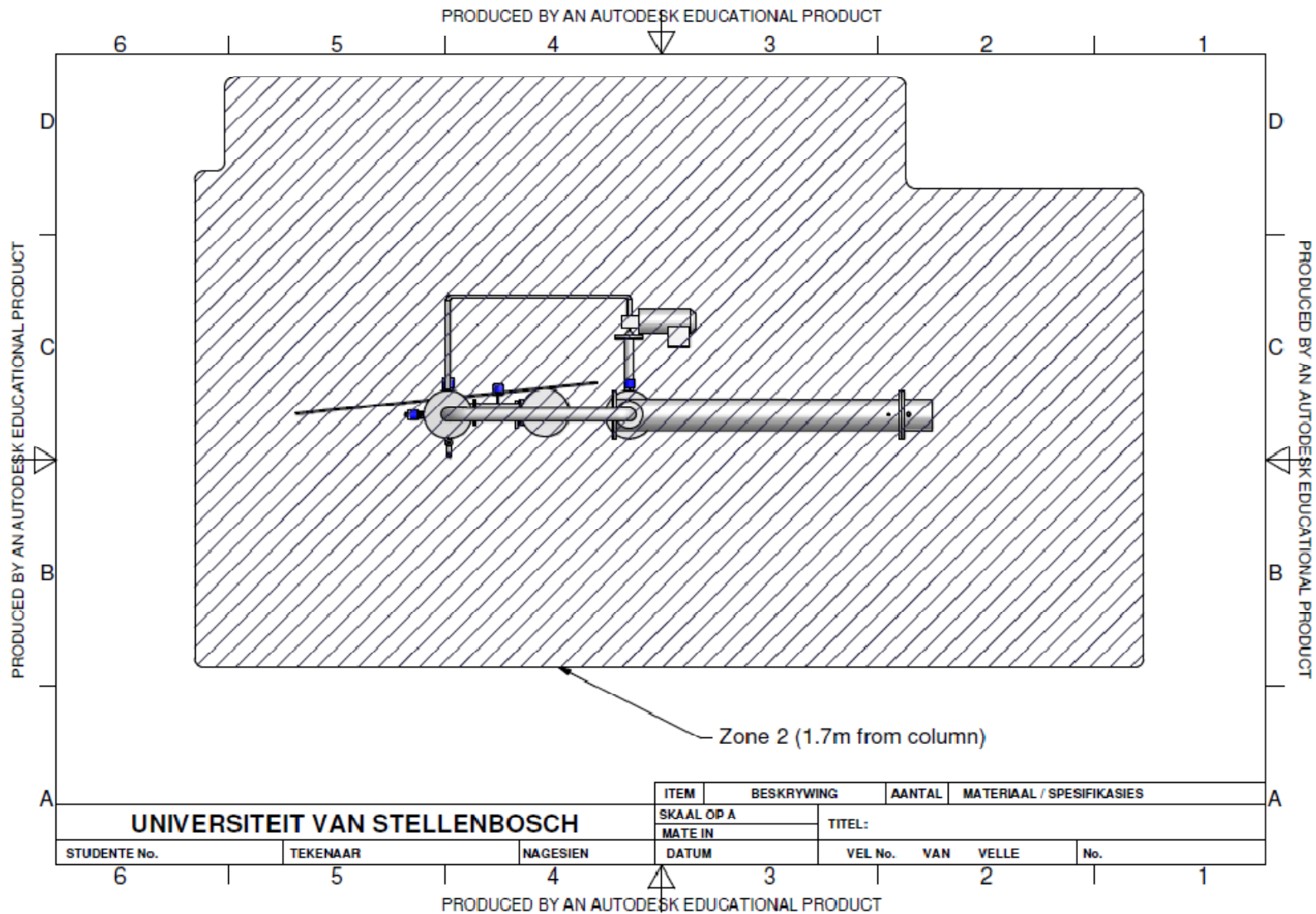


**Figure A 8 - Zoning sketch - Top view**

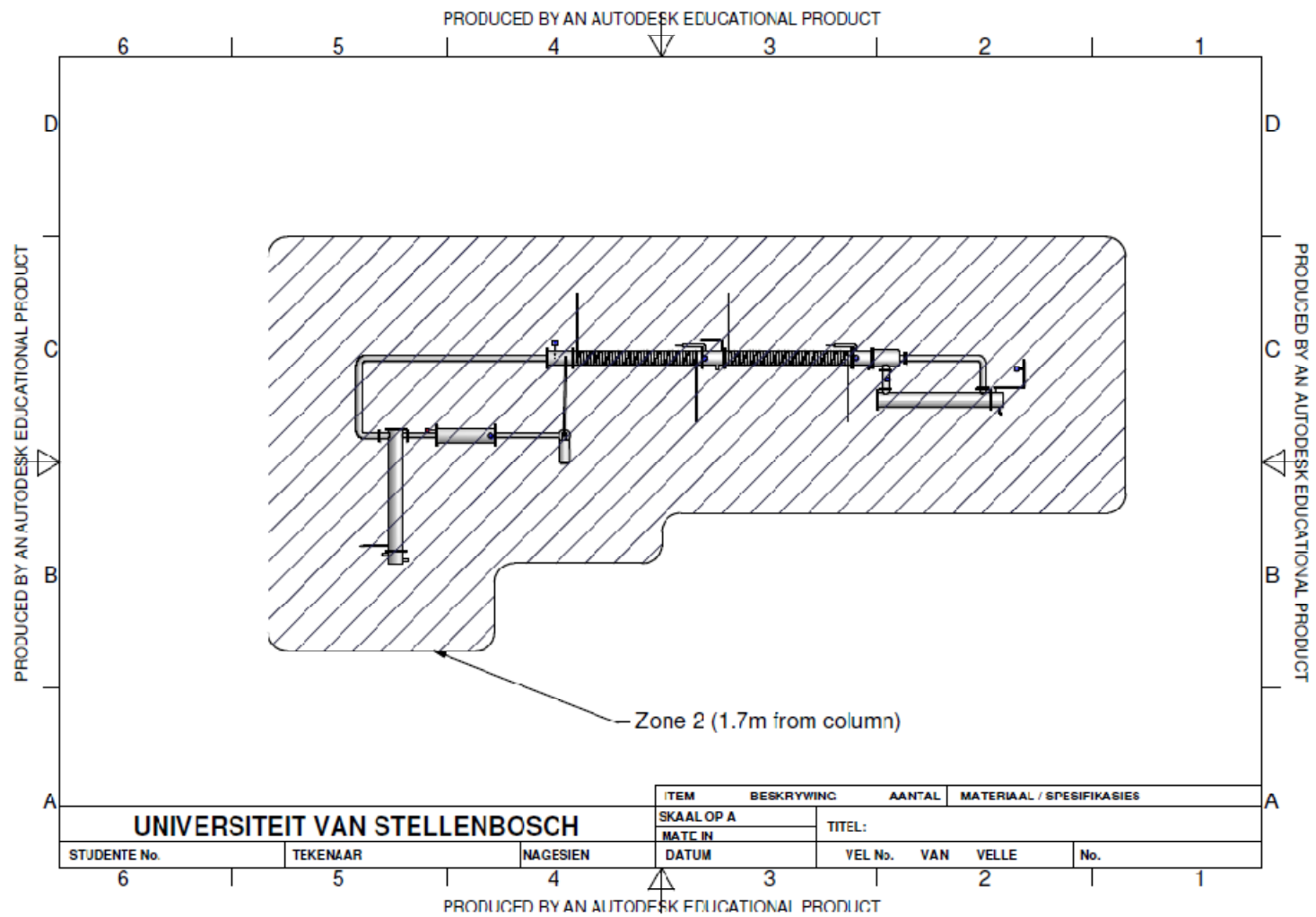


**Figure A 9 - Zoning sketch – Side view**



### 8.6.9 Hazard and Operability Study of Pilot Plant

HAZOP is procedure to critically examine the operability of process. During the HAZOP potential problems can be identified and provision for these problems can be made in the design. It is therefore necessary to do the HAZOP in the preliminary design stages and to update the HAZOP study if any changes are made to the design. The final HAZOP for the reboiler, condenser and pressure system is given in Table A 13, Table A 14 and Table A 15.

**Table A 13 – HAZOP of reboiler**

<b>Reboiler R-1</b>			
<b>Intention:</b> To vaporise liquid mixture			
<b>Lines</b>	Steam lines 4 and 5		
<b>Guide word</b>	<b>Deviation</b>	<b>Cause</b>	<b>Consequences and action</b>
<b>Line 4</b>			
<b>More</b>	Flow	Pneumatic valve (PCV-1) stuck open	Will lead to a higher vapour flow rate and possible increase in pressure: measure differential pressure over packed column
<b>Less of</b>	Flow	Pneumatic valve (PCV-1) stuck	Will lead to a lower vapour flow rate and possible decrease in pressure: measure differential pressure
<b>No</b>	Flow	Isolating valve close (GV-1), Pneumatic valve close (PCV-1) or pressure regulating valve close (PV-1)	No liquid will be vaporise: Differential pressure reading of zero
<b>Line 5</b>			
<b>No</b>	Flow	Blockage in line or isolating valve GV-2 can be closed	Reboiler will fill up with condensate: install side glass

**Table A 14 – HAZOP of pressure control system**

<b>Pressure control system</b>			
Control pressure in the column			
<b>Lines:</b>	9 and 14		
<b>Line 9</b>			
<b>Guide word</b>	<b>Deviation</b>	<b>Cause</b>	<b>Consequences and action</b>
<b>No</b>	Flow	NV-1 closed, PCV-2 closed	Pressure loss: Install pressure transmitter on system
<b>More</b>	Flow	NV-1 open, PCV-2 open	Pressure control system giving pressure fluctuations: Install absolute pressure transmitter, regulate pressure of N2
<b>Less of</b>	Flow	NV-1 partially closed, PCV-2 partially closed	Column will lose pressure: Install absolute pressure transmitter, Further open NV-1
<b>Line 14</b>			
<b>No</b>	Flow	NV-2 closed, PCV-3 closed	Pressure increase: Install absolute pressure transmitter on system
<b>More</b>	Flow	NV-1 open, PCV-2 open	Pressure fluctuations: Install absolute pressure transmitter
<b>Less of</b>	Flow	NV-1 partially closed, PCV-2 partially closed	Loss of pressure: Install absolute pressure transmitter

**Table A 15 – HAZOP of Condenser**

<b>Condenser C-1</b>			
<b>Intention:</b> Condenses the rising vapour			
<b>Lines:</b>	Cooling water lines 12 and 13		
<b>Lines 12 and 13</b>			
<b>Guide word</b>	<b>Deviation</b>	<b>Cause</b>	<b>Consequences and action</b>
<b>Less of</b>	Flow	GV-3 partially closed, GV-4 partially closed, Blockage of line	Can lead to a pressure increase in the system: install flow meter and pressure transmitter
<b>No</b>	Flow	GV-3 closed, GV-4 closed, Blockage of line	Lead to pressure increase in the column: Install pressure relieve valve, install flow meter with safety interlock to valve PCV-1

## 8.7 Raoult's Law

### 8.7.1 Calculations

The approximately 0.5°C differences in the temperature observed between the measured VLE data and the VLE data from (Zong et al. 1983) (see Section 4.1.1) can be explained with Raoult's law. According to Raoult's law the total pressure of an ideal system at equilibrium can be calculated with the Equation A 6.

$$P_{tot} = P_A^* x_A + P_B^* x_B \quad \text{A 6}$$

Where

$P_{tot}$  Total pressure of the system

$P_i^*$  Vapour pressure of the pure component i, calculated with Antoine equation.

$x_i$  Mole fraction of pure component in the solution

For binary mixture equation A 6 can be rewritten as:

$$P_A^* = \frac{P - P_B^* (1 - x_A)}{x_A} \quad \text{A 7}$$

The data from Zong et al. (1983) was taken at a pressure of 1.013 bar abs were as the pressure at Stellenbosch was measured to be 0.99 bar abs.

The Antoine equation for the pure components:

$$\log_{10} P^* = A - \frac{B}{T + C} \quad \text{A 8}$$

Where A, B and C are constants given in Table A 15, T is temperature in °C and  $P^*$  the vapour pressure of the pure component in mm Hg.

**Table A 16 – Antoine equation constants**

Component	A	B	C
2-Butanol	7.47429	1314.188	186.5
iso-butanol	8.53516	1950.94	237.147
p-xylene	6.99053	1453.43	215.31
o-xylene	7.00154	1476.393	213.872

The results for test 2 (see Figure 38 in Section 4.1.1) are given in Table A 17.

**Table A 17 – Results for VLE experiment, Test 2**

Total pressure	742.5	mm Hg
Temperature	103	°C
Composition of 2-butanol in liquid phase	0.49	mol/mol

The temperature for the system with the same composition at a pressure of 1.013 bar abs (760 mm Hg) can be calculated by substituting Antoine equation for both 2-butanol and iso-butanol into the Raoult's equation and then solving for the temperature.

$$P_{tot} = P_A^* x_A + P_B^* x_B$$

$$P_{tot} = 10^{\left[A - \frac{B}{T+C}\right]} x_A + 10^{\left[A - \frac{B}{T+C}\right]} (1 - x_A)$$

Substituting  $P_{tot} = 760$  mm Hg and  $x_A = 0.49$  mol/mol and solving for T.

$$T = 103.6 \text{ } ^\circ\text{C}$$

From this it can be seen that the temperature at 1.013 bar abs is approximately 0.5 °C higher than the temperature measured in this study at 0.99 bar abs and therefore explaining the temperature difference. The same was done for the xylene test system.

## 8.8 Thermodynamic Model

### 8.8.1 NRTL

The NRTL models were used to model the VLE line for both the 2-butanol/iso-butanol and o-xylene/p-xylene test mixtures. Working equations for the NRTL is given in equation:

$$g^E = RTx_a x_b \left[ \frac{\tau_{ba} G_{ba}}{x_a + x_b G_{ba}} + \frac{\tau_{ab} G_{ab}}{x_b + x_a G_{ab}} \right] \quad \text{A 9}$$

$$RT \ln \gamma_a = RTx_b^2 \left[ \frac{\tau_{ba} G_{ba}^2}{(x_a + x_b G_{ba})^2} + \frac{\tau_{ab} G_{ab}}{(x_b + x_a G_{ab})^2} \right] \quad \text{A 10}$$

$$RT \ln \gamma_b = RTx_a^2 \left[ \frac{\tau_{ba} G_{ba}}{(x_a + x_b G_{ba})^2} + \frac{\tau_{ab} G_{ab}^2}{(x_b + x_a G_{ab})^2} \right] \quad \text{A 11}$$

Constants obtained from DECHEMA given in (Section 4.1) and be used in the NRTL model in the following manner.

$$\begin{aligned} \tau_{12} &= \frac{(g_{12} - g_{22})}{RT} & \tau_{12} &= \frac{(g_{21} - g_{11})}{RT} \\ G_{21} &= \exp(\alpha_{21} \tau_{21}) & G_{21} &= \exp(\alpha_{21} \tau_{21}) \end{aligned}$$

Where

$g_{ij}$       Parameter for interaction between components i and j;  $g_{ij} = g_{ji}$

$\alpha_{ij}$       Nonrandomness parameter;  $\alpha_{ij} = \alpha_{ji}$

### 8.8.2 Diffusion Coefficients

Tyn and Calus (1975a) method for liquid diffusion coefficient [Absolute error = 4%]:

$$D_{AB} = 8.93 \times 10^{-8} \frac{V_B^{0.267}}{V_A^{0.433}} \frac{T}{\mu_B} \quad \mathbf{A \ 12}$$

Where

$D_{AB}$	Mutual diffusion coefficient of solute A at very low concentration in solvent B, cm <sup>2</sup> /s
$V_A$	Molar volume of solute A at its normal boiling temperature, cm <sup>3</sup> /mol
$V_B$	Molar volume of solvent at the normal boiling temperature, cm <sup>3</sup> /mol
$\mu_L$	Dynamic viscosity of solvent B, cP

The molar volume at the normal boiling temperature can be estimated with Tyn and Calus (1975b).

$$V_b = 0.285V_c^{1.048} \quad \mathbf{A \ 13}$$

Where

$V_b$	Molar volume at boiling point, cm <sup>3</sup> /mol
$V_c$	Critical molar volume, cm <sup>3</sup> /mol

Vapour phases diffusion coefficients (Fuller et al. 1966; Fuller et al. 1969):

$$D_{AB} = \frac{0.00143T^{1.75}}{PM_{AB}^{1/2} \left[ (\Sigma_v)_A^{1/3} + (\Sigma_v)_B^{1/3} \right]^2} \quad \mathbf{A \ 14}$$

Where

$D_{AB}$	Binary diffusion coefficient, cm <sup>2</sup> /s
T	Temperature, K

$M_A, M_B$	Molecular weights of A and B, g/mol
$M_{AB}$	$2[(1/M_A)+(1/M_B)]^{-1}$
P	Pressure, bar
$\Sigma_v$	Found for each component by summing atomic diffusion volumes in Table A 18

**Table A 18 – Atomic diffusion volumes**

Diffusion Coefficients	Diffusion Volume Increments
C	15.9
H	2.31
O	6.11
N	4.54
F	14.7
Cl	21
Br	21.9
I	29.8
S	22.9
Aromatic ring	-18.3
Heterocyclic ring	-18.3

### 8.8.3 Sample Calculations

**iii. Example:**

Estimate the liquid and vapour diffusion coefficients of 2-butanol (A) in iso-butanol (B) at 374.45 K and 1 bar abs if the viscosity of iso-butanol is 0.417 cP. The critical molar volumes of 2-butanol and iso-butanol are 269 and 274 cm<sup>3</sup>/mol (Gude and Teja 1995).

**iv. Solution:**

Calculating the molar volumes for A and B using Tyn and Calus (1975b)



$$V_A = 0.285 \cdot (269)^{1.048} = 100.28 \text{ cm}^3/\text{mol}$$

$$V_B = 0.285 \cdot (274)^{1.048} = 102.24 \text{ cm}^3/\text{mol}$$

For the liquid diffusion coefficients using Tyn and Calus (1975a):

$$\begin{aligned} D_{AB} &= 8.93 \times 10^{-8} \frac{V_B^{0.267} T}{V_A^{0.433} \mu_B} \\ &= 8.93 \times 10^{-8} \frac{100.28^{0.267} 374.45}{102.24^{0.433} 0.417} \\ &= 3.7 \times 10^{-5} \text{ cm}^2/\text{s} \end{aligned}$$

For the vapour diffusion coefficients (Fuller et al. 1966; Fuller et al. 1969):

From Table A 18:

$$\Sigma_A = 4(15.9) + 10(2.31) + 1(6.11) = 92.81 \text{ and}$$

$$\Sigma_B = 4(15.9) + 10(2.31) + 1(6.11) = 92.81$$

Substituting it into A 14:

$$\begin{aligned} D_{AB} &= \frac{0.00143T^{1.75}}{PM_{AB}^{1/2} \left[ (\Sigma_v)_A^{1/3} + (\Sigma_v)_B^{1/3} \right]^2} \\ &= \frac{0.00143 \cdot (374.45)^{1.75}}{(1) \cdot (74.12)^{0.5} \left[ (92.81)_A^{1/3} + (92.81)_B^{1/3} \right]^2} \\ &= 0.06457 \text{ cm}^2/\text{s} \end{aligned}$$

## 8.9 Measurement Error

The time to reach equilibrium is discussed in Section 4.3.2 and this section will focus on the experimental errors that can occur during the measuring of experimental values. The accuracy of these measurements will play a role when calculating the vapour flow factor and HETP.

The accuracy of the measurement that will influence the results is the:

- *Mole fractions obtained from the GC*
- *Temperature steam flowing to the boiler*
- *Temperature in the boiler*
- *Flow measurement of the condensed steam*

The effect of these measurements on the vapour flow factor and calculation in HETP given in Table A 18 and Table A 20.

**Table A 19 – Error in flow factor of the gas**

Measurement	Error in measurement	Effect on flow factor [%]
Flow rate of steam	± 0.01 kg	0.07
Temperature of steam	0.5 °C	0.06
Temperature in boiler	0.5 °C	0.18
Total error		0.32

**Table A 20 – Error in calculation of HETP**

Measurement	Error in measurement	Effect on HETP [%]
Mole composition by GC	0.3 %	1.7

From Table A 18 and Table A 20 it can be seen that an error of 0.32% and error of 1.7% can be expected in the vapour flow factor and HETP calculations. The pressure drop is dependent on the accuracy of the differential pressure transmitter and therefore an error of 0.58% can be expected in the pressure drop readings (see Table A 8).

## Sample calculations

Calculating HETP from experimental data over a packing section of 1.89 m high and compositions of 2-butanol above and below the bed:

Above the bed: 0.61 mol/mol

Below the bed: 0.18 mol /mol

Calculating the relative volatility above and below the bed with the equation derived in Section 4.1.2.

$$\alpha = 0.0886x + 1.2844$$

Thus the relative volatility above and below the bed are:

Above:

$$\begin{aligned}\alpha_1 &= 0.0886 \cdot (0.61) + 1.2844 \\ &= 1.34\end{aligned}$$

Below:

$$\begin{aligned}\alpha_2 &= 0.0886 \cdot (0.18) + 1.2844 \\ &= 1.30\end{aligned}$$

Taking the geometric average:

$$\begin{aligned}\alpha_{12} &= \sqrt{\alpha_1 \alpha_2} \\ &= 1.32\end{aligned}$$

Calculating the number of theoretical stages:

$$\begin{aligned}N_t &= \frac{\ln \left[ \left( \frac{x_{lk}}{1-x_{lk}} \right)_{above} \left( \frac{1-x_{lk}}{x_{lk}} \right)_{below} \right]}{\ln \alpha} \\ &= \frac{\ln \left[ \left( \frac{0.61}{1-0.61} \right)_{above} \left( \frac{1-0.18}{0.18} \right)_{below} \right]}{\ln(1.32)} \\ &= 6.95\end{aligned}$$

The HETP of the packing can now be determined from this and by knowing the height of the packed bed.

$$\begin{aligned}\text{HETP} &= \frac{h_{pb}}{N_t} \\ &= \frac{1.89}{6.95} \\ &= 0.272 \text{ m}\end{aligned}$$

Calculating the flow factor:

The flow rate of the gas was determined through an energy balance.

The values measured:

- Condensate flow rate
- Steam temperature at the inlet of the reboiler
- Temperature in the reboiler
- Composition in the reboiler

Energy input:

Take a condensate flow rate ( $\dot{c}$ ) of 12.5 kg/(10 min) or (0.021 kg/s) with a steam inlet temperature of 125 °C. Saturated steam at a temperature of 125 °C has a heat of vaporisation ( $\Delta h_{vap}$ ) of 2192.7 kJ/kg.

From this the energy input can be calculated by multiplying the condensate flow rate with the heat of vaporisation:

$$\begin{aligned}\text{Energy in} &= \Delta h_{vap} \cdot \dot{c} \\ &= 2192.7 \cdot 0.021 \\ &= 45.68 \text{ kW}\end{aligned}$$

The heat of vaporisation of the liquid mixture was calculated with a correlation by Majer and Svoboda (1985) and the correlation and its constants are given in table:

**Table A 21 – Heat of vaporisation**

$\Delta h_{vap} = A \exp(-\alpha T_r) (1 - T_r)\beta$ (kJ/mol)	Iso butanol	2-butanol
Temperature (K)	298. - 381.	298. - 372.
A (kJ/mol)	49.05	52.6
$\alpha$	-1.6587	-1.462
$\beta$	1.1038	1.0701
$T_c$ (K)	547.7	536

The measured temperature and composition of 2-butanol in the reboiler was 106 °C and 0.14 mol/mol. From this the individual heat of vaporization was calculated as 39.61 kJ/mol for 2-butanol and 42.01 kJ/mol for iso-butanol.

From this the mixtures heat of vaporisation ( $h_{vap,mix}$ ) was calculated by multiplying each components mol fraction with their heat of vaporisation and adding it together. This gave a mixtures heat of vaporisation of 42 kJ/mol.

The molar flow rate ( $\dot{n}$ ) through then obtained by dividing the energy input by the heat of vaporisation of the mixture:

$$\begin{aligned}\dot{n} &= \frac{\text{Energy in}}{h_{vap,mix}} \\ &= \frac{45.68}{42} \\ &= 1.09 \text{ mol/s} = 0.08 \text{ kg/s}\end{aligned}$$

The molar density is then calculated with the ideal gas law:

$$\frac{n}{V} = \frac{P}{RT}$$

Thus if the system is operating at a pressure of 1 000 kPa and the vapour temperature is 105.9 °C (378.9 K). Then the vapour density is equal to 31.5 mol/m<sup>3</sup> or 2.32 kg/m<sup>3</sup>.

From this the volumetric flow rate of vapour through the column can be calculated by dividing the molar flow rate by the molar density. This gives a volumetric flow rate of 0.0347 m<sup>3</sup>/s.

The velocity through the column can then be calculated by dividing the volumetric flow rate by the internal area of the column. This gives a velocity of 1.104 m/s.

The vapour flow factor is then vapour velocity times the square root of the vapour density, thus giving a vapour flow factor of 1.68 (m/s)(kg/m<sup>3</sup>)<sup>0.5</sup>.

## 8.10 Results

*Table A 22 – VLE data with butanol test mixture*

VLE Butanol	Temperature [°C]	2-butanol [mole %]	iso-butanol [mole %]	
1	Vapour	103	0.58	0.41913276
	Liquid	103	0.5	0.50
2	Vapour	103.5	0.53	0.47
	Liquid	103.5	0.44	0.56

*Table A 23 – VLE data with xylene test mixture*

VLE Xylene	Temperature [°C]	p-xylene [mole %]	o-xylene [mole %]	
1	Vapour	141	0.51	0.49
	Liquid	141	0.47	0.53
2	Vapour	140.8	0.58	0.42
	Liquid	140.8	0.54	0.46

**Table A 24 – Total reflux distillation experimental results for Flexipac 350Y HC, 2-butanol/iso-butanol (Figure 44 and Figure 47 )**

Run	F-factor (m/s)(kg/m <sup>3</sup> ) <sup>0.5</sup>	Conc. 2-butanol [wt%]				Temperatures [°C]					P <sub>top</sub> kPa	dP <sub>total</sub> mbar/m	Duty [kW]	HETP [m]		
		SP-1	SP-2	SP-3	SP-4	TI 102	TI 103	TI 104	TI 105	TI 106			Q <sub>reb</sub>	Bottom bed	Total bed	Top bed
1	1.31	13.47	17.66	45.84	78.33	93	92	90	86	82	60	3.2	28	0.495	0.481	0.481
2	1.60	13.47	16.43	45.75	78.77	93	92	90	87	81	60	5.2	34	0.467	0.462	0.462
3	1.91	11.56	15.95	45.21	79.76	94	93	91	87	83	60	7.2	41	0.462	0.448	0.448
4	2.33	8.33	11.34	41.10	81.98	93	93	90	86	82	60	10.4	50	0.400	0.380	0.380
5	2.46	7.19	10.47	39.64	82.53	93	93	90	86	82	60	12.8	53	0.394	0.367	0.367
6	2.71	5.88	7.67	36.78	83.47	94	93	91	86	82	60	15.2	59	0.349	0.331	0.331
7	2.74	5.20	6.99	34.00	83.41	94	93	91	86	82	60	17.6	59	0.353	0.323	0.323
8	1.42	14.75	14.80	40.55	79.12	77	76	74	70	65	30	4.8	22	0.565	0.502	0.502
9	1.88	11.01	13.66	42.04	80.90	77	77	74	71	66	30	6.4	29	0.508	0.470	0.470
10	2.21	9.34	11.63	38.49	82.41	77	77	74	70	66	30	8.8	34	0.496	0.433	0.433
11	2.51	7.13	8.17	36.51	82.83	78	78	75	70	66	30	13.6	39	0.414	0.387	0.387
12	2.70	5.79	6.64	35.31	83.40	78	78	75	70	66	30	17.6	42	0.379	0.363	0.363
13	2.92	5.47	5.91	32.55	82.75	79	79	76	71	67	30	23.2	46	0.379	0.357	0.357
14	1.39	14.60	18.84	45.49	75.26	106	105	103	100	94	100	3.2	38	0.427	0.424	0.424
15	1.62	13.74	17.97	46.35	76.17	106	106	103	100	94	100	4.8	44	0.398	0.407	0.407
16	2.11	11.19	15.96	41.53	77.39	106	106	104	100	96	100	7.2	58	0.414	0.378	0.378
17	2.29	9.32	13.60	41.28	78.62	107	106	104	100	95	100	8.8	63	0.365	0.347	0.347
18	2.64	7.02	9.40	37.72	79.56	107	107	104	100	96	100	12.8	72	0.310	0.301	0.301
19	2.75	5.30	7.04	33.70	80.10	107	107	104	100	96	100	14.4	75	0.287	0.275	0.275

**Table A 25 - Total reflux distillation experimental results for Flexipac 350Y HC, p-xylene/o-xylene (Figure 45 and Figure 48)**

Run nr	F-factor (m/s)(kg/m <sup>3</sup> ) <sup>0.5</sup>	Conc. p-Xylene [wt%]				Temperatures [°C]					Pressure [kPa]			Qreb [kW]	HETP [m]		
		SP-1	SP-2	SP-3	SP-4	TI 102	TI 103	TI 104	TI 105	TI 106	P <sub>atm</sub>	P <sub>top</sub>	dP <sub>total</sub>		Bottom bed	Total bed	Top bed
1	1.57	22.17	24.21	43.34	61.22	142	142	141	140	83	98.6	100	3.7	29.55	0.348	0.380	0.419
2	1.95	24.67	26.68	48.36	66.02	142	142	140	139	96	98.6	100	6	36.72	0.321	0.363	0.416
3	2.21	23.20	25.62	46.94	66.92	142	142	141	139	102	98.6	100	7.8	41.61	0.322	0.343	0.367
4	2.52	21.63	24.72	47.29	68.91	142	142	140	139	112	98	100	10.6	47.56	0.302	0.318	0.336
5	2.70	19.28	22.71	46.06	70.19	142	142	140	139	115	98	100	12.7	50.86	0.285	0.292	0.299
6	3.00	16.29	18.30	44.66	73.09	143	143	140	139	120	98	100	19.6	56.59	0.237	0.243	0.250
7	1.67	21.98	26.47	47.85	69.35	121	121	119	118	86	98.1	60	5.2	25.91	0.324	0.330	0.336
8	2.15	22.41	24.35	48.46	69.41	124	124	122	121	90	98.1	60	7.9	33.07	0.283	0.311	0.345
9	2.48	19.73	22.88	46.49	70.90	124	124	122	121	96	98.4	60	11.2	38.25	0.283	0.288	0.294
10	2.82	18.52	20.17	45.87	73.33	124	124	122	120	102	98.4	60	14.2	43.44	0.251	0.254	0.258
11	2.97	16.66	17.41	44.45	74.33	124	124	122	120	104	98.4	60	17.6	45.80	0.228	0.232	0.236
12	3.18	15.29	16.54	43.85	74.93	125	125	122	120	105	98.5	60	22.3	48.97	0.221	0.224	0.226
13	1.94	20.24	22.89	47.98	72.19	102	102	100	98	74	98	30	7	22.58	0.268	0.280	0.293
14	2.48	16.10	18.20	45.56	75.91	103	103	100	98	84	98	30	15.1	30.62	0.251	0.245	0.239
15	2.64	16.70	19.91	45.48	74.79	103	103	100	99	84	98.1	30	12.5	28.81	0.229	0.229	0.229
16	2.88	15.61	16.76	45.02	76.25	103	103	101	99	86	98.2	30	17.7	33.37	0.216	0.219	0.222
17	3.02	14.23	14.91	44.46	76.84	104	104	101	99	87	98.5	30	22.2	35.01	0.200	0.206	0.213
18	3.08	14.04	14.38	43.45	76.74	104	104	101	99	87	98.5	30	24.4	35.69	0.200	0.204	0.208



**Table A 26 - Total reflux distillation experimental results for Flexipac 350Y HC, p-xylene/o-xylene (Figure 46)**

Pressure	Run	F-factor (m/s)(kg/m <sup>3</sup> ) <sup>0.5</sup>	Total pressure drop over [mbar]				Pressure drop [mbar/m]		
			Top bed	Total column	Top distributor	Middle distributor	Top bed	Total column	Average
1 bar abs	1	1.71	2.38	5.02	0.17	0.45	0.79	0.78	0.79
	2	2.07	3.50	7.30	0.34	0.47	1.29	1.33	1.31
	3	2.41	4.59	9.59	0.38	0.76	1.85	1.85	1.85
0.6 bar abs	4	1.98	3.29	6.80	0.28	0.50	1.36	1.35	1.35
	5	2.37	5.06	10.50	0.36	0.61	2.25	2.28	2.26
	6	2.70	6.79	14.56	0.42	0.70	3.13	3.31	3.22
	7	3.00	9.02	18.50	0.49	1.42	4.27	4.14	4.21
	8	3.33	15.75	29.57	0.61	1.94	7.77	6.89	7.33
	9	3.42	19.46	34.98	0.65	1.11	9.71	8.53	9.12
	10	3.50	28.44	48.28	1.17	2.34	14.19	12.19	13.19
1 bar abs	11	2.46	4.73	9.90	0.38	0.69	1.92	1.95	1.94
	12	2.72	5.99	12.56	0.43	0.86	2.56	2.60	2.58
	13	2.82	7.60	15.96	0.45	0.90	3.41	3.72	3.56
	14	3.02	9.09	18.73	0.51	0.99	4.16	4.17	4.17
	15	3.19	13.44	25.55	0.56	1.13	6.43	6.26	6.35
	16	3.31	17.39	32.64	0.56	1.13	8.52	8.09	8.30
	17	3.38	33.33	o/r	2.25	4.5	16.07	o/r	16.07
0.3 bar abs	20	2.86	7.13	14.81	0.48	0.95	3.40	3.40	3.40
	21	3.12	9.63	19.24	0.55	2.18	4.68	4.23	4.46
	22	3.30	13.11	23.71	0.62	1.86	6.48	5.48	5.98
	23	3.52	16.15	29.09	0.67	2.05	8.07	6.83	7.45
	24	3.67	23.72	39.49	1.20	0.50	11.79	9.84	10.82
	25	3.79	35.75	o/r	2.66	5.32	17.38		17.38

**Table A 27 - Total reflux distillation experimental results for Mellapak 350Y, 2-butanol/iso-butanol (Figure 52, Figure 53 and Figure 55)**

Run nr	F-factor (m/s)(kg/m <sup>3</sup> ) <sup>0.5</sup>	Conc. 2-butanol [wt%]				Temperatures [°C]					P <sub>atm</sub> [kPa]	dP <sub>total</sub> [mbar/m]	Q <sub>reb</sub> [kW]	HETP [m]		
		SP-1	SP-2	SP-3	SP-4	TI 102	TI 103	TI 104	TI 105	TI 106				Bottom	Total bed	Top
1	1.67	0.14	0.18	0.61	0.89	106.7	105.9	102.3	99.1	92.3	99	1.3	46	0.272	0.304	0.348
2	1.85	0.13	0.17	0.59	0.90	106.9	106.2	102.4	98.9	93.1	99	1.6	51	0.262	0.282	0.309
3	1.99	0.11	0.15	0.57	0.91	107.1	106.3	102.6	98.9	94	99	1.9	55	0.257	0.266	0.277
4	2.07	0.11	0.14	0.55	0.91	107.3	106.5	102.9	98.9	94.1	99.5	2.3	57	0.252	0.256	0.261
5	2.20	0.09	0.12	0.53	0.92	107.6	106.8	103	98.9	94	99.5	3.3	60	0.241	0.239	0.238
6	2.32	0.07	0.10	0.51	0.92	107.9	107.2	103.2	98.9	94	99.55	4.9	64	0.228	0.229	0.229
7	2.37	0.07	0.09	0.50	0.92	108.1	107.4	103.3	98.9	94	99.6	6.6	65	0.220	0.223	0.226
8	2.44	0.06	0.08	0.26	0.92	108.4	107.6	103.8	98.9	94	99.7	8.0	67	0.343	0.216	0.156
9	2.54	0.02	0.02	0.18	0.83	109.6	108.7	106.7	99.6	95	99.8	15.9	69	0.217	0.196	0.172
Composition 1																
10	1.36	0.46	0.54	0.90	0.98	103.8	103	99.6	87.5	81.3	99.3	0.0	38	0.276	0.308	0.360
11	1.84	0.44	0.52	0.91	0.98	103.8	103	99.6	87.5	81.3	99.4	0.0	Area	0.258	0.278	0.311
12	1.96	0.43	0.51	0.91	0.99	104.2	103.1	99.8	88.9	83	99.4	0.0	0	0.252	0.262	0.281
Composition 2																
13	1.32	0.30	0.37	0.80	0.95	104.3	103.2	99.8	89.1	82.1	99.5	0.0	kg/m3	0.282	0.317	0.373
14	1.72	0.28	0.34	0.81	0.96	105.3	104.5	100.6	88.9	82.8	99.5	0.0	2	0.264	0.286	0.321
New distributor																
15	1.33	0.12	0.15	0.53	0.83	105.5	104.6	100.6	90.5	83.7	99.4	0.0	2	0.285	0.325	0.376
16	1.78	0.10	0.13	0.52	0.86	106.8	106.2	103	92.1	85.8	99.4	0.0	2	0.262	0.288	0.320
17	1.99	0.09	0.11	0.51	0.89	107.2	106.4	103	92.8	85.7	99.4	0.0	2	0.247	0.257	0.267
18	2.18	0.08	0.10	0.51	0.91	107.4	106.6	103.2	92.6	85.3	99.1	0.0	2	0.232	0.241	0.251
19	2.08	0.08	0.10	0.50	0.91	107.6	106.9	103.2	92.2	82.6	99.1	0.0	2	0.236	0.242	0.247
20	2.35	0.06	0.08	0.48	0.92	107.5	106.8	103.2	92.1	82.5	99.1	0.0	2	0.215	0.223	0.231

**Table A 28 - Total reflux distillation experimental results for Mellapak 350Y, 2-butanol/iso-butanol (Figure 54 and Figure 67)**

Pressure	Run	Gas capacity factor (m/s)(kg/m <sup>3</sup> ) <sup>0.5</sup>	mbar				Pressure drop [mbar/m]			
			Top bed	Total column	Top distributor	Middle distributor	Top bed	Bottom bed	Total column	Average
1 bar abs	1	1.67	2.63	5.47	0.23	0.42	1.27	1.28	1.27	1.27
	2	1.85	3.17	6.90	0.25	0.67	1.54	1.62	1.58	1.58
	3	1.99	3.90	8.22	0.29	0.64	1.91	1.95	1.92	1.93
	4	2.07	4.59	9.61	0.29	0.46	2.28	2.41	2.34	2.34
	5	2.20	6.68	13.84	0.32	0.94	3.36	3.29	3.32	3.33
	6	2.32	9.66	19.39	0.35	0.56	4.92	4.85	4.88	4.88
	7	2.37	12.07	25.51	0.36	0.26	6.19	6.97	6.57	6.58
	8	2.44	14.88	31.48	0.40	0.80	7.66	8.36	7.99	8.00
	9	2.54	32.11	o/r	1.29	1.24	15.91	o/r	o/r	15.91

